Modelling resilience and sustainability of complex human-environment systems in agriculture and ecology

by

Kathyrn Fair

A thesis
presented to the University of Waterloo
in fulfillment of the
thesis requirement for the degree of
Doctor of Philosophy
in
Applied Mathematics

Waterloo, Ontario, Canada, 2020

Examining Committee Membership

The following served on the Examining Committee for this thesis. The decision of the Examining Committee is by majority vote.

External Examiner:	Nina H Fefferman Professor, Department of Ecology & Evolutionary Biology, University of Tennessee, Knoxville
Supervisors:	Chris T Bauch Professor, Department of Applied Mathematics, University of Waterloo
	Madhur Anand Professor, School of Environmental Sciences, University of Guelph
Internal Members:	Sue Ann Campbell Professor, Department of Applied Mathematics, University of Waterloo
	Matthew Scott Associate professor, Department of Applied Mathematics, University of Waterloo
Internal-External Member:	Peter Deadman Associate professor, Department of Geography and Environmental Management, University of Waterloo

Author's Declaration

This thesis consists of material all of which I authored or co-authored: see Statement of Contributions included in the thesis. This is a true copy of the thesis, including any required final revisions, as accepted by my examiners.

I understand that my thesis may be made electronically available to the public.

Statement of Contributions

- Chapter 2: The work in this chapter was performed by Kathyrn R Fair (KRF) under the supervision of Prof. Chris T Bauch (CTB) and Prof. Madhur Anand (MA) resulting in a co-authored paper published in *Scientific Reports* [97]. Contributions are: CTB and MA conceived of the study, KRF analysed the model. All authors developed the model and wrote the manuscript.

- Chapter 3: The work in this chapter is based on a manuscript under review at *Global Change Biology* [98]. CTB and MA conceived of the study, KRF analysed the model and wrote the first draft. All authors developed the model and revised and commented on the manuscript.

- Chapter 4: The work in this chapter is based on a manuscript in preparation [96]. KRF conceived of the study, analysed the model and wrote the first draft. KRF, MA, and CTB developed the model. KRF and CTB revised and commented on the draft.

Abstract

As we move further into the Anthropocene, numerous challenges to sustainable development present themselves. Questions abound: How do we feed a growing population? What steps must we take to conserve ecologically valuable ecosystems? How can we create the greatest improvements in global food security and equality? The increasing impacts of climate change on Earth's systems only serve to heighten the importance of, and difficulty in, answering these questions. Given the complexity of the systems – trade networks, ecosystems, etc. – to which these questions pertain, it is crucial that we gain a comprehensive understanding of their dynamics before taking action. Without this, any changes to these complex human-environment systems could have unintended and potentially calamitous effects. As such, the value of modelling techniques for exploring the dynamics and potential futures of these complex systems is high. This thesis uses models to examine the behaviour and possible future trajectories of 3 such systems. We begin by delving into the temporal evolution of the global wheat trade network using a dynamic network model. A preferential attachment mechanism is found to provide a good fit to the empirical network, based on several key metrics. Our modelled trade network is quite fragile to shocks. However, as it grows towards 2050, its resilience to attacks will increase. Next, we implement a spatially-explicit agent-based model for the forest-grassland mosaics of Southern Brazil. These ecologically valuable systems are fragile, with simulated mosaics persisting only over a narrow range of conditions. Mosaics may cease to exist in scenarios where climate change impacts greatly reduce fire-mediated recruitment thresholds. When climate change effects are less severe mosaics that do not disappear exhibit substantial alterations to their spatial structure. Finally, we explore the dynamics of a human metapopulation linked through a trade network. Centrality to the network is key to obtaining high food per capita, and differences in centrality may result in inequalities between patches. Inequalities and issues of food security can also arise when patch-level behaviours differ. Larger and more regular network structures facilitate more equal patch-level outcomes and higher levels of food security. However, when patch-level import behaviours are heterogeneous, the best course of action is to first modify these behaviours before adjusting the network topology. Across all 3 projects, modelled systems display complex behaviours. This emphasizes the necessity of further development of models for complex human-environment systems that can provide a more complete understanding of system dynamics and potential futures. The insights gained from these models can be used to inform policies for facilitating positive outcomes in real-world complex systems.

Acknowledgements

First, I would like to thank my supervisors, Dr. Chris T Bauch and Dr. Madhur Anand, for their support, guidance, and insight throughout my undergraduate and graduate education.

Thanks to Dr. Sue Ann Campbell and Dr. Matthew Scott for their guidance both during their classes and as members of my PhD advisory and examination committee. Thank you to Dr. Nina H Fefferman and Dr. Peter Deadman for sitting on my PhD examination committee.

I would like to thank my grad school friends for their help, companionship, humour, and shared enjoyment of time spent outside the office. To my friends outside of the department: thank you for your support, and for sharing in good meals, trips to the dog park, and relaxing evenings.

Finally, thank you to my family for their love and support, and their patience regarding phone calls that quickly devolved into monologues on the minutiae of my research.

Table of Contents

List of Tables

List of Figures

Chapter 1

Introduction

Recently, the field of "complexity science" has emerged as an attempt to grapple with complex systems that have proved intractable via the established methods of more traditional disciplines. Through interdisciplinary collaborations, researchers have attempted to gain insight on, and in some cases predict, the behaviour of such complex systems.

Definitions of complexity, and of complex systems, vary widely (see [176] for example). Here, we consider a system to be "complex" if it contains a large number of components interacting with each other in such a way that the system displays behaviour not evident from analysis of its constituents [338].

Commonly cited properties of complex systems include non-linearity, hierarchical organization, feedback, emergence, self-organization, robustness and lack of central control, and numerosity [176, 338]. Though neither necessary nor sufficient conditions for classifying a system as "complex" they do provide us with a reasonable set of guidelines for distinguishing between complex and simple systems [338]. As such, we will describe them briefly to give an idea of the scope of complex systems, and complexity science.

Mathematically speaking, a function, $f(x)$, is considered to be linear if it satisfies 2 properties;

1. Additivity: $f(x+y) = f(x) + f(y)$,
2. Homogeneity: $f(\alpha x) = \alpha f(x)$.

Functions that do not satisfy these properties are considered to be non-linear. Applying this thinking to systems, we say a system is non-linear if a change to its input does not lead

to a proportional change in output [176]. For example, there is a non-linear relationship between the amount of time an athlete spends training and their performance [305]. Going from not training at all to training 1 hour/week should improve performance, but we cannot assume that if they begin training 5 hours/week they will perform 5 times better than on a 1 hour/week schedule. Additionally, training 15 hours/week is unlikely to lead to a 15-fold increase in performance, and may result in a drop in performance due to fatigue.

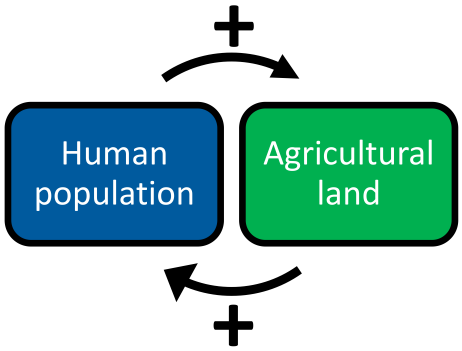

Figure 1.1: **Positive feedback loop between human population and agricultural land.** Visualization of the positive feedback loop between human population and agricultural land [42].

In a system with feedback, the behaviour of a component will impact the behaviour of other components, creating a "feedback loop" if these other components in turn influence the original component. For example, when playing chess, the moves made by the "white" player influence the moves the "black" player makes, in turn affecting the gameplay of the "white" player. Feedback may be "positive"; if 2 components have a positive feedback loop increases in the first will result in increases in the second, in turn resulting in further increases to the first, creating an amplifying effect. An example of this is the relationship between human population and food production (Figure 1.1), as human population increases, food production must increase to meet growing demand, and this increased food supply will in turn result in further population growth (unless populations undergo a demographic transition) [42]. In contrast, negative feedback has a dampening effect, where increases in one component result in decreases to the other, or vice versa. Blood pressure regulation in the human body involves a negative feedback; baroreceptors detect when blood pressure has become too low or too high, and signal for an increase (respectively decrease) in heart rate to return blood pressure to within the desired range [133].

Self-organization in a system (also know as spontaneous order) means that random local interactions between components can result in some global order [47, 176]. This phenomenon arises in complex systems across a variety of fields, including biology, physics,

economics, and linguistics. The collective behaviour of schools of fish, or flocks of birds (e.g. Figure 1.2), arises from self-organization [66, 135, 47]. Additionally, it has been argued that the market economy is self-organizing, via an "invisible hand", and as a result distributes resources more efficiently than if its order was determined by some overall design [236].

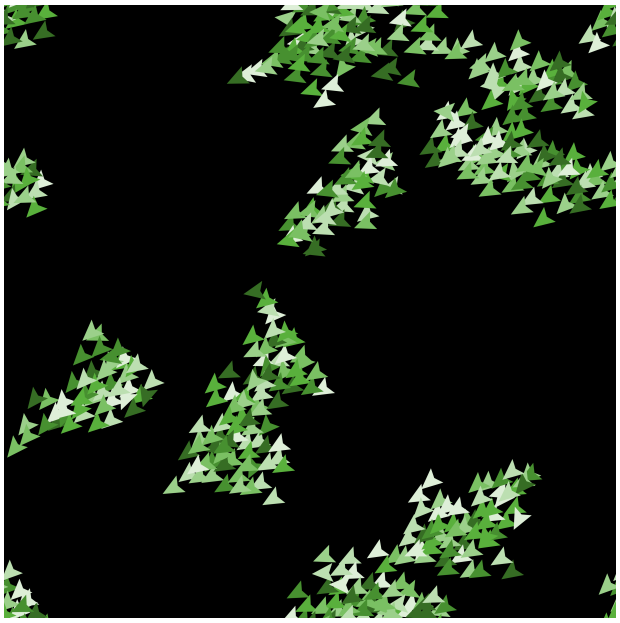

Figure 1.2: **Simulated self-organization of flocking birds.** Flocking model implemented in NetLogo [324, 323].

The concepts of robustness and lack of central control are strongly linked to the idea of self-organization. Systems that are self-organized, and thus not governed by some centrally dictated order, tend to be robust to perturbations [176]. Returning to our earlier example of a school of fish, the behaviour of the school is not likely to be greatly impacted by the removal of a single fish; the remaining individuals in the school will re-order themselves to maintain some overall organization. Conversely, if we removed the keystone from an archway, we would expect that the archway would collapse, as the keystone's role in the arch's ability to bear weight is crucial to the order of the system; its removal leaves us with a disordered pile of rubble.

For complex systems, the behaviour and properties of the system as a whole differ from that of its constituent parts. This phenomenon is known as "emergence" as these characteristics emerge when we consider not only individual components of the system, but how they interact with each other to create some larger whole [176, 150]. As such,

self-organization is an example of emergence [67]. Complex systems have components that often display very simple behaviours. However, the collective behaviour of the entire system resulting from the interactions between these components is very complex [150]. This collective behaviour can be difficult to predict as, with a large number of components, the number of potential interactions that must be considered is vast.

Emergent behaviour is often a result of the hierarchical organization of complex systems; the robust order created by the interactions of components at lower levels leads to a distinct pattern of behaviour at a higher level [176]. The interaction of components, not only within their level of the hierarchy, but across levels, contributes to complexity. For example, the Fédŕation Internationale de Football Association (FIFA) is the global governing body for the sport of football, which governs regional football associations such as the Union of European Football Associations (UEFA). These regional associations in turn oversee national associations such as England's Football Association, and so on. These components of the global system of organized football interact within their level of the hierarchy. However cross-level interactions also occur, as when FIFA sanctions regional associations for breaching the rules governing the sport.

As is evident from the above discussion, complex systems display numerosity; they are made up of a large number of components that participate in a multitude of interactions [176, 338]. This characteristic is quite intuitive; if there are very few components to a system and/or if they very rarely interact, the behaviour of the system will tend to be quite simple. Consider, for example, 2 people playing rock paper scissors; there are only 2 players, who are engaging in a single round of play, where the permutations (e.g. rock/rock, rock/scissors, etc.) are quite limited. The numerosity of this system is quite low, especially in contrast to something like a massively multiplayer online role-playing game (MMORPG). Here, millions of players are interacting with each other, often multiple times, and are able to engage in a much broader range of actions than simply choosing between rock, paper, and scissors.

Understanding and predicting the behaviour of complex systems is a challenging task. One method for doing so is through mathematical models. In order to do this we must find a way of representing these systems that simplifies them while preserving their essential characteristics. Once we have arrived at some satisfactory representation of the system we may begin to model its behaviour. Through such models, we can gain insight into the function of the system, and how it might behave in future. By using models to perform *in silico* experiments, we can explore possible future trajectories for these systems without the costs and potential for unintended consequences that would be incurred if we attempted to manipulate aspects of the real-world system itself.

1.1 A brief history of network models for complex systems

Complex systems can be conceptualized as networks of interconnected components. In such a network the components of the complex system are "nodes" that are connected to each other via "edges". Through this representation, we retain key information about the system's structure of interactions [338]. By reducing complex systems to their essential characteristics in this way, we can better facilitate their analysis and modelling.

Using networks as a framework for studying complex systems is a relatively recent development [36, 216, 3, 338, 19, 320]. However, it is rooted in graph theory, which originated in the 18^{th} century. The city of Königsberg in Prussia, spread across both sides of the Pregel river and the island of Kneiphof, possessed 7 bridges. This lead to a mathematical puzzle, known as the "Seven Bridges of Königsberg"; how to leave one point in the city, cross all 7 bridges exactly once, and return to the original location. While it was widely believed that no such route existed, no proof of this was presented until Leonard Euler tackled the problem in 1735 [92, 5]. He did so by creating a graph, treating each piece of land as a node, and each bridge as a link. This was the first time a mathematical proof had been demonstrated using a graph, and his published work on the topic is considered to be the very first "graph theory" paper [92, 5, 18].

Fast-forwarding to the 20^{th} century, scientists became interested in studying systems by modelling them as components interacting on a lattice. Perhaps the most famous of these, the Ising model (Figure 1.3) comes from statistical mechanics [163, 226]. First proposed in 1920 to demonstrate ferromagnetism, this model describes atomic "spins" arranged on a lattice. These spins have one of two states (-1, $+1$). Through interactions with neighbouring spins, a spin may "flip" from -1 to $+1$ or vice versa. Another example is the "voter models" developed in the 1970s, which describe the process of opinion formation [151, 65]. Here each node in the lattice represents a voter, who has an opinion state (0 or 1). Voters are randomly selected, and their opinion changes with some probability, based on the opinion of one of their neighbours. For example, if the neighbour has opinion state 1 and the selected voter has state 0, the selected voter flips their opinion state to 1. In such models, consensus can occur where all voters have the same opinion state. However, coexistence between opinion states, where the system reaches an equilibrium with both opinions, is also possible. In this case, clustering of like opinions will be evident.

Lattices have also been employed to explore evolutionary game theory, as in pioneering work on the spatial Prisoner's Dilemma by Nowak & May from 1992 [221]. This model explored how cooperative behaviour evolves in a spatial setting, where at each round of

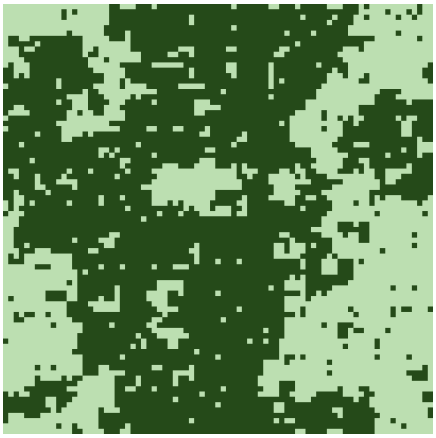

Figure 1.3: **Spatial distribution of spins in the 2-dimensional Ising model.** Model implemented in NetLogo [324, 325], +1 spin shown in dark green, −1 spin in light green.

the game, agents situated on the nodes of a lattice play the Prisoner's Dilemma with their neighbours. The Prisoner's Dilemma consists of 2 players, who choose whether they will cooperate with the other, or defect, based on a set of payoffs for pursuing each of these strategies (Table 1.1) [301, 242]. When $T > R > P > S$, it is clear that both players obtain the best payoff by defecting. If Player Y defects, so should Player X (since $P > S$), and if Player Y cooperates Player X should still defect as $T > R$ (similarly for Player Y) [301, 242, 221]. While this behaviour is simply laid out for a single round of the game between 2 individuals, outcomes are much more complex when the game is played on a lattice. Nowak & May found that this implementation of the Prisoner's Dilemma leads to spatial patterns of cooperators and defectors that vary temporally, with both strategies persisting indefinitely. Depending on the payoffs for different strategies, the spatial patterns generated can vary widely. This work has implications for cooperative behaviour in biological systems (e.g. between molecules, or organisms), with the authors suggesting the spatial structure that emerges in such models is essential to the evolution of cooperation [221].

Table 1.1: **Payoffs in the Prisoner's Dilemma.** (x, y) indicate the payoffs for players X and Y respectively, for the given set of strategies.

		Player Y	
		Cooperate	Defect
Player X	Cooperate	$(x, y) = (R, R)$	$(x, y) = (S, T)$
	Defect	$(x, y) = (T, S)$	$(x, y) = (P, P)$

These models are precursors to the modern network models used in complexity science. However, due to their use of regularly structured lattices they are unable to capture the observed complexity of real-world systems [338]. The field of "network science", which begin to gain in prominence in the late 1990s with two seminal works by Watts & Strogatz and Barabási & Albert, provides an alternative [19, 320]. By employing networks, which have more intricate structure and the potential to evolve temporally, analyses and modelling efforts are better able capture the characteristics of real-world systems [338].

1.2 Basics of network science

Networks consist of components known as nodes (or vertices), connected to each other by edges (or links). Networks may be undirected (Figure 1.4a), where only the presence/absence of a connection is considered, or directed, where edges have some inherent direction (from one node to another), as in Figure 1.4b. Depending on the system being considered, the directionality of interactions may or may not be essential information. A network of actors that have collaborated with each other on films would not require directed edges. However, directionality is important to a network of academic citations; it is key that we know whether paper i cited paper j or vice versa.

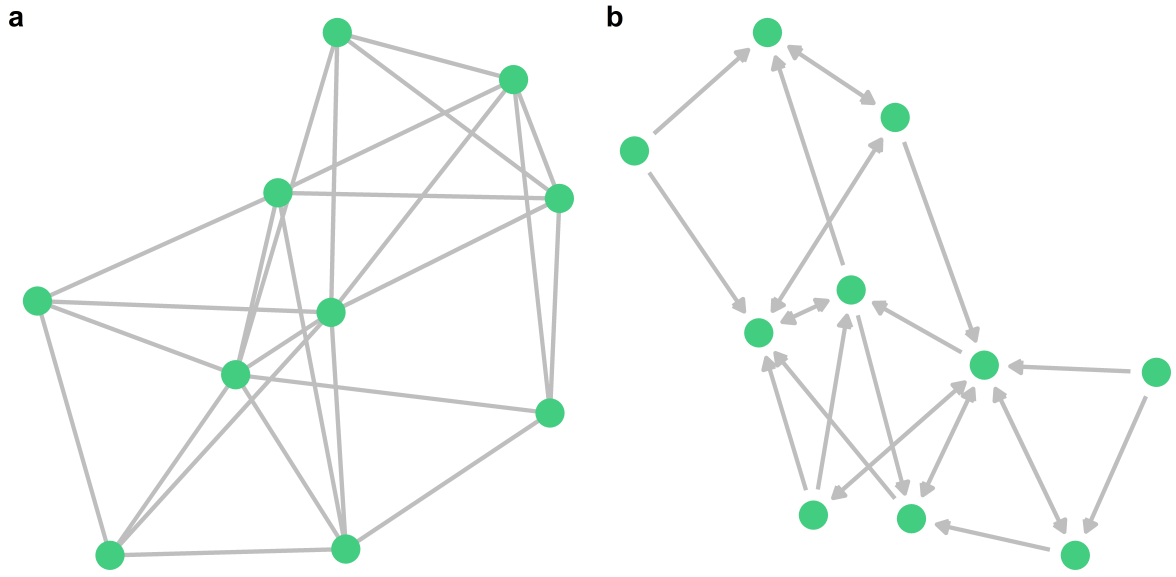

Figure 1.4: **Edge types in networks.** Network with a) undirected and b) directed edges.

A network containing N nodes can be represented via an $N \times N$ adjacency matrix, A. For an undirected network, we say that each element a_{ij} of the matrix A contains some value

$$a_{ij} = \begin{cases} 1 \text{ if node } i \text{ is connected to node } j, \\ 0 \text{ if node } i \text{ is not connected to node } j, \end{cases} \tag{1.1}$$

where $a_{ij} = a_{ji}$, creating a symmetric network. For a directed network elements are defined as

$$a_{ij} = \begin{cases} 1 \text{ if there is an edge to node } i \text{ from node } j, \\ 0 \text{ if node } i \text{ is not connected to node } j \end{cases} \tag{1.2}$$

such that we can store information on the direction of an edge [18].

The properties of networks, both at the network- and node-level, can be quantified in a variety of ways. A few of the most common metrics, which are useful to us in describing types of networks, are listed in Table 1.2. In regular networks (Figure 1.5a) all nodes have the same number of edges, and thus the same degree [217]. In contrast, random networks (Figure 1.5c) do not guarantee that all nodes will have the same number of edges. For a set number of nodes, random networks can be generated either by randomly placing a fixed number of edges between these nodes, or by connecting pairs of nodes via edges with some probability p (in which case the number of edges is not fixed) [18, 217].

Table 1.2: **A selection of common network metrics.** Metrics for classifying network types.

Metric	Description	Source
Average node degree	Average number of edges connected to a node within a network	[18, 261]
Assortativity	Measures the extent to which nodes with similar characteristics (e.g. similar node degree) tend to connect to each other	[18]
Average path length	Average length of the shortest paths (along edges) between pairs of nodes in a network	[18]
Average clustering coefficient	Describes the degree to which a node's neighbours are themselves linked, averaged over the network	[217, 261]

The Watts-Strogatz algorithm can be used to generate both random and regular networks (Figure 1.5). By beginning with a ring lattice (a regular network) with a fixed number of nodes and edges per node, and randomly rewiring each edge with probability p, we can generate a regular ($p = 0$) or a random network ($p = 1$). Networks generated for $p \in (0, 1)$ may exhibit high clustering (like a lattice) and short path lengths between nodes

(like a random network); these have been dubbed "small-world" networks (Figure 1.5b) [320, 292]. Many real-world networks exhibit small-world properties including food webs, power grids, and trade networks [160, 271, 326].

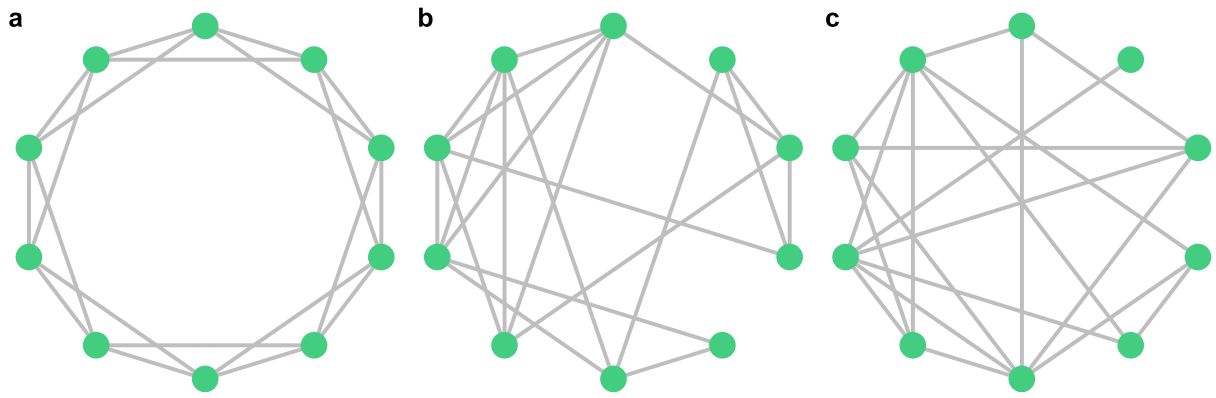

Figure 1.5: **Common network types.** Using the Watts-Strogatz algorithm with different rewiring probabilities, p, we can generate a) regular ($p = 0$), b) small-world ($p = 0.25$), and c) random ($p = 1$) networks with 10 nodes and 20 edges [320].

Networks that follow power-law degree distributions, called "scale-free" networks (e.g. Figure 1.6a), are another commonly discussed network type due to their purported (though disputed, see for example [41]) ubiquity in the real world [217, 19]. Definitions of what requirements must be met to deem a network as "scale-free" vary, however it is generally agreed that, in these networks, the probability that a node has degree k is given by

$$P(k) \sim k^{-\gamma} \tag{1.3}$$

where $\gamma > 1$ (e.g. Figure 1.6b) [41]. Networks of this type can be generated via a preferential attachment mechanism, such as in the Barábasi-Albert (BA) model [19]. In the BA model, we begin with m_0 nodes, and at each step add a new node with $m \leq m_0$ edges. The probability that a new edge is connected to a node i already present in the system is proportional to node i's degree (k_i), and is given by

$$\Pi(k_i) = \frac{k_i}{\sum_j k_j} \tag{1.4}$$

such that new nodes preferentially attach to nodes that are already highly connected [19].

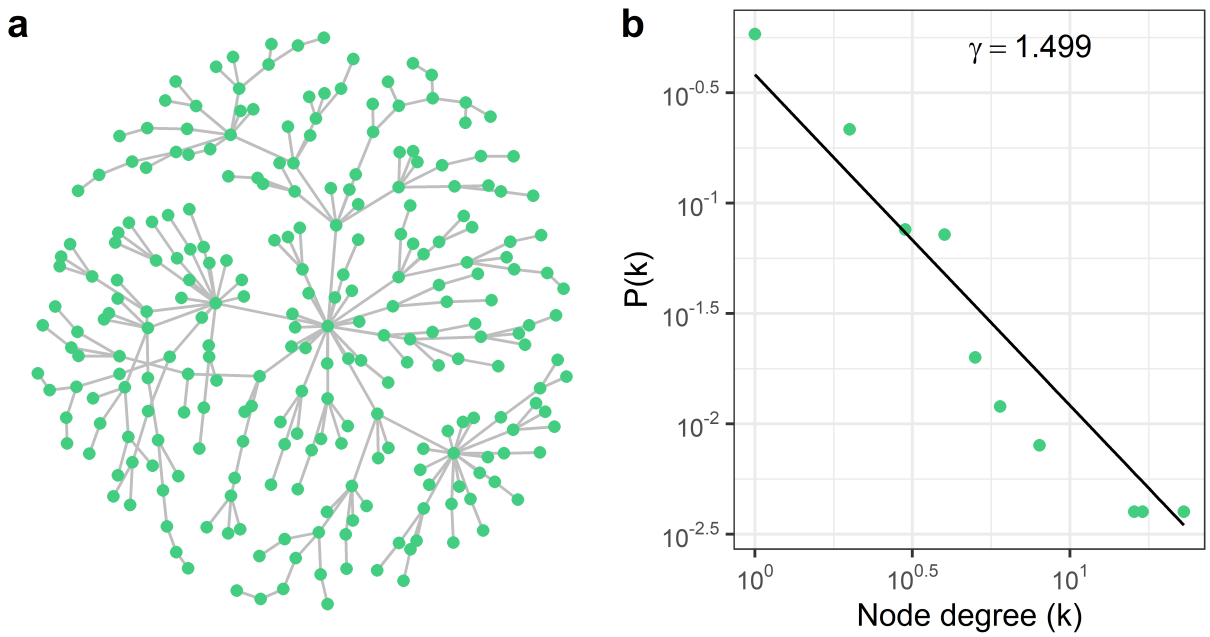

Figure 1.6: **Characteristics of scale-free network degree distributions.** a) A scale-free network with 250 nodes and 249 edges generated using the Barábasi-Albert model. b) The degree distribution (green points) and associated power-law fit (black line) for the generated network where $P(k) \sim k^{-1.499}$.

1.3 Sustainability, resilience, and vulnerability in complex systems

Discussions around the impacts of an increasing human population have been ongoing at least since Thomas Malthus first published "An Essay on the Principle of Population" in 1798. Therein he raised concerns about the viability of feeding a population that grows exponentially while food supply grows arithmetically; a concept now known as the "Malthusian Law Of Population" [189]. Though his dire predictions of a malnourished global population have not come to pass, in part due to technological advances such as the manufacture of nitrogen fertilizer, new debates have ignited surrounding our consumption of natural resources and anthropogenic impacts on ecosystems [297, 193, 126]. In 1972, "The Limits to Growth" was published and proclaimed that yet another disaster awaited humanity - one of civilization collapse in the 21st century, if the rates at which human population, food production, resource depletion, industrialisation, and pollution have been

increasing remain constant [199, 193]. Unlike Malthus, the authors of this report appear to have been vindicated in their assertions, based on comparisons of their predictions to actual post-1972 trajectories (see for example [303, 304, 126]).

The linked concepts of "sustainability" and "sustainable development" may provide us with an avenue for avoiding such a catastrophic outcome for humanity in the 21st century. While numerous definitions of these concepts exist, we focus on the characterization introduced in the 1987 report "Our common future" from the World Commission on Environment and Development. In it, sustainable development was defined as "development that meets the needs of the present without compromising the ability of future generations to meet their own needs" [225]. Thus, the long-term goal of sustainability – balancing the maintenance of environmental integrity with the fulfilment human needs – can be met through sustainable development [168, 332]. Sustainability can be conceptualized using the "triple bottom line" framework which describes it as a goal that can only be attained if social, environmental, and economic sustainability are achieved (Figure 1.7). These 3 types of sustainability are known as the "bottom lines" or pillars of sustainability [165]. Other frameworks have also been proposed, such as the "circles of sustainability" which introduces cultural sustainability as a 4th pillar [167].

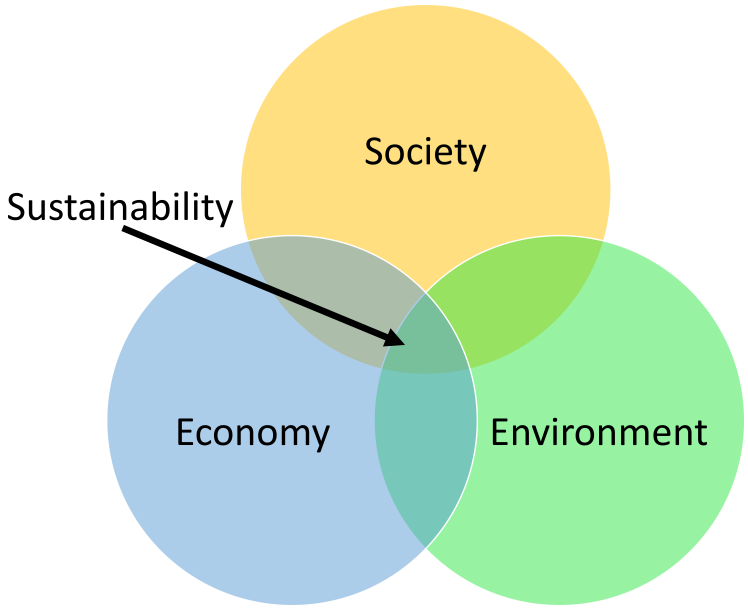

Figure 1.7: **The 3 pillars of sustainability.** Social, environmental, and economic sustainability are the 3 pillars or "bottom lines" of sustainability, all of which are required for sustainability to be achieved [165].

The United Nations Sustainable Development Goals (SDGs) were introduced in 2015 as "the blueprint to achieve a better and more sustainable future for all". Included are 17 goals for improving global sustainability by 2030 [214, 212]. Of these, 3 address issues integral to the work presented in this thesis:

- Goal 2: "End hunger, achieve food security and improved nutrition and promote sustainable agriculture",
- Goal 13: "Take urgent action to combat climate change and its impacts",
- Goal 15: "Protect, restore and promote sustainable use of terrestrial ecosystems, sustainably manage forests, combat desertification, and halt and reverse land degradation and halt biodiversity loss" [214].

Though we do not discuss methods for combating climate change, our exploration of climate change impacts may be useful to designing effective strategies to combat its impacts on ecosystems. Additionally, as noted in [99], achievement of Goal 1: "End poverty in all its forms everywhere" and Goal 4: "Ensure inclusive and equitable quality education and promote lifelong learning opportunities for all." relies upon advancement towards Goal 2. Poor food security can impede productivity and educational attainment, inhibiting economic development and making it more difficult to break out of cycles of poverty [99, 33, 158]. It is clear from these SDGs that issues of food security, climate change, and ecosystem conservation are integral to sustainability.

The sustainability of a complex system depends strongly on its resilience [182, 156, 333]. While there are numerous characterizations and types of resilience, Holling's definition of ecological resilience is most useful to us here. Ecological resilience is the perturbation (or shock, or disturbance) that can be absorbed by a system before it loses its self-organization and undergoes a transition to a different stable state. This definition does not require that a system be at (or near) an equilibrium, meaning we may still apply it to systems displaying transient dynamics [153, 154, 155, 234]. Resilient systems adapt in the face of perturbations or changing conditions; they are robust to disturbance [181, 156, 306]. Systems that are unable to do so may be vulnerable, where vulnerability is characterized as the likelihood of a system sustaining damage due to the introduction of a perturbation [302, 306]. As such, consideration of resilience, vulnerability, and robustness are key to contextualizing complex systems (the internet, trade networks, financial systems, ecosystems, etc.) in terms of sustainable development [197, 245, 145, 287, 82, 277, 234, 214, 316, 332, 306].

1.4 Study systems

This thesis explores the behaviour of several complex coupled human-environment systems (HES) [187]. In HES, human and environmental components interact to create complex behaviours, such as the human systems driving emissions of greenhouse gasses and the Earth's climate system [180] or human social behaviours and disease dynamics [318]. The introduction of human influence to environmental systems may alter their dynamics and stability [27, 180, 136]. Thus, gaining insight into the behaviour of these systems is vital, as they are essential to humanity's continued existence. In addition to describing our study systems, we briefly discuss modelling techniques for these systems to provide context for our work in later chapters.

1.4.1 Agri-food trade networks

Agri-food trade networks (e.g. wheat trade within South America in 2017, as in Figure 1.8) are a key component of the global food supply system. Here the nodes are trading entities (e.g. countries, cities), and the edges represent trade routes between them. These networks display several properties of complex systems, most notably hierarchies of trade (from the company to the country level), and self organization. The structure of these networks is not determined by some overall guiding design, but by the multitude of interactions (trades) between components. Previous work has characterized trade networks as small-world [271, 326]. In addition to the high clustering and short average path length characteristic of small-worldness, these networks display heterogeneous degree distributions [89, 174, 51, 287, 110, 330].

Trade in agri-food products is crucial to the maintenance of food security, as it facilitates the redistribution of food supplies to meet demand. In a world where an expanding population with shifting consumption patterns will require additional food resources from a shrinking pool of viable agricultural land, the role of trade networks will become increasingly important [258, 123, 177, 75]. Additionally, due to the environmental impacts of trade and its role in driving land-use changes (e.g. deforestation), this complex system has far-reaching effects [123, 177, 75]. Some authors have suggested that the clustering in these networks, and their skewed degree distributions make them a "weak link" for food security due to the potential for trade disruption in a globalizing world [89, 330, 174, 51, 287, 110]. However, others have stated that the temporal evolution of trade networks is not resulting in a lower level of food security, and that their growth may make them less vulnerable to certain types of disruptions [238, 263].

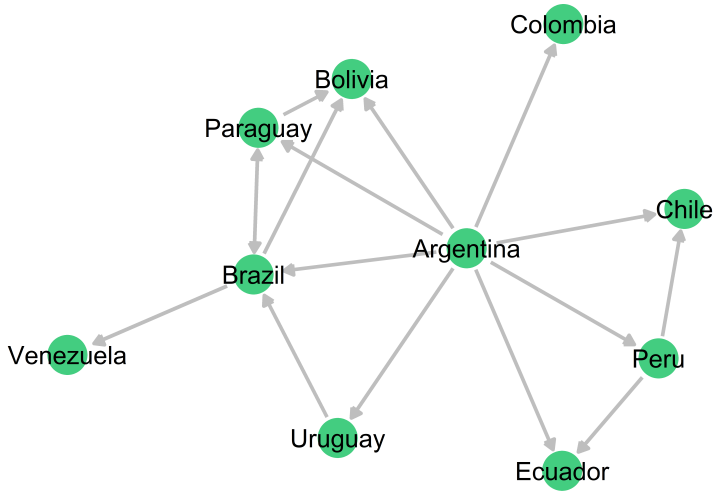

Figure 1.8: **Wheat trade in South America.** Visualization of the wheat trade network within South America in 2017 using data from the Food and Agriculture Organization of the United Nations [108].

Depending on the aims of a project, different types of models will be appropriate for describing trade networks. If the focus is on the dynamic evolution of the trade network itself, network formation models (e.g. preferential attachment) are developed, as in [117, 116, 110, 7, 94, 95, 288]. However, if the interaction of trade with other factors, such as human population growth or land use, is the area of interest it is often simpler to use a static network (which does not experience structural change during simulation) as in [81, 82, 287]. Here, temporal dynamics are driven by the behaviours of the trading entities (nodes), which interact with each other via a fixed network structure.

1.4.2 Forest-grassland mosaics

Forest-grassland mosaics are complex systems consisting of distinct patches of forest and grassland coexisting in close proximity. They occur around the globe, from the Atlantic forest-*Campos* grassland system in Southern Brazil (Figure 1.9), to Nigeria's Jos Plateau forest-grassland mosaics, and the montane forests in India's South Western Ghats [224, 72, 80, 286, 29, 279, 39, 219]. In these systems, the self organization of forest and grassland species into distinct clusters creates an overall "mosaic" pattern. Temporal trends in the dominant land cover (from forest to grassland or vice versa) are driven by feedback loops and threshold responses to changing disturbance regimes [136, 31, 34, 275, 286].

Figure 1.9: **Forest-grassland mosaics in Southern Brazil.** Satellite image of the forest-grassland mosaics surrounding the municipality of Cambará do Sul (29.02° S, 50.08° W) in the state of Rio Grande do Sul generated using data from the Sentinel-2A satellite [2].

These unique ecosystems face disruptions due to the expansion of agricultural land over both the natural forest and grassland states, as well as exotic species invasion, and climate change [136, 224, 72, 80, 31, 227, 45, 293]. Previous fieldwork and modelling have shown that fire, rainfall, and other aspects of environmental conditions are crucial to the maintenance of forest-grassland systems [311, 280, 208, 1, 282, 253, 252, 278, 314]. Given the ongoing effects of climate change on temperature, precipitation, and the frequency and severity of disturbances (fire, hurricanes, etc.) in regions containing mosaics, the continued stability of these systems is far from guaranteed [279, 29, 192]. Additionally,

mosaic ecosystems are highly biodiverse and rich in endemic species, some of which (e.g. the Paraná Pine in Brazil) are endangered [136, 31, 209, 227, 275, 45, 293, 72]. As such, these systems have high conservation value, and will need to be managed carefully in the face of a broad range of threats. By building models of these systems, we can gain insight into how to maintain the coexistence of forest and grassland, and potentially assist in site selection for conservation reserves [220].

Previous models of these systems have generally focused on their stability (e.g. [136, 279, 282, 310, 161] amongst others). In mosaic ecosystems, forest and grassland can be conceived of as alternative stable states, creating a system with bi-stability. Models of forest-grassland bi-stability are "compartmental", dividing the mosaic into sub-populations with distinct characteristics, described as proportions of the total population. This can be done by species (e.g. tree species in one compartment, grassland species in another, shown in Figure 1.10a) [161] or by land use types (e.g. agricultural land, natural grassland, natural forest as in [136]). Once this compartmental structure is established, we can define rates of change that determine how individuals within the population move between compartments, which is generally done using ordinary differential equations (ODEs). By analysing the ODEs, we are able to determine what stable equilibria the system has. If both stable grassland and stable forest equilibria are possible (under a certain parameter regime) the system has forest-grassland bi-stability, and we can interpret this as a region of the parameter space where mosaic ecosystems occur. The idea behind this is that if (at a sufficiently fine scale) forest and grassland are alternative stable states, stochastic processes and spatial heterogeneity will mean that at a broader scale we observe both stable forest and stable grassland states. Perturbations to the system (e.g. disturbances such as fire) will cause shifts from a forest to a grassland state (or vice versa) at the fine scale (Figure 1.10b), creating overall temporal shifts in the proportions of forest and grassland.

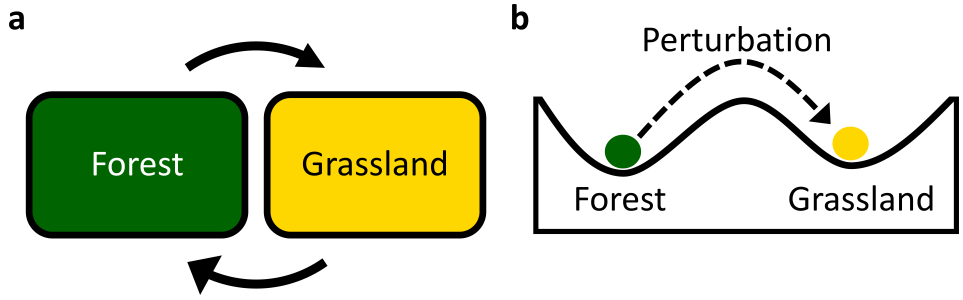

Figure 1.10: **Alternative stable states in forest-grassland mosaics.** a) A compartmental mosaic ecosystem model that produces forest-grassland bi-stability. b) A perturbation causing a shift from a stable forest to a stable grassland state in a bi-stable mosaic ecosystem.

While compartmental models are convenient in that they allow us to analyse the stability of mosaic ecosystems, they do not incorporate spatial structure. Spatial interactions (e.g. fire spread) are essential to maintaining the stability of these systems [308, 266, 264, 34, 335, 311, 253, 252, 314]. Thus, non-spatial models may be disregarding spatial information that is key to an accurate analysis of mosaic stability. Spatial models for these systems can represent them in a variety of ways, from dividing the mosaic landscape into discrete cells [314, 266, 264, 34] to considering a continuous landscape where densities of tree cover vary [335]. Often, discretization of the mosaic is achieved by treating it as a lattice (Figure 1.11) where each cell of the landscape is a node connected by edges to nearby cells. Here, each cell has a "state" property, which provides information on what the cell contains (e.g. forest or grassland). Probabilities that a cell transitions from one state to the other can be defined to describe how processes such as forest recruitment and forest fire drive system dynamics.

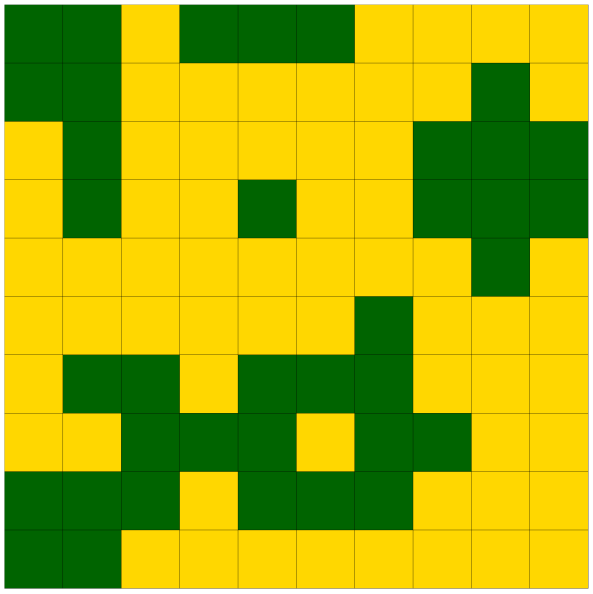

Figure 1.11: **Stylized forest-grassland mosaic.** Representation of a forest-grassland mosaic as cells containing forest (green) or grassland (yellow) on a lattice.

1.5 Thesis outline

In this thesis we apply modelling techniques to several important complex systems, as described in the previous section. These projects aim to enhance our understanding of system behaviours, while also incorporating a predictive aspect. Through the development of such models, we can gain insight into several challenges to the realization of sustainable development over the remainder of the 21st century.

We begin in Chapter 2 by building a model of trade network growth, as applied to international wheat trade. This model employs a preferential attachment mechanism, similar to that described in Section 1.2. While some previous work modelling the formation of trade networks has been undertaken (e.g. [117, 116, 110, 7, 94, 95, 288]), these have considered the trade network as a whole. This leads us to our goal of developing a commodity-specific model of network evolution. Using this model, we explore how network growth is impacted by shocks (e.g. climate change, disease spread) and their effect on network resilience. This chapter has been published in Scientific Reports [97].

Chapter 3 describes the development of a spatially-explicit agent-based model of Southern Brazil's forest grassland mosaics. This work expands on several previous non-spatial models of forest-grassland mosaics [161, 136, 310, 282] to explore how environmental conditions and disturbance regimes impact the spatial structure of these systems. In addition, we consider specific scenarios of changing environmental conditions/disturbance regimes driven by climate change, to project potential futures for these ecosystems. This chapter [98] is currently in submission with Global Change Biology.

In Chapter 4 we develop a model linking human population growth to land-use and food trade. This ODE model divides Earth's land, food supply, and human population into metapopulations located in spatially distinct "patches" linked by a network of trade. Unlike previous work, we explicitly model not only human population and food supply, but the land area required for food production [254, 81, 82]. Using this model, we explore how both the characteristics of the patches, and of the network structure that they are embedded in, impact model behaviour. We characterise behaviour in terms of outcomes for the human population (e.g. food per capita, inequality in per capita food supply, population size, etc.). This chapter [96] is being prepared for submission.

We conclude in Chapter 5 with a discussion of the complex behaviours exhibited by our modelled systems, as well as the implications of these models for sustainability. The thesis closes with final remarks and suggestions for future work.

Chapter 2

Dynamics of the global wheat trade network and resilience to shocks

This chapter is based on the paper: Kathyrn R Fair, Chris T Bauch, and Madhur Anand. Dynamics of the global wheat trade network and resilience to shocks. *Scientific reports*, 7(1):1-14, 2017.

Abstract

Agri-food trade networks are increasingly vital to human well-being in a globalising world. Models can help us gain insights into trade network dynamics and predict how they might respond to future disturbances such as extreme weather events. Here we develop a preferential attachment (PA) network model of the global wheat trade network. We find that the PA model can replicate the time evolution of crucial wheat trade network metrics from 1986 to 2011. We use the calibrated PA model to predict the response of wheat trade network metrics to shocks of differing length and severity, including both attacks (outward edge removal on high degree nodes) and errors (outward edge removal on randomly selected nodes). We predict that the network will become less vulnerable to attacks but will continue to exhibit low resilience until 2050. Even short-term shocks strongly increase link diversity and cause long-term structural changes that influence the network's response to subsequent shocks. Attacks have a greater impact than errors. However, with repeated attacks, each attack has a lesser impact the previous attack. We conclude that dynamic models of multi-annual, commodity-specific networks should be further developed to gain insight into possible futures of global agri-food trade networks.

2.1 Introduction

As nations become more interconnected in the era of globalisation, trade networks play an increasingly significant role in the well-being of nation states. The ways in which countries select trading partners; the global impact of local economic crises due to globalisation; and how country-level characteristics are affected by network metrics can be explored by analysing these complex systems [178]. A significant amount of research has characterized trade networks and described how they change over time. However, a crucial subset of these networks–trade in agri-food commodities–has not been explored in as much depth. Trade in agri-food products will become more crucial to maintaining food security as global population growth, urbanization, increasing demand, and shifting consumption patterns decrease land resource availability [258, 43]. At a global scale, the success or failure of sustainable development goals – heavily dependent on improved food security [99, 33, 158, 214, 212] – is tied to the dynamics of these trade networks.

Potential risks to the agri-food network are abundant, with more emerging due to a variety of factors. In trade networks shocks generally manifest as the sudden inability of countries to export due to a negative supply shock that alters network structure [289, 263, 118, 119]. A myriad of triggers can cause these shocks. The globalisation of agri-food

trade has led to the threat of contaminants spreading across international borders, forcing countries to close their borders to trade and affecting billions of people [78, 327, 330]. Reductions in availability and quality of cereal crops due to extreme weather conditions impacting major agricultural producers will only be worsened by climate change [331, 238, 322]. Food crops being utilised in fuel production and higher demand for meat in low-income nations results in increased pressure on global stocks of vegetable and cereal crops [331]. Other shocks that could impact global food supply include agro-terrorism, crop pests, and epidemics [238, 244, 251, 170, 84]. During food shortages countries often cease exporting agri-food commodities [93, 238, 272, 205, 299, 76, 296, 83, 132, 10, 28, 100]. For example, as a result of the global food crisis in 2008 trade restrictions were imposed by 6 of the top 17 wheat exporters and 4 of the top 9 rice exporters [238, 272]. These export restrictions caused increased global prices and led to other countries imposing export restrictions, resulting in even higher global prices in what has been dubbed a "multiplier effect" [121]. As network connectivity increases these disturbances could severely impact low-income countries, which depend greatly on imports of staple foods during shortages and are heavily burdened by the resulting price shocks [74, 238]. Thus, an understanding of how resilient trade networks are to shocks, and potential areas of vulnerability is essential ton maintaining food security.

Previous network analyses of the agri-food trade network as a whole [89, 287]: the virtual water trade network [289, 263, 174, 52, 51, 70]; and commodity-specific trade networks [20, 330, 331, 238, 118, 119] have been undertaken with some consideration of shocks in relation to food security [289, 331, 263, 89, 238, 118, 119, 110]. These studies have led to conflicting views on how globalisation has impacted global food security in these networks. Several reference the heterogeneous degree distributions of these networks or their clustering as sources of vulnerability [89, 330, 174, 51, 287, 110], while others state that the globalisation of trade has had little negative effect on global food security [263]. Network vulnerability, measured using the magnitude of damage to network structure resulting from shocks, is one aspect of network resilience. Definitions of resilience encompass not only the robustness of a network to damage resulting from shocks but also the speed at which it recovers from shocks [245]. Further research, especially regarding the resilience of trade networks for globally important staple foods, could provide useful insights and guide the development of food security policy.

Models that examine the self-organization of components within a trade network are useful for understanding mechanisms that determine network structure [190]. By modelling a network it becomes possible to perform experiments *in silco* to gain insights into system dynamics, both in terms of future growth and shock scenarios. This can help ensure that policy is pro-active instead of reactive [238].

A review of the literature reveals that most trade network models focus either on network formation or on simulating shocks. Network formation models generate a network according to growth rules and treat the final network as a static, single-year "snapshot" of the empirical network with different model parametrisations for each snapshot. Shock simulation models generally do not include growth mechanisms, meaning that the interaction between network growth and response to shocks is not considered [119, 238, 289]. These approaches do not permit an examination of the concurrent multi-year effects of temporal network evolution and shocks on these networks–areas we propose to explore here.

Additionally, network formation models have been formulated for only the network of all globally traded goods (WTN: the world trade network) [117, 116, 110, 7, 94, 95] and the virtual water trade network (VWTN) [288], to our knowledge. Because networks for individual commodities often have structural differences compared to the entire WTN, models describing their evolution could differ in important ways from those created to represent the entire WTN. Therefore models of individual commodity networks should be further studied since they may yield unique insights [20].

To gain insight into these international trade networks, an understanding of how their overall structure emerges from interactions between countries is critical. Two main theories as to how trade networks evolve have been proposed. Maoz found that partnerships in the WTN form according to preferential attachment (PA) based on the total degree centrality of nodes [190]. Preferential attachment captures the fact that nation states that are already central to the network are often more desirable as potential partners [190, 90]. Alternatively, Garlaschelli and Loffredo assert that the mechanism driving the growth of the WTN is a "good get richer" system, represented by a model based on the hidden variable hypothesis (HVH). In this case, each node has an intrinsic fitness impacting the probability of connection. They identified the hidden variable (fitness) for the WTN as annual GDP and used this to model the growth of the WTN in specific years [117, 116].

While the HVH requires knowledge of economic data (e.g. GDP), the PA model does not. Hence, its relative simplicity and fewer data requirements, together with the current knowledge gap on applying PA models for such problems, make it an attractive prospect for modelling dynamics of single commodity agri-food networks. Based on this review of the literature, we formulated 2 questions to motivate our work. First, can a preferential attachment model describe the growth of a trade network for a specific commodity over many years? Second, if a PA model can describe such a network, how does that model predict the network will respond to shocks? Our corresponding objectives were twofold: to fit a PA model for a commodity-specific network using empirical data, and to use our model to predict the response of that network to shocks.

To this end, we constructed a dynamic network model of the global wheat trade network that builds on previous work by considering the temporal evolution of the network and how shocks impact it over time. The PA model was calibrated to describe the time evolution of the empirical network. We carried out a vulnerability analysis of both empirical and model networks to ascertain potential weaknesses, and to determine whether the network is evolving over time to become more or less resilient in the face of shocks.

The global wheat trade network (Figure 2.1a) was chosen for analysis due to its global importance to food security. From 1986-2010 wheat was the highest traded agri-food commodity by volume, and in the top 10% of agri-food commodities both in regard to number of countries trading and the number of trades [107]. Shocks impacting this network have had significant impacts on global food security, most recently during the 2007-08 world food crisis and in 2010-11 when several major producers imposed export restrictions [205, 299, 76, 296, 83, 238, 125, 100, 10]. An additional cause for concern is that climate change driven shocks impacting global agri-food trade, and the wheat trade network specifically, are expected to occur more frequently as we move further into the 21st century [101, 298].

2.2 Methods

2.2.1 Definition of empirical network

We began by defining the network we sought to model as a subset of the entire global wheat trade network. To define a network we followed an approach similar to the existing practice of creating a "backbone" network. These networks include only those edges corresponding to the largest trades by volume and together accounting for 80 % of total trade volume. This method is used to simplify analysis of trade networks while also retaining salient aspects of network structure [89, 174, 122, 238, 288].

Previous research defines a backbone network for static networks and often over a single year only. In contrast, we defined a "continuous wheat trade network" by including only edges where trade was sustained over at least 3 years (Subsection A.1.1). We therefore simplified the model by avoiding having to determine when and how edges should be deleted. Also, using 3 years instead of 1 year increases the chance that our network reflects the long-term features of network structure. We also assume that countries connected by a trade link persisting over multiple years have a higher probability of being impacted by a shock than countries that are only infrequently part of the network. Thus, continuous trade networks are of interest when modelling long-term dynamics and the long-term impact of shocks on the biggest traders.

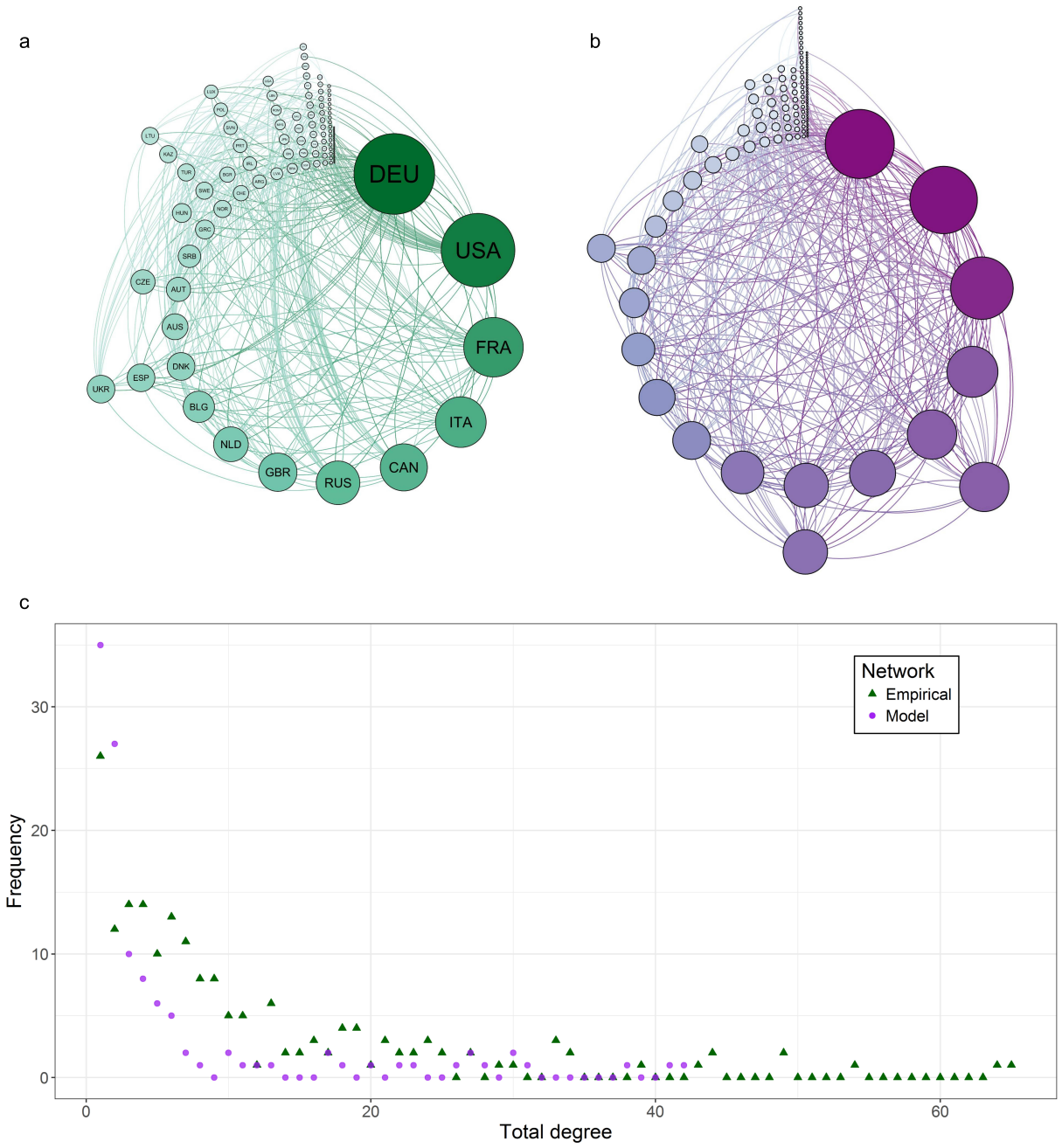

Figure 2.1: **Comparison of empirical and model continuous wheat trade networks.** (a) Empirical network. (b) Exemplar model network. (c) Comparison of degree distributions for empirical and exemplar model networks. All sub-figures correspond to the year 2013. For (a) and (b), nodes are arranged clockwise, and in size and colour, by total degree.

While our network is not defined in the same way a conventional backbone network, it accounts for 66% of total trade volume despite containing only 30% of the trades, on average (Figure A.7). By 2013, there were 108 countries engaged in 363 continuous trade partnerships in this network [107]. The correlation between a country's total degree in the continuous trade network and its total trade volume in the empirical network is positive and significant at the 5% level (Figure A.8). This suggests that countries important to our continuous trade network are also important in a conventionally-defined backbone network. The characteristics of the empirical network are further described in Subsection 2.2.5.

2.2.2 Overview of model network

We developed a preferential attachment (PA) model in order to mechanistically describe the empirical network. The PA theory of trade network formation operates on the premise that well-connected countries (namely, countries with high total degree centrality) are more appealing to prospective trading partners [190, 90]. As already noted in the Introduction, PA theory has not been applied to trade networks for specific commodities, to our knowledge. Additionally, using a PA model does not require annual GDP as input data, in contrast to the Hidden Variable Hypothesis (HVH) model, and therefore offers the possibility of a more parsimonious theoretical model.

However, to create our PA model, we built on certain aspects of the HVH model of trade network formation proposed by Garlaschelli *et al.* (see following subsections for details) [117, 116]. For a PA model to describe a commodity network, the number of nodes in the network must grow over time, and new nodes must initiate trades with highly-connected pre-existing nodes (i.e. the network must be disassortative). These characteristics are observed in the continuous wheat trade network we wish to model (Figure A.4)

Our model of the wheat trade network (Figure 2.1b) contains m directed, unweighted edges and is represented by an $N \times N$ matrix A where N is the total number of countries in the world. The $(i,j)^{th}$ element of the matrix contains information on import from country j to country i ($A(i,j) = 1$ if i imports from j, and $A(i,j) = 0$ otherwise). The way trade partnerships are formed to populate this matrix is discussed in Subsection 2.2.3. The rate of network growth, in terms of number of edges, was estimated by extrapolating 26 years of data from the United Nations Food and Agriculture Organization (FAO) (Subsection A.1.2) [107]. As we considered a directed network, imports and exports between countries i and j were represented as separate partnerships: if these countries engage in reciprocal trade, they will possess 2 partnerships. All simulations were run in Matlab R2014b [195]. Network analysis was conducted using the igraph package (version 1.0.1) [68] for Rstudio (version 3.2.2) [259]. Network visualization was conducted using Gephi (version 0.8.2) [24].

2.2.3 Trade probability calculations in network model

The probability of a trade (import or export) occurring depends on the fitness of both countries involved in the potential trade. For the PA model, a country's trade fitness depends on their total degree centrality [190, 90]. We defined the probability $P_t[x_i(m), x_j(m)]$ of a trade between countries i and j when there are m directed edges in the network as

$$P_t[x_i(m), x_j(m)] = \frac{\alpha x_i(m) x_j(m) + \epsilon}{1 + \beta x_i(m) x_j(m)}, \tag{2.1}$$

where $x_i(m)$ and $x_j(m)$ are the fitness for country i and country j when there are m directed edges in the network, and $\epsilon \ll 1$ is some small probability of the formation of an edge between countries i and j when one or both has zero fitness (i.e. one or both are not yet engaged in any trade partnerships). α and β are free parameters, which we fit to match characteristics of the empirical network (Subsection 2.2.5) [116]. α scales the overall probability of connection whereas β controls how strongly the probability of connection depends on fitness. For example, a very small β-value ($\beta \ll 1$) would allow approximating Equation 2.1 by $P_t[x_i(m), x_j(m)] \approx \alpha x_i(m) x_j(m) + \epsilon$, and the product $x_i(m) x_j(m)$ would have a large impact on the overall probability.

It could be argued that a country with high export fitness would tend not to have high import fitness. In this case, separate probabilities of import and export should be calculated based on import and export fitness values for each country. However, we do not believe this to be necessary. We examined the top 20 wheat importing and exporting countries by year for 1961-2011, determining that 25% of countries were in the top 20 for both import and export volume each year [107]. Similar results have been found for the maize network from 2000-2009 [330]. This overlap between the largest importers and exporters suggests that there is considerable overlap between import and export fitness.

We defined the fitness of country i, when there are m directed edges in the network, as

$$x_i(m) = \frac{l_i(m)}{m}, \tag{2.2}$$

where $l_i(m)$ is number of edges connected to country i when there are m directed edges in the network (the country's total degree). The degree of each node (country) is recalculated every time a new edge is added to the network. Thus, a country's fitness is dictated by the fraction of total trades it is involved in, and is a unit-less quantity. Both the trade probability and fitness equations are adapted from previous research [116].

2.2.4 Model network formation

At each time-step a series of events occur, which may lead to a new edge being added to the network (Figure A.7). The likelihood of a new edge being formed increases with the fitness values of the countries involved in the potential trade. Our model permits reciprocal trades, where a country both imports and exports the same good with the same partner country. We allow for this as our analysis shows reciprocal trade within the continuous wheat trade network (Figure A.4), and Shutters and Muneepeerakul note the existence of reciprocal trades within agricultural trade networks [274]. However, self-loops, where a country attempts to trade with itself, are excluded.

Initial attempts to emulate the observed characteristics of the empirical network, as described in Comparison of Empirical and Model Networks, revealed that our model networks were not as disassortative as the empirical network. To address this, we introduced a step of rewiring the network after the addition of each new edge using the Maslov-Sneppen rewiring algorithm (MSRA), which has been shown to increase disassortativity. This algorithm ensures that node degree is not impacted by rewiring and edges are uniquely defined [194, 239]. Our rewiring led to a better fit of model to empirical network in terms of assortativity (Figure A.5) [239]. The number of attempts to rewire the network ($R(m)$) decays exponentially as the number of directed edges (m) in the network increases:

$$R(m) = Ce^{-\lambda m}. \tag{2.3}$$

This functional form was chosen as it results in a good fit to the increases in assortativity over time in the empirical network. Rewiring acts as a random assignment of trade partnerships for countries that are already engaging in trade. The good fit to the empirical network provided by an exponentially decaying number of rewiring attempts indicates that as the network grows, the PA mechanism becomes increasingly dominant over these random partnership assignments.

2.2.5 Comparison of model and empirical networks

We utilised a grid sweep to calibrate values of α, β, and ϵ from Equation 2.1 as well as C and λ from Equation 2.3. This generated approximately 5000 possible parameter sets (Subsection A.1.3). Previous analysis has calculated α and β for an HVH model of the WTN in individual years [116]. However, we wanted a single set that would replicate characteristics of the empirical trade network over multiple years. Thus, we carried out a parameter fitting instead of calculating values for specific years. The fitting sought

a parameter set which resulted in a good fit to the number of nodes, reciprocity, and assortativity coefficient of the empirical network for 1986-2011. The number of nodes and reciprocity were chosen as fitting metrics as the functional forms for trade probabilities taken from Garlaschelli *et al.* are related to the number of nodes and network reciprocity [117, 116]. The requirement on assortativity arises because an assortative network responds differently to shocks than a disassortative network [22, 197, 260].

To determine the best parameter sets, 25 networks were generated for each parameter set and network metrics were averaged over these networks. The mean squared error (MSE) from 1986-2011 between the model and empirical networks for assortativity, number of nodes and reciprocity was calculated for each parameter set. For each metric the MSE values were normalized, and then a combined normalized MSE over these metrics was generated. Parameter sets were ranked according to their combined normalized MSE, and the 100 "best" sets with the lowest MSE were used for all subsequent analysis.

We focused on a subset of network metrics to simplify analysis. To pick these metrics we examined a wide range of metrics for empirical agri-food commodity trade networks [107]. This analysis revealed strong correlations between many metrics, allowing us to reduce the number of measures needed to describe a network fully (Section A.2). Average path length, assortativity, and average clustering coefficient were thereby chosen as network metrics. The average path length is the average of the all the shortest paths between pairs of nodes; assortativity, by degree, is a measure of the extent to which nodes of a similar degree tend to connect to each other; the average clustering coefficient describes the degree to which a node's neighbours are themselves linked, averaged over the entire network. [18]

We also included the sizes of the giant strong component (GSC) and giant weak component (GWC) because of their relevance to network vulnerability analysis [244, 251, 170, 84, 157, 4, 317, 171, 232, 17, 320]. The GSC and GWC are defined as the largest strongly- and weakly- connected components within the network, respectively [170]. The size of a component – a collection of connected nodes – is given by the number of nodes it contains [244, 251, 84]. In a directed network, a strongly-connected component contains nodes that can all reach each other. A weakly-connected component contains all nodes in the strongly connected component, as well as any nodes that could reach all other nodes in the component if the network were undirected [170].

In addition to metrics of the vulnerability of networks to shocks we included 3 others that are thought to impact network resilience: density, symmetry, and heterogeneity (the latter 2 in terms of node in- and out-degree) [115]. Network density is the fraction of the maximum possible number of links that are present in the network [217]. Symmetry, in terms of node in- and out-degree, describes the extent to which nodes with a high in-degree

also tend to have high out-degree. Degree heterogeneity measures the heterogeneity in the in- and out-degree distributions of the network [115]. Network analysis often includes a consideration of whether the degree distribution of the network follows a power-law. The presence of a power-law distribution can can be determined using the Kolmogorov-Smirnov (KS) statistic. However, the KS statistic is not accurate for networks containing small numbers of nodes (approximately 100 or fewer nodes) [63]. Thus, the KS statistic was only used to determine the shape of the degree distribution in networks containing more than 100 nodes. For all other metrics, a network was generated for each of the 100 best parameter sets, and metrics were averaged across these 100 networks for comparison to the empirical network.

2.2.6 Shock simulation

To ascertain the resilience of the wheat trade network and its response to shocks we simulated shocks to the model networks and compared the effects of different types of shocks on model network structure. Throughout the shock analysis 1 network was generated for each of the 100 best parameter sets, and metrics were averaged across these 100 networks. Shocks to agri-food trade networks generally result in countries imposing export restrictions, while continuing to import [238, 109, 110, 205, 299, 76, 296, 83, 132, 125, 100]. Thus, we implemented shocks that result in nodes having their outgoing (export) edges removed [238, 109, 110].

Studies have considered 2 types of shocks to a network: errors and attacks [238, 4, 244, 183, 169]. In the case of an error we removed the outgoing edges of randomly selected nodes to test the network's error tolerance [4, 183, 169]. For an attack, nodes with the highest connectivity are targeted, as these are assumed to be the most important nodes in the network [4, 164]. We defined connectivity in terms of total degree centrality, meaning the nodes with the most trade partners were targeted for outward edge removal. The total degree metric was not recalculated between removals; we used a simultaneous attack that assumes all countries targeted would be impacted at roughly the same time, as this reduces computational time [157, 164]. In addition to single shocks, we experimented with introducing multiple shocks to the networks.

We also explored variations. Attacks with removals based on out-degree centrality (removal of the countries with the most export links) were simulated [169]. A sequential attack was considered, as it may not be realistic to assume that cessation of exports in multiple countries occurs simultaneously, and 1 country's change in trade status will impact the centrality of other countries in the network [164]. Details of how shocks were implemented appear in Subsection A.1.4.

We use empirical data to determine approximate ranges for the number of countries affected by a shock (1-15 countries) and the number of years in which a shock would impact a country's exports (1-5 years) (Subsection A.1.5). Hence we classified the types of shocks by severity–low (3 countries cease exports) or high (15 countries cease exports)–as well as by duration–short (1 year) or long (5 years). Additionally, in the case of multiple shocks, a gap of 2 years occurs between shocks [238, 294, 205, 299, 76, 296, 83, 132, 125, 100, 10].

Previous analysis has most often considered the effect of a shock on a static network where nodes are removed, and an evaluation of the shock impact immediately afterwards is carried out [4, 169, 183, 244, 188]. However, our focus was on the effect of shocks on the wheat trade network as it evolves in time, to ascertain the impact of shocks over a larger time frame. In some cases, the impact of shocks on trade networks has been measured by dynamically redistributing volumes of trade [110, 238, 178, 169]. As we have the simpler case of an unweighted network, no trade volume redistribution was considered. The effect of exogenous disturbances to our networks was ascertained by introducing shocks of different duration and severity during the process of network formation and evaluating their impact on network metrics.

Several metrics were used to determine network vulnerability and resilience, as well as the extent to which a shock has impacted a network. Average path length indicates the speed at which a shock will disseminate through a network, with a small average path length indicating quick spread, as most nodes in the network will tend to be near each other [89, 273]. The robustness to errors and vulnerability to attacks displayed by disassortative networks necessitates measurement of the assortativity coefficient [22, 197, 260]. The average clustering coefficient is a measure of cliquishness within networks, with clustering reducing network efficiency and resulting in increased vulnerability to attacks [197, 317, 320, 157]. The sizes of the GSC and GWC are respectively lower and upper bounds on the maximum size of a shock, given that the shock begins in the giant component [170].

When networks have a positive symmetry metric, high symmetry, heterogeneity, and density contribute to network resilience [115]. Networks with power-law degree distributions are "scale-free," and are robust where errors are concerned but are extremely fragile with regards to attacks [4, 317]. This is because their high degree heterogeneity means removing highly connected nodes results in rapid increases in network diameter and eventual network fragmentation [4].

2.3 Results

2.3.1 Comparison of empirical and model networks

Fitting a PA model to an empirical network evolving over several decades while using as few parameters as possible to avoid over-fitting the data is challenging. Nevertheless, the 100 best parameter sets provide a reasonable fit to the empirical network metrics (Figure A.5), as well as to the rest of the measured metrics (Figure 2.2), from 1986-2011 both qualitatively and quantitatively. For the majority of metrics the empirical data falls within 2 standard deviations of the mean of the model networks. The GSC size and symmetry for model networks, while not displaying a good fit quantitatively, nevertheless display similar trends to those for the empirical network (Figure 2.2d, f). From 1986-2011, the global wheat trade network experienced several shocks [205, 299, 76, 296, 83, 238, 132, 272, 125, 100, 10]. Thus, discrepancies between metrics in the empirical and model networks may be impacted by the fact that our network simulations did not include shocks during calibration. Due to the influence of the assortativity coefficient on network vulnerabilities we also fitted the model using only assortativity as a measure of goodness-of-fit in an attempt to more closely match the metric in the empirical network. While this led to a better quantitative fit to the assortativity coefficient the increasing trend was lost (Figure A.10) so we proceeded with the best parameter sets ranked by the normalized MSE. The addition of network rewiring steps that decay in number over time (Equation 2.3) suggests that PA with an additional random component drives network formation. The fact that a decaying number of rewiring attempts leads to a good fit regarding network assortativity (Figure 2.2b) indicates that as the size of the network increases, fitness plays a larger role in how edges are formed, as compared to random chance.

Calculation of the Kolmogorov-Smirnov statistic indicated that we should reject the hypothesis that the degree distributions for our empirical and model networks fit a power-law distribution (KS statistic calculated at the 5% significance level for each year in which number of nodes exceeded 100). As Konar *et al.* found that the degree distribution of the global VWTN was fit well by an exponential decay distribution with the decay coefficient given by the average degree of the network, we re-calculated the KS statistic to determine whether the same was true of our networks [174]. These calculations revealed that the exponential decay distribution provided a good fit to our network's degree distributions at 5% significance, measured yearly. As a result, we cannot draw conclusions about network vulnerability using the scale-free property. However, because exponential networks also have a highly skewed node degree distribution, other network metrics can be utilised to make many of the same judgments, as we will subsequently show.

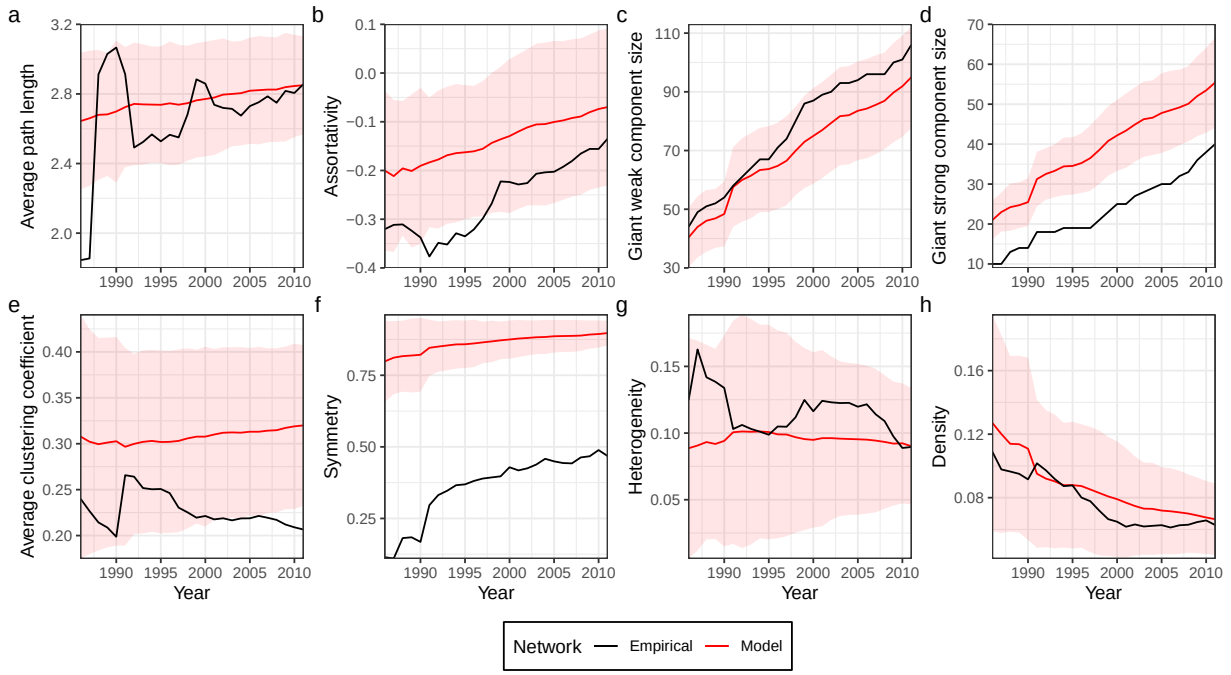

Figure 2.2: **Selected empirical and model network metrics, 1986-2011.** Red lines represent the mean metrics for model networks generated using the top 100 parameter sets ranked by least MSE normalized over assortativity, number of nodes, and reciprocity. The envelopes represents a range of ±2 standard deviations from the mean metrics for the model networks. Black lines represent the metrics of the empirical network.

To illustrate the similarities between the model and empirical network, we visualized a single-year snapshot of the empirical continuous wheat trade network (Figure 2.1a) and an exemplar model network (Figure 2.1b) for 2013. These networks show several similarities including complex structure and heterogeneous degree distributions (Figure 2.1c).

2.3.2 Shocks and model network growth

Notably, even shocks with low duration and severity, which result in 1-year export bans for $< 2\%$ of nodes, have substantial and long-lasting effects on model network metrics (Figure 2.3, Figure 2.4). These impacts are especially heightened when networks experience attacks (Figure 2.4). In the short term, networks affected by shocks will experience slower spread of subsequent shocks due to increased average path length (Figure 2.3a, Figure 2.4a). They will also have a broader range of maximum shock sizes (higher maximum and lower

minimum bounds due to changes in GWC and GSC size) (Figure 2.3c, d, Figure 2.4c, d). Additionally, these networks will be more heterogeneous, and less dense and symmetric, resulting in short-term changes in network resilience (Figure 2.3f-h, Figure 2.4f-h).

Increasing the severity or duration of a shock will increase its impact on network metrics. For errors, increasing the duration of a shock by 500% was more effective than increasing its severity by the same factor, with regards to changes in network metrics (Figure 2.3). For attacks, the opposite was generally true: a severe shock had more influence on network metrics than a longer duration shock (Figure 2.4). An exception to these trends is assortativity. While the error scenario leads to increases in assortativity for short duration shocks, long shocks result in an overall decrease this metric (Figure 2.3b). Under an attack scenario, low-severity shocks cause a decrease in assortativity, while high severity shocks result in an increase (Figure 2.4b). The long-term impacts of shocks on assortativity are much more durable for low-severity attacks than for high-severity attacks or errors of any severity and increased duration leads to a larger impact (Figure 2.3b, Figure 2.4b).

The long-lasting effects of shocks on network resilience are minimal under an error scenario: by 2050 network heterogeneity, symmetry and density are approximately the same for shocked and unshocked networks (Figure 2.3f-h). Similar trends in density and heterogeneity exist when a network is attacked (Figure 2.4g, h). However, the long-term resilience of the network under attacks will be lowered due to the considerable and long-lasting decreases in symmetry (Figure 2.4f). Shock type does not impact the upper bound on maximum shock size (by increasing the GWC size) in the long term, though attacks will result in a larger lower bound on shock size (larger GSC size) as shown in Figure 2.3c, d and Figure 2.4c, d.

Interpreting the meaning of changes in assortativity and average clustering coefficients (ACC) lead us to a contradiction. Networks that have experienced attacks, and are thus more disassortative than networks that have experienced an error or are unshocked, should be the most vulnerable to any subsequent attack. However, based on ACC, attacks will result in networks that are the least vulnerable to subsequent attacks due to their low clustering (Figure 2.3e, Figure 2.4e). It is unclear whether the lowered ACC or the increased disassortativity will have the dominant impact on vulnerability. This discrepancy is discussed further in Subsection 2.3.3.

As the network evolves it approaches a constant low level of assortativity and clustering, suggesting that the network is evolving to be less vulnerable to attacks (Figure 2.3b, e, Figure 2.4b, e). As a result, the network's resilience varies over time: symmetry increases and density and heterogeneity decrease, on the whole (Figure 2.3f-h, Figure 2.4f-h). Low levels of network heterogeneity and density may indicate that poor network resilience will

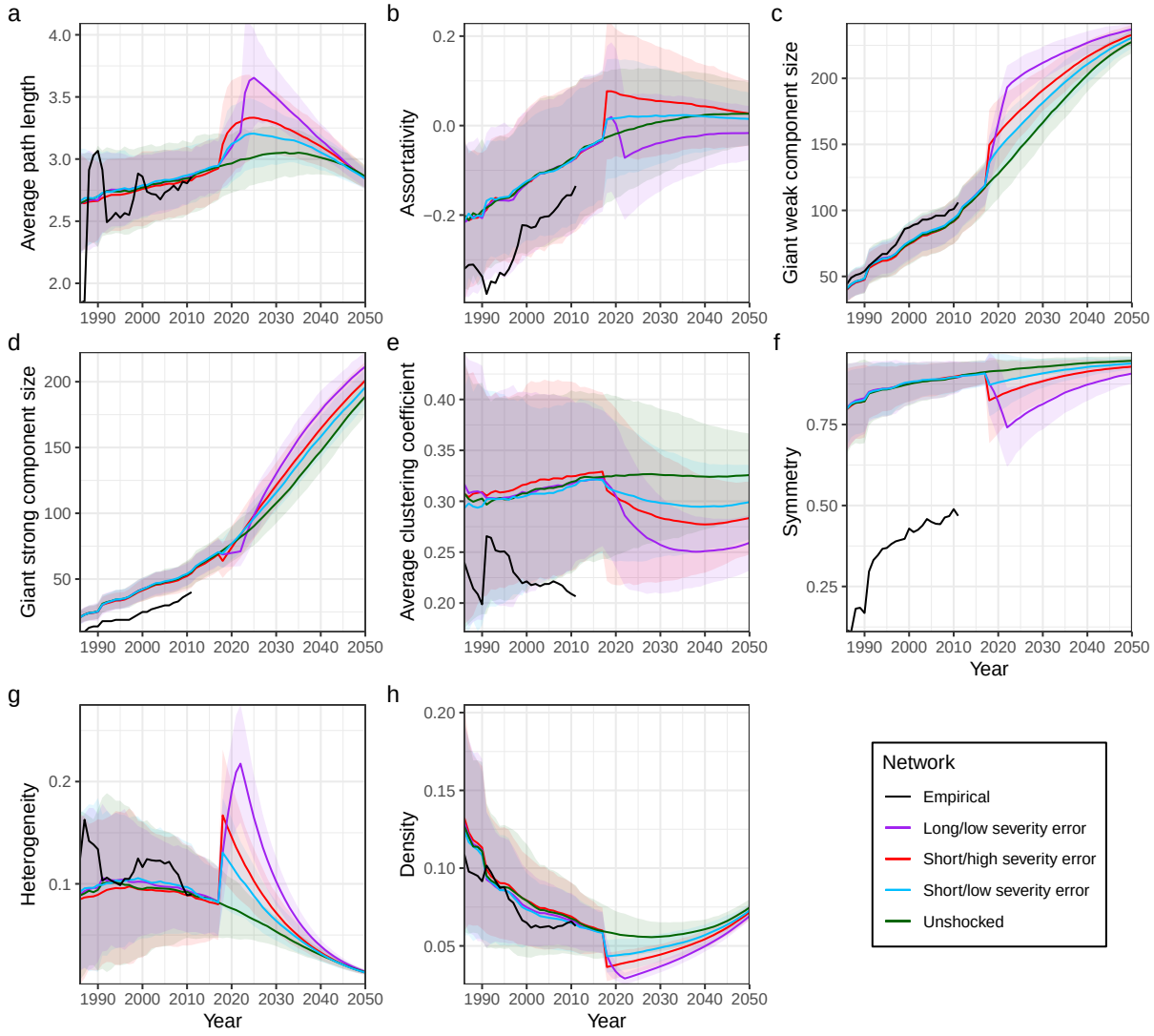

Figure 2.3: **Future errors have substantial impacts on model network metrics.** Shocks occurred in 2017-18. Coloured lines represent the mean metrics for model networks generated using the top 100 parameter sets ranked by least MSE normalized over assortativity, number of nodes, and reciprocity. The envelopes represent a range of ±2 standard deviations from the mean metrics for the model networks. Black lines represent the metrics of the empirical network using data from 1986 to 2011.

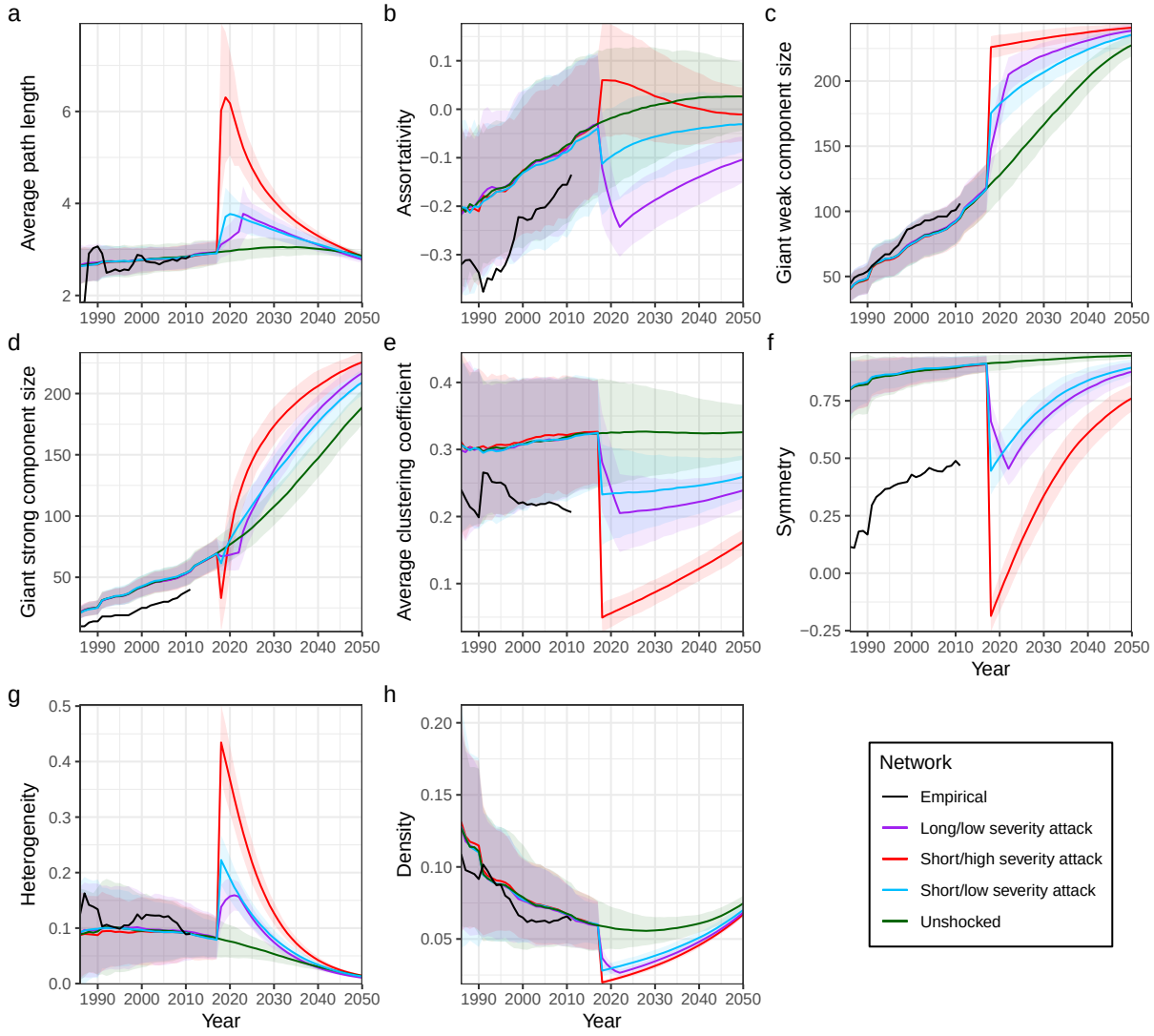

Figure 2.4: **Future attacks have substantial impacts on model network metrics.** Shocks occurred in $2017 - 18$. Coloured lines represent the mean metrics for model networks generated using the top 100 parameter sets ranked by least MSE normalized over assortativity, number of nodes, and reciprocity. The envelopes represent a range of ± 2 standard deviations from the mean metrics for the model networks. Targets with largest total degree are selected for attacks. Black lines represent the metrics of the empirical network using data from 1986 to 2011.

persist as we approach 2050 (Figure 2.3f-h, Figure 2.4f-h). For both errors and attacks, networks show some long-term resilience (Figure 2.3a, g, h, Figure 2.4a, g, h). Regardless of whether a shock has been introduced to the network, the majority of the 244 countries in the world are included in the GWC by the year 2050, though shocks increase the size of this component, as well as of the GSC (Figure 2.3c, d, Figure 2.4c, d). As the giant strong component grows to include all countries in the world, a larger number of countries will have the potential to be impacted by shocks. Additionally, all shock types produce long-lasting reductions in network clustering, creating a less cliquish trade network (Figure 2.3e, Figure 2.4e).

While the mean changes in network metrics are unique for each combination of shock type, duration, and severity, variability in the impact of a specific shock on the network means that a variety of different shocks can result in similar outcomes. This is especially clear for long-term predictions of the influence of errors: by 2050 there is a large overlap between the potential effects of all 3 error scenarios considered (Figure 2.3).

2.3.3 Consequences of repeated shocks

We simulated the effect of repeated shocks, considering multiple shocks of the same type and sets of shocks in which both errors and attacks occurred. All shocks had the same duration. With respect to most metrics, a previous attack reduces the short-term impact of subsequent attacks: each additional attack has a lesser impact on network metrics than the preceding attack (Figure 2.5). This observation helps to resolve the contradiction described in the previous section–our results indicate that in the short term, for a network that has experienced an attack, decreased vulnerability to attacks resulting from lowered ACC outweighs increased vulnerability to attacks due to increased disassortativity. An exception to this trend is the giant strong component size, which decreases by a larger amount with every subsequent attack (Figure 2.5d).

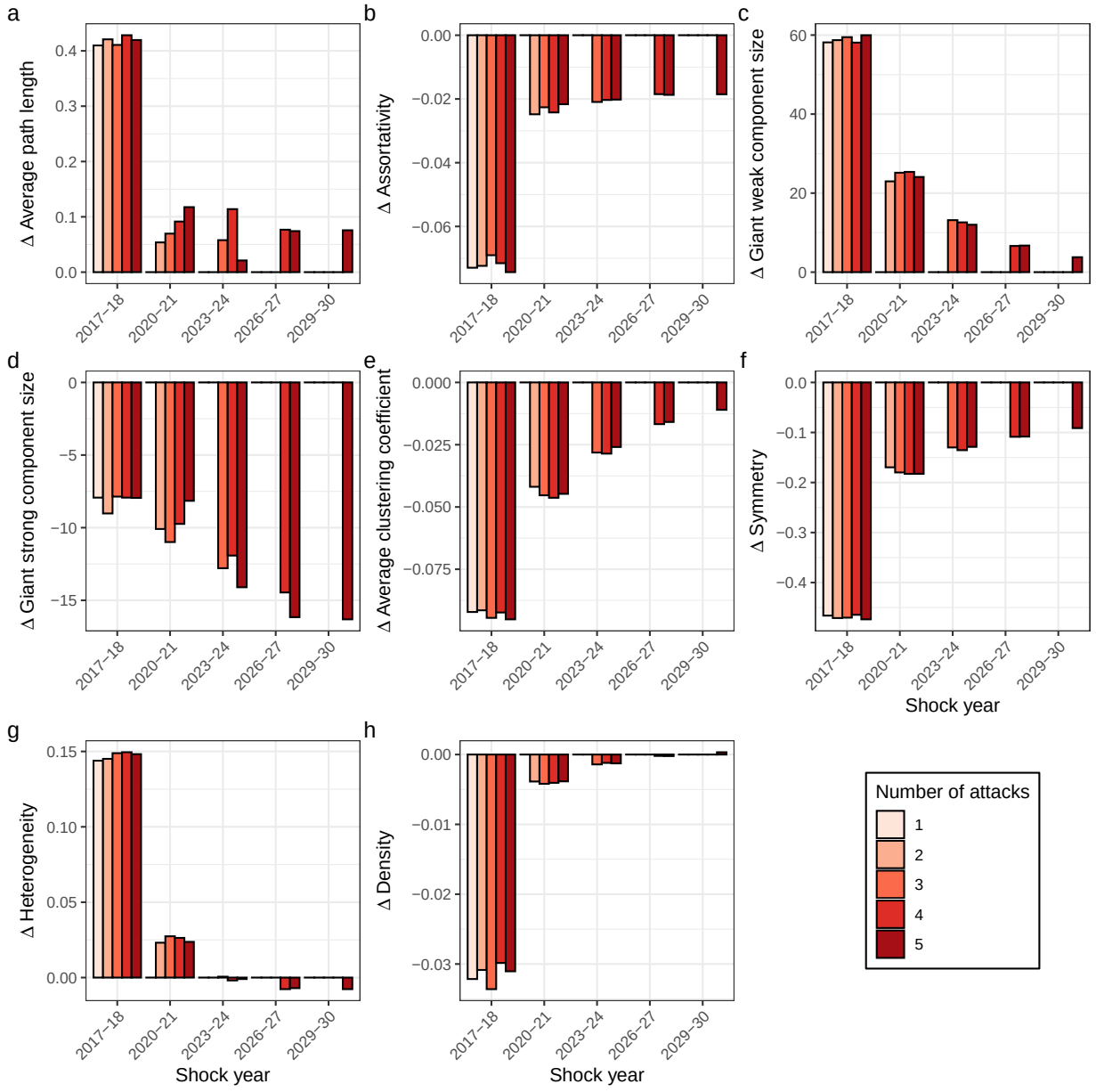

Figure 2.5: **Introducing multiple attacks has a lessening impact on model network metrics with each new iteration.** All attacks are low severity/short duration, with a gap of 2 years between every attack. Bars represent the mean change in metrics for model networks generated using the top 100 parameter sets ranked by least MSE normalized over assortativity, number of nodes, and reciprocity. Bars are only shown for years where an attack occurred; changes caused by the temporal evolution of the network in unshocked years are not included.

Sequences of shocks that include the largest number of attacks will have the most substantial long-term effects on the network, leading to lasting changes across a broad range of metrics. For most metrics the type and occurrence of the first shock, as well as the type of the second shock, influence long-term outcomes (Figure A.11, Figure A.12). Average path length, heterogeneity, and density metrics show remarkable resilience. Regardless of the number, type, magnitude, and duration of shocks, by 2050, a shocked network be similar to an unshocked network in regards to these metrics (Figure 2.3a, g, h, Figure 2.4a, g, h, Figure A.11, Figure A.12). As with the single shock scenarios, variation in the outcome of different types and combinations of shocks means that disparate shock scenarios may have comparable outcomes. For example, both double shocked networks that were initially attacked, regardless of the type of the second shock, show similar metrics as we approach 2050 (Figure A.12). Due to the short time between shocks (2 years), the natural growth process of the network does not significantly impact responses to shocks.

2.3.4 Comparison of attack strategies

For attacks on our model networks the use of a sequential versus simultaneous attack does not lead to noticeably different outcomes on any time-scale in the duration/severity scenarios (Figure A.13). We also considered whether attacks that targeted the countries with the largest number of export links, instead of those with the largest number of trade links, would result in more damage to the network. However, for all duration and severity levels, targeting countries based on total degree and out-degree are equally damaging (Figure 2.4, Figure A.12). This result suggests that countries highly ranked in terms of total degree will also be highly ranked by out-degree in our network, in general. This is true of the empirical network where there is a significant correlation between total degree and out-degree (Figure A.13).

2.4 Discussion

We developed a dynamic model for the time evolution of the global agri-food wheat trade network to explore the impact of shocks on its structure and its response to subsequent shocks. In order to fit the model, we also constructed an empirical global wheat trade network consisting of continuous trade partnerships and analysed its network metrics. It was found that a preferential attachment model with network rewiring was able to replicate the temporal evolution of crucial metrics in the empirical network in many respects, despite not requiring country-level data such a GDP. Based on analysing time evolution of historical

metrics in the empirical network and network model predictions of future trends, we predict that the network is evolving to be less vulnerable to attacks, though its resilience may remain low for the next few decades. We also experimented with applying shocks to the model network to determine the effect of factors such as extreme weather events or agro-terrorism on its dynamics. We found that even short-term shocks (1-year duration) have substantial and long-lasting effects on its structure, increasing the diversity of links as well as determining its response to subsequent shocks. While attacks have the largest impact on networks, for repeated attacks the damage from each subsequent shock will be smaller than from the last. Different network metrics are affected in different ways by attacks, but on the whole, attacks make the network less vulnerable to subsequent shocks.

Previous analyses of global trade networks have led to conflicting predictions regarding the food security risks associated with the globalisation of trade, and the potential for the disruption of trade. Global wheat and rice trade networks have been shown to be transitioning to a "robust yet fragile" state where they are vulnerable to attacks but robust against errors [238, 110]. Conversely, Sartori & Schiavo found that the world trade network's time evolution, while resulting in increased connectivity, has not led to higher levels of instability [263]. Our predictions regarding the future of the continuous wheat trade network show a transition towards a more stable network configuration where countries maintain trade links with a diverse group of partners. This pattern of growth suggests that the network is evolving to be less vulnerable to attacks, in agreement with Puma *et al.*, although attacks still have the potential to damage the network severely [238]. However, the network is vulnerable to errors, due to low levels of cliquishness and slight assortativity. Extreme climate events, such as floods, droughts, and heat stress, are predicted to increase in frequency, both globally and in regions of Europe where most of the world's wheat is produced, over the remainder of the 21st century [101, 298]. Thus, strategies for lessening the impact of shocks on the network will become increasingly crucial to global food security and are an important area for future research.

The time evolution of the continuous wheat trade network's resilience is less clear than the time evolution of vulnerability due to opposing trends in resilience-related metrics. Network density is predicted to decrease over the next decade but will begin to increase beyond this time period and contribute to higher levels of resilience. This increase in density will result from new links being added to the network much more frequently than new nodes. Despite high symmetry, low levels of network density and heterogeneity indicate that network resilience may be poor for a considerable portion of the next century. There is some debate as to whether the methods used to arrive at these metrics as universal measures of network resilience are as broadly applicable as has been asserted [300]. However, most of our conclusions do not depend on the interpretation of these metrics.

The network was predicted to respond differently to changes in duration and severity of shocks for attacks versus errors. This discrepancy may suggest that strategies for dealing with them should differ. For example, containing the spread of a shock should be a higher priority than facilitating recovery of impacted nodes when the network is affected by an attack, whereas in the case of an error, recovery should be the higher priority. However, the variability in the impact of a specific shock means that shocks of different type, severity, and duration may have similar impacts on network evolution. Attacks reduce network vulnerability to future shocks of the same type. While it would be preferable for the network to remain attack-free, any attack will create a positive externality by reducing the impact of a subsequent attack that occurs while the network is recovering. Longer gaps between shocks, allowing more time for network recovery, would reduce the overall impact of shocks. However, the frequency of shocks impacting agri-food trade networks is expected to increase during the 21st century, meaning that short gaps between shocks are a reasonable assumption [298, 101].

The choice of sequential or simultaneous attacks did not significantly impact the effectiveness of an attack. However, this result is likely dependent on our network and the severity of attacks. Sequential attacks and attacks based on other centrality measures should be explored in future, as previous work has shown that these variations on the attack strategy can be substantially more damaging than simultaneous attacks, and those based on total degree centrality, for both simulated and empirical networks [157, 164]. As well, model extensions could provide further insight into mechanisms of network growth. For example, established exporters of a specific commodity are more attractive to potential importers, suggesting that preferential attachment based on out-degree should be considered [23, 109].

While there appears to be a lack of analyses of the network effects of shocks on agri-food trade networks, analyses of shocks on financial networks are consistent with our simulations. Reductions in network density and symmetry following a shock are evident both in our model networks and in international financial networks following the 2008 financial crisis [57]. The global banking network also exhibited a reduction in density following the financial crisis, and showed significant changes in several network metrics up to 4 years after the crisis, suggesting protracted effects from shocks [204]. In addition to these global effects of shocks, the impact of export bans can have long-lasting effects for individual countries. For example, the 1997 outbreak of foot and mouth disease in Taiwan led to export bans and severely reduced the country's pork export [35]. As of 2013, the average yearly export volume since 1997 was 0.02% of the average volume in the 8 years preceding the outbreak [107]. Additionally, Japan (one of the largest importers of Taiwanese pork pre-outbreak) was forced to seek alternative trade partnerships as a result

of the shock. In 1996, Japan's largest source of pork was Taiwan, but by 2005 they had ceased importing from Taiwan and had increased the volume of their imports from the United States, Denmark, and Canada. Japan showed similar shifts in trade partnerships in response to the outbreak of Avian Influenza in Southeast Asia in 2003-2004 [35]. In addition to illustrating the long-term effects of shocks, these case studies provide support for our assumed mechanism of network restructuring following a shock.

As noted in the model description, the number of nodes in the network must grow over time and the network must be disassortative for a preferential attachment model to be appropriate for describing network evolution. Some of our model networks become slightly assortative as we approach 2050. This may suggest that PA will decrease in importance as a driver of network growth, and models used for more long-term predictions should consider different mechanisms of network growth. Our work has focused on the wheat trade network, meaning that the impact of a shock that originated in another commodity network and spread to the wheat network, or vice versa, cannot be evaluated. One extension of this work could be to consider a multi-network model where the impact of a such a shock could be quantified. Additionally, it is important to note that the continuous network we have modelled does not include countries that only infrequently engage in wheat trade. As a result, we are unable to quantify the impact of shocks on these countries. However, our predictions indicate that the number of nodes in our network is approaching the number of countries in the world, thus decreasing the number of countries excluded from our model.

Finally, we suggest that a useful continuation of this work would be extending the model to include edge weights using methods from previous research [21, 288, 7]. This would give us a more complete picture of wheat trade network dynamics as we move toward 2050. As well, it would allow for more realistic predictions of shock outcomes, and thus impacts on food security. Not all trade partnerships would have the same volume and thus shocks impacting higher volume partnerships would have a larger impact on global trade than those impacting low-volume trades [119].

This work demonstrates that the multi-year time evolution of specific commodity networks and the shocks that afflict them can be mechanistically modelled to provide insight into dynamics and response to future shocks under various possible scenarios. Future research should continue developing these models for the trade networks of other major agri-food commodities so their dynamics can be compared and contrasted to gain greater insights into the dynamics of empirical networks.

Chapter 3

Spatial structure in protected forest-grassland mosaics: exploring futures under climate change

This chapter is based on the paper: Kathyrn R Fair, Chris T Bauch, and Madhur Anand. Spatial structure in protected forest-grassland mosaics: exploring futures under climate change. *In review*, 2020.

Abstract

In mosaic ecosystems, multiple land types coexist as alternative stable states exhibiting distinct spatial patterns. These ecosystems occur worldwide but are under threat from anthropogenic disturbances. Designating protected areas is one approach to preserving natural mosaic ecosystems. However, climate change will also impact protected areas, yet there are few spatially explicit models of mosaic dynamics under climate change that can predict its effects. We construct a spatially explicit agent-based model for a natural forest-grassland mosaic, parametrized for the mosaics of Southern Brazil. This model is used to investigate how spatial structure of these systems change under different environmental conditions and disturbance regimes, including climate change. By including local spatial interactions and fire-mediated tree recruitment, our model reproduces many important spatial features of real-world protected mosaics, including the number of forest patches and overall forest cover. We observe that multiple changes in environmental conditions have significantly greater impact on tree cover and mosaic spatial structure than single changes. This sensitivity reflects the narrow range of conditions under which simulated mosaics persist and emphasizes the fragility of these ecosystems. Our simulations predict that climate change impacts on the fire-mediated forest recruitment threshold will lead to substantial increases in forest cover, with potential for complete mosaic loss under RCP 6.0 and 8.5 scenarios. Forest cover is predicted to continue increasing centuries after climate change impacts have stabilized, and scenarios where mosaics are able to persist display altered spatial structure at both the patch and landscape level. Our model is relatively simple and yet predicts several realistic aspects of spatial structure as well as plausible responses to likely regional climate shifts. Hence, further development of these models could help protect these unique ecosystems, such as by informing site selection for new conservation areas that will be favourable to forest-grassland mosaic under future climates.

3.1 Introduction

Understanding how population dynamics are impacted by climate is a key challenge for ecologists in a world undergoing anthropogenic climate change [50, 61, 235, 60, 11]. Empirical studies and models of tree-grass coexistence have revealed that environmental conditions, including fire and rainfall, are crucial to the bistability observed in forest-grassland mosaics and savannas [311, 280, 208, 1, 282, 253, 252, 278, 314]. Changes to these conditions influence how mosaics respond to disturbances and, along with feedback loops and ecological thresholds, cause the proportion of each land-state to vary temporally

[161, 136, 31, 34, 275, 286]. Several models of tree-grass coexistence indicate that increased rainfall and/or reduced fire frequency contribute to the encroachment of woody species over grassland [282, 49]. However, climate change impacts on these complex systems are expected to vary greatly between regions [49, 140, 206, 146]. As a result, it has been suggested that the development of region-specific models should be pursued [206]. Additionally, the importance of spatial context has been stressed; spatial aspects of disturbances (such as fire), competition for resources, and ecological thresholds influence the relative prevalence of different land states in these ecosystems, as well as ecosystem stability [308, 266, 264, 34, 335, 311, 253, 252, 314].

Forest-grassland mosaics, where natural forest and grassland land-states can persist as alternative stable states for ecosystems, occur around the world [224, 72, 80, 136, 161, 286, 29, 279, 39, 219, 31]. However, many natural forest-grassland mosaics are endangered, with the conversion of both forest and grassland into agricultural land leading to substantial reductions in natural land states [136, 224, 72]. Designating protected areas can help preserve mosaic ecosystems, but even well-protected areas of natural forest-grassland mosaic could be threatened by climate change. Mosaic ecosystems are expected to experience changes in temperature, precipitation, and the frequency of disturbances such as fire and hurricanes [279, 29, 192]. In South America, climatic predictions suggest that the forest-grassland mosaics of Southern Brazil may experience pressure due to higher forest expansion rates from increasing rainfall [34, 192]. Knowledge about how forest-grassland mosaics respond to climate change could help efforts such as site selection [220] for new protected areas that are predicted to be favourable under future climates.

These considerations motivate our objective: to construct and analyse a spatially-explicit model of forest-grassland mosaics, parametrized for Southern Brazil. We use this model to explore how environmental conditions and disturbance regimes, including those resulting from climate change, impact spatial structure. Through these experiments we can gain insights into the resilience of these complex systems, and assess their vulnerability to climate change impacts. Our agent-based model (ABM), where each patch of land is an 'agent', is based on previous non-spatial models for forest-grassland mosaics [161, 136, 310, 282]. We calibrate the model using empirical data, and compare model output to real-world mosaics using several landscape metrics. Following this, we explore how altering parameter value(s) impacts forest cover and spatial configuration. Through these simulation experiments we gain insights into how mosaic persistence and spatial structure are influenced by land-state transition dynamics. Finally, we consider scenarios where land state transitions are impacted by climate change through changes in precipitation. The effects of climate change are measured both through changes in forest cover, and in alterations to the spatial structure of the landscape via changing disturbance regimes.

3.2 Methods

3.2.1 Study system

Brazilian forest-grassland mosaics (23° to 30° S, 55° to 48° W) are selected as our study system due to their high conservation value, and the availability of empirical data for parameter fitting and model comparison. Southern Brazil's mosaics consist of Atlantic forest and *Campos* grassland – ecosystems with high species richness [31, 209, 227]. This species richness, combined with the fact that the Atlantic forest is home to the endangered Paraná Pine (*Araucaria angustifolia*) and other endemic species, makes Brazil's forest-grassland mosaics some of the most biodiverse on Earth [31, 275, 136]. However, both Atlantic forest and *Campos* are incurring losses as land is converted for human use [227, 31].

To evaluate our model's performance, we use satellite images of the Brazilian forest-grassland mosaics as a reference. As our model does not include the impact of direct anthropogenic activities (logging, etc.), we want to compare our model to an area that had not been strongly influenced by humans. Established in 1959, Aparados da Serra (AdS) National Park, one of the oldest in Brazil, is situated at a point where the Atlantic Forest and *Campos* grassland meet to create a mosaic [230]. While human-driven changes to the area cannot be discounted, especially prior to the creation of the park, their impacts are limited in comparison to unprotected areas.

Image files covering the forest-grassland mosaics located within AdS (29.07°-29.15° S, 50.10°-50.01° W) captured by the Sentinel-2A satellite are obtained through the Copernicus Open Access Hub [2]. We generate a normalized difference vegetation index (NDVI) image (10m spatial resolution) using the spectral bands 4 (Red) and 8 (Near-infrared/NIR) with the raster package for R (Version 3.5.1) to identify forested areas [144, 241, 211]. NDVI, calculated as $\text{NDVI} = \frac{\text{NIR}-\text{Red}}{\text{NIR}+\text{Red}}$ operates on the principle that areas with dense vegetation, such as forests, reflect a higher proportion of near-infrared radiation than visible light, and thus the pixels of an image containing forest will have high NDVI values [211].

The NDVI image is classified using a k-means clustering algorithm to identify cells with similar NDVI values using the R stats package [291]. The classified groups of cells were sorted into "forest" and "non-forest" categories by comparing the results of the clustering algorithm to a "true colour" image created by stacking bands 2 (Blue), 3 (Green) and 4 (Figure 3.1). These categories are used to generate a "forest mask" of the image; a binary representation indicating forest and non-forest areas. This mask image is split into 16 landscapes of 200×200 cells (4 km^2), arranged in a 4×4 grid and centred on the original image to minimize edge effects (Figure B.1).

Figure 3.1: **Forest-grassland mosaics in Southern Brazil's Aparados da Serra National Park.** True colour image of the mosaics in Aparados da Serra National Park (29.07°-29.15° S, 50.10°-50.01° W) generated using data from the Sentinel-2A satellite [2].

For each landscape, forest patches (connected components) are labelled, and several key landscape- and patch-level metrics describing the spatial distribution of forest were calculated (Table 3.1) using the SDMTools package for R [315, 241, 55, 198]. We repeat this process at 20m resolution generating 4 landscapes (Figure B.1). Considering multiple scales allows us to evaluate our model without explicitly defining a cell size for the simulated landscapes. We are unable to include 30m and 40m resolutions as both result in only 1 landscape, making any meaningful comparison difficult.

Table 3.1: **Spatial metrics for describing mosaics.** Metrics used to describe the spatial configuration of land states.

Metric	Description
Forest cover	Percent of cells in landscape classified as forest
Number of patches	Number of forest patches (connected components, queen's case) in landscape
Landscape Shape Index (LSI)	Measures aggregation of forest patches in landscape, describes complexity of landscape structure (higher LSI corresponds to a more complex landscape)
Effective Mesh Size (EMS)	Area of forest accessible from a randomly chosen forest cell in landscape, describes the probability that two randomly chosen forest cells are connected (higher EMS corresponds to lower landscape fragmentation)
Patch area	Area of forest patch (cell area = 1 unit^2)
Patch perimeter	Perimeter of forest patch, including internal holes (cell edge = 1 unit)
Shape index (SI)	Complexity of forest patch (higher SI corresponds to a more complex patch); perimeter/$\sqrt{\text{area}}$

3.2.2 Base model

Our ABM uses mechanisms similar to those employed in the ordinary differential equation (ODE) model developed by Innes *et al.* [161], with alterations to discretize the system and add spatial structure. The ABM describes a landscape divided into cells, which can be in a forest (F) or grassland (G) state at any given time-step. Rates of change for forest and grassland populations are converted to probabilities of transition between states for individual cells. Introducing spatial structure allows us to implement transitions influenced by local conditions. The model is parametrized by drawing realistic parameter ranges from

empirical data on tropical tree-grass systems, and selecting a set of base parameters to represent conditions in Southern Brazilian forest-grassland mosaics (Table 3.2).

A landscape, comprised of $N = 40000$ cells, is represented by a 2-D square lattice. The lattice has dimensions of 200×200 cells and is mapped onto a torus. The dynamics of a cell are influenced by the land-state of adjacent cells (Moore neighbourhood, radius 1). These spatially constrained local interactions drive the dynamics of the system at the landscape level, leading to the emergence of some overall organization.

Transition probabilities for the ij^{th} cell are given by

$$P_{ij}^{F \to G} = \nu(1 - {F^L}_{ij}) + \varepsilon_\nu \tag{3.1}$$

and

$$P_{ij}^{G \to F} = \alpha {F^L}_{ij} H({F^L}_{ij} - T_{ij}) + \varepsilon_\alpha, \tag{3.2}$$

where

$${F^L}_{ij} = \frac{1}{9} \sum_{n \in R} (\text{state}_n = F) \tag{3.3}$$

is the local proportion of forest, i.e. the proporotion of forest in the Moore neighbourhood, R, of the ij^{th} cell, including the ij^{th} cell itself such that $R = \{(i-1, j-1), (i-1, j), \ldots, (i+1, j), (i+1, j+1)\}$. As cells have only 2 possible states, $1 - {F^L}_{ij} = {G^L}_{ij}$. Density-dependent forest recruitment and mortality rates have coefficients α and ν respectively. We also include some small probability that land-state transitions occur randomly, both for recruitment (ε_α) and mortality (ε_ν). For simplicity we set $\varepsilon_\nu = \varepsilon_\alpha = \varepsilon$ where $\varepsilon > 0$. However, $\varepsilon \ll 1$, and thus land state changes are largely driven by density-dependent dynamics.

Density-dependent forest recruitment and mortality transitions are utilized because forest mortality will increase with grassland cover, and recruitment with tree cover [282, 310, 243]. In forest-grassland mosaics, fire decreases the forest recruitment rate by killing or limiting the growth of saplings and contributes to mortality for both saplings and mature trees. Fire frequency decreases dramatically for sufficiently high cover, as dense tree stands are better able to resist the onset of fire than trees that sparsely populate grassland areas [29, 279, 266, 148]. This combination of factors means that below some threshold forest cover level recruitment is suppressed by fire and increases greatly once the threshold is met or exceeded [161, 13, 266].

We use a step function, $H(x)$, to describe this threshold mechanism, where

$$H({F^L}_{ij} - T_{ij}) = \begin{cases} 1, & {F^L}_{ij} - T_{ij} \geq 0 \\ 0, & {F^L}_{ij} - T_{ij} < 0 \end{cases} \tag{3.4}$$

with T_{ij} representing a fire-mediated ecological threshold to forest recruitment in the ij^{th} cell [266, 161, 136].

To illustrate how spatially heterogeneous factors may impact the recruitment threshold, we allow T_{ij} to vary; each $T_{ij} = T^L - S/9 + (1/9) * \text{Round}(\text{rand}(0,1) * 2S)$ where $T^L = 4/9$ and $S = 3$. The value of S is tuned, and is meant to capture the broad range of forest cover over which fire can occur [311, 280]. Thus, $T_{ij} \in \left\{\frac{1}{9}, \ldots, \frac{7}{9}\right\}$, the distribution of T_{ij} values is symmetric around $T^L = \frac{4}{9}$, and $\lim_{N\to\infty} \overline{T}_{ij} = \lim_{N\to\infty}(\sum_{i=1}^{\sqrt{N}} \sum_{j=1}^{\sqrt{N}} T_{ij})/N = T$, where T is a landscape-level mean threshold value. For simplicity, we restrict ourselves to a finite set of possible T_{ij} values as $F_{ij} \in \left\{\frac{0}{9}, \frac{1}{9}, \ldots, \frac{8}{9}, \frac{9}{9}\right\}$. While we experimented with other distributions, and different levels of variability, they were unable to consistently produce mosaic outcomes using the baseline parametrization or resulted in forest patches with high regularity (i.e. approximately circular patches), which do not resemble those in real-world mosaics.

This heterogeneity in threshold values can be interpreted as the result of several factors that we do not explicitly model. First, while we do not define the size of a cell in our simulation, we assume they have roughly the same dimensions as the cells in our satellite data (10m, 20m resolution, see Subsection 3.2.1 for further detail). However, the threshold value of 40% often cited is based on analysis over large areas and we cannot discount the possibility of heterogeneity within smaller spatial units [13, 335, 311]. Thus, we allow localized heterogeneity in threshold values, but require that $\overline{T}_{ij} \approx T^L \approx 40\%$, as the landscape will be closer in size to the areas surveyed in empirical studies. Heterogeneity may result from differences in the density of tree stands, not captured by our binary land-state classification, that impact the ability of trees in a neighbourhood to resist fire [223]. Spatial variation in fire intensity and frequency may alter the threshold locally [266, 139, 149]. Additionally, tree cover is influenced by spatially heterogeneous factors, such as soil texture and wild herbivory, that can impact fire regimes [328, 262, 237, 281, 12]. Finally, we note that, in South America, fires still occur regularly in locations with high tree cover, meaning fire can dampen recruitment even in largely forested areas [280, 311].

3.2.3 Base model analysis

The model is implemented in C++. Throughout simulations we track the total proportion of forest in the landscape at time t, given by $F(t) = \sum_{i=1}^{\sqrt{N}} \sum_{j=1}^{\sqrt{N}} (\text{state}_{ij}(t) = F)/N$. Simulation runs are initialized by creating a landscape of either all forest (if desired $F(0) \geq 0.5$) or all grassland cells (if desired $F(0) =< 0.5$), then seeding it with small patches. Seeding is done by randomly changing the land-state of 2×2 cell blocks, alternating between changing grassland to forest, and vice versa. The process is repeated until the proportions of forest cells in the landscape match the desired $F(0)$ value, where $F(0) \in \{0.05, 0.15, \ldots, 0.85, 0.95\}$. A more systematic seeding of the landscapes – to match current clustering in real-world mosaics – may reduce the run-time of the simulations. However, we use this random initialization as we do not want the model's ability to produce mosaic-like spatial patterns to depend on a pre-determined layout.

Table 3.2: **Parameters for mosaic model.** Parameter ranges are generated from empirical data, with base values chosen to represent conditions in Southern Brazil's forest-grassland mosaics. Threshold-related parameters are unitless, land-state transition rates are annual, but contribute to unitless probabilities within each timestep (year).

Parameter	Description	Range	Base value	Sources
T^L	Base cell-level threshold to forest recruitment	$[0.24, 0.45]$	4/9	[13, 311, 280, 335, 279]
S	Controls range of cell-level recruitment thresholds	tuned	3	[311, 280]
α	Forest recruitment rate	$[0.1, 0.5]$	0.3	[310, 136, 215]
ν	Forest mortality rate	$[0.01, 0.26]$	0.05	[91, 310, 215, 30, 147, 141, 162, 136]
ε	Random land-state transition rate	$[0, 0.0001]$	0.000025	[161], tuning

Once initialized, the model is run for $500,000$ time-steps (representing years) to allow the simulated landscapes to develop spatial structure and settle to a relatively stable level of forest cover. All simulations where, within the final $100,000$ time-steps, $\max(F) - \min(F) > 0.05$ are discarded as they have not stabilized. The remaining simulations are classified as being in a certain state based on the proportion of forest cells in the landscape; grassland (G) if $F(500,000) < 0.05$, mosaic (M) if $0.05 \leq F(500,000) < 0.6$, and forest ($F$) if $F(500,000) \geq 0.6$ [145]. These final time-step states are not necessarily equilibrium states for the system. They may also be long-term transients, a common occurrence in ecological models that incorporate spatial structure and/or stochasticity [131, 129, 130].

However, as many real-world ecological systems take long periods of time to reach a steady state, their dynamics along the trajectory towards this equilibrium remain an important area of study.

As with the real-world mosaics, we calculate spatial metrics for each simulated landscape (Table 3.1). We note that while the model employs periodic boundary conditions, the patch labelling process does not consider that a patch on the edge of the landscape may be part of a larger continuous area that continues on the opposite boundary. After comparing our base model to real-world mosaics, we explore the parameter space to determine how parameters interact to produce the simulated landscapes. We consider how varying one or more parameter value from the base set changes both the model outcomes – what landscape states are possible (F, G, M, or some combination thereof) – and the spatial structure of the landscape. As in the base model, we discard any simulations that do not stabilize.

3.2.4 Climate projections

In order to model the impact of climate change on Brazil's forest-grassland mosaics, we need climate projections that are both specific to the geographic region and cover a length of time at least on par with the time-scales over which mosaics experience change. Our variables of interest are mean annual temperature (MAT) and mean annual precipitation (MAP). Though seasonality and extremes in temperature and precipitation undoubtedly influence mosaics, we focus on yearly averages as a starting point for modelling climate impacts. Projections generated from global climate models (GCMs) give the best available estimates of future climate change impacts. GCM simulations can be used to explore different climate change scenarios, known as Representative Concentration Pathways (RCPs), named for the levels of radiative forcing they forecast for the year 2100 (2.6, 4.5, 6.0, and 8.5 W/m^2 respectively) [313].

While mosaics may exhibit climate change-driven changes within the next half-century, we seek to explore trends over a larger time frame. To generate long-term trends for MAT and MAP specific to our region of interest we begin with data on global CO_2 concentrations for 1765-2500, combining historical measurements (1765-2004) with projections for the RCPs (2005-2500), compiled by Meinshausen *et al.* (Figure B.2) [201, 312, 62, 112, 248]. Previous models have assumed that the change in MAT relative to pre-industrial temperatures (ΔT_c) varies with CO_2 according to the equation

$$\Delta T_c = \frac{S}{\ln(2)} \ln\left(\frac{CO_2}{CO_{2(t=1765)}}\right) \tag{3.5}$$

where S is the equilibrium climate sensitivity (change in equilibrium global average temperature for a doubling of atmospheric CO_2 concentration from pre-industrial levels) and $CO_{2(t=1765)} = 278.05158$ ppm is the pre-industrial concentration [172, 44, 173, 201, 200, 265]. The IPCC 5th Assessment Report estimated that $S \in (1.5, 4.5)$°C [285] while the IPCC 4th Assessment Report stated a likely value of 3 °C for S with $S \in [2, 4.5]$°C [56].

For changes in MAP relative to pre-industrial levels (ΔP) we use

$$\Delta P = 365 \left(A \ln \left(\frac{CO_2}{CO_{2(t=1765)}} \right) + B\Delta T_c + C \ln \left(\frac{CO_2}{CO_{2(t=1765)}} \right) \Delta T_c \right) \tag{3.6}$$

where $CO_{2(t=1765)}$ and ΔT_c are as described previously, and ΔP is given in mm/year [124]. Coefficients A, B and C approximate partial derivatives

$$\begin{aligned} A &\approx \frac{\partial P}{\partial(\ln(CO_2))} \text{ at } T_c = 0 \text{ (control temperature)} \\ B &\approx \frac{\partial P}{\partial T_c} \text{ at } CO_{2(t=1765)} \\ C &\approx \frac{\partial^2 P}{\partial T_c \partial(\ln(CO_2))} \end{aligned} \tag{3.7}$$

but include effects from other sources [124]. Units for A are mm, for B and C are mm/°C.

Historical data for Brazil's forest-grassland mosaics yields "current" (year=1990) climate data (MAT ≈ 18.17°C, MAP ≈ 1620 mm, taken as averages of the 1960-1990 mean values within the region) [143, 142]. Additionally, we obtain GCM climate projections specific to Southern Brazil's forest-grassland mosaics for the years 2050 (2041-2060 average) and 2070 (2061-2080 average) [143, 142]. MAT and MAP values for each RCP at 2050 and 2070 are taken as the mean of the projections from the set of GCMs for which a complete data set is available (containing RCP 2.6, 4.5, 6.0, and 8.5 projections for 2050 and 2070) in the WorldClim database. These models are CCSM4, GISS-E2-R, HadGEM2-AO, HadGEM2-ES, IPSL-CM5A-LR, MIROC-ESM-CHEM, MIROC-ESM, MIROC5, MRI-CGCM3, and NorESM1-M [142, 143].

To determine an S value for Equation 3.5 we minimize the sum of the squared errors (SSE) between the GCM-predicted temperature changes and the corresponding change predicted using Equation 3.5. Errors are in predicted changes from 1990 to 2050 and from 1990 to 2070, across all RCPs. We obtain $S \approx 3.36$, falling within the range proposed by the IPCC [285]. Using this S-value, we project changes in temperature to obtain MAT projections for the mosaics (Figure B.2).

Our projections for ΔT_c and the CO_2 projections from Hijmans *et al.* are inserted into Equation 3.6 at 2050 and 2070 for all RCPs, and we minimize the SSE for projected precipitation changes between the GCMs and Equation 3.6 to obtain $A \approx -0.24$, $B \approx 0.226$, $C \approx -0.000745$ [143]. When minimizing, we require $|A|, |B|, |C| \in [0, 1]$ and $A, C < 0$, $B > 0$ so that our coefficients have the same sign and similar magnitude to those stated for global precipitation change by Good *et al.* [124]. Our coefficient values differ from those for global precipitation change as we are considering changes at a much finer scale. Using these fitted parameters, we generate precipitation projections (Figure B.2). While there is some deviation from the GCM-based projections for MAT and MAP, particularly for RCP 2.6, Equation 3.5 and Equation 3.6 perform reasonably well, given their simplicity.

3.2.5 Climate change mechanisms

To model how climate change impacts manifest in forest-grassland mosaics, we need to link system dynamics to climate variables. Climatic variation, distinct from that caused by anthropogenic climate, influences system dynamics over large timescales. However, the rapid and substantial increases in atmospheric CO_2 since the beginning of the Industrial Revolution depart from the trend shown over the past $800,000$ years, with current concentrations of around 400 ppm the highest in 3 million years [334, 32]. This recent rapid acceleration in emissions has resulted in changes impacting system dynamics on a much shorter timescale than those resulting from natural climatic shifts. Simulations are run for $500,000$ time-steps with our base parameter set, as in the original model. Following this, they are run for an additional 511 time-steps, representing the years 1990-2500. While climate change was undoubtedly impacting these ecosystems prior to 1990, detailed data on climatic variables and fire regimes has only recently become available.

Forest recruitment as a function of precipitation can be modelled as

$$\alpha(P) = \alpha_{max} \frac{P}{h_P + P} \tag{3.8}$$

where P represents MAP, α_{max} is the maximum recruitment rate, and h_P is the MAP at which recruitment is reduced to 50% of α_{max} [310]. Given that our base and maximum recruitment rates are 0.3 and 0.5 respectively (Table 3.2), and precipitation in 1990 was 1619.897 mm/yr, we assume $\alpha(1619.897) = \alpha(P(5000001)) = 0.3$, $\alpha_{max} = 0.5$, and find $h_P = \frac{2}{3}(1619.897) \approx 1080$ mm/yr. Using Equation 3.8 and our precipitation values from Equation 3.6 we model how recruitment changes with precipitation and create projections from 1990-2500 for each RCP (Figure B.3).

As the threshold to recruitment is fire-mediated, and the probability of fire varies with MAP, we assume that threshold values (T_{ij}) are impacted by changes in precipitation [311]. Recent empirical work suggests that fire frequency is highest at intermediate MAP values, with van Nes *et al.* showing that the probability of fire as a function of MAP can be modelled with a logistic optimum function [233, 309, 311]. We assume that the fire-mediated threshold will vary with MAP according to a similar relationship, such that

$$T_{ij}(P) = \frac{T_{ij}^{B}}{\delta}\left(\frac{\kappa}{1+e^{-\left(p_1\left(\frac{P-P_0}{P_0}\right)^2+p_2\left(\frac{P-P_0}{P_0}\right)+p_3\right)}}\right) \tag{3.9}$$

where T_{ij}^{B} is the threshold defined for the base model, κ modifies the maximum value ($\kappa/2$) of the logistic optimum function, P_0 is the location of the peak in fire frequency, and δ is the probability of fire in the year 1990, ensuring that $T_{ij}(1619.897) = T_{ij}^{B}$. Logistic optimum parameters ($p_1 = -7.57,\ p_2 = 0.00649,\ p_3 = -2.48 \times 10^{-6}$) are taken from van Nes *et al.*, who fit a logistic optimum function to empirical data for South America [311]. We obtain $P_0 = 1354$ mm/yr and $\kappa = 0.06704$ using a non-linear least-squares estimate of the fit of a logistic optimum function to the data presented in [311] for fire probability as a function of MAP for South America, and thus find $\delta \approx 0.02868$. The mean (landscape-level) threshold as a function of precipitation, and as projected over time are shown in Figure B.3.

3.3 Results

3.3.1 Base model

In this subsection, we report temporal trends in model behaviour, and demonstrate the model's ability to consistently produce mosaic landscapes. For our base parameter set (Table 3.2), all simulations begin with a short period of substantial landscape restructuring as cell-level interactions lead the initial random layout of the landscape to shift to one with distinct clustering. This results in large changes in forest cover (e.g. Figure 3.2a ($t = 0$) and b ($t = 50$)). Following this restructuring period, short timescale small amplitude fluctuations (Figure 3.2f) in forest cover occur, as boundaries between forest and grassland shift (e.g. Figure 3.2c ($t = 5000$) and d ($t = 500000$)). These fluctuations are overlaid on long-term trends in forest cover change (Figure 3.2e). The direction and final outcome of these long-term trends depends on initial forest cover (Figure B.4). For our base parameter set, approximately 95% of simulations stabilize and are included in our analysis.

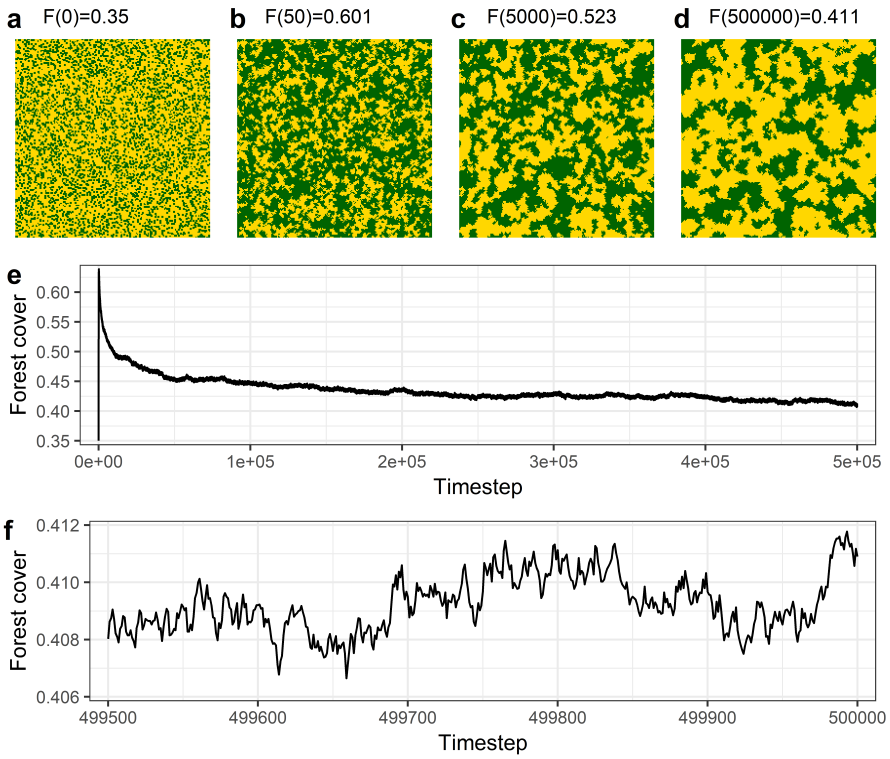

Figure 3.2: **Distinct spatial structure emerges from local cell-level interactions in simulated landscapes.** (a)-(d) visualize a landscape at various time-steps to show forest patch formation, (e),(f) show associated time-series for forest cover on the landscape. Simulation uses base parameter set, with $F(0) = 0.35$.

3.3.2 Comparison to real-world mosaics

In this subsection we contrast modelled and real-world mosaics, highlighting our model's ability to produce realistic landscapes (see Table 3.1 for spatial metric definitions). The base model returns a mean forest cover close to those for landscapes from Aparados da Serra National Park (Figure 3.3a). We observe $F + M$ states, with the 10m resolution landscapes covering a broader range of forest covers than the base model, while 20m landscapes display a narrower range. The base model has a similar mean for number of forest patches as the 20m data (Figure 3.3b), and all ranges for the base model have large regions of overlap with those from AdS. However, mean landscape shape index in the model was markedly higher than in AdS (Figure 3.3c), accompanied by lower effective mesh size (Figure 3.3d).

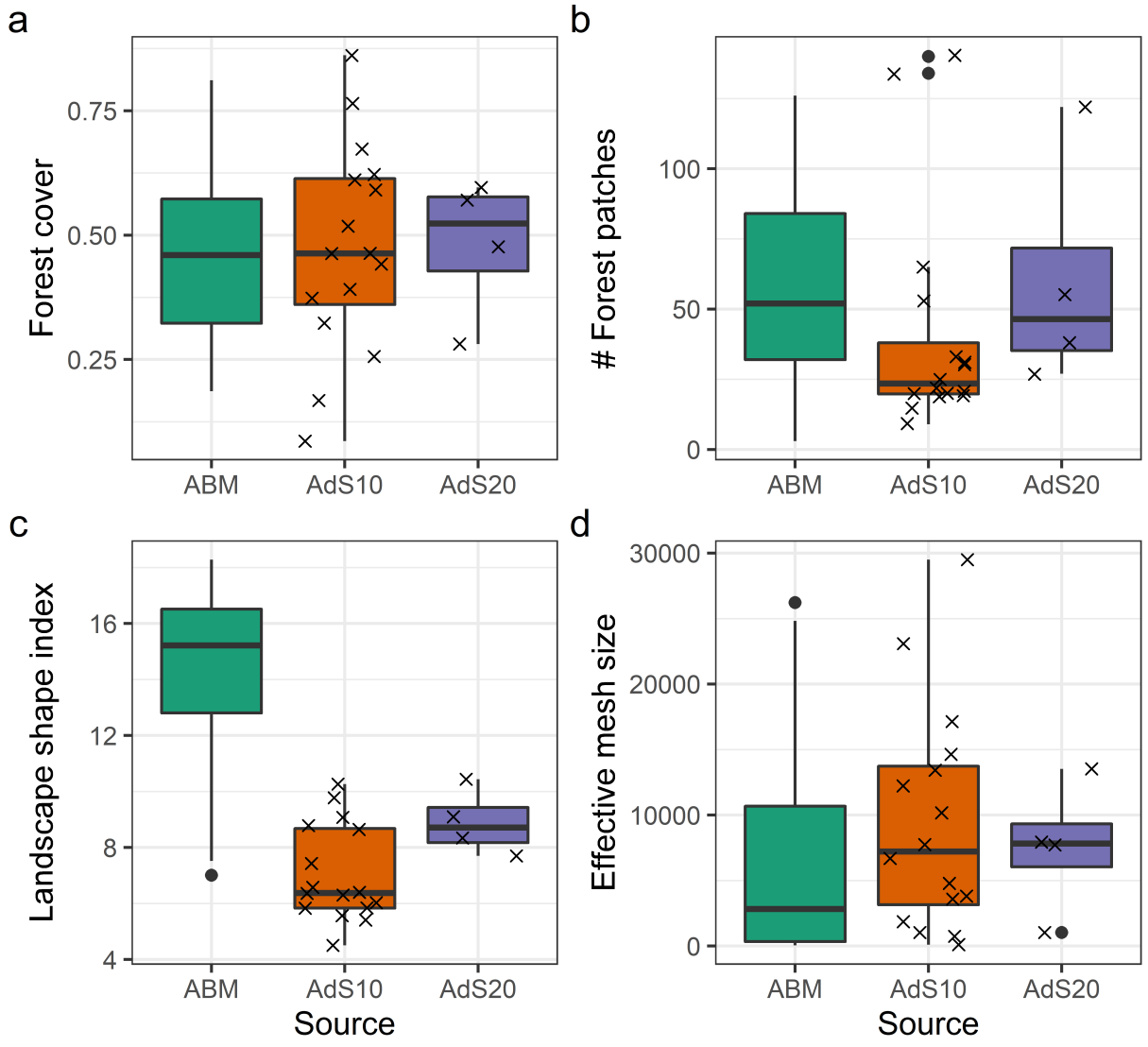

Figure 3.3: **Simulated and real-world mosaics display similar landscape-level spatial characteristics.** 10m and 20m resolution landscapes from Aparados da Serra national park compared to simulated landscapes for (a) forest cover (b) number of forest patches (c) effective mesh size (d) landscape shape index. Solid dots indicate outliers, while ×'s indicate observations for each landscape in the satellite image. 250 simulations are run for each $F(0)$, discarding any that do not stabilize.

To compare the model to AdS on a finer scale, we also consider the distribution of patch-level characteristics within a landscape. Distributions for these metrics are similar for AdS across spatial resolutions; the majority of patches have low area and perimeter values, leading to low shape index values (Figure B.5). Small, simple patches are also common in the base model, though they do not occur as frequently as in AdS, especially at 10m resolution. Mean count distributions decay at a similar rate, however modelled landscapes may contain larger numbers of patches with area and perimeter values roughly in the 10-100 unit range than we observe in the AdS data. Overall, the model captures the diverse range of possible configurations for real-world mosaic landscapes.

3.3.3 Exploring parameter space

In this subsection we illustrate the narrow range of parameter values under which mosaics can persist, indicating that these ecosystems may be vulnerable to external shocks. We additionally demonstrate that while changes to individual parameter values (representing the mosaic's response to environmental conditions) may impact mosaic structure, the results are magnified when multiple parameters are changed.

A broad range of forest cover levels and spatial characteristics (Figure 3.4, Figure 3.5, Figure B.6-Figure B.16), can be obtained by varying parameters. Patch area and landscape effective mesh size change with forest cover in a consistent way regardless of any parameter variation. At low forest cover, patch areas are small and effective mesh size is low, while at high forest cover the effective mesh size is high and a small number of large patches dominate the landscape, with all others having very small areas (Figure B.6, Figure B.8, Figure B.10, Figure B.12-Figure B.14). This consistency does not hold for other spatial metrics; simulations run with different parameter sets may result in landscapes with the same forest cover level but with distinct spatial configurations, depending on the parameter(s) varied (Figure 3.4, Figure 3.5, Figure B.6-Figure B.16).

When the recruitment rate exceeds 0.19 mosaics landscapes, where $F(500000) \in [0.05, 0.6)$, occur (Figure 3.4a). The relationship between $F(0)$ and the final level of forest cover holds regardless of recruitment, with higher initial cover corresponding to higher final cover. When forest cover exceeds 50%, α-values above base result in a higher maximum patch perimeter (Figure 3.4b), with larger increases corresponding to higher α-values. This results in higher shape index (SI) values for these patches, and thus higher landscape shape index (LSI) values (Figure B.6). Recruitment slightly below base may result in fewer forest patches for landscapes with approximately $20 - 30\%$ forest cover (Figure 3.4c), leading to lower LSI values (Figure B.6).

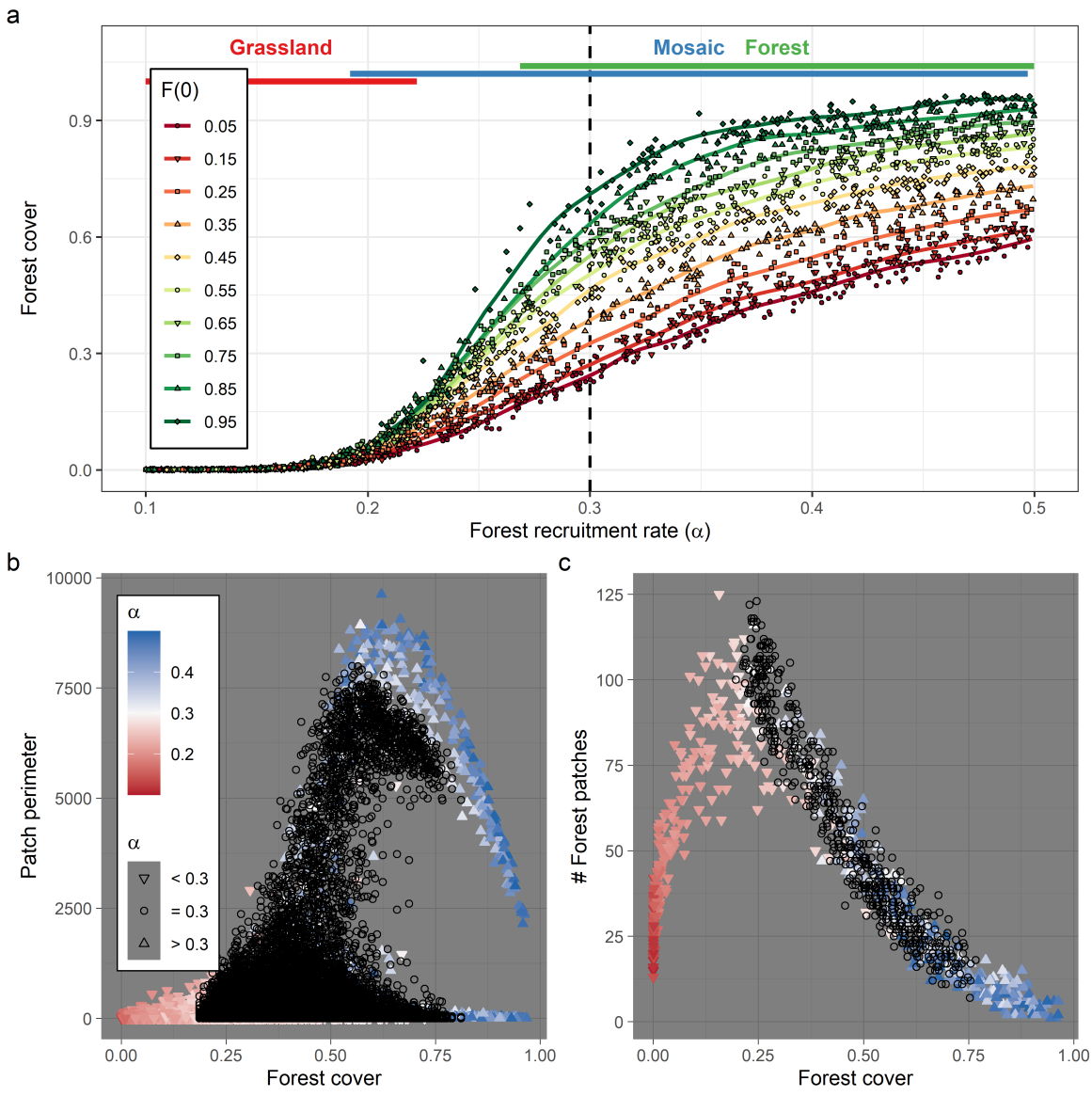

Figure 3.4: **Forest recruitment impacts landscape forest cover and spatial structure.** (a) Effect of recruitment on forest cover. Points indicate individual simulations, lines show a LOESS (locally estimated scatter plot smoothing) curve for each $F(0)$. Vertical dashed line marks base recruitment rate, horizontal bars indicate ranges of α for which different landscape outcomes are possible. (b) and (c) display the effect of recruitment on perimeter and number of forest patches. Here colour corresponds to α-value for each α-vary run (black for base), shape indicates the value in relation to base α. 250 simulations run for each $F(0)$, discarding any that do not stabilize, with 25% of points shown in (b) and (c) to avoid over plotting

Mosaic outcomes are only possible when the tree mortality rate is near its base value, $\nu \in (0.034, 0.074)$ (Figure B.7). Within the range of ν-values that admit mosaic outcomes, higher tree mortality reduces the range of possible forest cover levels. For forest cover in $20 - 30\%$ mortality slight above base can result in fewer forest patches (Figure B.7) and a lower LSI (Figure B.8). As well, for landscapes with approximately 55% or more forest, mortality below base leads to higher perimeter (Figure B.7) and SI (Figure B.8) values for large patches, with larger deviation from base mortality corresponding to larger changes in these metrics, and thus in LSI (Figure B.8).

In order to generate mosaic outcomes, the random land-state transition rate must be less than 0.00017 (Figure B.9) For moderate to high ε we get all F states, and if $\varepsilon = 0$ we get $F + G + M$ (Figure B.9), a combination not possible when varying either recruitment or mortality rates (Figure 3.4a, Figure B.7). Exceeding base ε boosts the number of forest patches in landscapes with at least 40% forest cover, and for those with at least 60% additionally results in higher maximum patch perimeter (Figure B.9), increasing their SI (Figure B.10). These changes result in higher LSI for landscapes with approximately 50% or more forest cover (Figure B.10).

When varying both tree recruitment and mortality (Figure 3.5a, Figure B.11), mosaics occur in the region enclosed by the lines $\nu = 0.1\alpha + 0.0013$ and $\nu = 0.24\alpha + 0.0039$. The band of $\alpha - \nu$ combinations that admit mosaic outcomes widens with increased mortality and recruitment, suggesting that high density-dependent turnover rates facilitate the persistence of mosaics. Interaction between α and ε results in different combinations of outcomes, with mosaics possible in the region enclosed by $\varepsilon = 0.029\ e^{-27\alpha} - 0.00014$ and $\alpha = 0.5825 - \frac{0.42\varepsilon}{0.000085+\varepsilon}$ (Figure 3.5b, Figure B.11). Mosaics can occur for (ν, ε) between $\varepsilon = 0.47\nu^2 - 0.049\nu + 0.00096$ and $\nu = \frac{0.055\varepsilon}{\varepsilon+0.00019} + 0.024$ (Figure 3.5c, Figure B.11). Unlike the case of the $\alpha - \nu$ plane, the band of parameter combinations that admit mosaic outcomes does not widen as parameter values increase for the $\alpha - \varepsilon$ and $\nu - \varepsilon$ planes. Here, ε increase results in an narrowing of the range of α (or ν) values under which mosaics can occur.

On all 3 planes, the range of parameters under which mosaics occur is small, and the base parameter set is located in a region where slight alterations in one or more transition rate could lead to mosaic states only (Figure 3.5, Figure B.11). Within the region of parameter space that admits a specific landscape state there will be variation in the forest cover level (higher forest cover for mosaics in a $F + M$ region than an M region, etc.) creating smooth transitions between landscape states (Figure 3.5). A high random land-state transition rate facilitates the persistence of mosaics when forest recruitment is lower (or mortality higher) than would admit mosaic outcomes when ε is at base, suggesting frequent random transitions favour the establishment of forest in our model. This relates to the

fire-mediated recruitment threshold, which prevents forest recruitment in neighbourhoods with low forest cover. In such a neighbourhood, the only avenue for forest establishment is random land-state transition, with higher random transition rates facilitating increased forest growth. Random land-state transitions do not provide the same benefit to grassland establishment, as there is no threshold to forest mortality.

Plots of patch perimeter, area, and shape index (as well as effective mesh size) vs. forest cover when varying 2 parameters do not depart noticeably from plots of the same data when varying 1 parameter (Figure B.12- Figure B.14). For the $\alpha - \nu$ plane, the same is true when plotting landscape shape index and number of forest patches vs. forest cover (Figure B.12). However, for the $\alpha - \varepsilon$ and $\nu - \varepsilon$ planes, varying both parameters can result in more complex landscapes with substantially higher numbers of forest patches, and larger landscape shape index values, than if only 1 parameter is varied (Figure B.13, This is achieved through high ε values, combined with low α values in the case of the $\alpha - \varepsilon$ plane (Figure B.15) and high ν values for the $\nu - \varepsilon$ plane (Figure B.16). While the number of forest patches and LSI are boosted in both cases, combining high ε with low α creates the largest departure from base.

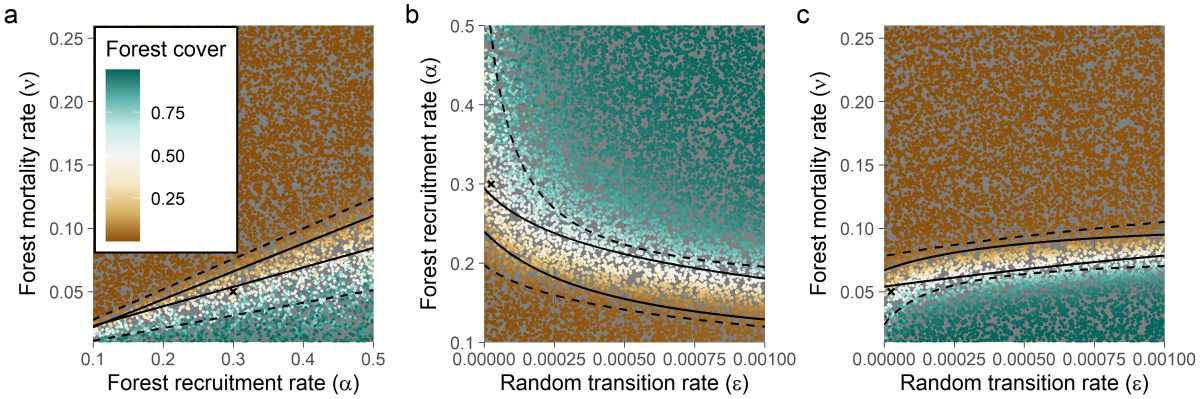

Figure 3.5: **Mosaics occur in a narrow region of parameter space.** Forest cover due to combined effect of (a) forest recruitment and mortality, (b) forest recruitment and random land-state transitions, and (c) forest mortality and random land-state transitions. Location of base rates are indicated with $\times$. For each parameter plane 10000 simulations are run (1000 for each $F(0)$), discarding any that do not stabilize. Dashed lines enclose the region where mosaics occur, with solid lines enclose the region where only mosaics are possible.

3.3.4 Climate change scenarios

The results in this subsection will demonstrate how Brazil's mosaics may be impacted by climate change, with potential for drastic increases in forest cover causing mosaic loss, as well as structural changes to remaining mosaics. We also note that delays between changes in external conditions and system responses could be a feature of climate-impacted mosaics.

A range of outcomes is possible, depending both on the RCP considered, and what parameter(s) are impacted by climate change (Figure 3.6). Changes to the recruitment threshold have a substantial impact on forest cover (Figure 3.6a); under RCP 6.0 and 8.5 they result in complete loss of mosaics (by 2210 and 2130 respectively) due to increased forest cover. RCP 4.5 results in some loss of mosaics, with the mean forest cover level exceeding the mosaic range by 2440. Under RCP 2.6, forest cover decreases slowly from the mid 2300s onwards, a result of precipitation decreasing towards its pre-1990 level. Projected long-term forest cover is highly variable for RCP 2.6 and 4.5 but not for RCP 6.0 or 8.5. Climate-impacted recruitment has a much smaller impact on forest cover (Figure 3.6b), as recruitment is still limited by the fire-mediated threshold. However, we do still observe small increases in forest cover (<1%) by 2500 under RCP 4.5, 6.0 and 8.5. When both recruitment and the recruitment threshold are climate-impacted, forest cover increases slightly faster than when only the threshold is impacted (Figure 3.6a) but long-term outcomes are similar. Due to these considerations, we focus on results from the climate-impacted threshold for the remainder of the section.

For decadal changes in threshold and forest cover (Figure B.17) the timing of the initial change in value, maximum absolute change, and stabilization do not coincide. We define the time of initial change and stabilization for threshold as the first year where $\Delta T > 0$ and $\Delta T = 0$ respectively (with the latter following the former). For forest cover we take the first year where $\Delta F > \max(\Delta F_{Base})$ and $\Delta F < \max(\Delta F_{Base})$ such that the forest cover change is measured in comparison to a scenario with no climate change. The majority of simulations show a delay between when the threshold begins to vary and when forest cover begins to change (Figure 3.7a). The maximum absolute change in threshold precedes the maximum absolute change in forest cover for all RCP, with the gap between these two events decreasing as we move from RCP 4.5 through RCP 6.0 to RCP 8.5 (Figure 3.7b). In all RCP 8.5 simulations, forest cover stabilizes before the threshold (Figure 3.7c), as forest cover quickly reaches its maximum value (of approximately 100%) due to the swift and substantial decrease in threshold under this scenario (Figure B.17). However, for RCP 4.5 and 6.0, forest cover may take decades or centuries to stabilize. As RCP 2.6 scenarios do not experience forest cover stabilization (Figure 3.6a), we do not include them in Figure 3.7c.

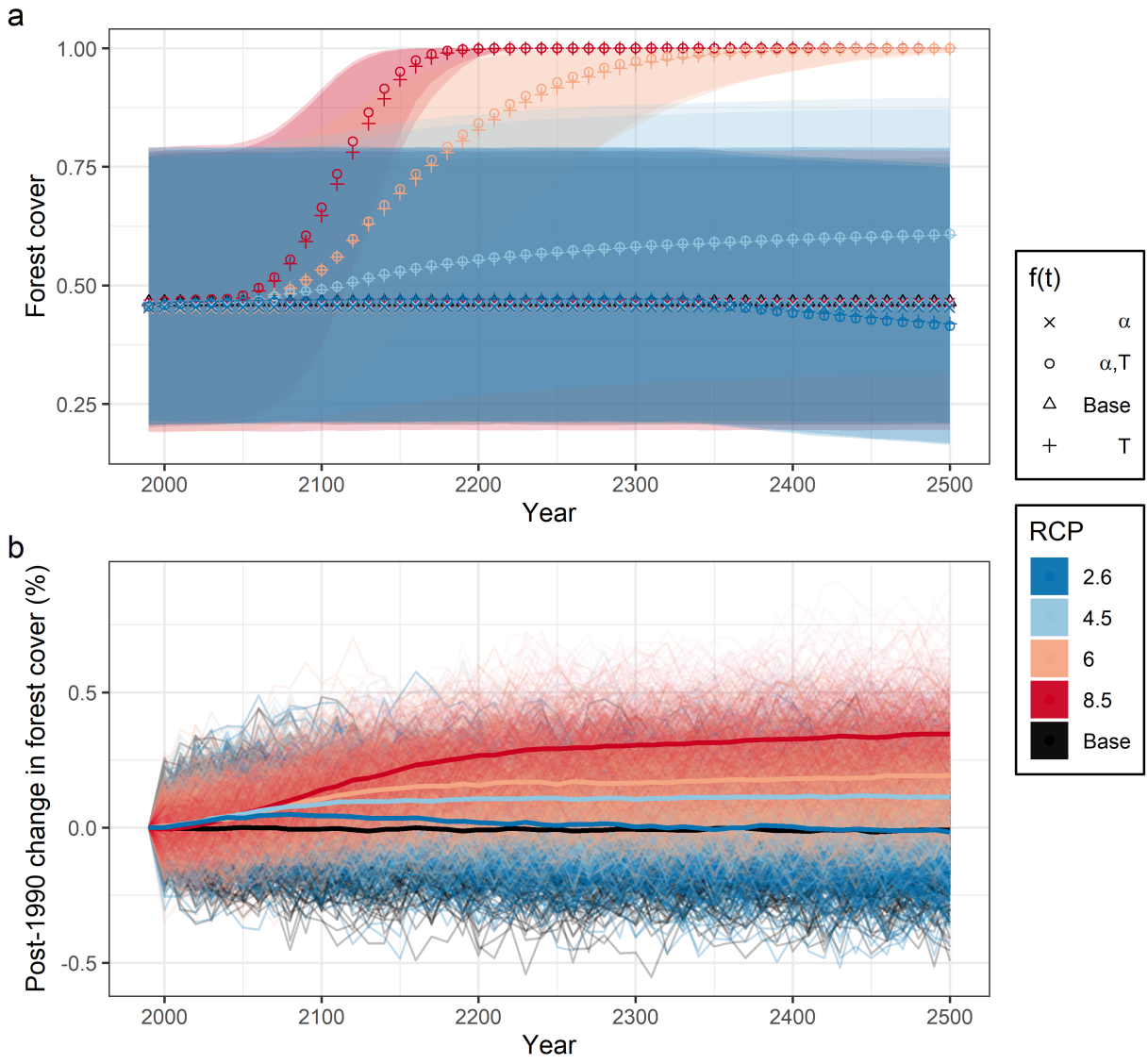

Figure 3.6: **Climate impacts on the forest recruitment rate and threshold to recruitment can lead to increases in forest cover.** a) Points indicate mean values for each scenario, envelopes indicate the associated min/max range. b) Climate-impacted recruitment only, thick lines indicate means for each RCP, thin lines represent individual runs. For each scenario 500 simulations are run.

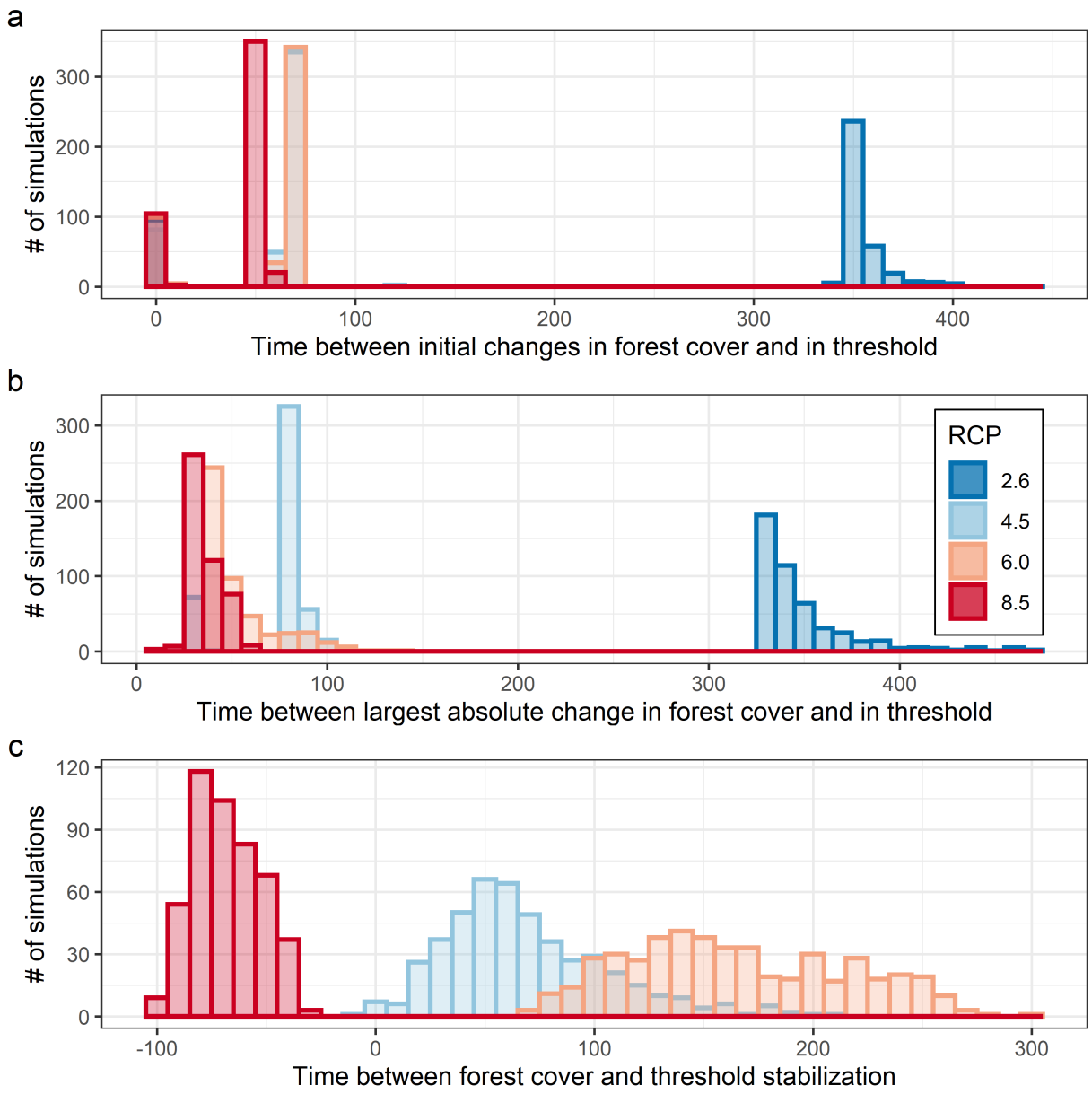

Figure 3.7: **Climate impacted mosaics may experience delays between shifts in external conditions and system responses.** Delays between a) initial changes, b) largest absolute decadal changes c) stabilization in threshold and forest cover.

A climate-impacted threshold alters the spatial layout of landscapes, despite no substantial changes in the number of patches (Figure B.18). For forest cover roughly between 50% and 75%, patches with mid-level values for area, perimeter, and shape index occur (Figure B.18). Additionally landscapes with $25-75\%$ forest cover will have lower landscape shape index values and, for forest cover in $50-75\%$, lower effective mesh size values than those where threshold is held constant. Under RCP 6.0 and 8.5 these alterations occur as part of a transition to a landscape with a single connected forest patch and $> 99\%$ forest cover. However, for RCP 2.6 and 4.5, we observe that these changes persist to the end of the simulations (Figure 3.8). Spatial structure in mosaics with climate-impacted recruitment does not differ greatly from that in those with constant recruitment (Figure B.19), while mosaics where both recruitment and threshold are impacted have similar structure to those where only the threshold varies over time (Figure B.20).

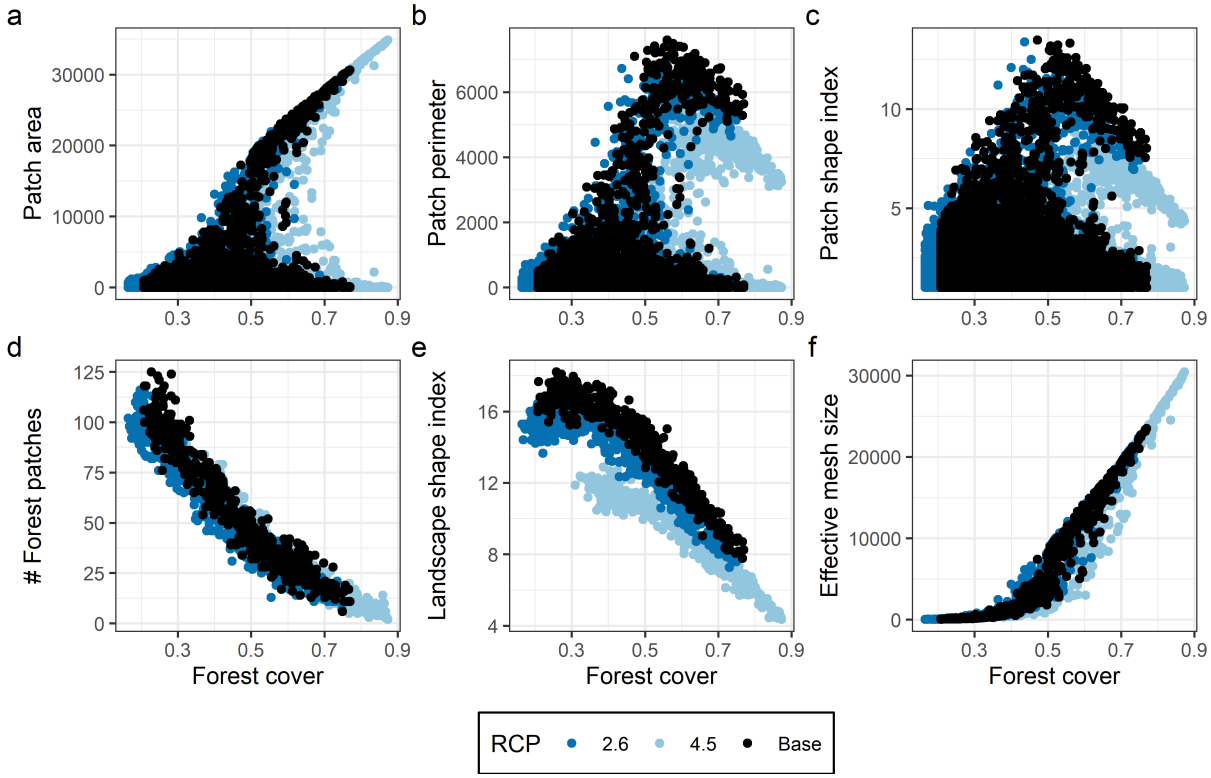

Figure 3.8: **Mosaics with climate impacted recruitment thresholds exhibit alterations to spatial structure.** (a) patch area (b) patch perimeter (c) patch shape index (d) number of forest patches (e) landscape shape index and (f) effective mesh size of landscapes under RCP 2.6 and 4.5. For each scenario 500 simulations are run.

3.4 Discussion

We developed and analysed a spatially-explicit model of forest-grassland mosaic dynamics, parametrized for the Atlantic forest-*Campos* grassland mosaics of Southern Brazil. The model, through the inclusion of fire-mediated tree recruitment and local spatial interactions, reproduces key spatial features of real-world protected mosaics. This model is used to examine how disturbances and environmental conditions influence the spatial structure of these complex systems, with special emphasis on the effects of anthropogenic climate change. Model analysis shows that mosaics are vulnerable to disturbances altering conditions in the landscape. They persist only under a narrow range of conditions, and when multiple aspects of system conditions are altered the impact is substantially higher than if a single condition is changed. Simulations with a climate-impacted recruitment threshold show marked increases in forest cover for all but the RCP 2.6 trajectory, with RCP 6.0, and 8.5 trajectories leading to total mosaic loss. Additionally, results suggest that even after changes to the threshold cease it may take centuries for forest cover to stabilize, with mosaics experiencing lasting changes to spatial structure.

Our model reproduces aspects of the diverse range of spatial characteristics exhibited by the Brazilian forest-grassland mosaics, both at the patch and landscape level. Some discrepancies between the model and the empirical data were observed–particularly with respect to the landscape shape index–but these are to be expected considering the simplicity of the model. Real-world mosaics are subject to human activities (deforestation, construction of roads, etc.) not considered in our model that could explain the differences in the shape index. The extent of these aspects would be lessened in national parks like Aparados da Serra, but not non-existent. Factors including soil heterogeneity and topography, not included in this model, may also impact these elements of spatial structure. Additionally, our assumption of constant transition rates is not realistic over extended time periods; even prior to the advent of anthropogenic climate change some variation in conditions impacting system dynamics would have occurred.

Simulations show that mosaics persist under a limited range of conditions, indicating that these complex ecosystems are not robust to multiple perturbations. This is further highlighted by the fact that our base parameter values (representing the Brazilian forest-grassland mosaics) occur in a region of the parameter planes where small changes to conditions could shift the system away from a regime where both mosaics and forest are possible. When forest mortality and recruitment rates are high mosaics can persist under a broader range of conditions than when land-state changes occur less frequently, suggesting high density-dependent transition rates facilitate mosaic persistence. Land state transition rates influence landscape spatial structure, impacting patch perimeter and shape index, the

number of patches, and landscape shape index values. If the random land-state transition rate, along with either the forest mortality rate or the recruitment rate, depart from their base value the effect on spatial structure is magnified.

Our climate change simulations suggest that increasing CO_2 levels will lead to forest expansion, due to climate change driven increases in precipitation. Higher recruitment rates in simulated climate change scenarios result in slightly higher forest cover. However, the majority of increases in forest cover are driven by reductions to the fire-mediated recruitment threshold. These reductions occur due to increases in precipitation, which lower the probability (and likely severity, though we do not consider this) of fire.

This result agrees with those of previous models of forest-grassland mosaic and savannah systems, both general [282] and specific to other geographic regions [49], that point to increased rainfall and reduced fire frequency as drivers of increases in woody species prevalence. Under RCP 6.0 and 8.5, where precipitation increases greatly resulting in substantial reduction in fire probability, grassland disappears entirely. As empirical studies and models have shown that precipitation and fire play key roles in the maintenance of tree-grass bistability [311, 279, 208, 1, 282, 278, 314], it follows that climatic shifts altering the balance of these factors could destabilize the mosaic, causing a shift to a forested state. Our model's prediction of increases in forest cover for Southern Brazilian mosaics, considered alongside previous model results projecting that climate change will lead to forest expansion in savanna regions of Northern Brazil [206] and forest loss in portions of the Amazon Basin [146], point to the diversity of responses to climate change, and the necessity of region-specific modelling. However, we might reasonably assume that our results generalize to forest-grassland mosaics outside of our study system, if they share a similar set of properties (fire-mediated recruitment, projected increases in precipitation). The extent of forest expansion in such systems would depend on several factors including the magnitude of precipitation increase and the location of the threshold in the absence of climate change impacts, both of which we would expect to vary geographically [311].

In most scenarios where climate change impacts the recruitment threshold, notable events (time of initial change, largest absolute change, and time of stabilization) in the time series of the evolving recruitment threshold precede the corresponding events in the forest cover time series. This suggests that even given a scenario where emissions are capped, the full impact of climate change could take decades or even centuries to become apparent. Additionally, our work indicates that for scenarios where mosaics persist with a climate-impacted threshold (RCP 2.6, 4.5), the spatial structure of the system will experience long-lasting impacts both at the patch and landscape level. Changes to the distributions of patch area and perimeter will alter patch complexity, and at higher forest cover levels lead to lower landscape complexity. This modified spatial structure may influence species

biodiversity as, at intermediate forest cover levels, patch area has a positive effect on species richness and abundance of forest specialist species inhabiting the Atlantic Forest [229].

Given the high ecological value of these ecosystems, strategies for protecting them – both from climate change and direct human impacts like deforestation – should be developed. Finding a balance between supporting human populations and preserving the integrity of mosaic structure and biodiversity will be key to achieving sustainable development in regions where mosaics occur [168, 332]. Models like the one developed here may prove useful in this regard, for example as tools to aid in identifying areas with conditions suitable for the establishment of protected areas [220].

The addition of land-use dynamics to the model would provide greater insight into the majority of forest-grassland mosaics that are not in conservation areas. Deforestation of the Atlantic forest has been extensive, with less than 20% of the original extent in Rio Grande do Sul state remaining [250, 137]. Deforestation leads to increasing atmospheric CO_2 levels and results in changes in surface albedo, both of which contribute to climate change effects [38]. In addition to this, the *Campos* grassland in the region is threatened by the expansion of agriculture and silviculture [227]. With only 0.15% of *Campos* protected within conservation units, the combination of climate and land use changes could hasten the disappearance of these ecologically valuable grasslands, and the loss of mosaics [137, 227, 77]. We did not include land-owner decision-making because our objectives were to study spatial structure of natural forest-grassland mosaics. However, modelling land-owner decision-making [136] in a spatial context could provide insights into how to promote sustainable development in these regions, including the preservation of natural forest-grassland mosaics on private lands, in the climate change era. As well, we did not consider tree species and age, in order to keep our model as simple as possible. Rates of carbon accumulation and storage are influenced by these characteristics, as well as the diversity of species, suggesting they could be incorporated into future models [284, 114]. This is especially crucial given the forest expansion predicted by our model; young trees will not have the same capacity for carbon storage as old growth forest. Additionally, climatic changes may lead to different species composition in forested areas, and thus altered carbon storage capacity. Such feedbacks between deforestation and climate change, as well as the net outcome of climate-driven forest expansion combined with deforestation should be explored. Finally, extensions of this work should consider how other aspects of system dynamics, such as the tree mortality and random land-state transition rates, will be impacted by anthropogenic climate change.

Given the narrow range of environmental conditions for which we observe forest-grassland mosaics in our model system, and the projected loss of mosaics under climate change, we conclude that more detailed mechanistic models of mosaic ecosystems should be developed.

These could expand on our work by incorporating tree species and age structure and/or explicitly modelling direct human activities e.g. deforestation. Such models could be used to target existing areas with ecosystem mosaics that are most likely to survive climate change, as well as inform site selection for new locations that could be restored as forest-grassland mosaics. Our simple model can reproduce many realistic spatial characteristics of these systems, suggesting that developing canonical predictive models for forest-grassland mosaics in the climate change era is both achievable and worthwhile.

Chapter 4

Human metapopulation interactions on a trade network: implications for food security and equality

This chapter is based on the paper in progress: Kathyrn R Fair, Madhur Anand, and Chris T Bauch. Human metapopulation interactions on a trade network: implications for food security & equality. *In progress*, 2020.

Abstract

As the Earth's population expands over the remainder of the 21st century, demands placed on the global food system will heighten. Given the integral role that international agri-food trade plays in maintaining food security, it is crucial to understand how the dynamics of human population growth, land use, and food supply interact with the network structures that facilitate food distribution. We use agricultural trade data to develop a metapopulation model that couples human populations to agricultural land use and food production in patches, where food is traded between patches through small-world networks. This model demonstrates that outcomes for human populations are strongly linked to their behavioural response to changes in food per capita. Inequality in the system grows over time, though the rate and magnitude of increase depends strongly on the drivers of inequality. Inequality is measured in terms of differences in food and non-agricultural land per capita, making this not only an issue of inequality but one of food security. Larger or more regularly structured networks lead to lower levels of inequality than smaller or more randomly structured networks. The most central patches on the trade network attain more food per capita due to their increased access to imports. When efficiency differences between patches create inequalities, they are sufficiently small that efforts to reduce inequality should focus on network topology. However, inequalities resulting from differences in patch-level import behaviours increase substantially and rapidly, leading to a case where import behaviours should be modified before alterations to network topology are considered. We conclude that trade network structure–all else being equal–can have significant impacts on food security and equality. Models of this type should be further developed, especially for the purpose of exploring the effects of shocks to network structure, and climate change impacts.

4.1 Introduction

The global population is expected to continue to grow over the remainder of the century, reaching 10.9 billion by the year 2100 [222]. Producing enough food for this population, especially given expected shifts in consumption patterns, is a challenge that has been emphasized in the literature [123, 177, 104, 255]. According to one estimate, a 60% increase in food production by 2050 (from 2006/07 levels) will be needed to meet growing demand [6]. This production increase may partially be achieved through increased yields and agricultural intensification [123, 270], however recent studies suggest that expansion of agricultural land area will also be required [228, 270, 177, 329, 267, 255]. This raises concerns, not only due to the environmental impact of converting natural land states (e.g.

forested land) for agricultural use, but because of the finite amount of land suitable for agriculture, some of which will be lost to urbanization and land degradation [123, 177]. In order to practice sustainable development as we move further into the 21st century, an understanding of how human population growth interacts with the global food system to impact land use and food security will be a necessity [99, 212, 214].

A crucial aspect of the global food system is trade; around 23% of food calories produced for human consumption move through international trade networks [87]. From 1986-2009 the amount of calories traded increased by more than 200%, with a more than 50% increase in the number of edges in the trade network [87]. Food trade impacts human population growth, food security, land-use changes, and the environmental impacts of food production [123, 177, 75]. These effects may be positive, such as the redistribution of food to efficiently meet demand, or negative, as when increased agricultural exports lead to increased deforestation [123, 75].

The interplay between human population, land use, food production, and agri-food trade creates a complex coupled human-environment system (HES). Within this system, the effects of feedbacks between population growth and agricultural land use play out across the trade network linking human metapopulations, and lead to the emergence of complex dynamics. One avenue for exploring these interactions is through models, which can be used to conduct *in silico* experiments. While numerous models of resource-limited human populations have been developed, most focus on a single population (e.g. [207, 69, 71, 40, 103, 303, 199, 82], amongst others), with a select few exploring the dynamics of metapopulations [81, 254, 14, 196, 247, 82, 287]. These metapopulation models have considered the effects of migration [254, 14], conflict and bargaining between populations over common resources [196, 73, 247], and the transfer of resources between populations [254, 81, 82, 287]. This latter avenue of exploration is tied closely to the goal of understanding how trade impacts human population growth.

Our objective is to explore how metapopulation structure – not only the inclusion of trade, but the structure of the trade network, and the parameters controlling demand-driven trade dynamics – impacts a system where human population, food supply, and agricultural land area are coupled. To this end, we develop a simple ordinary differential equation (ODE) model based on previous work exploring linked metapopulations [81] and land use change [228]. This model will be parametrized with empirical data, and fit to historical trends in agricultural land use, food supply, and human population growth at the global level, a model validation exercise that has not been employed in previous work [254, 81, 82]. Our model will further explore how trade impacts the dynamics of human population growth while accounting for the use of agricultural land to produce resources, unlike in previous models [254, 81, 82, 287]. We introduce a net population growth rate

function that incorporates both the resource-limited population growth assumed in previous models [81, 254, 82, 287] and the observed demographic transition towards lower fertility rates for populations with developed economies [256, 26, 210, 179]. By developing a simple but empirically validated model of this complex system, we provide a framework for exploring hypotheses about the interaction of trade, land use, and human population dynamics. Through experimentation, we can ascertain how this complex system impacts global food security and land use. Insights gained from this analysis, and future analyses of specific scenarios (trade wars, climate change impacts, etc.), will enhance our understanding of how to meet the challenge of feeding a growing population while simultaneously engaging in sustainable development.

4.2 Methods

4.2.1 Global model

We begin with a single-patch (global) model of human population, agricultural land use, agricultural yield, and food supply. Agricultural yield, Y, human population, P, agricultural land, A, and food supply, F, change according to

$$\frac{dY}{dt} = r_Y Y \left(1 - \frac{Y}{K_Y}\right) \tag{4.1}$$

$$\frac{dP}{dt} = P\left(\alpha_0 e^{-\sigma F/P}\left(\rho - \frac{P}{F}\right) - \delta\right) \tag{4.2}$$

$$\frac{dA}{dt} = \kappa b^A (T - A) - \zeta A \tag{4.3}$$

$$\frac{dF}{dt} = f(1-s)YA - cF. \tag{4.4}$$

All parameter definitions are stated in Table 4.1. As in [228] we assume yield undergoes logistic growth. Food supply increases proportionally to agricultural yield and land area, and we assume that no food is held in reserve over time ($c = 1$). Human population growth is density-dependent, with the birth rate changing dynamically with per capita food supply. The total habitable land area, T, is the sum of agricultural land A, and non-agricultural land, which pools natural land states, urban area, etc.

Previous models have focused on resource-limited population growth, where increased access to resources raises the net population growth rate [81, 254, 82, 287]. The construction

of our net human population growth rate function (Equation 4.2) is intended to capture both resource-limited growth, and the occurrence of a demographic transition towards lower fertility rates when resources are sufficiently abundant. This phenomenon has been observed as countries become increasingly developed, leading to slowed population growth and in some cases a net population decrease [256, 26, 210, 179]. The transition is likely driven by a variety of socio-economic factors; not only higher levels of wealth, but increases in the level of health, education, and other factors that are positively correlated with wealth [256, 8, 210].

In order to incorporate this demographic transition into our model, which does not explicitly consider any measure of wealth, we utilize food per capita as a wealth proxy. We justify this by observing that more developed countries tend to have have higher per capita food supply, a consequence of food demand increasing with wealth – up to a point – as well as the higher levels of consumer-level food waste in developed countries [257, 106, 59, 336, 120]. This allows us to construct our net population growth function, assuming that in a resource-scarce regime food per capita is either the limiting resource or a proxy for wealth as the limiting resource, and in a resource-abundant regime it acts as a proxy for wealth. Combining these behaviours creates an overall curve, whereby the net growth rate increases to some maximum with increasing food per capita, prior to decreasing gradually at higher levels of food per capita. This curve resembles a Holling type-IV functional response [152, 290], and agrees with a previously proposed relationship between fertility and wages [175]. While there is some evidence to suggest that at very high levels of development (as measured using human development index) fertility will begin to increase, creating a "J-curve" [210], this result has been disputed [113].

Finally, we introduce a function, b^A, that determines the response to changes in per capita food supply through adjustments to the rate of agricultural land expansion. This function is given by

$$b^A = \frac{1}{1 + e^{\gamma^A(\beta^A - P/F)}} \tag{4.5}$$

where γ^A controls the steepness, and β^A the midpoint of the sigmoid. With this function, as P/F increases (food per capita decreases), the rate of agricultural land expansion increases.

Refer to Subsection C.1.1 for details of the fitting exercise carried out on the global model to obtain parameters for use in the metapopulation model. Global model trajectories using the parametrization resulting from this fit are presented in Section C.2.

4.2.2 Metapopulation model

With all definitions as for the global model, we can formulate a metapopulation model with N patches as

$$\frac{dY_i}{dt} = r_{Y_i} Y_i \left(1 - \frac{Y_i}{K_{Y_i}}\right) \tag{4.6}$$

$$\frac{dP_i}{dt} = P_i \left(\alpha_{0_i} e^{-\sigma_i F_i/P_i} \left(\rho_i - \frac{P_i}{F_i}\right) - \delta_i\right) \tag{4.7}$$

$$\frac{dA_i}{dt} = \kappa_i b_i^A \left(T_i - A_i\right) - \zeta_i A_i \tag{4.8}$$

$$\frac{dF_i}{dt} = f_i(1-s_i)Y_i A_i \left(1 - \lambda_i \mu_i \sum_{j=1, j\neq i}^{N} M_{ij} b_j^I\right) + b_i^I \sum_{j=1, j\neq i}^{N} M_{ji} \lambda_j \mu_j (1-s_j) f_j Y_j A_j - c_i F_i \tag{4.9}$$

where μ_i is the fraction of patch i's production that is exported, with $1 - \mu_i$ consumed locally. These patches may be thought of as countries, cities, or any other human metapopulation that exists within a trade network.

The (undirected, unweighted) trade network is represented as an $N \times N$ adjacency matrix M. We use undirected networks to describe trade, as the dynamic resource flows within the model will have some net direction without prior specification. Thus,

$$M_{ij} = M_{ji} = \begin{cases} 1 & \text{if patch } i \text{ has a trade link with patch } j \ (i \leftrightarrow j), \\ 0 & \text{if patches } i \text{ and } j \text{ are not connected.} \end{cases} \tag{4.10}$$

The networks our model is simulated on are discussed further in Subsection 4.2.3.

We assume that the population of a patch will adjust import demand in response to changes in per capita food supply according to a function given by

$$b_i^I = \frac{1}{1 + e^{\gamma_i^I \left(\beta_i^I - P_i/F_i\right)}} \tag{4.11}$$

where γ_i^I controls the steepness, and β_i^I the midpoint of the import demand sigmoid for patch i. With this sigmoid function, as P_i/F_i increases (per capita food decreases), import demand increases.

We define a normalization factor, λ_i, to ensure that a patch does not export more than a fraction μ_i of its production. The value of λ_i depends on external demand for patch i's food, according to the relationship

$$\lambda_i = \left(\sum_{j=1, j \neq i}^{N} M_{ij} b_j^I \right)^{-1} \tag{4.12}$$

such that each trade partner is able to access an equal share of food, given their demand relative to the demand of all other connected partners.

Given these definitions for b_i^I and λ_i we can reduce Equation 4.9 to

$$\frac{dF_i}{dt} = f_i(1 - s_i)Y_i A_i(1 - \mu_i) + b_i^I \sum_{j=1, j \neq i}^{N} M_{ji} \lambda_j \mu_j (1 - s_j) f_j Y_j A_j - c_i F_i \tag{4.13}$$

for simplicity.

4.2.3 Model analyses

To gain insight into how inter-patch trade interacts with patch-level dynamics to impacts system outcomes, we perform several experiments manipulating different aspects of the trade mechanism and patch-level behaviour within the model. First, we consider a simple case of "identical demand response" where $\gamma^I = \gamma^A = \gamma$ and $\beta^I = \beta^A = \beta$ to explore how the slope and midpoint of the demand sigmoids impact model outcomes. This experiment is carried out under both "low" and "high" yield scenarios (see Subsection C.1.1 for further details). We also explore a "distinct demand response" scenario where $\beta^I \neq \beta^A$ such that, for a given level of food per capita, demand levels for agricultural expansion and import of food are not equal.

Empirical studies have shown that real-world trade networks are small-world [271, 326]. As such, we use small-world networks as the basis for the trade networks we simulate our metapopulation model on. The "small-world" property indicates that the network displays high clustering (like a lattice) and a short average path length (like a random network) [320, 292]. We quantify the small-worldness of our networks using the small-world measure developed by Telesford *et al* [292]. For the purposes of our analysis, we call a network "small-world" if the small-world measure (ω) returns $\omega \in [-0.5, 0.5]$ for that network [292]. For further information on the network science concepts and metrics used in this analysis please refer to Subsection C.1.2.

Table 4.1: **Baseline parameters for metapopulation model.** Values are drawn directly from (or fit using ranges from) empirical data, where possible. Parameters related to human population growth (listed above line) fit to data on net population growth rate, independent of remainder of model fitting. Units of δ, r_Y, κ, ζ, f, and c are 1/year, μ and s are unitless, α_0 has units of tonnes/(person $*$ year), K_Y has units of tonnes/hectare, γ^A and γ^I have units of tonnes/person, σ, ρ, β^A, and β^I have units of (tonnes/person)$^{-1}$, T is given in billions of hectares.

Parameter	Description	Value	Range	Source
δ	Base death rate	0.0113	N/A	[222]
α_0	Controls maximum net growth rate	0.028	$[0, 1]$	fitting, [108]
σ	Controls steepness of birth rate decrease with increasing food per capita	2.1013	$[1, 10]$	fitting, [108]
ρ	Controls food per capita where net growth becomes negative due to food scarcity	6.25	$[5, 6.25]$	fitting, [108]
K_Y	Yield carrying capacity (low, high yield)	3.5, 7	$[2, 7]$	[228]
r_Y	Yield growth rate (low, high yield)	0.0301, 0.0245	$[0, 1]$	fitting, [108]
κ	Agricultural land conversion rate	0.0031	$[0, 0.1]$	fitting, [108]
T	Total habitable land area	9.6251	N/A	[108]
ζ	Agricultural land abandonment rate	0.001	$[0.001, 0.1]$	fitting, [185, 137, 136, 48]
f	Proportion of agri-food resources produced that are available as human food, annually	0.75	$[0.745, 0.755]$	fitting, [53, 108]
s	Proportion of food production unavailable due to pre-consumer food waste/loss	0.0689	$[0.02, 0.2]$	fitting, [106]
μ	Proportion of food produced that is available for export	0.16	N/A	[108]
c	Consumption rate, inclusive of consumer-level food waste/loss	1	N/A	N/A
β^A	Controls location of midpoint for agricultural land conversion sigmoid	N/A	$[0, 10]$	N/A
γ^A	Controls steepness of agricultural land conversion sigmoid	N/A	$[0, 10]$	N/A
β^I	Controls location of midpoint for trade sigmoid	N/A	$[0, 10]$	N/A
γ^I	Controls steepness of trade sigmoid	N/A	$[0, 10]$	N/A

Both "demand response" experiments are carried out on networks of 10 and 100 nodes, to demonstrate results at multiple scales. We do not proscribe a set number of edges across all networks of the same size, thus allowing for a range of network densities. Instead we generate networks with some fixed N and a randomly selected neighbourhood size and rewiring probability. Any networks that are not sufficiently small-world are discarded.

Following this, we explore how running simulations on networks with different structures (i.e. different levels of small-worldness) impacts outcomes both at the global and patch level. This is done by rewiring regular networks using the Watts-Strogatz algorithm, to shift from very regular networks (at low rewiring probabilities) through small-world networks (at intermediate rewiring probabilities) to very random networks (at high rewiring probabilities). This rewiring exercise is carried out on 100 node networks, with 2 different edge densities, to illustrate the effect of network density on outcomes.

Finally, we experiment with a heterogeneous parametrization of the model to ascertain how heterogeneity in patch-level behaviour impacts global and patch-level outcomes. Here we particularly focus on how differences in patch-level behaviour interact with node-level network metrics to result in unequal outcomes between patches. These simulations are carried out on 100 node networks with small-world characteristics.

All simulations are run for 100 time-steps (years), with any results where the time-series is not explicitly referenced indicative of outcomes at $t = 100$. This time-frame is chosen as the assumptions that go into the construction and parametrization of models describing human behaviours are generally only valid over short periods, due to factors such as technological and societal change. For our model, this would include the constant parameter values for processes such as land conversion, as well as the assumption of a static trade network. The 100 time-step run was chosen as it has a similar length to the projections (to 2100) used by the United Nations and the Intergovernmental Panel on Climate Change to explore population growth, Shared Socioeconomic Pathways (SSPs) for climate change, and other phenomena [249, 222]. This means that we are studying transient as opposed to equilibrium behaviour. However, given the rate at which change in human systems occurs, it is reasonable to assume that any equilibrium behaviour we could study by extending the time series would be invalidated as our model assumptions would no longer be reasonable.

This model is implemented in Matlab (Version 2016b), with equations solved numerically using ODE45 (adaptive 4^{th}-5^{th} order Runge-Kutta method). In all experiments, we initialize the model by assuming global population, agricultural area, food supply, and available land are divided evenly amongst patches, in order to isolate the effects of trade. Using data from our global model (corresponding to the year 2013) as our $t = 0$ initial-

ization, $P_i(0) \approx 7.20/N$ ($\times 10^7$), $A_i(0) \approx 5.00/N$ ($\times 10^7$ hectares), $F_i(0) \approx 6.41/N$ ($\times 10^7$ tonnes) and $Y_i(0) \approx 1.86$ (tonnes/hectare). We initialize using model data instead of empirical data so that if the metapopulation model is reduced to a global model we will not see a discrepancy in results.

In addition to tracking the model variables, we consider several other measures to enhance our understanding of food security and inequality in the system. Food per capita (FPC), already a driver of model dynamics, is also indicative of food availability, one of the 4 main pillars of food security. We additionally examine patch-level import dependency, a measure of stability in food security [105]. If a patch is highly reliant on imports for its food supply, any disruption (to the network, or in other patches) that impacts their ability to import will have a drastic effect. Import dependence is calculated as (imports/food supply) where food supply is (as demonstrated by Equation 4.13) made up of domestic production + imports − exports. We also consider the amount of non-agricultural land per capita (LPC) calculated as (total area − agricultural area)/person. We can interpret this as a measure of the per capita availability of natural land states as well as urban area for housing. When we present global mean values for FPC and LPC, these are weighted by patch-level population. Inequality between patches is described in terms of food per capita [86], and non-agricultural land per capita. We quantify these inequalities using the Gini index, which measures inequality between values within a distribution. It ranges between 0 and 1, where higher values correspond to greater inequality. Index values are calculated using the reldist package (Version 1.6-6) for R, with patch-level observations weighted by patch population size [127, 128]. We can think of high Gini index values for food per capita as inequalities in food security, while for non-agricultural land per capita this may indicate inequalities in access to housing, natural land states, etc.

4.3 Results

4.3.1 Exploring patch-level behaviours

Identical demand response

We begin by considering a simple case where the demand response curves (b_i^A, b_i^I) are identically parametrized ($\gamma_i^A = \gamma_i^I = \gamma$, $\beta_i^A = \beta_i^I = \beta \ \forall \ i \in \{1, \ldots, N\}$) to explore the relationship between β and γ (Figure 4.1). The β-value controls the "desired" food per capita (smaller β indicates that a higher food per capita must be achieved for demand to drop below 50%), and the γ-value indicates the "efficiency" of the response to changes

in food per capita (higher γ indicates a steeper response curve). Thus, variable values on the (β, γ) plane indicate how model outcomes are impacted by the interplay between the desired food per capita and the efficiency of patches in adjusting their demand to achieve that value. We explore parameter planes while simulating the model on small-world networks with either 10 or 100 nodes (Refer to Subsection 4.2.3 for network details).

As response efficiency increases (higher γ), we see a shift from outcomes where population, agricultural land, and food supply (Figure 4.1a-f) have moderate values, to a regime where more extreme outcomes are possible (roughly $\gamma > 2.5$). Unlike in the low-γ region of the plane, the demand response is efficient enough that we observe starkly different outcomes, depending on the desired food per capita, over the time period considered. Here, increasing desired food per capita (decreasing β) results in increases in global agricultural land and food supply, with a lower population (and thus higher food and non-agricultural land per capita, as in Figure 4.1i-l).

The switch from a large food- and land-poor population to a smaller food- and land-rich population occurs in the region where β is near 1. To understand this, we revisit our initialization; food per capita in each patch at $t = 0$ is approximately 0.89 (and thus $P_i(0)/F_i(0) \approx 1.12$). If β is much larger than 1, demand for agricultural expansion and food imports is low early in the time-series, and as populations grow they are unable to obtain enough food to maintain or increase their food per capita. Thus, these populations experience higher growth rates, exacerbating the issue of low food per capita. By the time food per capita has become low enough that patches experience high demand and start to increase agricultural expansion and food imports, they already have large populations and little food. In the time-span of our simulations, they are unable to transition to a smaller population with a more abundant supply of food. In contrast, if $\beta < 1$ the initial trajectory is one of agricultural expansion accompanied by food import, allowing patches to obtain higher food per capita early in the simulation run. Populations in these patches shift to the right on our net population growth rate curve, experience slowed net population growth, and are able to further increase their food per capita over the timespan we consider.

Increasing response efficiency tends to decrease inequality between patches, both in terms of food per capita and non-agricultural land per capita when $\beta > 1$ (Figure 4.1m-p). However, when $\beta < 1$ inequality values remain relatively consistent regardless of the γ-value. The level of import dependency (Figure 4.1g,h) doesn't change substantially, though some $N = 10$ networks experience slightly lower values.

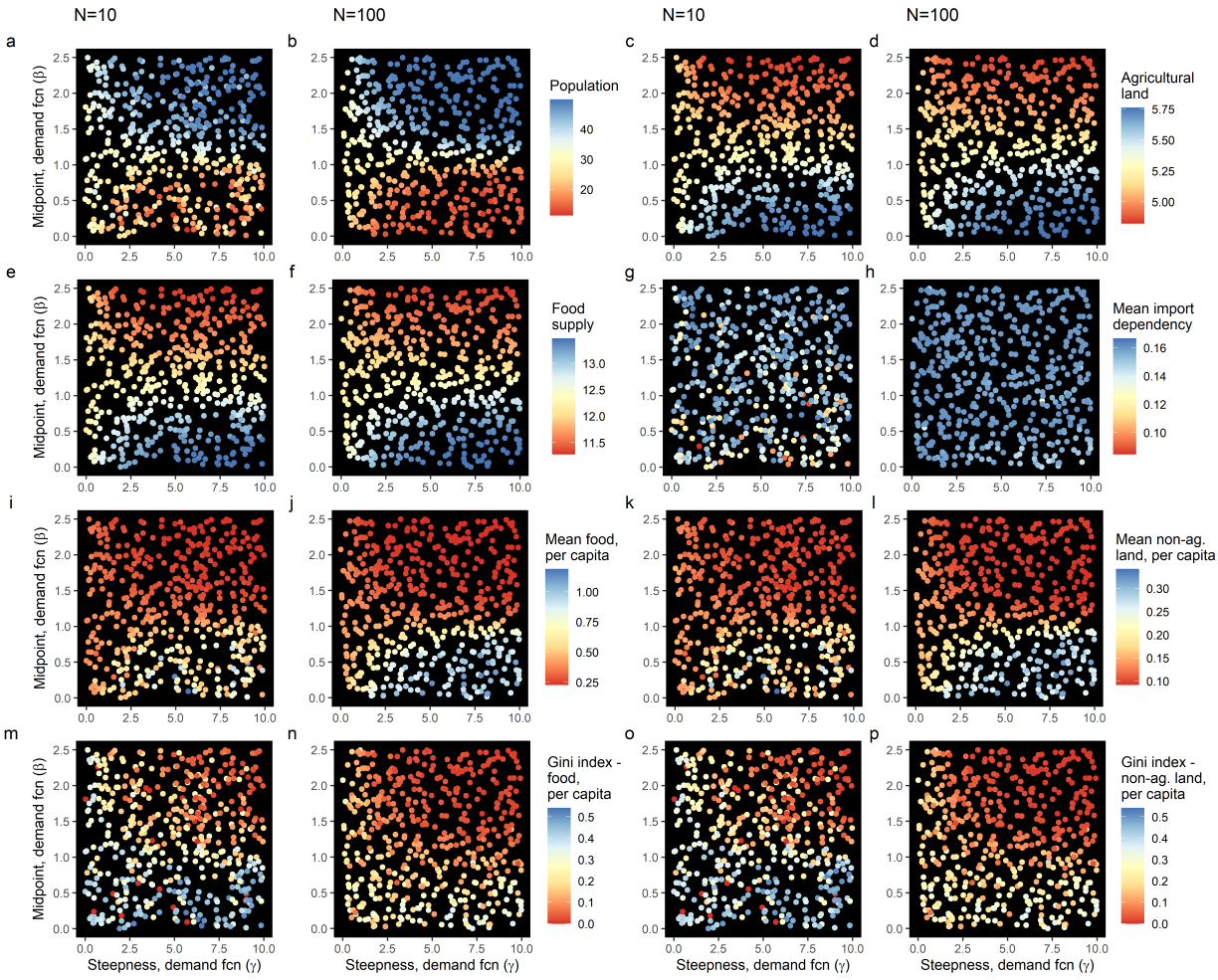

Figure 4.1: **Steepness and midpoint of demand response sigmoid influence system outcomes under a "low" yield scenario.** (γ, β) parameter planes for global values of (a)-(b) population ($\times 10^7$ people) (c)-(d) agricultural land ($\times 10^7$ hectares) (e)-(f) food supply ($\times 10^7$ tonnes) (g)-(h) mean level of import dependency, mean per capita (i)-(j) food (tonnes/person) and (k)-(l) non-agricultural land (hectares/person and Gini index, per capita (m)-(l) food and (o)-(p) non-agricultural land. Results are for a low-yield scenario. 500 simulations run for each of $N = 10$, $N = 100$, randomly selecting a network and parameter values.

Results are qualitatively similar for 10 and 100 patch networks, though in $N = 100$ networks the demarcation between regions where different model outcomes are possible are more sharply defined (especially for population), while $N = 10$ networks show more variation in measures of inequality and import dependency. In larger networks higher per capita values for food and non-agricultural land are attainable when $\beta < 1$, as are lower levels of inequality. We observe similar patterns if the "high" yield scenario is assumed. However, as in the global model, the higher yield will result in higher food supply and thus a smaller population, due to the transition to lower net growth rates in food-rich populations (Figure C.4). Throughout the remainder of the analysis, we focus on the "low" yield scenario.

Distinct demand response

Here we explore the effect of distinct demand response curves for b_i^A and b_i^I by considering a case where $\beta_i^A = \beta^A \; \forall \; i \in \{1, \ldots, N\}$ and $\beta_i^I = \beta^I \; \forall \; i \in \{1, \ldots, N\}$ but $\beta^A \neq \beta^I$. We assume that patches will have identical efficiency ($\gamma_i^A = \gamma_i^I = \gamma \; \forall \; i \in \{1, \ldots, N\}$) as patches with efficient economies should tend to have both high trade and agricultural efficiency (similarly for inefficient economies). Using $\beta^A \neq \beta^I$ represents a scenario where the food per capita at which demand drops below 50% differs between demand for agricultural expansion and imports. For example, a patch will keep importing after it has stopped expanding agricultural land if $\beta_A > \beta_I$, or keep expanding its agricultural land after it has stopped importing if $\beta_I > \beta^A$. As in Section 4.3.1, the model is simulated on small world networks where $N = 10$ or $N = 100$ (see Subsection 4.2.3 for network details).

β^I has little effect on population, agricultural land area, and food supply at the global level, especially for $N = 100$ networks, with model outcomes almost entirely determined by the value of β^A (Figure 4.2a-f). This makes intuitive sense; β^A controls the amount of agricultural land, meaning that for a given β^A there is a finite amount of food available. Due to the homogeneous parametrization of all patches, all the β^I value does is determine how food available for export is distributed.

Though these global outcomes are insensitive to β^I, it impacts per capita food and non-agricultural land outcomes when $\beta^A < 1$, with $\beta^I > 1$ leading to high values for these measures, while for $\beta^I < 1$ these values decrease with smaller β^I, with a larger drop-off in the $N = 10$ networks (Figure 4.2i-l). When $\beta^I < 1$, there are differences in levels of inequality on either side of $\beta^A = 1$ (Figure 4.2m-p), especially in the $N = 10$ network. A combination of $\beta^A, \beta^I < 1$ results in the highest levels of inequality on these parameter planes. The level of import dependency remains relatively constant, with a slightly broader range of values possible in $N = 10$ networks (Figure 4.2g,h).

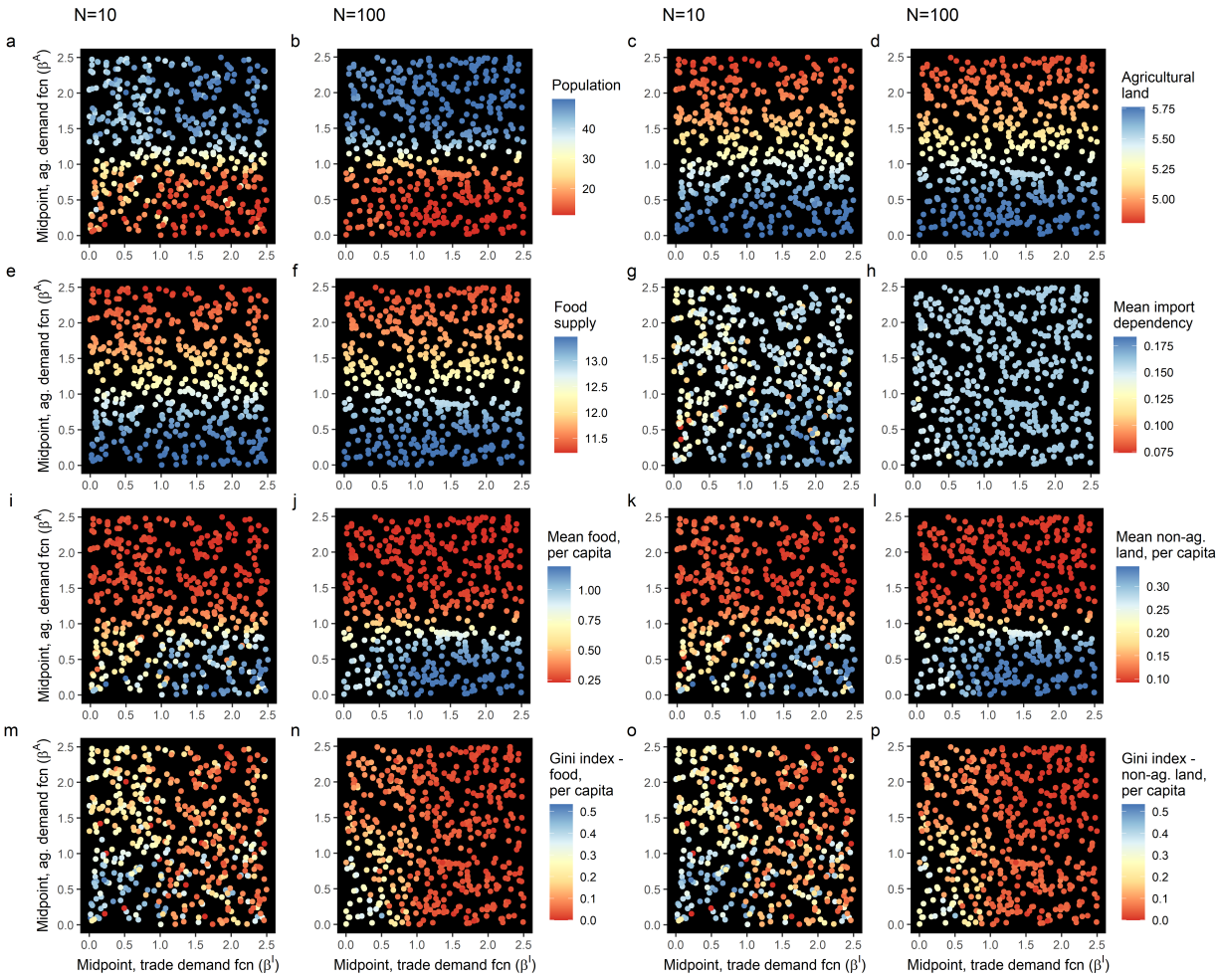

Figure 4.2: **Midpoints of demand response sigmoids for agricultural land expansion and imports influence system outcomes.** (β^I, β^A) parameter planes for global values of (a)-(b) population ($\times 10^7$ people) (c)-(d) agricultural land ($\times 10^7$ hectares) (e)-(f) food supply ($\times 10^7$ tonnes) (g)-(h) mean level of import dependency, mean per capita (i)-(j) food (tonnes/person) and (k)-(l) non-agricultural land (hectares/person and Gini index, per capita (m)-(l) food and (o)-(p) non-agricultural land. 500 simulations run for each of $N = 10$, $N = 100$, randomly selecting a network and parameter values.

4.3.2 Network properties

Having established how patch behaviour impacts model outcomes, we explore the effects of network structure. We limit ourselves to a $\{\beta_i^A, \gamma_i^A, \beta_i^I, \gamma_i^I\}$ set that results in outcomes at $t = 100$ similar to those from our global model for the year 2100. This allows us to observe the effects of network structure when global outcomes align with plausible real-world trajectories. The set chosen is $\{\beta_i^A, \gamma_i^A, \beta_i^I, \gamma_i^I\} = \{0.25, 7.5, 0.25, 7.5\}$, where we pick the β_i^I, β_i^A values from the region of (β^I, β^A) space where inequality is high to better observe how network structures impact inequality.

Simulations are run on networks generated using the Watts-Strogatz algorithm with different re-wiring probabilities (p). For each rewiring probability, 25 networks are generated. We experiment with 100 node networks with either 1700 or 2600 edges, giving us network densities of 0.343 and 0.525 respectively. These densities are chosen to match those for the undirected real-world international agri-food trade network from the years 1986 and 2016 (the first and final year available in FAO trade data) as closely as possible [108]. We consider 2 densities to explore how the number of edges interacts with the rewiring probability, as previous work has shown the number of edges in real-world agri-food trade networks is increasing over time [97, 87, 70, 118].

Network topology and global outcomes

For higher density networks we do not achieve highly random networks even when $p = 1$ (Figure 4.3a). Lower density networks experience more drastic and larger increases in the small-world measure, with the small-world measure becoming positive (indicating a network that is more random than regular) when $p > 0.1$. In lower density networks a higher rewiring probability leads to lower values for average path length and average clustering coefficient, while in the higher density network the average path length remains constant throughout (Figure 4.3b,c). Networks at both densities experience changes in their average clustering coefficient over a similar range of p-values.

As networks become less regular and more random the global population increases (Figure 4.3d). While the change in population from $p = 0$ to $p = 1$ is substantial, agricultural land and food supply only experience small decreases, as does the mean import dependency (Figure 4.3e-g). Mean food and non-agricultural land per capita levels both show marked decreases (Figure 4.3h,i). Random structures promote inequality, with our Gini index values increasing substantially as the rewiring probability increases (Figure 4.3j,k). These results hold at both network densities, though for $0.1 < p < 1$ simulations on lower-density networks have higher populations, lower mean food per capita, etc.

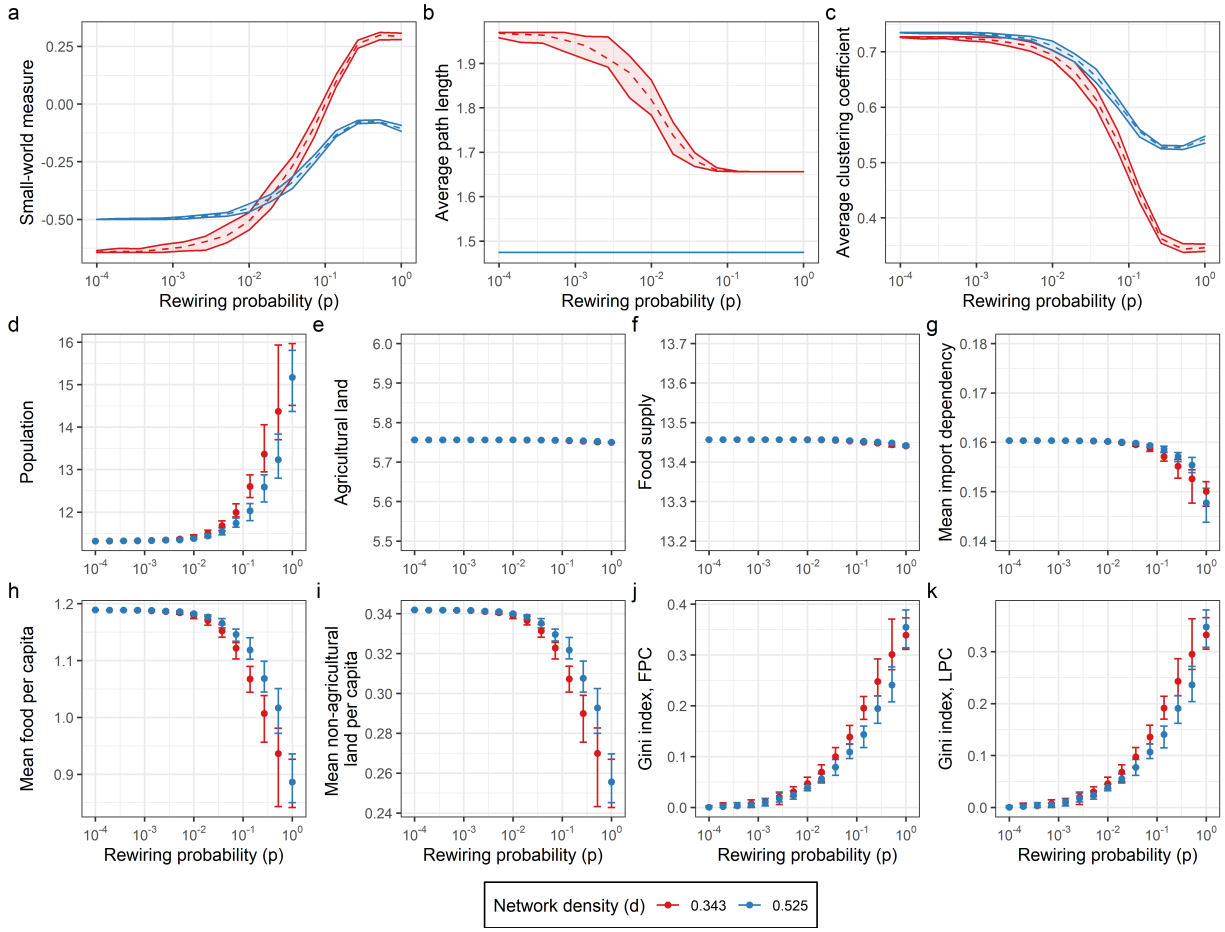

Figure 4.3: **Network structure impacts system outcomes.** Effect of rewiring probability on network (a) small-world measure (b) average path length (c) average (local) clustering coefficient. Effect of rewiring probability on system (d) population ($\times 10^7$ people) (e) agricultural land ($\times 10^7$ hectares) (f) food supply ($\times 10^7$ tonnes) (g) mean level of import dependency, mean per capita (h) food (tonnes/person) and (i) non-agricultural land (hectares/person) and Gini index, per capita (j) food and (k) non-agricultural land. In (a)-(c) dashed lines indicate mean value for all simulations with a network density and rewiring probability, while ribbons show the range of outcomes. For (d)-(k) bars indicate the range of outcomes, points indicate mean values for all simulations with a given network density and rewiring probability. 25 networks generated for each rewiring probability (p-value) and density.

Node centrality and patch-level outcomes

Regardless of rewiring probability, more central patches (in terms of node degree, betweenness, closeness, or eigenvector centrality) will have higher food per capita at $t = 100$ (Figure 4.4). This is due to the fact that being situated more centrally in the network gives patches more access to food through imports. The effect on food per capita is reduced for networks generated using lower rewiring probabilities as these networks are more regular and differences in centrality between the most and least central node will be smaller.

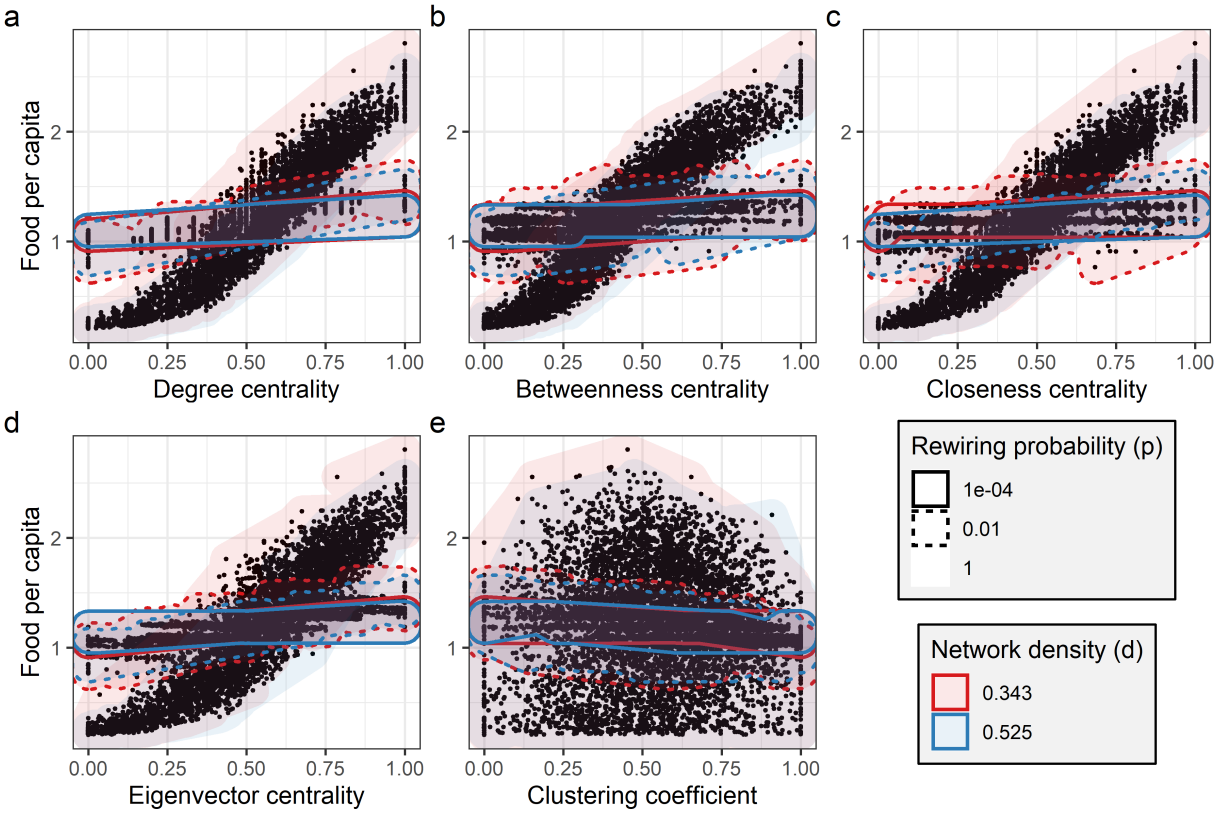

Figure 4.4: **Node-level metrics are indicators of patch-level food per capita.** Relationship between patch-level food per capita (tonnes/person) and (a) degree centrality (b) betweenness centrality (c) closeness centrality (d) eigenvector centrality (e) clustering coefficient. All metrics are normalized to facilitate comparison across networks. Hulls are drawn around groups of points to indicate they correspond to nodes from networks with different densities and rewiring probabilities.

It is unsurprising that all 4 centrality measures show similar results, as these metrics are highly correlated [184, 307]. However, unlike the centrality measures, local clustering coefficient does not appear to impact food per capita outcomes (Figure 4.4e). Patches positioned on nodes with the same clustering coefficient experience a broad range of food per capita values, particularly when $p = 1$. Thus, being positioned on a node located in a highly clustered region of the network does not confer any advantage or disadvantage in terms of food per capita outcomes.

4.3.3 Heterogeneous patch-level behaviours

Given that we have established how network centrality influences outcomes when all patches have identical parametrizations, it is interesting to consider what outcomes are possible when parametrization is heterogeneous. These experiments are carried out on our high-density networks (100 nodes, 2600 edges), with $p = 0.5$. This p-value is chosen as it is in the range of rewiring probabilities that result in the highest mean value for the small-world measure (Figure 4.3a). We assume these networks are a reasonable representation of real-world agri-food trade networks due to their small-world and large number of edges. In considering patch-level outcomes we focus on degree centrality as our key network metric, as our previous analysis suggests it is a consistent predictor of outcomes for patches situated on nodes in networks with a constant density.

Heterogeneous efficiency

We consider a simple case where $\beta_i^A = \beta_i^I = \beta = 0.25 \ \forall \ i \in \{1, \ldots, N\}$, but 50% of patches are efficient ($\gamma_i^A = \gamma_i^I = \gamma_i = 7.5$) and thus all remaining patches are inefficient ($\gamma_i^A = \gamma_i^I = \gamma_i = 2.5$) in adjusting their imports and agricultural land expansion in response to changes in food per capita. Patches are randomly assigned either the "efficient" or the "inefficient" γ_i-value, so there is no correlation between nodes based on patch efficiency.

At the global level, introducing heterogeneity in patch efficiency results in trajectories that are in some cases similar to those for the homogeneous low-efficiency case (population, food and non-agricultural per capita, import dependency) or high efficiency case (Gini index values), while "splitting the difference" on agricultural land area and food supply (Figure 4.5). Heterogeneity in patch efficiency results in a more unequal world; Gini index values are higher than in simulations with homogeneous parametrizations, and increase more rapidly over the time-span considered (Figure 4.5g, h). Initial increases in the mean patch-level food per capita (Figure 4.5e) are followed by a downturn. For all but the 100%

high efficiency case, this decline results in the mean patch-level food per capita being lower at the end of the simulation than at initialization. Thus, while trajectories may at first appear promising, these improvements in mean food per capita prove to be unsustainable.

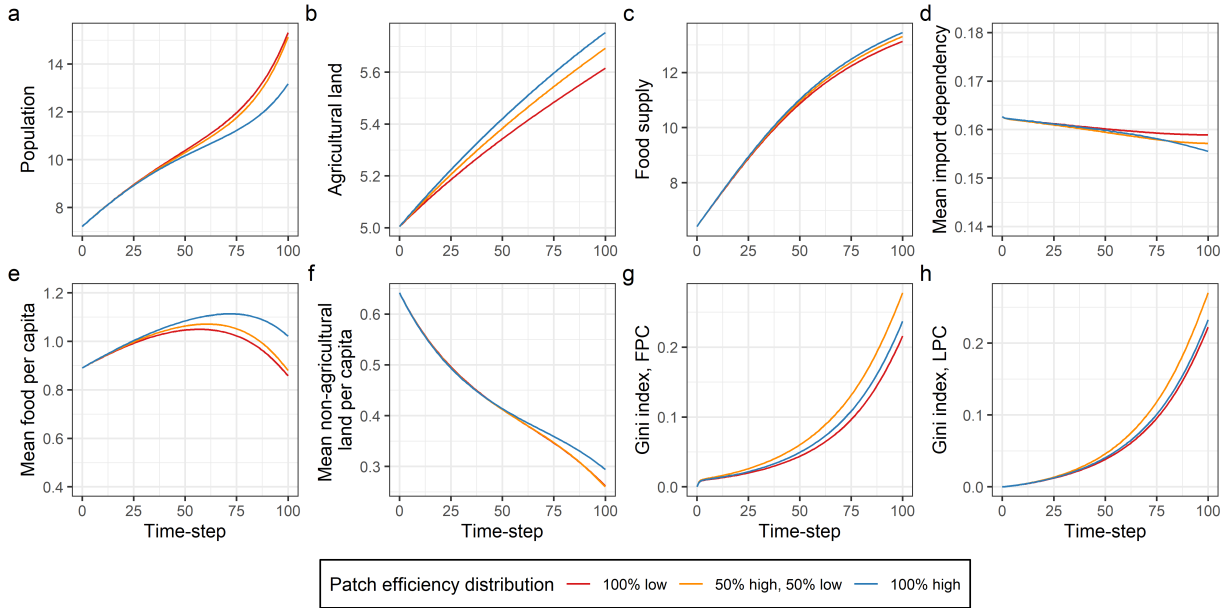

Figure 4.5: **Heterogeneity in patch efficiency impacts system outcomes.** The effect of heterogeneity in patch efficiency on (a) population ($\times 10^7$ people) (b) agricultural land ($\times 10^7$ hectares) (c) food supply ($\times 10^7$ tonnes) (d) mean level of import dependency, mean per capita (e) food (tonnes/person) and (f) non-agricultural land (hectares/person) and Gini index, per capita (g) food and (h) non-agricultural land.

In the heterogeneously parametrized network, high efficiency patches tend to have lower populations and higher food and non-agricultural land per capita (Figure 4.6a, e, f) than those with low efficiency (and as compared to high efficiency patches in a homogeneously parametrized network). While high efficiency patches benefit, low efficiency patches lose out; they have larger populations, and lower food and non-agricultural land per capita values than low efficiency patches in homogeneously parametrized networks. These trends persist throughout the time-span we consider, with the gaps in outcomes widening over time (Figure 4.6) resulting in increasing Gini index values (Figure 4.5g, h).

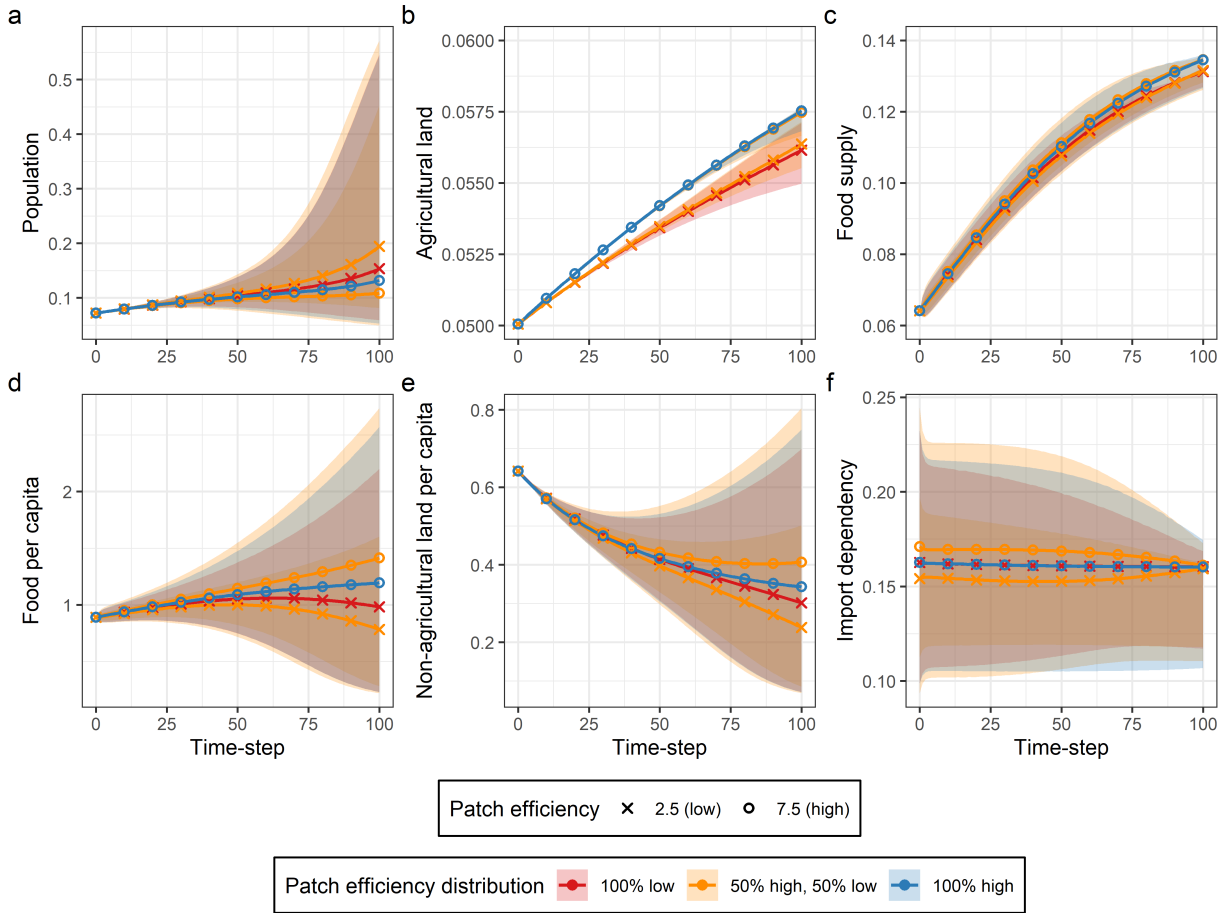

Figure 4.6: **Heterogeneity in patch efficiency impacts patch-level outcomes differently for high- and low-efficiency patches.** The effect of heterogeneity in patch efficiency on (a) population ($\times 10^7$ people) (b) agricultural land ($\times 10^7$ hectares) (c) food supply ($\times 10^7$ tonnes), per capita (d) food (tonnes/person) (e) non-agricultural land (hectares/person) (f) import dependency. Lines indicate the mean outcome for patches by (patch efficiency/efficiency distribution) group, ribbons the range of possible outcomes across all patches in that group.

Finally, we consider how patch efficiency interacts with node degree to influence patch-level outcomes (Figure 4.7) focusing on per capita food and non-agricultural land. We fit separate linear regressions for groups of points belonging to each combination of patch efficiency and high efficiency proportion. Regardless of the parametrization, centrality in the network is important to obtaining high per capita outcomes (Figure 4.7e,f). However, depending on how simulations are parametrized, the spread in outcomes between patches

located on the most and least central nodes in a network varies (i.e. there are differences in the slopes of the linear regressions between groups). In simulations with heterogeneously parametrized patches, high efficiency patches gain more by being more central, and low efficiency nodes less, than in simulations where all patches have the same efficiency. Thus, this heterogeneity in efficiency provides an advantage to the high efficiency nodes.

Discrepancies in per capita outcomes caused by heterogeneous parametrization are substantially smaller than those resulting from differences in network centrality. For example, the gap in food per capita between the most centrally located high efficiency patch under different parameterizations (0.256 tonnes/person) is substantially smaller than between the least and most centrally located high efficiency patch under the same parameterization (1.86 or 1.93 tonnes/person), as shown in Figure 4.6e. Considerations of low efficiency patches and/or differences in non-agricultural land per capita result in similar outcomes.

High efficiency patches are more quick to expand their agricultural area in response to demand, and thus tend to have more agricultural area (Figure 4.7b). Being positioned on a less central node results in a patch having a larger agricultural land area. These differences are quite small, however they are slightly more pronounced for low efficiency patches. Patches located less centrally cannot obtain as much food through trade and must do so through agricultural expansion. Unsurprisingly, these patches also tend to have lower levels of import dependency (Figure 4.7d).

Finally, the level of non-agricultural land per capita in patches located on nodes at the periphery of the network is a cause for concern (Figure 4.7f). The least central low-efficiency nodes have less than 0.06 ha of non agricultural land per capita, below the current global average for urban area required per capita [228, 16]. These patches have populations that would be experiencing housing issues due to lack of available land, and additionally would have lost substantial amounts of natural land-states as they would need to be converted for urban land-use.

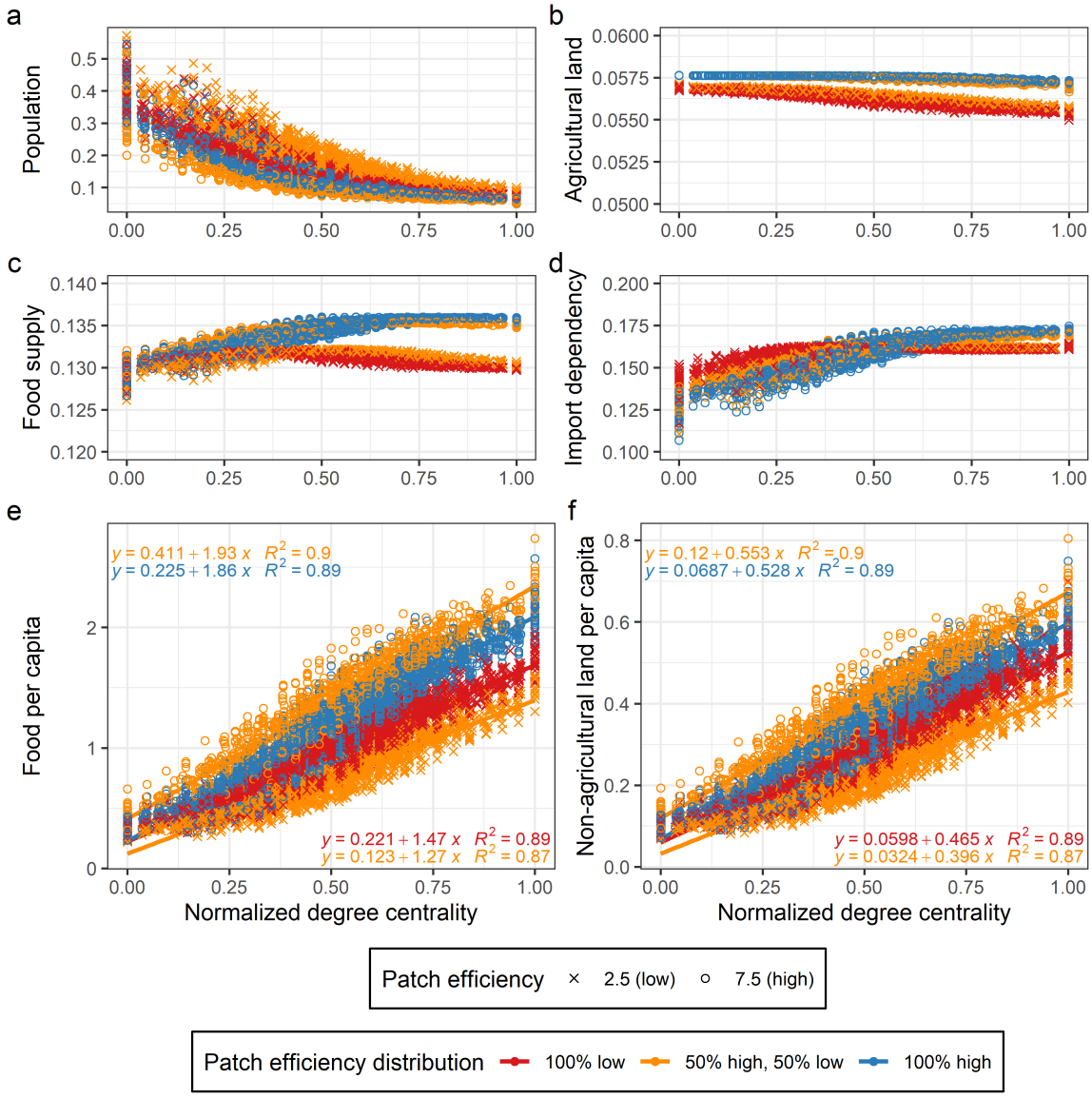

Figure 4.7: **Inequalities due to differences in patch efficiency compound those stemming from differences in node centrality.** Combined effects of patch efficiency level, node centrality on (a) population ($\times 10^7$ people) (b) agricultural land ($\times 10^7$ hectares) (c) food supply ($\times 10^7$ tonnes) (d) import dependency, per capita (e) food (tonnes/person) and (f) non-agricultural land (hectares/person). Analysis of covariance tests for FPC and LPC as functions of normalized degree centrality show models controlling for interaction between patch efficiency and high efficiency proportion outperform those controlling only for patch efficiency or high efficiency proportion (in all cases $p < 2.2 \times 10^{-16}$) [54, 64].

Heterogeneous import behaviour

We consider a simple case where $\gamma_i^A = \gamma_i^I = \gamma = 7.5$, $\beta_i^A = 0.25 \; \forall \; i \in \{1, \ldots, N\}$, but 50% patches have a β^I from the region of the (β^I, β^A) plane where outcomes between patches are highly unequal ($\beta_i^I = 0.25$) while the remainder have $\beta_i^I = 1.25$ from a region with low inequality (Figure 4.2m-p). A smaller β_i^I value indicates that a higher level of food per capita must be attained for import demand to fall below 50%. As these low β_i^I values result in unequal outcomes in a homogeneously parametrized simulation, we call patches where $\beta_i^I = 0.25$ "greedy". If $\beta_i^I = 1.25$ patches have much lower import demand at high levels of food per capita than when $\beta_i^I = 0.25$. Due to this, we dub these $\beta_i^I = 1.25$ patches "restrained". In a homogeneously parametrized simulation where $\beta^I = 1.25$, low-inequality outcomes are attained that have higher food per capita than if $\beta_i^I = 0.25$. Patches are randomly assigned either the "greedy" or the "restrained" β_i^I-value, so there is no correlation between nodes based on patch import behaviours.

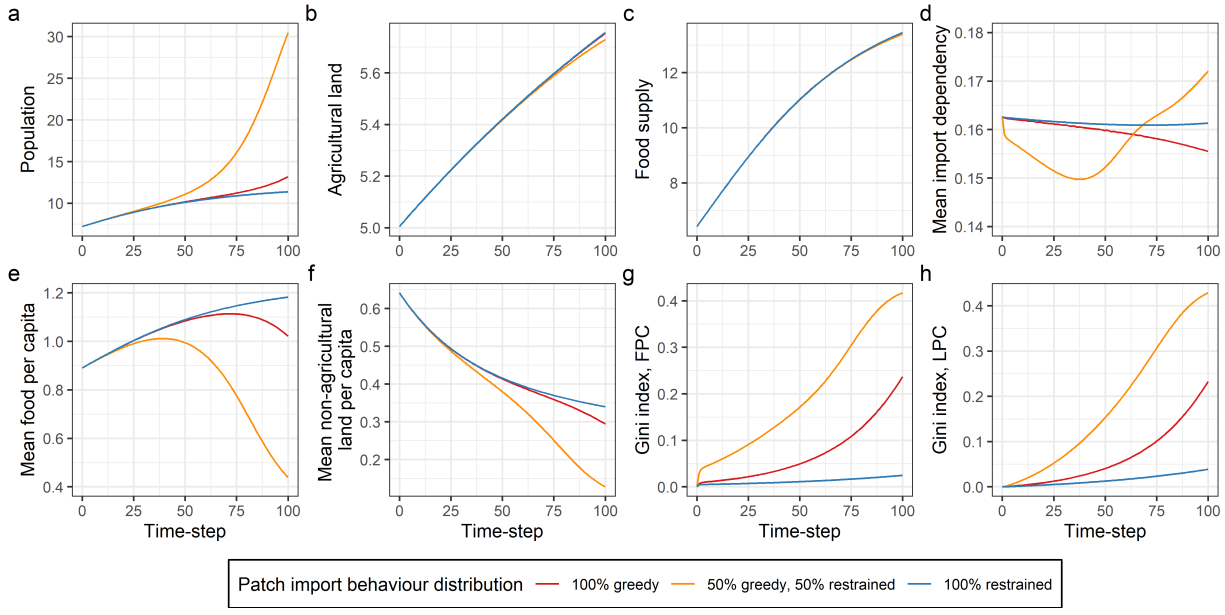

Figure 4.8: **Heterogeneity in patch import behaviours impacts system outcomes.** The effect of heterogeneity in patch import behaviours on (a) population ($\times 10^7$ people) (b) agricultural land ($\times 10^7$ hectares) (c) food supply ($\times 10^7$ tonnes) (d) mean level of import dependency, mean per capita (e) food (tonnes/person) and (f) non-agricultural land (hectares/person), and Gini index, per capita (g) food (h) non-agricultural land.

Global behaviour in the heterogeneous simulations departs substantially from that displayed in homogeneous simulations. Here, a spike in population occurs, driven by decreases in per capita food levels, and is accompanied by increases in inequality and decreases in non-agricultural land per capita (Figure 4.8). Initially increasing trajectories for mean food per capita under the 100% "greedy" and 50/50 split parameterizations do not persist, with a particularly pronounced downturn under the 50/50 split parameterization.

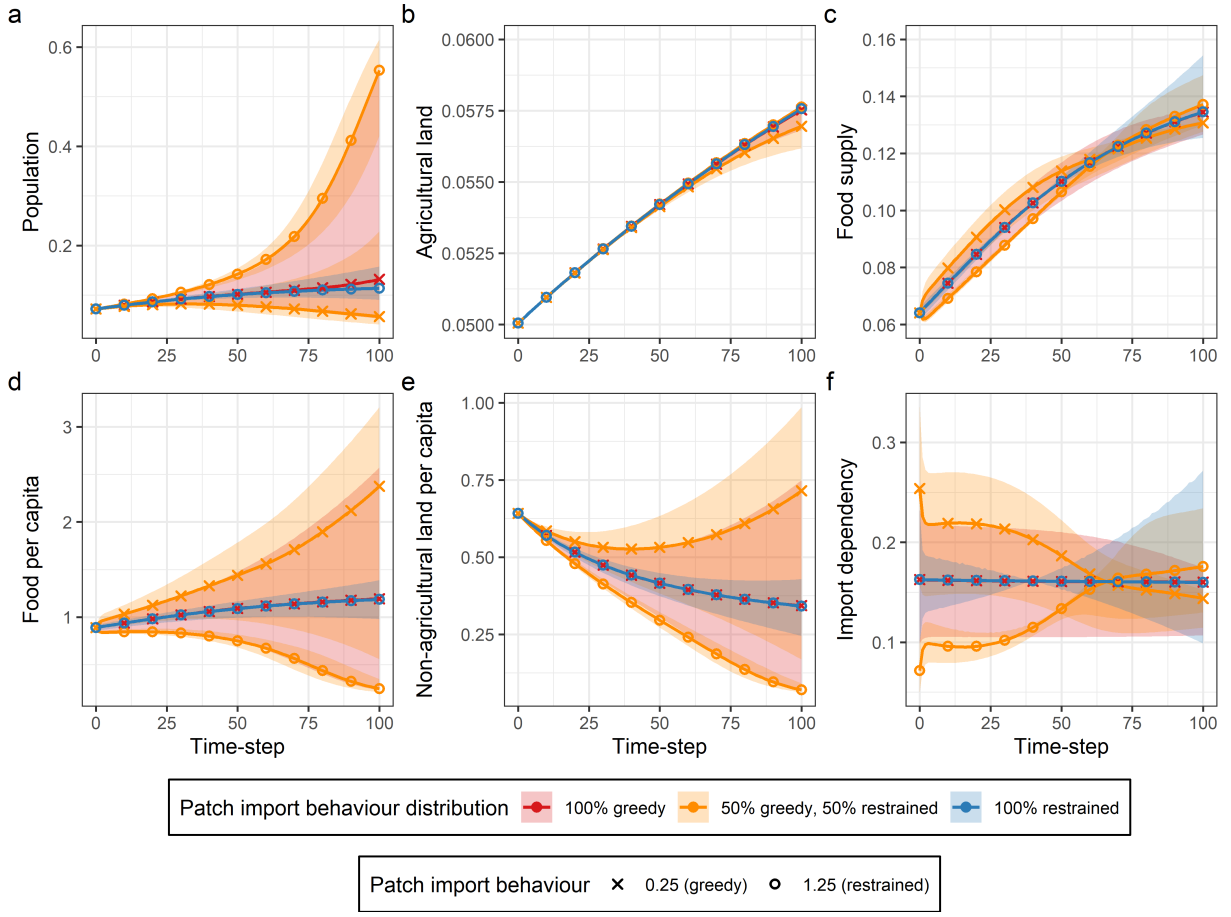

Figure 4.9: **Heterogeneity in patch import behaviour impacts patch-level outcomes.** The effect of heterogeneity in patch import behaviour on (a) population ($\times 10^7$ people) (b) agricultural land ($\times 10^7$ hectares) (c) food supply ($\times 10^7$ tonnes), per capita (d) food (tonnes/person) (e) non-agricultural land (hectares/person) (f) import dependency. Lines indicate the mean outcome for patches by (patch import behaviour/import behaviour distribution) group, ribbons the range of possible outcomes across all patches in that group.

The substantial inequalities in both food and non-agricultural land per capita in the heterogeneously parametrized simulations stem from the fact that though "greedy" patches obtain high food per capita values and undergo a demographic transition, "restrained" patches get caught in a feedback loop between decreasing food per capita and increasing net growth rates (Figure 4.9). While the "greedy" patches obtain substantial amounts of food through import from the start of the simulations, these "restrained" patches do not begin to ramp up their imports until approximately 25% of the way through. They only attain import dependence similar to that experience in homogeneously parametrized networks at the 60% mark. Their unwillingness to import food unless it becomes scarce means that they lose out to the "greedy" patches and experience notably worse outcomes.

For "restrained" patches, who import sparingly as compared to their "greedy" neighbours, centrality to the trade network provides a minor advantage (Figure 4.10e). The effects for "greedy" patches are much larger due to their tendency towards high import demand. The benefit of heterogeneous parametrization for "greedy" patch outcomes is marked. To obtain at least as much food per capita as the least-central "greedy" patch in the heterogeneously parametrized simulations, a "greedy" patch in a homogeneous simulation must be on a node with a degree centrality value in the top 29%. In contrast, all "restrained" patches are worse off than they would be in a homogeneously "restrained" parametrization, and than their "greedy" counterparts in the heterogeneous simulations.

Centrality also impacts agricultural land areas, particularly for "greedy" patches (Figure 4.10b). In both heterogeneously and homogeneously parametrized simulations, "restrained" patches have roughly the same agricultural area regardless of centrality. However, "greedy" patches that are more central tend to have less agricultural land. One consequence of this is that the "restrained" patches in heterogeneously parametrized simulations have very little non-agricultural land per capita due to their large populations. As a result, housing their populations would leave them with very little area for natural land-states. The same is true for the least central "greedy" patches in a homogeneously parametrized simulation.

We experiment with different proportions of greedy patches (Figure 4.11, Figure 4.12) to further explore these effects. Inequality in the system is at its height when 75% of patches are "greedy" (Figure 4.11g,h). While below 75% reducing the proportion of "greedy" patches leads to decreased inequality overall, this is not accompanied by an increase in the average per capita food and non agricultural land until $< 25\%$ of patches are 'greedy".

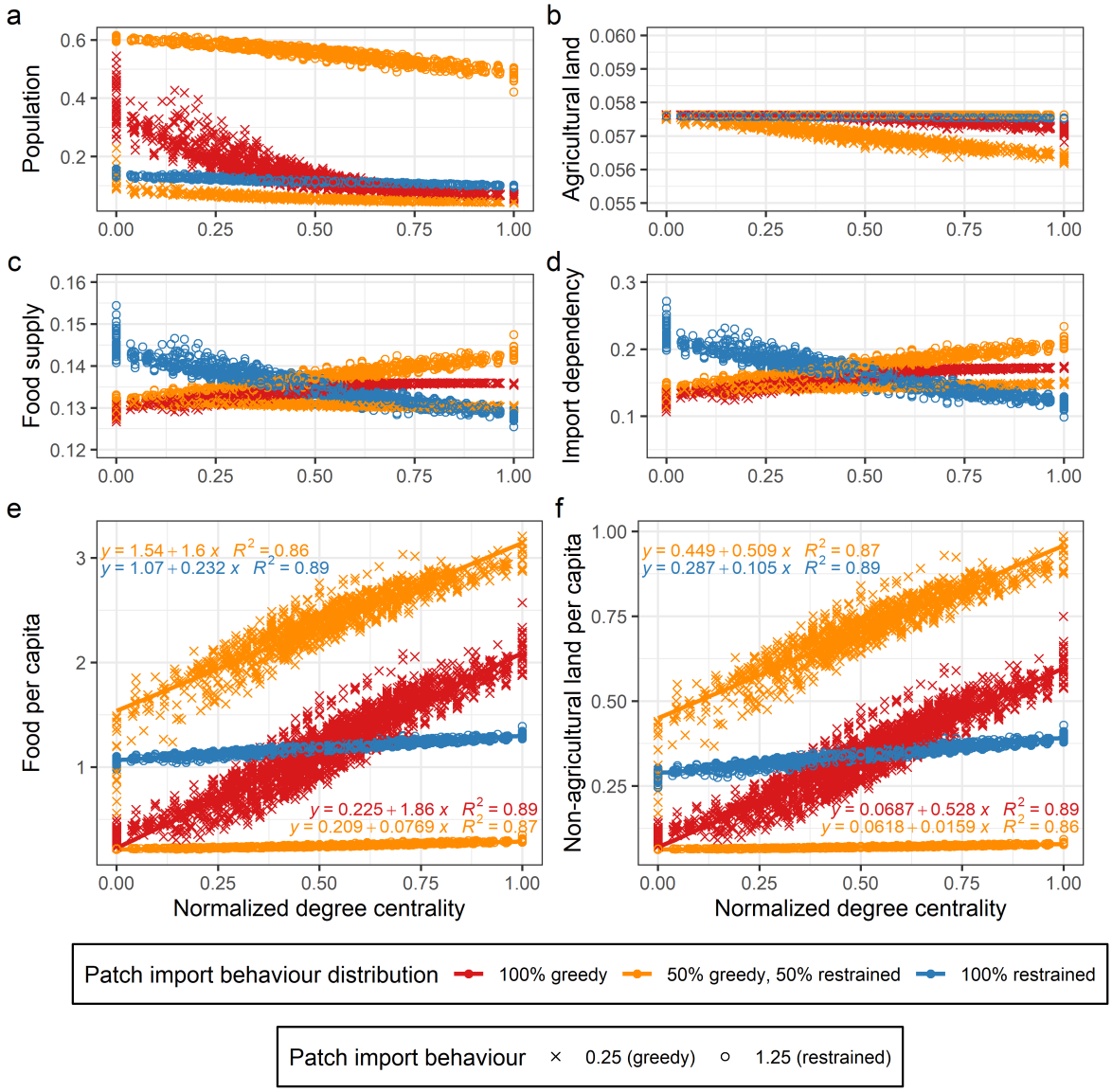

Figure 4.10: **Inequalities due to differences in patch import behaviour are substantial and interact with those caused by node centrality differences.** Combined effects of patch import behaviour, node centrality on (a) population ($\times 10^7$ people) (b) agricultural land ($\times 10^7$ hectares) (c) food supply ($\times 10^7$ tonnes) (d) import dependency, per capita (e) food (tonnes/person) (f) non-agricultural land (hectares/person). Analysis of covariance tests for FPC and LPC as functions of normalized degree centrality show models controlling for interaction between patch import behaviour and proportion of greedy patches outperform those controlling only for patch import behaviour or proportion of greedy patches (in all cases $p < 2.2 \times 10^{-16}$) [54, 64].

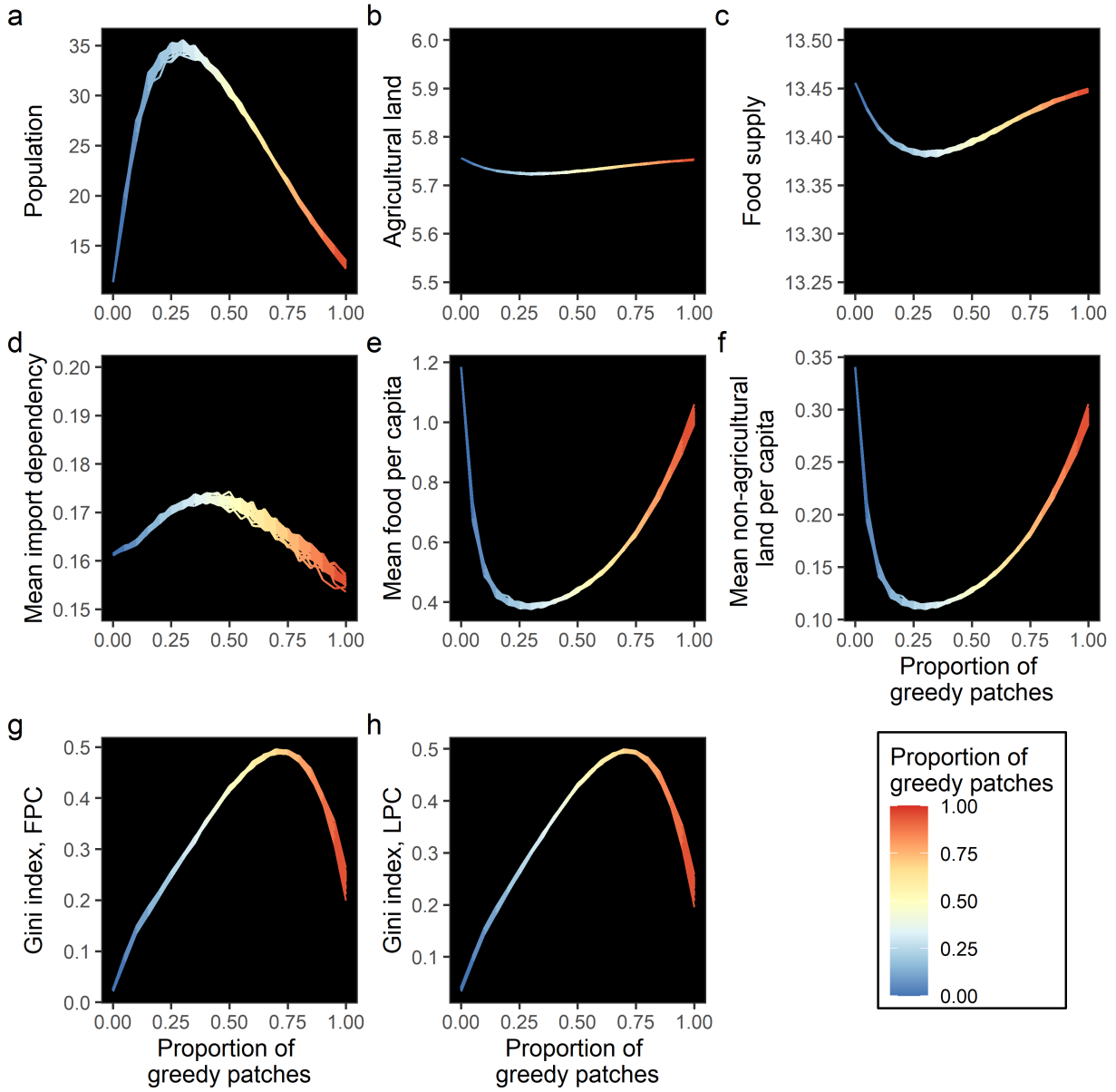

Figure 4.11: **Proportions of patches with different import behaviours impact system outcomes.** Effect of different proportions of patches with "greedy" and "restrained" import behaviours on (a) population ($\times 10^7$ people) (b) agricultural land ($\times 10^7$ hectares) (c) food supply ($\times 10^7$ tonnes) (d) mean level of import dependency, mean per capita (e) food (tonnes/person) (f) non-agricultural land (hectares/person), and Gini index, per capita (g) food (h) non-agricultural land.

It becomes increasingly advantageous to be a "greedy" patch as the proportion of "greedy" patches decreases. The fewer "greedy" patches there are, the higher the food and non-agricultural land per capita they can attain (Figure 4.12d,e). Patches with "restrained" behaviour also benefit as the proportion of greedy patches decreases, though the increases in their per capita outcomes for some percentage reduction in "greedy" patches is much lower than for "greedy" patches. Especially at low proportions of "greedy" patches, "restrained" patches bear more responsibility for food production (Figure 4.12b).

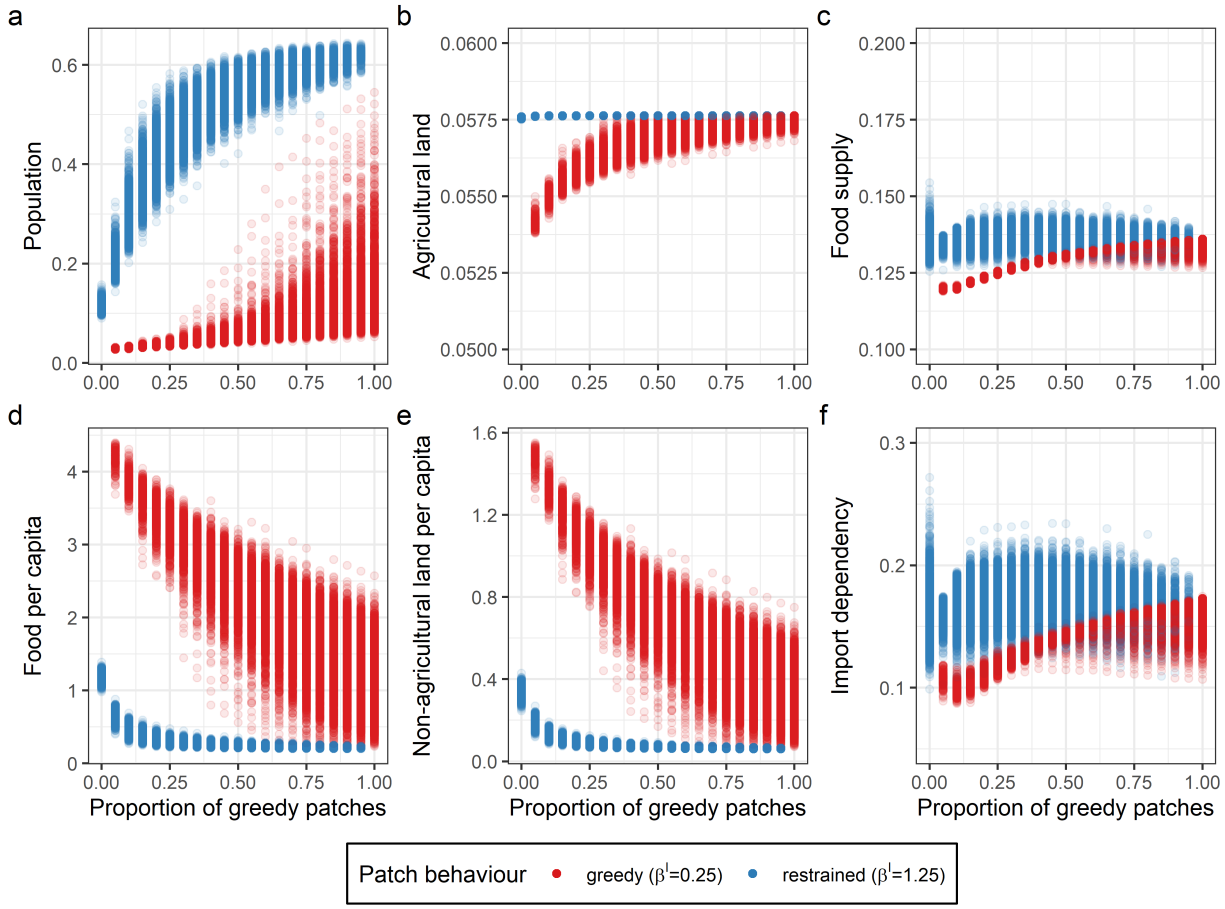

Figure 4.12: **"Restrained" patches lose out in metapopulations where "greedy" patches are present.** The effect of different proportions of patches with "greedy" and "restrained" import behaviours on patch-level (a) population ($\times 10^7$ people) (b) agricultural land ($\times 10^7$ hectares) (c) food supply ($\times 10^7$ tonnes), per capita (d) food (tonnes/person) (e) non-agricultural land (hectares/person) (f) import dependency.

4.4 Discussion

This study explores how the coupled dynamics of human population growth and food production systems are impacted by trade. We developed and analysed a simple metapopulation model that expands on previous work in this area (e.g [81, 82], amongst others) to incorporate land-use dynamics and demographic transitions in human populations. We consider both how the behaviour of trading entities (patches) and the topology of the network on which trades occur impact system outcomes. Much of this discussion focuses on the linked ideas of equality (in access to food, as well as land for housing and natural land states), food security, and sustainability [214, 212].

Metapopulations trading on larger networks experience lower levels of inequality, in terms of food and non-agricultural land per capita. This is likely due to the structure of small-world networks, where even as network size increases, maximal path-lengths between nodes remain relatively low. This facilitates increasingly efficient redistribution of resources with larger network sizes, as noted by Dolfing *et al.* [82]. Centrality in the network is found to be key to patches attaining high food per capita, consistent with results from a previous model [82]. As such, a regular network structure where all nodes are equally central eliminates inequalities resulting from network topology.

Despite the fact that regular network structure results in low levels of inequality, this topology may be impracticable for some real-world trade networks. Countries tend to specialize their production, so certain goods will need to be imported even at high levels of food per capita [269]. There are costs (economic, environmental, etc.) associated with the transport of goods (e.g. with creating and maintaining edges between nodes). Thus, having short average path lengths between nodes helps minimize the cost of obtaining these necessary imports while allowing for efficient redistribution of goods [134, 159, 326]. The structure of regular networks means that unless they have a high edge density (which will have associated costs to maintain), they will tend to have longer average path lengths than small-world networks of an equivalent size and density [320, 292]. Thus, if your neighbours in a regularly structured agri-food trade network do not possess the good you need to import, the cost of doing so may become quite substantial. Small-world networks appear to provide a reasonable compromise between efficient (and cost-effective) food distribution and the minimization of inequality.

During simulations with heterogeneous efficiency, high efficiency patches enjoy a transition to more slowly growing populations with higher food and non-agricultural land per capita. In contrast, low efficiency patches are caught in a "poverty trap" [15] where they experience a feedback loop between increased population growth and decreased food

per capita. This results in large populations and the persistence of low food (and non-agricultural land) per capita for these patches. Low efficiency patches could be thought of as representing countries or cities where the agents (government, corporations, etc.) that oversee changes to agricultural land area and trade flows provide poor governance and/or are hampered by corruption, creating cross-patch inequities. This discrepancy in patch-level efficiency exacerbates inequalities resulting from network topology. The case of a metapopulation where some patches pursue a "greedy" import strategy, while others are "restrained" is similar. Restrained patches fall into a "poverty trap" more severe than that experienced by low efficiency patches in heterogeneously parametrized simulations.

This suggest that, in a scenario where patches can switch import behaviour during a simulation run, even a low initial percentage of "greedy" patches could drive the system towards a state where all patches are "greedy". Tackling the issue from the opposite end, namely a metapopulation where there are few "restrained" patches, we see a similar problem with attaining 100% "restrained" patches. Even if individual patches switch to a "restrained" behaviour with a goal of improving overall equality and per capita outcomes, they would both need to endure an initial bump in inequality in the 75%-100% "greedy" region, and succeed in convincing at least 75% of patches to adopt a "restrained" behaviour.

In addition to the consequences for food security and inequality we explore in these scenarios, other socio-economic factors may compound these impacts. Previous studies have shown that poor countries tend to feel the effect of shocks in trade networks most severely, as they often depend on a small number of large exporters [79, 85, 74, 238]. Though we do not consider shocks in this model, we might expect that patches at the periphery of the trade network – which are already experiencing food insecurity due to low availability – would have this exacerbated by vulnerability to shocks.

These peripheral patches also tend to bear more of the weight of agricultural production. When some patches pursue a "greedy" import strategy while others are "restrained", the "greedy" patches lean on imports from "restrained" patches and are thus able maintain smaller agricultural land areas. This highlights the real-world phenomenon of a displacement or "leakage" effect, wherein countries increase imports to meet demand while protecting their natural land states. The effect of this is the displacement of agricultural land expansion to other countries. If these countries have weaker protections for natural land states (e.g. displacement from developed to tropical countries) this can have serious environmental impacts [177, 276].

Issues of food security, equality, and the sustainable use of land-based ecosystems are central to the Sustainable Development Goals (SDGs) established by the United Nations (UN) [212, 214]. This works demonstrates that the dynamics of human metapopulation

interactions on agri-food trade networks are crucial to the success or failure of sustainable development. Interventions to the system that reduce inequalities in food supply and result in improvements to food security, while avoiding the disappearance of natural land states, would constitute progress towards the SDGs.

Effective strategies for reducing inequality and improving food security in the system depend heavily on the drivers of inequality. When all patches are identically parametrized, inequalities arise solely from differences in network centrality. Here, working towards parity in centrality measures by creating a more regular network structure will reduce inequality and enhance food security. Similarly, given the relative magnitudes of the inequalities stemming from network topology and differences in efficiency between patches, network restructuring would provide the largest gains in equality and food security in that scenario. Once parity or near-parity is achieved (i.e. the gap in food per capita between patches on the most and least central nodes a network is on par with that between heterogeneously and homogeneously parametrized networks), measures involving adjustments to patch level efficiency may be worth pursuing. However, when inequalities result from differences in patch import behaviour, it makes sense to change patch behaviour before restructuring the network. Here, changes to network topology could be considered once behaviour differences are minimized. While none of these interventions substantially impact the global agricultural land area required to feed the human population, they would result in a more even distribution of agricultural land between patches. This outcome does not, of course, preclude the unsustainable use of ecosystems within patches. However, it does reduce the likelihood of high stress to ecosystems within specific patches, namely those shouldering a disproportionate share of the responsibility for food production. Thus, improved environmental sustainability could be an additional benefit of these interventions.

Reductions in inequality (accompanied by increased food security) through adjustments to patch behaviour may prove more expedient to implement, as they would not require large-scale network restructuring. However, as the scenario of "greedy" and "restrained" behaviour demonstrates, this could require substantial sacrifices from the patches altering their behaviour. On the other hand, changes to network topology would likely prove difficult due to the necessity of a coordinated effort by a large numbers of patches. Despite this, there are potential added benefits from interventions which alter network topology. Previous work indicates that node (patch in our model) resilience to shocks and resource variability can be improved by increasing the number or diversity of trade partnerships that node engages in [191, 82]. It has additionally been suggested that increasing the number of nodes in a network can improve resilience [82]. The potential for increased patch-level resilience through partnership addition/diversification could motivate patches to engage in small-scale efforts at network restructuring.

One clear avenue for extending the model is allowing patches to switch their import behaviour during the simulation run based on the relative payoffs of a "greedy" vs. "restrained" strategy. Models of dynamic strategy switching in human populations already exist for a variety of applications, including vaccination behaviour [25], climate change mitigation [46], and conservation of natural land-states [136]. As such, they are well-established in the literature and could easily be adapted for our purposes. Other extensions to this model could incorporate a variety of modifications for enhanced realism. The incorporation of a dynamically evolving network model akin to that developed in [97] would improve our understanding of how changes to network structure in an increasingly globalized world impact outcomes. Including a broader range of land-use types (urban areas, etc.) similarly to [228], would provide more information on the potential for land scarcity as the human population expands over the remainder of the 21st century. Finally, the inclusion of dynamically varying parameters for mechanisms such as agricultural expansion (similar to [246]) would make longer simulation runs more justifiable, allowing us to explore long-term system behaviours.

Our model could be used to explore scenarios pertinent to themes from the UN SDGs, including food security, equality, sustainable ecosystem use, and climate change mitigation [212, 214]. For example, we could investigate the impact of shocks to the network structure (resulting from armed conflict, trade wars, disease, etc.) on system food security and equality [97]. Alternatively we could explore how climate change interacts with land use and human population growth to influence food security, equality, and land use. Changes to patch-level dynamics such as fluctuations in food availability caused by climate variability under climate change (as in [82]) may be examined. Climate change scenarios could also include alterations in the availability of land suitable for agriculture and in yields, along with feed-backs between agricultural land-use/production and climate [104, 270, 123, 231]. This latter aspect would provide greater insight on strategies for climate change mitigation as a component of sustainable development.

Given the wide range of confounding factors that must be accounted for when designing resilient and equitable food systems, modelling is a useful tool for identifying key areas for improvement. This work demonstrates the efficacy of simple differential equation models for exploring the dynamics of human metapopulations linked through trade. The insights gained from simulating scenarios using such models will enhance our understanding of the challenges for sustainable development facing humanity as we approach 2100.

Chapter 5

Conclusion

The aim of this thesis was to use modelling techniques to explore the dynamics of several real-world complex systems. The topics explored – trade, land use, climate change, human population growth – are relevant to our understanding of potential futures for humanity in the 21st century. Our analysis placed an emphasis on gaining insight into the trajectories of these systems, given the multitude of impediments that must be overcome to succeed in sustainable development. We begin our conclusion with an overview of the complex behaviours exhibited in our modelled systems, and then transition to a discussion of the larger implications of this work within a sustainability framework. Finally, we put forth our closing remarks and suggest potential future work in this area.

5.1 Complex systems behaviour in modelled systems

This trio of models highlights the complexity of real-world systems, and the difficulties faced by those seeking to predict and influence their behaviour. In all 3, highly stylized descriptions of the behaviour of system components gave rise to complicated - and in some cases unintuitive - dynamics. All of the modelled systems displayed numerosity, with many components engaging in a myriad of interactions. However, as this is the most intuitive concept related to complex systems, we do not discuss it in great depth. We instead focus on a discussion of the remaining traits of complex systems introduced in Chapter 1, and the linked ideas of robustness, resilience, and vulnerability in complex systems.

Our model of the dynamic evolution of trade networks highlighted the complicated higher-level behaviours that emerge from simple interactions between components in complex systems. A basic preferential attachment mechanism, whereby new nodes entering the

network had a bias towards establishing trade partnerships with highly connected nodes, gave rise to complex network structure mimicking that of the real-world wheat trade network. The effect of feedbacks was also apparent; with preferential attachment, nodes with high centrality are more attractive to prospective trade partners and thus accumulate even more trade partnerships, creating a positive feedback loop.

By applying shocks to our modelled trade networks we were able to explore one aspect of their resilience, and observe how that resilience evolved over time. We discovered that these networks become more resilient to shocks as they grow. However, this work emphasized that, despite this, their resilience is still quite low and shocks may have significant and lasting effects on the structure of the system. Additionally, we noted that the response of components (nodes) within the system to shocks reduced their vulnerability to future occurrences of the same.

Our simulated mosaics display numerous hallmarks of complex systems. The fire-mediated threshold to recruitment imitates the feedbacks in real world systems where when forest cover is higher, the impact of fire on forest recruitment is lessened, in turn resulting in increased forest cover. Non-linearities abound, from the abrupt decrease in forest recruitment at low levels of forest cover as a result of the fire-mediated threshold to recruitment, to the response of the fire-mediated threshold and forest recruitment rates to climate change driven variations in precipitation. The self-organization of forest patches into configurations that facilitate their persistence despite the presence of disturbances (fire, etc.) results in the emergence of complex spatial patterns at the landscape scale.

While the forest clusters in this system evolve towards configurations that are robust to perturbations, the system as a whole is fragile. Mosaics persist under only a small range of environmental conditions even in the absence of climate change effects. Scenarios where climate-driven increases in precipitation are substantial result in the partial or complete loss of mosaic ecosystems. Additionally, mosaics that endure in scenarios with more modest increases in precipitation show substantially altered spatial structure.

Feedbacks, both linear and non-linear, drive the dynamics of our metapopulation model. The interaction of patches through trading mechanisms results in diverse outcomes, both globally and locally. Outcomes at the global level are impacted by, and impact, outcomes at the patch level. Though not explicitly modelled, patch-level outcomes will have impacts, at a lower level of the hierarchy, for the human populations occupying them.

This model demonstrates how heterogeneity – in network topology and/or in patch level characteristics – can result in inequalities that create vulnerabilities in the system. Uneven distribution of food across the trade network may leave individual patches at a disadvantage in the face of food shortages. Additionally, patches that bear a disproportionately large

amount of responsibility food production may find their natural ecosystems at risk due to the expansion of agricultural land area. However, interventions that alter the topology of the trade network, or aim to reduce heterogeneity in patch-level behaviour may make these systems more robust.

5.2 Broader implications for sustainability

The implications of this work for sustainability are wide ranging. Food security, equality, and the conservation of valuable ecosystems are central to the motivation for the projects presented here, and to achieving sustainable development. Underpinning all of this is the question of how to work towards these goals in an age of climate change. Policy to meet the challenge of this question will need to be holistic, and empirically supported. When data is sparse, or non-existent - as in the case of providing future projections - modelling approaches are a useful tool for building this support.

Both our dynamic trade network model and metapopulation model consider how food security is impacted by network structure. In our dynamic trade network model, shocks to the trade network result in the disruption of food trade flows. Such disruptions would create food shortages at nodes within the network (representing countries), reducing the stability of their food access, and thus their food security. The definition of resilience we explored in this model is a measure of the extent to which shocks to the network damage its structure. Resilience has major implications for food security; networks with low resilience will experience large structural changes, and thus significant impacts on their ability to redistribute food efficiently. Our work indicated that the resilience of the wheat trade network is low (though increasing). Given that wheat is a staple crop around the world, a lack of resilience in this network could reverberate through the entire global food system.

Issues of inequality and poverty may also arise in relation to shocks. Previous studies have shown that shocks to trade networks have a disproportionately large impact on poor countries, due to cross-country income inequalities [79] and their reliance upon a small number of trade partners [85, 74, 238]. Thus, not only do shocks impact food security, they have a disproportionately large impact on poorer countries, contributing to global inequalities. While we do not explicitly model shocks in our metapopulation model, we might think of the patches that experience food insecurity due to a lack of availability and are positioned on nodes at the periphery of the network, as analogous to poor countries. These patches would experience additional food insecurity as a result of the temporal instability in their access to food imports.

Inequalities in access to non-agricultural land (e.g. urban area, natural land states) are also rampant in our metapopulation model results. Due to being on the periphery of the network, or possessing characteristics such as low efficiency or a "restrained" importing behaviour, certain patches experience low levels of non-agricultural land per capita. As there are limits on the minimum land area required to house a human population, this likely indicates the loss of natural land states in these patches, which will have serious ecological implications. In severe cases, where the per capita level becomes extremely low, this could also result in overcrowding within the patch due to high population densities. Equity may also be an issue in systems where patches have different levels of efficiency. Inefficiency in response to changes in food per capita could be caused by factors such as poor governance or corruption (by/within governments, corporations, etc). In this case, the resulting disparities would be issues of inequity, not inequality.

In metapopulation simulations, some patches – by virtue of their "greedy" import behaviour or centrality to the network – are able to maintain high levels of food and non-agricultural land per capita. They pass on the responsibility of food production to other patches, and are able to retain large areas of non-agricultural land. Given their small population sizes, and thus minimal need for large urban areas, these patches are likely able to conserve large tracts of natural land states. These patches are analogous to countries that introduce protections for natural land states and supplement their food stocks through increased imports as opposed to agricultural expansion [177]. This is known as the displacement, or "leakage" effect [202, 177]. In some cases, countries are even able to reduce their agricultural area and engage in reforestation [202]. The consequence of their actions is the expansion of agricultural land area in countries that are less able to protect natural land states (e.g. developing nations). This can have severe environmental impacts, such as when the demand for agricultural products is met by tropical countries who engage in deforestation to expand agricultural land area [177, 202].

Our model of forest-grassland mosaics is the project that most directly addresses the challenges of climate change. It demonstrates the fragility of these ecologically valuable ecosystems to climate change. The loss of mosaics would significantly impact biodiversity in Southern Brazil, and could have ramifications for the persistence of endangered and endemic species such as *Araucaria angustifolia*, the Paraná pine. However, climate change is a common thread throughout this thesis. Manifestations of climate change impacts, such as severe weather effects, changing patterns of disease, or climate-influenced armed conflict, might all result in disruptions to the global food system [9, 218, 138]. This could play out through shocks to the trade network, alterations to agricultural yields, or changes to the availability/viability of land for agriculture. The effects of these disturbances will be felt by human populations and the distribution of associated costs is likely to be uneven.

These results highlight barriers to sustainable development, and in particular the UN Sustainable Development Goals (SDGs) [214, 212]. The goal of ending hunger may be impeded by food insecurities arising from shocks to agri-food trade networks. These networks are, as of yet, not particularly resilient and have topologies that contribute to inequalities in per capita food supply. This lack of food security will have ramifications for sustainable development goals pertaining to education and poverty [99, 33, 158, 79, 85]. Environmental sustainability may also be hampered by climate change impacts on ecologically valuable ecosystems, such as forest-grassland mosaics [31, 209, 227, 31, 275, 136], and the environmental cost of trade patterns that result in the loss of natural land states [177, 202].

Though these challenges are substantial in magnitude, our work presents some avenues for facilitating sustainable development. First, restructuring of trade networks for increased equality and resilience [191, 82] could help enhance global food security and promote positive outcomes for the eradication of poverty and improved access to quality education [99, 33, 158]. However, as we highlight in Chapter 4, there may be difficulties with this approach due to the high levels of inequality that occur on the trajectory towards a system where food security and equality are high. Second, we may see a similar range of benefits from the reduction or elimination of disparities in the import behaviours and/or efficiency of agents within food trade networks. Finally, models of forest-grassland mosaics under climate change could aid in optimal site selection for creating protected areas [220], thus contributing to ecological sustainability.

5.3 Closing remarks and future work

These models highlight the challenge of understanding and predicting the behaviour of complex systems. Despite this, it is clear why complex systems modelling has gained such prominence. Models allow us to gain insight into these systems, as they are able to capture unintuitive aspects of their dynamics, such as non-linear feedbacks and the emergence of complex behaviour. Through our model analysis we were able to disentangle some drivers of behaviour in our study systems. However, given the simplicity of these models, it is easy to imagine that performing such an exercise on a real-world system would prove much more difficult.

We emphasize that researchers should resist the temptation to instinctively assume that complex systems require complex models. Not only will this introduce the potential for over-fitting, making model results difficult to generalize, it may also reduce the clarity of insight that can be gained from modelling techniques. Given the complex behaviours demonstrated in our models, it is unlikely that any meaningful insight would result from

attempting to incorporate a high level of detail without a strong understanding of basic system dynamics. Thus, we stress that ramping up model complexity without first exploring the potential of parsimonious models is a flawed approach.

In his seminal 1959 paper, "The science of muddling through", Charles E. Lindblom asserted that any policy change should be incremental, due to the complexity of the decision-making space [186, 203]. This has been pointed to as a reasonable guideline for approaching complex systems thinking [240]. We believe this advice should also be applied to the modelling of complex systems; models do not need to be revolutionary, rather they should seek to be evolutionary. Additionally, we urge that – where possible – these simple models should utilize empirical data for parametrization and validation. Without this, it is difficult to engender much confidence in the predictions and insights they give rise to.

Given these considerations, we suggest several potential avenues for further modelling projects designed to make incremental improvements on the work presented here. As previously mentioned, adding a dynamic trade network to our metapopulation model would give a fuller view of how the temporal evolution of trade structures interacts with the behaviours of trading agents to influence system outcomes. This could easily be accomplished using a version of our dynamic preferential attachment model modified to describe trade in all agri-food products [97]. Another possibility would be the incorporation of direct anthropogenic effects into our mosaic model (e.g. deforestation, etc. for agricultural land use) by a demand-driven mechanism similar to that for non-agricultural land conversion in our metapopulation model. This could additionally incorporate the effects of external demand on the conversion of natural land states if we also included a metapopulation structure with trade links. Thinking in the opposite direction, we could instead incorporate mechanisms from our mosaic model into our metapopulation model. The addition of dynamic climate effects on agricultural yields and the amount of land suitable and/or available for agricultural use (analogous to the effects on natural land states in a mosaic) could provide us with a view of how global food systems will be impacted by climate change.

Across these extensions, opportunities arise for exploring specific scenarios to enhance our understanding of possible futures and policy effects. We could consider how following the Shared Socioeconomic Pathways (SSPs) – describing socioeconomic trajectories with different levels of sustainable development and associated climate outcomes to 2100 [249, 222] – impacts model outcomes. Different SSPs would correspond to different levels of frequency and severity for climate-driven disturbances (altered patterns of disease, armed conflict, severe weather,etc.) introduced to the models, as well as different parametrizations [9, 218, 138]. Through these experiments, we could observe whether the levels of sustainable development inherent to these pathways translate to commensurate outcomes in our models. Alternatively, instead of assuming fixed socioeconomic pathways to 2100,

we could explore interventions aimed at facilitating sustainable development to ascertain which policies might prove most effective in achievement of the UN SDGs. These interventions could cover a broad range of goals depending on the model structure, from the conservation of natural land states, to climate change mitigation and food security enhancement. This sort of scenario analysis would prove helpful in designing policy for a sustainable future.

The development of more sophisticated models, tailored to specific complex systems and scenarios with relevance to issues of sustainability is essential. Through simulation experiments we can not only gain insight into current and future system dynamics but see the effects of different perturbations and interventions. Thus, models can be used to explore both potential threats to system stability and function, and the strategies used to combat or preempt them. As such, they are important tools for facilitating sustainable development.

References

[1] Francesco Accatino, Carlo De Michele, Renata Vezzoli, Davide Donzelli, and Robert J Scholes. Tree–grass co-existence in savanna: interactions of rain and fire. *Journal of Theoretical Biology*, 267(2):235–242, 2010. 15, 43, 66

[2] European Space Agency. Copernicus open access hub. Retrieved from `https://scihub.copernicus.eu/` August 12, 2018., 2018. 15, 45, 46

[3] Réka Albert and Albert-László Barabási. Statistical mechanics of complex networks. *Reviews of modern physics*, 74(1):47, 2002. 5

[4] Réka Albert, H. Jeong, and Albert-László Barabási. Error and attack tolerance of complex networks. *Nature*, 406(6794):378–382, 2000. 28, 29, 30, 146

[5] Gerald Alexanderson. About the cover: Euler and königsberg's bridges: A historical view. *Bulletin of the american mathematical society*, 43(4):567–573, 2006. 5

[6] Nikos Alexandratos and Jelle Bruinsma. World agriculture towards 2030/2050: the 2012 revision. *ESA Working paper No. 12-03*, 2012. 70

[7] A. Almog, T. Squartini, and D. Garlaschelli. A gdp-driven model for the binary and weighted structure of the international trade network. *New J. Phys.*, 17(1):013009; 10.1088/1367–2630/17/1/013009, 2015. 14, 18, 22, 41

[8] George Alter and Gregory Clark. The demographic transition and human capital. *The Cambridge Economic History of Modern Europe*, 1:43–69, 2010. 73

[9] Sonia Altizer, Richard S Ostfeld, Pieter TJ Johnson, Susan Kutz, and C Drew Harvell. Climate change and infectious diseases: from evidence to a predictive framework. *science*, 341(6145):514–519, 2013. 104, 106

[10] K. Anderson and S. Nelgen. Trade barrier volatility and agricultural price stabilization. *World Dev.*, 40:36–48, 2012. 21, 23, 30, 31, 141, 147

[11] Miguel B Araújo, Richard G Pearson, Wilfried Thuiller, and Markus Erhard. Validation of species–climate impact models under climate change. *Global Change Biology*, 11(9):1504–1513, 2005. 43

[12] Sally Archibald, WJ Bond, WD Stock, and DHK Fairbanks. Shaping the landscape: fire–grazer interactions in an african savanna. *Ecological Applications*, 15(1):96–109, 2005. 49

[13] Sally Archibald, David P Roy, Van Wilgen, W Brian, and Robert J Scholes. What limits fire? an examination of drivers of burnt area in southern africa. *Global Change Biology*, 15(3):613–630, 2009. 48, 49, 50

[14] Robert L Axtell, Joshua M Epstein, Jeffrey S Dean, George J Gumerman, Alan C Swedlund, Jason Harburger, Shubha Chakravarty, Ross Hammond, Jon Parker, and Miles Parker. Population growth and collapse in a multiagent model of the kayenta anasazi in long house valley. *Proceedings of the National Academy of Sciences*, 99(suppl 3):7275–7279, 2002. 71

[15] Costas Azariadis and John Stachurski. Poverty traps. *Handbook of economic growth*, 1:295–384, 2005. 97

[16] Deborah Balk, Francesca Pozzi, Gregory Yetman, Uwe Deichmann, and Andy Nelson. The distribution of people and the dimension of place: methodologies to improve the global estimation of urban extents. In *International Society for Photogrammetry and Remote Sensing, proceedings of the urban remote sensing conference*, pages 14–16, 2005. 89

[17] Albert-László Barabási. Scale-free networks: a decade and beyond. *Science*, 325(5939):412–413, 2009. 28

[18] Albert-László Barabási. *Network science*. Number 59, 64, 236-237. Cambridge University Press, 2016. 5, 8, 28, 182

[19] Albert-László Barabási and Réka Albert. Emergence of scaling in random networks. *science*, 286(5439):509–512, 1999. 5, 7, 9

[20] M. Barigozzi, G. Fagiolo, and D. Garlaschelli. Multinetwork of international trade: A commodity-specific analysis. *Phys. Rev. E*, 81:046104, 2010. 21, 22

[21] Alain Barrat, Marc Barthélemy, and Alessandro Vespignani. Weighted evolving networks: coupling topology and weight dynamics. *Phys. Rev. Lett.*, 92(22):228701, 2004. 41

[22] J. Bascompte, P. Jordano, and J. M. Olesen. Asymmetric coevolutionary networks facilitate biodiversity maintenance. *Science*, 312(5772):431–433, 2006. 28, 30

[23] T. Baskaran, F. Blöchl, T. Brück, and F. J. Theis. The heckscher-ohlin model and the network structure of international trade. *Int. Rev. Econ. Financ.*, 20(2):135–145, 2011. 40

[24] Mathieu Bastian, Sebastien Heymann, and Mathieu Jacomy. Gephi: An open source software for exploring and manipulating networks. 2009. 25

[25] Chris T Bauch. Imitation dynamics predict vaccinating behaviour. *Proceedings of the Royal Society B: Biological Sciences*, 272(1573):1669–1675, 2005. 100

[26] Chris T Bauch. Wealth as a source of density dependence in human population growth. *Oikos*, 117(12):1824–1832, 2008. 72, 73

[27] Chris T Bauch, Ram Sigdel, Joe Pharaon, and Madhur Anand. Early warning signals of regime shifts in coupled human–environment systems. *Proceedings of the National Academy of Sciences*, 113(51):14560–14567, 2016. 13

[28] Kathy Baylis, Maria Christina Jolejole-Foreman, and M Mallory. Impact of wheat and rice export ban on indian market integration. In *Agricultural & Applied Economics Association's 2013 AAEA & CAES Joint Annual Meeting, Washington, DC, August*, pages 4–6, 2013. 21

[29] Brian Beckage, Louis J Gross, William J Platt, and FS Gilliam. Modelling responses of pine savannas to climate change and large-scale disturbance. *Applied Vegetation Science*, 9(1):75–82, 2006. 14, 15, 44, 48

[30] SW M Beckert, MAD Rosot, and NC Rosot. Crescimento e dinâmica de araucaria angustifolia (bert.) o. ktze. em fragmento de floresta ombrófila mista. *Embrapa Florestas-Artigo em periódico indexado (ALICE)*, 2014. 50

[31] Hermann Behling and Valério DePatta Pillar. Late quaternary vegetation, biodiversity and fire dynamics on the southern brazilian highland and their implication for conservation and management of modern araucaria forest and grassland ecosystems. *Philosophical Transactions of the Royal Society B: Biological Sciences*, 362(1478):243–251, 2007. 14, 15, 16, 44, 45, 105

[32] Bernhard Bereiter, Sarah Eggleston, Jochen Schmitt, Christoph Nehrbass-Ahles, Thomas F Stocker, Hubertus Fischer, Sepp Kipfstuhl, and Jerome Chappellaz. Revision of the epica dome c co2 record from 800 to 600 kyr before present. *Geophysical Research Letters*, 42(2):542–549, 2015. 53

[33] Robert E Black, Harold Alderman, Zulfiqar A Bhutta, Stuart Gillespie, Lawrence Haddad, Susan Horton, Anna Lartey, Venkatesh Mannar, Marie Ruel, Cesar G Victora, et al. Maternal and child nutrition: building momentum for impact. *The Lancet*, 382(9890):372–375, 2013. 12, 20, 105

[34] Carolina Casagrande Blanco, Simon Scheiter, Enio Sosinski, Alessandra Fidelis, Madhur Anand, and Valério D Pillar. Feedbacks between vegetation and disturbance processes promote long-term persistence of forest–grassland mosaics in south brazil. *Ecological Modelling*, 291:224–232, 2014. 14, 17, 44

[35] Don P Blayney, John Dyck, and David Harvey. Economic effects of animal diseases linked to trade dependency. *Amber Waves*, 4(2):22, 2006. 40, 41

[36] Stefano Boccaletti, Vito Latora, Yamir Moreno, Martin Chavez, and D-U Hwang. Complex networks: Structure and dynamics. *Physics reports*, 424(4-5):175–308, 2006. 5

[37] Phillip Bonacich. Power and centrality: A family of measures. *American journal of sociology*, 92(5):1170–1182, 1987. 182

[38] Gordon B Bonan. Forests and climate change: forcings, feedbacks, and the climate benefits of forests. *science*, 320(5882):1444–1449, 2008. 67

[39] William J Bond and Catherine L Parr. Beyond the forest edge: ecology, diversity and conservation of the grassy biomes. *Biological conservation*, 143(10):2395–2404, 2010. 14, 44

[40] James A Brander and M Scott Taylor. The simple economics of easter island: A ricardo-malthus model of renewable resource use. *American economic review*, pages 119–138, 1998. 71

[41] Anna D Broido and Aaron Clauset. Scale-free networks are rare. *Nature communications*, 10(1):1–10, 2019. 9

[42] A Duncan Brown et al. *Feed or feedback: agriculture, population dynamics and the state of the planet*. International Books, 2003. 2

[43] J. Bruinsma. *World agriculture: towards 2015/2030: an FAO perspective*. Earthscan, 2003. 20

[44] Mikhail Ivanovich Budyko. The earth's climate: past and future. 1982. 52

[45] Milind Bunyan, Sougata Bardhan, Shibu Jose, et al. The shola (tropical montane forest)-grassland ecosystem mosaic of peninsular india: a review. *American Journal of Plant Sciences*, 3(11):1632, 2012. 15, 16

[46] Thomas M Bury, Chris T Bauch, and Madhur Anand. Charting pathways to climate change mitigation in a coupled socio-climate model. *PLoS computational biology*, 15(6), 2019. 100

[47] Scott Camazine, Jean-Louis Deneubourg, Nigel R Franks, James Sneyd, Eric Bonabeau, and Guy Theraula. *Self-organization in biological systems*, volume 7. Princeton university press, 2003. 2, 3

[48] J Elliott Campbell, David B Lobell, Robert C Genova, and Christopher B Field. The global potential of bioenergy on abandoned agriculture lands. *Environmental science & technology*, 42(15):5791–5794, 2008. 76

[49] Domenico Caracciolo, Erkan Istanbulluoglu, Leonardo Valerio Noto, and Scott L Collins. Mechanisms of shrub encroachment into northern chihuahuan desert grasslands and impacts of climate change investigated using a cellular automata model. *Advances in water resources*, 91:46–62, 2016. 44, 66

[50] Stephen R Carpenter. Ecological futures: building an ecology of the long now. *Ecology*, 83(8):2069–2083, 2002. 43

[51] J. A. Carr, P. D'Odorico, F. Laio, and L. Ridolfi. On the temporal variability of the virtual water network. *Geophys. Res. Lett.*, 39(6):6; 10.1029/2012GL051247, 2012. 13, 21

[52] J. A. Carr, P. D'Odorico, F. Laio, and L. Ridolfi. Recent history and geography of virtual water trade. *PLoS ONE*, 8(2):e55825; 10.1371/journal.pone.0055825, 2013. 21

[53] Emily S Cassidy, Paul C West, James S Gerber, and Jonathan A Foley. Redefining agricultural yields: from tonnes to people nourished per hectare. *Environmental Research Letters*, 8(3):034015, 2013. 76

[54] John M Chambers, Anne E Freeny, and Richard M Heiberger. Analysis of variance; designed experiments. In *Statistical models in S*, pages 145–193. Routledge, 2017. 90, 94

[55] Fu Chang, Chun-Jen Chen, and Chi-Jen Lu. A linear-time component-labeling algorithm using contour tracing technique. *Computer Vision and Image Understanding*, 93(2):206–220, 2004. 47

[56] IPCC Climate Change et al. The physical science basis. *Contribution of working group I to the Fourth Assessment Report of the Intergovernmental Panel on Climate Change*, 996, 2007. 52

[57] Matteo Chinazzi, Giorgio Fagiolo, Javier A Reyes, and Stefano Schiavo. Post-mortem examination of the international financial network. *J. Econ. Dyn. Control.*, 37(8):1692–1713, 2013. 40

[58] Alexander P Christensen. NetworkToolbox: Methods and measures for brain, cognitive, and psychometric network analysis in R. *The R Journal*, pages 422–439, 2018. 181

[59] Xavier Cirera and Edoardo Masset. Income distribution trends and future food demand. *Philosophical Transactions of the Royal Society B: Biological Sciences*, 365(1554):2821–2834, 2010. 73

[60] James S Clark, David M Bell, Michelle H Hersh, and Lauren Nichols. Climate change vulnerability of forest biodiversity: climate and competition tracking of demographic rates. *Global Change Biology*, 17(5):1834–1849, 2011. 43

[61] James S Clark, Steven R Carpenter, Mary Barber, Scott Collins, Andy Dobson, Jonathan A Foley, David M Lodge, Mercedes Pascual, Roger Pielke, William Pizer, et al. Ecological forecasts: an emerging imperative. *science*, 293(5530):657–660, 2001. 43

[62] Leon Clarke, James Edmonds, Henry Jacoby, Hugh Pitcher, John Reilly, and Richard Richels. Scenarios of greenhouse gas emissions and atmospheric concentrations. 2007. 51

[63] A. Clauset, C. R. Shalizi, and M. E. Newman. Power-law distributions in empirical data. *SIAM Rev.*, 51(4):661–703, 2009. 29

[64] William S Cleveland, Eric Grosse, William M Shyu, John M Chambers, and Trevor J Hastie. Statistical models in s. *Local regression models*, pages Chapter–8, 1992. 90, 94

[65] Peter Clifford and Aidan Sudbury. A model for spatial conflict. *Biometrika*, 60(3):581–588, 1973. 5

[66] Iain D Couzin, Jens Krause, et al. Self-organization and collective behavior in vertebrates. *Advances in the Study of Behavior*, 32(1):10–1016, 2003. 3

[67] Marc Crommelinck, Bernard Feltz, and Philippe Goujon. *Self-organization and emergence in life sciences*. Springer, 2006. 4

[68] Gabor Csardi and Tamas Nepusz. The igraph software package for complex network research. *InterJournal*, Complex Systems:1695, 2006. 25, 181

[69] Simone D'Alessandro. Non-linear dynamics of population and natural resources: The emergence of different patterns of development. *Ecological Economics*, 62(3-4):473–481, 2007. 71

[70] Carole Dalin, Megan Konar, Naota Hanasaki, Andrea Rinaldo, and Ignacio Rodriguez-Iturbe. Evolution of the global virtual water trade network. *Proceedings of the National Academy of Sciences*, 109(16):5989–5994, 2012. 21, 83

[71] Thomas R Dalton, R Morris Coats, and Badiollah R Asrabadi. Renewable resources, property-rights regimes and endogenous growth. *Ecological Economics*, 52(1):31–41, 2005. 71

[72] Arundhati Das, Harini Nagendra, Madhur Anand, and Milind Bunyan. Topographic and bioclimatic determinants of the occurrence of forest and grassland in tropical montane forest-grassland mosaics of the western ghats, india. *PloS One*, 10(6):e0130566, 2015. 14, 15, 16, 44

[73] David De la Croix and Davide Dottori. Easter island's collapse: a tale of a population race. *Journal of Economic Growth*, 13(1):27–55, 2008. 71

[74] Angus Deaton and Guy Laroque. On the behaviour of commodity prices. *Rev. Econ. Stud.*, 59(1):1–23, 1992. 21, 98, 103

[75] Ruth S DeFries, Thomas Rudel, Maria Uriarte, and Matthew Hansen. Deforestation driven by urban population growth and agricultural trade in the twenty-first century. *Nature Geoscience*, 3(3):178, 2010. 13, 71

[76] M. Demeke, G. Pangrazio, and M. Maetz. Country responses to the food security crisis: nature and preliminary implications of the policies pursued. *FAO Economic and Social Development Department* http://www.fao.org/documents/card/en/c/506db788-bb64-4715-a211-1448442ed637/, 2009. 21, 23, 29, 30, 31, 141, 147

[77] Pedro Ferreira Develey, Robberson Bernal Setubal, Rafael Antunes Dias, Glayson Ariel Bencke, et al. Conservação das aves e da biodiversidade no bioma pampa aliada a sistemas de produção animal. *Revista Brasileira de Ornitologia*, 16(4):308–315, 2008. 67

[78] M. Dilley and T. E Boudreau. Coming to terms with vulnerability: a critique of the food security definition. *Food Policy*, 26:229–247, 2001. 21

[79] Tiziano Distefano, Francesco Laio, Luca Ridolfi, and Stefano Schiavo. Shock transmission in the international food trade network. *PloS one*, 13(8), 2018. 98, 103, 105

[80] AP Dixon, D Faber-Langendoen, C Josse, J Morrison, and CJ Loucks. Distribution mapping of world grassland types. *Journal of Biogeography*, 41(11):2003–2019, 2014. 14, 15, 44

[81] Zachary Dockstader, Chris T Bauch, and Madhur Anand. Interconnections accelerate collapse in a socio-ecological metapopulation. *Sustainability*, 11(7):1852, 2019. 14, 18, 71, 72, 97

[82] Alexander G Dolfing, Jasper RFW Leuven, and Brian J Dermody. The effects of network topology, climate variability and shocks on the evolution and resilience of a food trade network. *PloS one*, 14(3):e0213378, 2019. 12, 14, 18, 71, 72, 97, 99, 100, 105

[83] K. Dollive. The impact of export restraints on rising grain prices. *U.S. International Trade Comission Office of Economics Working Paper* https://www.usitc.gov/publications/332/EC200809A.pdf, 2008. 21, 23, 29, 30, 31, 141, 147

[84] C. Dubé, C. Ribble, D. Kelton, and B. McNab. A review of network analysis terminology and its application to foot-and-mouth disease modelling and policy development. *Transbound. Emerg. Dis.*, 56:73–85, 2009. 21, 28

[85] Christopher Bren d'Amour, Leonie Wenz, Matthias Kalkuhl, Jan Christoph Steckel, and Felix Creutzig. Teleconnected food supply shocks. *Environmental Research Letters*, 11(3):035007, 2016. 98, 103, 105

[86] Paolo D'Odorico, Joel A Carr, Kyle F Davis, Jampel Dell'Angelo, and David A Seekell. Food inequality, injustice, and rights. *BioScience*, 69(3):180–190, 2019. 78

[87] Paolo D'Odorico, Joel A Carr, Francesco Laio, Luca Ridolfi, and Stefano Vandoni. Feeding humanity through global food trade. *Earth's Future*, 2(9):458–469, 2014. 71, 83

[88] Timur V. Elzhov, Katharine M. Mullen, Andrej-Nikolai Spiess, and Ben Bolker. *minpack.lm: R Interface to the Levenberg-Marquardt Nonlinear Least-Squares Algorithm Found in MINPACK, Plus Support for Bounds*, 2016. R package version 1.2-1. 179

[89] M. Ercsey-Ravasz, Z. Toroczkai, Z. Lakner, and J. Baranyi. Complexity of the international agro-food trade network and its impact on food safety. *PLoS one*, 7(5):e37810, 2012. 13, 21, 23, 30, 141

[90] G. Ergün and G. J. Rodgers. Growing random networks with fitness. *Physica A*, 303:261–272, 2002. 22, 25, 26

[91] Fernando DB Espírito-Santo, Manuel Gloor, Michael Keller, Yadvinder Malhi, Sassan Saatchi, Bruce Nelson, Raimundo C Oliveira Junior, Cleuton Pereira, Jon Lloyd, Steve Frolking, et al. Size and frequency of natural forest disturbances and the amazon forest carbon balance. *Nature Communications*, 5:3434, 2014. 50

[92] Leonhard Euler. Solutio problematis ad geometriam situs pertinentis. *Commentarii academiae scientiarum Petropolitanae*, pages 128–140, 1741. 5

[93] M. Fader, D. Gerten, M. Krause, W. Lucht, and W. Cramer. Spatial decoupling of agricultural production and consumption: quantifying dependences of countries on food imports due to domestic land and water constraints. *Environ. Res. Lett.*, 8:014046, 2013. 21

[94] G. Fagiolo. The international-trade network: gravity equations and topological properties. *J. Econ. Interact. Coor.*, 5(1):1–25, 2010. 14, 18, 22

[95] G. Fagiolo, T. Squartini, and D. Garlaschelli. Null models of economic networks: the case of the world trade web. *J. Econ. Interact. Coor.*, 8(1):75–107, 2013. 14, 18, 22

[96] Kathyrn R Fair, Madhur Anand, and Chris T Bauch. Human metapopulation interactions on a trade network: implications for food security & equality. *In progress*, 2020. iv, 18

[97] Kathyrn R Fair, Chris T Bauch, and Madhur Anand. Dynamics of the global wheat trade network and resilience to shocks. *Scientific reports*, 7(1):1–14, 2017. This article is licensed under a Creative Commons Attribution 4.0 License (https://creativecommons.org/licenses/by/4.0/). Changes were made to the original article for inclusion as Chapter 2. iv, 18, 83, 100, 106

[98] Kathyrn R Fair, Chris T Bauch, and Madhur Anand. Spatial structure in protected forest-grassland mosaics: exploring futures under climate change. *In review*, 2020. iv, 18

[99] Shenggen Fan and Paul Polman. An ambitious development goal: Ending hunger and undernutrition by 2025. In Andrew Marble and Heidi Fritschel, editors, *2013 Global Food Policy Report*, chapter 2, pages 15–28. International Food Policy Research Institute (IFPRI), 2014. 12, 20, 71, 105

[100] T. Fellmann, S. Hélaine, and O. Nekhay. Harvest failures, temporary export restrictions and global food security: the example of limited grain exports from russia, ukraine and kazakhstan. *Food Security*, 6:727–742, 2014. 21, 23, 29, 30, 31, 141, 147

[101] C. B Field, V Barros, and T. F. Stocker. Managing the risks of extreme events and disasters to advance climate change adaptation. special report of the intergovernmental panel on climate change (ipcc). Technical report, Intergovernmental Panel on Climate Change, Geneva (Switzerland); Cambridge University Press, New York, NY (United States), 2012. 23, 39, 40

[102] G Fischer, E Hizsnyik, S Prieler, H van Velthuizen, and D Wiberg. Scarcity and abundance of land resources: competing uses and the shrinking land resource base. *SOLAW Background Thematic Report - TR02*, 2012. 179

[103] JC Flores, Mauro Bologna, and Deterlino Urzagasti. A mathematical model for the andean tiwanaku civilization collapse: Climate variations. *Journal of theoretical biology*, 291:29–32, 2011. 71

[104] Jonathan A Foley, Ruth DeFries, Gregory P Asner, Carol Barford, Gordon Bonan, Stephen R Carpenter, F Stuart Chapin, Michael T Coe, Gretchen C Daily, Holly K Gibbs, et al. Global consequences of land use. *science*, 309(5734):570–574, 2005. 70, 100

[105] Food and Agriculture Organization of the United Nations. An introduction to the basic concepts of food security, 2008. 78

[106] Food and Agriculture Organization of the United Nations. Global food losses and food waste – extent, causes and prevention, 2011. 73, 76

[107] Food and Agriculture Organization of the United Nations. Faostat statistical database, 2016. Data retrieved July 11, 2016. 23, 25, 26, 28, 40, 144, 147

[108] Food and Agriculture Organization of the United Nations. Faostat statistical database, 2019. Data retrieved September 15, 2019. 14, 76, 83, 179, 181

[109] R. Foschi, M. Riccaboni, and S. Schiavo. Preferential attachment in multiple trade networks. *Phys. Rev. E*, 90(2):022817, 2014. 29, 40

[110] N. J. Foti, S. Pauls, and D. N. Rockmore. Stability of the world trade web over time–an extinction analysis. *J. Econ. Dyn. Control*, 37(9):1889–1910, 2013. 13, 14, 18, 21, 22, 29, 30, 39

[111] Linton C Freeman. A set of measures of centrality based on betweenness. *Sociometry*, pages 35–41, 1977. 182

[112] Junichi Fujino, Rajesh Nair, Mikiko Kainuma, Toshihiko Masui, and Yuzuru Matsuoka. Multi-gas mitigation analysis on stabilization scenarios using aim global model. *The Energy Journal*, pages 343–353, 2006. 51

[113] Fumitaka Furuoka et al. Looking for a j-shaped development-fertility relationship: Do advances in development really reverse fertility declines. *Economics bulletin*, 29(4):3067–3074, 2009. 73

[114] Lars Gamfeldt, Tord Snäll, Robert Bagchi, Micael Jonsson, Lena Gustafsson, Petter Kjellander, María C Ruiz-Jaen, Mats Fröberg, Johan Stendahl, Christopher D Philipson, et al. Higher levels of multiple ecosystem services are found in forests with more tree species. *Nature communications*, 4:1340, 2013. 67

[115] Jianxi Gao, Baruch Barzel, and Albert-László Barabási. Universal resilience patterns in complex networks. *Nature*, 530(7590):307–312, 2016. 28, 29, 30

[116] D. Garlaschelli, T. Di Matteo, T. Aste, G. Caldarelli, and M. I. Loffredo. Interplay between topology and dynamics in the world trade web. *Eur. Phys. J. B*, 57:159–164, 2007. 14, 18, 22, 25, 26, 27, 28, 145

[117] D. Garlaschelli and M. I. Loffredo. Fitness-dependent topological properties of the world trade web. *Phys. Rev. Lett.*, 93:188701, 2004. 14, 18, 22, 25, 28, 145

[118] Jessica A Gephart and Michael L Pace. Structure and evolution of the global seafood trade network. *Environmental Research Letters*, 10(12):125014, 2015. 20, 21, 83

[119] Jessica A. Gephart, E. Rovenskaya, U. Dieckmann, M. L. Pace, and Å. Brännström. Vulnerability to shocks in the global seafood trade network. *Environ. Res. Lett.*, 11(3):035008, 2016. 20, 21, 22, 41, 146

[120] PW Gerbens-Leenes, Sanderine Nonhebel, and Martinus S Krol. Food consumption patterns and economic growth. increasing affluence and the use of natural resources. *Appetite*, 55(3):597–608, 2010. 73

[121] Paolo E Giordani, Nadia Rocha, and Michele Ruta. Food prices and the multiplier effect of export policy. *CESifo Working Paper Series*, 2012. 21

[122] J. B. Glattfelder and S. Battiston. Backbone of complex networks of corporations: The flow of control. *Phys. Rev. E*, 80(3):36104, 2009. 23, 141

[123] H Charles J Godfray, John R Beddington, Ian R Crute, Lawrence Haddad, David Lawrence, James F Muir, Jules Pretty, Sherman Robinson, Sandy M Thomas, and Camilla Toulmin. Food security: the challenge of feeding 9 billion people. *science*, 327(5967):812–818, 2010. 13, 70, 71, 100

[124] Peter Good, William Ingram, F Hugo Lambert, Jason A Lowe, Jonathan M Gregory, Mark J Webb, Mark A Ringer, and Peili Wu. A step-response approach for predicting and understanding non-linear precipitation changes. *Climate dynamics*, 39(12):2789–2803, 2012. 52, 53

[125] Ashok Gulati and Shweta Saini. India's political economy responses to the global food price shock of 2007–08. *WIDER Working Papers 2015*, 2015. 23, 29, 30, 31, 147

[126] Charles AS Hall and John W Day. Revisiting the limits to growth after peak oil: In the 1970s a rising world population and the finite resources available to support it were hot topics. interest faded—but it's time to take another look. *American scientist*, 97(3):230–237, 2009. 10, 11

[127] Mark S. Handcock. *Relative Distribution Methods*. Los Angeles, CA, 2016. Version 1.6-6. Project home page at urlhttp://www.stat.ucla.edu/ handcock/RelDist. 78

[128] Mark S. Handcock and Martina Morris. *Relative Distribution Methods in the Social Sciences*. Springer, New York, 1999. ISBN 0-387-98778-9. 78

[129] Alan Hastings. Transient dynamics and persistence of ecological systems. *Ecology Letters*, 4(3):215–220, 2001. 50

[130] Alan Hastings, Karen C Abbott, Kim Cuddington, Tessa Francis, Gabriel Gellner, Ying-Cheng Lai, Andrew Morozov, Sergei Petrovskii, Katherine Scranton, and Mary Lou Zeeman. Transient phenomena in ecology. *Science*, 361(6406):eaat6412, 2018. 50

[131] Alan Hastings and Kevin Higgins. Persistence of transients in spatially structured ecological models. *Science*, 263(5150):1133–1136, 1994. 50

[132] D. Headey. Rethinking the global food crisis: the role of trade shocks. *Food Policy*, 36:136–146, 2011. 21, 29, 30, 31, 141, 147

[133] Cherly M Heesch. Reflexes that control cardiovascular function. *Advances in Physiology Education*, 277(6):S234, 1999. 2

[134] Elhanan Helpman, Marc Melitz, and Yona Rubinstein. Estimating trade flows: Trading partners and trading volumes. *The quarterly journal of economics*, 123(2):441–487, 2008. 97

[135] Charlotte K Hemelrijk and Hanno Hildenbrandt. Schools of fish and flocks of birds: their shape and internal structure by self-organization. *Interface focus*, 2(6):726–737, 2012. 3

[136] Kirsten A Henderson, Chris T Bauch, and Madhur Anand. Alternative stable states and the sustainability of forests, grasslands, and agriculture. *Proceedings of the National Academy of Sciences*, 113(51):14552–14559, 2016. 13, 14, 15, 16, 18, 44, 45, 49, 50, 67, 76, 100, 105

[137] Kirsten A Henderson, Mateus Reis, Carolina C Blanco, Valério D Pillar, Rodrigo C Printes, Chris T Bauch, and Madhur Anand. Landowner perceptions of the value of natural forest and natural grassland in a mosaic ecosystem in southern brazil. *Sustainability science*, 11(2):321–330, 2016. 67, 76

[138] Stephanie C Herring, Nikolaos Christidis, Andrew Hoell, James P Kossin, Carl J Schreck III, and Peter A Stott. Explaining extreme events of 2016 from a climate perspective. *Bulletin of the American Meteorological Society*, 99(1):S1–S157, 2018. 104, 106

[139] Steven I Higgins, William J Bond, and Winston SW Trollope. Fire, resprouting and variability: a recipe for grass–tree coexistence in savanna. *Journal of Ecology*, 88(2):213–229, 2000. 49

[140] Steven I Higgins and Simon Scheiter. Atmospheric co 2 forces abrupt vegetation shifts locally, but not globally. *Nature*, 488(7410):209, 2012. 44

[141] Pedro Higuchi, Ary T Oliveira-Filho, Daniel P Bebber, Nick D Brown, Ana Carolina Silva, and Evandro LM Machado. Spatio-temporal patterns of tree community dynamics in a tropical forest fragment in south-east brazil. *Plant Ecology*, 199(1):125–135, 2008. 50

[142] Robert J Hijmans, Susan E Cameron, Juan L Parra, Peter G Jones, and Andy Jarvis. Cmip5 30-seconds. Retrieved from http://worldclim.org/cmip5_30s January 1, 2019. 52

[143] Robert J Hijmans, Susan E Cameron, Juan L Parra, Peter G Jones, and Andy Jarvis. Very high resolution interpolated climate surfaces for global land areas. *International Journal of Climatology: A Journal of the Royal Meteorological Society*, 25(15):1965–1978, 2005. 52, 53

[144] Robert J. Hijmans, Jacob van Etten, Joe Cheng, Matteo Mattiuzzi, Michael Sumner, Jonathan A. Greenberg, Oscar Perpinan Lamigueiro, Andrew Bevan, Etienne B. Racine, Ashton Shortridge, and Aniruddha Ghosh. *Raster: Geographic Data Analysis and Modeling*, 2017. R package version 2.6-7. 45

[145] Marina Hirota, Milena Holmgren, Egbert H Van Nes, and Marten Scheffer. Global resilience of tropical forest and savanna to critical transitions. *Science*, 334(6053):232–235, 2011. 12, 50

[146] Marina Hirota, Carlos Nobre, Marcos Daisuke Oyama, and Mercedes MC Bustamante. The climatic sensitivity of the forest, savanna and forest–savanna transition in tropical south america. *New Phytologist*, 187(3):707–719, 2010. 44, 66

[147] William A Hoffmann, Ryan Adasme, M Haridasan, Marina T de Carvalho, Erika L Geiger, Mireia AB Pereira, Sybil G Gotsch, and Augusto C Franco. Tree topkill, not mortality, governs the dynamics of savanna–forest boundaries under frequent fire in central brazil. *Ecology*, 90(5):1326–1337, 2009. 50

[148] William A Hoffmann, Erika L Geiger, Sybil G Gotsch, Davi R Rossatto, Lucas CR Silva, On Lee Lau, M Haridasan, and Augusto C Franco. Ecological thresholds at the

savanna-forest boundary: how plant traits, resources and fire govern the distribution of tropical biomes. *Ecology letters*, 15(7):759–768, 2012. 48

[149] Ricardo M Holdo, Anthony RE Sinclair, Andrew P Dobson, Kristine L Metzger, Benjamin M Bolker, Mark E Ritchie, and Robert D Holt. A disease-mediated trophic cascade in the serengeti and its implications for ecosystem c. *PLoS Biology*, 7(9):e1000210, 2009. 49

[150] John H Holland. *Emergence: From chaos to order*. OUP Oxford, 2000. 3, 4

[151] Richard A Holley and Thomas M Liggett. Ergodic theorems for weakly interacting infinite systems and the voter model. *The annals of probability*, pages 643–663, 1975. 5

[152] Crawford S Holling. Principles of insect predation. *Annual review of entomology*, 6(1):163–182, 1961. 73

[153] Crawford S Holling. Resilience and stability of ecological systems. *Annual review of ecology and systematics*, 4(1):1–23, 1973. 12

[154] Crawford S Holling. *Resilience of ecosystems: local surprise and global change*. Number 5. Cambridge University Press, 1985. 12

[155] Crawford S Holling. Cross-scale morphology, geometry, and dynamics of ecosystems. *Ecological monographs*, 62(4):447–502, 1992. 12

[156] Crawford S Holling. Understanding the complexity of economic, ecological, and social systems. *Ecosystems*, 4(5):390–405, 2001. 12

[157] P. Holme, B. J. Kim, C. N. Yoon, and S. K. Han. Attack vulnerability of complex networks. *Phys. Rev. E*, 65(5):056109, 2002. 28, 29, 30, 40, 146

[158] Sue Horton and R Steckel. Global economic losses attributable to malnutrition 1900–2000 and projections to 2050. *The economics of human challenges*, pages 247–272, 2013. 12, 20, 105

[159] David Hummels. Transportation costs and international trade in the second era of globalization. *Journal of Economic perspectives*, 21(3):131–154, 2007. 97

[160] Mark D Humphries and Kevin Gurney. Network 'small-world-ness': a quantitative method for determining canonical network equivalence. *PloS one*, 3(4), 2008. 9

[161] Clinton Innes, Madhur Anand, and Chris T Bauch. The impact of human-environment interactions on the stability of forest-grassland mosaic ecosystems. *Scientific reports*, 3(1):1–10, 2013. 16, 18, 44, 47, 48, 49, 50

[162] Graziela Iob and Emerson M Vieira. Seed predation of araucaria angustifolia (araucariaceae) in the brazilian araucaria forest: influence of deposition site and comparative role of small and 'large'mammals. *Plant Ecology*, 198(2):185–196, 2008. 50

[163] Ernst Ising. Beitrag zur theorie des ferromagnetismus. *Zeitschrift für Physik*, 31(1):253–258, 1925. 5

[164] S. Iyer, T. Killingback, B. Sundaram, and Z. Wang. Attack robustness and centrality of complex networks. *PLoS ONE*, 8(4):e59613; 10.1371/journal.pone.0059613, 2013. 29, 40, 146

[165] Elkington J. Enter the triple bottom line. In Richardson J Henriques A, editor, *The triple bottom line: does it all add up?*, chapter 1, pages 1–16. Earthscan, London, 2004. 11

[166] A. Jamakovic and S. Uhlig. On the relationships between topological measures in real-world networks. *Netw. Heterog. Media*, 3(2):345, 2008. 148

[167] Paul James. *Urban sustainability in theory and practice : circles of sustainability*. Advances in urban sustainability series. Routledge, Abingdon, Oxon ;, 2014. 11

[168] Eila Jeronen. *Sustainability and Sustainable Development*, pages 2370–2378. Springer Berlin Heidelberg, Berlin, Heidelberg, 2013. 11, 67

[169] Q. Ji, H. Zhang, and Y. Fan. Identification of global oil trade patterns: an empirical research based on complex network theory. *Energ. Convers. Manage.*, 85:856–865, 2014. 29, 30, 146

[170] R. R. Kao, L. Danon, D. M. Green, and I. Z. Kiss. Demographic structure and pathogen dynamics on the network of livestock movements in great britain. *P. Roy. Soc. B-Biol. Sci.*, 273:1999–2007, 2006. 21, 28, 30

[171] I. Z. Kiss, D. M. Green, and R. R. Kao. Infectious disease control using contact tracing in random and scale-free networks. *J. Roy. Soc. Interface*, 3(6):55–62, 2006. 28

[172] Reto Knutti and Gabriele C Hegerl. The equilibrium sensitivity of the earth's temperature to radiation changes. *Nature Geoscience*, 1(11):735, 2008. 52

[173] Reto Knutti, Maria AA Rugenstein, and Gabriele C Hegerl. Beyond equilibrium climate sensitivity. *Nature Geoscience*, 10(10):727, 2017. 52

[174] M. Konar, C. Dalin, S. Suweis, N. Hanasaki, A. Rinaldo, and I. Rodriguez-Iturbe. Water for food: The global virtual water trade network. *Wat. Resour. Res.*, 47(5):5; 10.1029/2010WR010307, 2011. 13, 21, 23, 31, 141

[175] Michael Kremer and Daniel L Chen. Income distribution dynamics with endogenous fertility. *Journal of Economic growth*, 7(3):227–258, 2002. 73

[176] James Ladyman, James Lambert, and Karoline Wiesner. What is a complex system? *European Journal for Philosophy of Science*, 3(1):33–67, 2013. 1, 2, 3, 4

[177] Eric F Lambin and Patrick Meyfroidt. Global land use change, economic globalization, and the looming land scarcity. *Proceedings of the National Academy of Sciences*, 108(9):3465–3472, 2011. 13, 70, 71, 98, 104, 105

[178] K. M. Lee, J. S. Yang, G. Kim, J. Lee, K. I. Goh, and I. M. Kim. Impact of the topology of global macroeconomic network on the spreading of economic crises. *PLoS ONE*, 6:e18443; 10.1371/journal.pone.0018443, 2011. 20, 30

[179] Ronald Lee. The demographic transition: three centuries of fundamental change. *Journal of economic perspectives*, 17(4):167–190, 2003. 72, 73

[180] Timothy M Lenton, Hermann Held, Elmar Kriegler, Jim W Hall, Wolfgang Lucht, Stefan Rahmstorf, and Hans Joachim Schellnhuber. Tipping elements in the earth's climate system. *Proceedings of the national Academy of Sciences*, 105(6):1786–1793, 2008. 13

[181] Simon A Levin. Ecosystems and the biosphere as complex adaptive systems. *Ecosystems*, 1(5):431–436, 1998. 12

[182] Simon A Levin. Fragile dominion: complexity and the commons. perseus. *Reading, MA*, 1999. 12

[183] C. Li, H. Zhao, and X. Zhang. A local-clustered evolving network model. *ICIC-EL*, 2(2):193–199, 2008. 29, 30, 146

[184] Cong Li, Qian Li, Piet Van Mieghem, H Eugene Stanley, and Huijuan Wang. Correlation between centrality metrics and their application to the opinion model. *The European Physical Journal B*, 88(3):65, 2015. 86

[185] Shengfa Li and Xiubin Li. Global understanding of farmland abandonment: A review and prospects. *Journal of Geographical Sciences*, 27(9):1123–1150, 2017. 76

[186] Charles E Lindblom. The science of "muddling through". *Public administration review*, pages 79–88, 1959. 106

[187] Jianguo Liu, Thomas Dietz, Stephen R Carpenter, Marina Alberti, Carl Folke, Emilio Moran, Alice N Pell, Peter Deadman, Timothy Kratz, Jane Lubchenco, et al. Complexity of coupled human and natural systems. *science*, 317(5844):1513–1516, 2007. 13

[188] Z. Liu, Y. Lai, N. Ye, and P. Dasgupta. Connectivity distribution and attack tolerance of general networks with both preferential and random attachments. *Phys. Lett. A*, 303(5):337–344, 2002. 30

[189] T.R. Malthus. *An essay on the principle of population, as it affects the future improvement of society. With remarks on the speculations of Mr. Godwin, M. Condorcet, and other writers.* printed for J. Johnson, St. Paul's Church-Yard: London, 1798. 10

[190] Z. Maoz. Preferential attachment, homophily, and the structure of international networks, 1816-2003. *Conflict Manag. Peace*, 29:341–369, 2012. 21, 22, 25, 26

[191] Philippe Marchand, Joel A Carr, Jampel Dell'Angelo, Marianela Fader, Jessica A Gephart, Matti Kummu, Nicholas R Magliocca, Miina Porkka, Michael J Puma, Zak Ratajczak, et al. Reserves and trade jointly determine exposure to food supply shocks. *Environmental Research Letters*, 11(9):095009, 2016. 99, 105

[192] José A Marengo, R Jones, Lincoln M Alves, and Maria C Valverde. Future change of temperature and precipitation extremes in south america as derived from the precis regional climate modeling system. *International Journal of Climatology: A Journal of the Royal Meteorological Society*, 29(15):2241–2255, 2009. 15, 44

[193] Julian D Marshall and Michael W Toffel. Framing the elusive concept of sustainability: A sustainability hierarchy. *Environmental science & technology*, 39(3):673–682, 2005. 10, 11

[194] S. Maslov and K. Sneppen. Specificity and stability in topology of protein networks. *Science*, 296(5569):910–913, 2002. 27

[195] MATLAB. *version 8.4.0.150421 (R2014b)*. The MathWorks Inc., Natick, MA, 2014. 25

[196] John W Maxwell and Rafael Reuveny. Resource scarcity and conflict in developing countries. *Journal of peace Research*, 37(3):301–322, 2000. 71

[197] Robert M May, Simon A Levin, and George Sugihara. Ecology for bankers. *Nature*, 451(7181):893–894, 2008. 12, 28, 30

[198] K McGarigal, S.A. Cushman, and E. Ene. Fragstats v4: Spatial pattern analysis program for categorical and continuous maps. Computer software program produced by the authors at the University of Massachusetts, Amherst. Available at the following web site: http://www.umass.edu/landeco/research/fragstats/fragstats.html, 2012. 47

[199] DH Meadows, DL Meadows, J Randers, WW Behrens III, et al. *The Limits to growth; : a report for the Club of Rome's project on the predicament of mankind*. Universe Books, New York, 1972. 11, 71

[200] Malte Meinshausen and Steven J Smith. Rcp concentration calculations and data final version, background data, acknowledgements and further info. Retrieved from http://www.pik-potsdam.de/~mmalte/rcps/ November 15, 2018. 52

[201] Malte Meinshausen, Steven J Smith, K Calvin, John S Daniel, MLT Kainuma, Jean-Francois Lamarque, Km Matsumoto, SA Montzka, SCB Raper, K Riahi, et al. The rcp greenhouse gas concentrations and their extensions from 1765 to 2300. *Climatic change*, 109(1-2):213, 2011. 51, 52

[202] Patrick Meyfroidt, Thomas K Rudel, and Eric F Lambin. Forest transitions, trade, and the global displacement of land use. *Proceedings of the National Academy of Sciences*, 107(49):20917–20922, 2010. 104, 105

[203] Andrea Migone and Michael Howlett. Charles e. lindblom,"the science of muddling through". In *The Oxford Handbook of Classics in Public Policy and Administration*. Oxford University Press, 2015. 106

[204] Camelia Minoiu and Javier A Reyes. A network analysis of global banking: 1978–2010. *J. Financ. Stabil.*, 9(2):168–184, 2013. 40

[205] S. Mitra and T. Josling. Food export restrictions: review of the 2007-2010 experience and considerations for disciplining restrictive measures. *IPC Position Paper Agricultural and Rural Development Policy Series* http://www.ictsd.org/downloads/2009/02/exportrestrictions_final.pdf, 2009. 21, 23, 29, 30, 31, 141, 147

[206] Glenn R Moncrieff, Simon Scheiter, Liam Langan, Antonio Trabucco, and Steven I Higgins. The future distribution of the savannah biome: model-based and biogeographic contingency. *Philosophical Transactions of the Royal Society B: Biological Sciences*, 371(1703):20150311, 2016. 44, 66

[207] Safa Motesharrei, Jorge Rivas, and Eugenia Kalnay. Human and nature dynamics (handy): Modeling inequality and use of resources in the collapse or sustainability of societies. *Ecological Economics*, 101:90–102, 2014. 71

[208] Brett P Murphy and David MJS Bowman. What controls the distribution of tropical forest and savanna? *Ecology letters*, 15(7):748–758, 2012. 15, 43, 66

[209] N Myers, RA Mittermeier, CG Mittermeier, GAB Da Fonseca, and J Kent. 2000: Biodiversity hotspots for conservation priorities. *Nature*, 403:853–858, 2000. 16, 45, 105

[210] Mikko Myrskylä, Hans-Peter Kohler, and Francesco C Billari. Advances in development reverse fertility declines. *Nature*, 460(7256):741–743, 2009. 72, 73

[211] NASA. Measuring vegetation (ndvi & evi). Retrieved on February 7, 2019 from: https://earthobservatory.nasa.gov/features/MeasuringVegetation, 2000. 45

[212] United Nations. About the sustainable development goals. Retrieved from https://www.un.org/sustainabledevelopment/sustainable-development-goals/ on March 27,2020. 12, 20, 71, 97, 98, 100, 105

[213] United Nations. Economic commission for europe (2015) un/locode country names iso 3166-1. Retrieved from http://www.unece.org/cefact/locode/countries.html. 144

[214] United Nations. Transforming our world: The 2030 agenda for sustainable development, 2015. Retrieved from https://sustainabledevelopment.un.org/post2015/transformingourworld on March 27, 2020. 12, 20, 71, 97, 98, 100, 105

[215] Alison G Nazareno and Maurício S dos Reis. At risk of population decline? an ecological and genetic approach to the threatened palm species butia eriospatha (arecaceae) of southern brazil. *Journal of Heredity*, 105(1):120–129, 2013. 50

[216] Mark E.J. Newman. The structure and function of complex networks. *SIAM review*, 45(2):167–256, 2003. 5

[217] Mark E.J. Newman. *Networks: an introduction*. Number 134. Oxford University Press, 2010. 8, 9, 28, 181, 182

[218] Ragnhild Nordås and Nils Petter Gleditsch. Climate change and conflict. *Political geography*, 26(6):627–638, 2007. 104, 106

[219] Myers Norman. Biodiversity hotspots revisited. *BioScience*, 53(10):916–917, 2003. 14, 44

[220] Shane Nowack, Chris T Bauch, and Madhur Anand. A local optimization framework for addressing conservation conflicts in mosaic ecosystems. *PloS one*, 14(5), 2019. 16, 44, 67, 105

[221] Martin A Nowak and Robert M May. Evolutionary games and spatial chaos. *Nature*, 359(6398):826–829, 1992. 5, 6

[222] United Nations Department of Economic and Social Affairs Population Division. World population prospects 2019, online edition, 2019. 70, 76, 77, 106, 179

[223] Ary T Oliveira-Filho, José Márcio De Mello, and José Roberto S Scolforo. Effects of past disturbance and edges on tree community structure and dynamics within a fragment of tropical semideciduous forest in south-eastern brazil over a five-year period (1987–1992). *Plant Ecology*, 131(1):45–66, 1997. 49

[224] David M Olson and Eric Dinerstein. The global 200: a representation approach to conserving the earth's most biologically valuable ecoregions. *Conservation Biology*, 12(3):502–515, 1998. 14, 15, 44

[225] World Commission on Environment and Development. *Our common future*. Oxford paperbacks. Oxford University Press, Oxford, UK, 1987. 11

[226] Lars Onsager. Crystal statistics. i. a two-dimensional model with an order-disorder transition. *Physical Review*, 65(3-4):117, 1944. 5

[227] Gerhard E Overbeck, Sandra C Müller, Alessandra Fidelis, Jörg Pfadenhauer, Valério D Pillar, Carolina C Blanco, Ilsi I Boldrini, Rogerio Both, and Eduardo D Forneck. Brazil's neglected biome: the south brazilian campos. *Perspectives in Plant Ecology, Evolution and Systematics*, 9(2):101–116, 2007. 15, 16, 45, 67, 105

[228] Chris Pagnutti, Chris T Bauch, and Madhur Anand. Outlook on a worldwide forest transition. *PLoS One*, 8(10):e75890, 2013. 70, 71, 72, 76, 89, 100, 180

[229] Renata Pardini, Adriana de Arruda Bueno, Toby A Gardner, Paulo Inácio Prado, and Jean Paul Metzger. Beyond the fragmentation threshold hypothesis: regime shifts in biodiversity across fragmented landscapes. *PloS one*, 5(10):e13666, 2010. 67

[230] ParksWatch.org. Duke university parkswatch: Aparados da serra national park. Retrieved on February 7, 2019 from: http://www.parkswatch.org/parkprofile.php?l=eng&country=bra&park=asnp&page=inf&p=bra, 2004. 45

[231] Martin L Parry. *Climate change and world agriculture*. Routledge, 2019. 100

[232] R. Pastor-Satorras and A. Vespignani. Epidemic spreading in scale-free networks. *Phys. Rev. Lett.*, 86(14):3200–3203, 2001. 28

[233] Juli G Pausas and Eloi Ribeiro. The global fire–productivity relationship. *Global Ecology and Biogeography*, 22(6):728–736, 2013. 54

[234] Charles Perrings. Resilience in the dynamics of economy-environment systems. *Environmental and Resource Economics*, 11(3-4):503–520, 1998. 12

[235] Owen L Petchey, Mikael Pontarp, Thomas M Massie, Sonia Kéfi, Arpat Ozgul, Maja Weilenmann, Gian Marco Palamara, Florian Altermatt, Blake Matthews, Jonathan M Levine, et al. The ecological forecast horizon, and examples of its uses and determinants. *Ecology letters*, 18(7):597–611, 2015. 43

[236] Christina Petsoulas. *Hayek's liberalism and its origins: His idea of spontaneous order and the Scottish Enlightenment*. Routledge, 2013. 3

[237] Herbert HT Prins and Henk P van der Jeugd. Herbivore population crashes and woodland structure in east africa. *Journal of Ecology*, pages 305–314, 1993. 49

[238] M. J. Puma, S. Bose, S. Y. Chon, and B. I. Cook. Assessing the evolving fragility of the global food system. *Enviro. Res. Lett.*, 10:024007, 2015. 13, 21, 22, 23, 29, 30, 31, 39, 98, 103, 141, 147

[239] J. Qu, S. Wang, M. Jusup, and Z. Wang. Effects of random rewiring on the degree correlation of scale-free networks. *Sci. Rep.*, 5:15450; 10.1038/srep15450, 2015. 27

[240] Sarah Quarmby. What are the implications of complex systems thinking for policy? Retrieved from https://blogs.lse.ac.uk/politicsandpolicy/complex-systems-thinking-for-policy/ on March 23, 2020., 2018. 106

[241] R Core Team. *R: A Language and Environment for Statistical Computing*. R Foundation for Statistical Computing, Vienna, Austria, 2020. 45, 47, 179, 181

[242] Anatol Rapoport, Albert M Chammah, and Carol J Orwant. *Prisoner's dilemma: A study in conflict and cooperation*, volume 165. University of Michigan press, 1965. 6

[243] Zak Ratajczak, Paolo D'Odorico, and Kailiang Yu. The enemy of my enemy hypothesis: Why coexisting with grasses may be an adaptive strategy for savanna trees. *Ecosystems*, 20(7):1278–1295, 2017. 48

[244] S. Rautureau, B. Dufour, and B. Durand. Targeted surveillance of cattle trade using social network analysis tools. *Rev. Epid. San. Anim.*, 59/60:58–60, 2011. 21, 28, 29, 30, 146

[245] Aura Reggiani. Network resilience for transport security: Some methodological considerations. *Transp. Policy*, 28:63–68, 2013. 12, 21

[246] Rafael Reuveny and Christopher S Decker. Easter island: historical anecdote or warning for the future? *Ecological Economics*, 35(2):271–287, 2000. 100

[247] Rafael Reuveny and John W Maxwell. Conflict and renewable resources. *Journal of Conflict resolution*, 45(6):719–742, 2001. 71

[248] Keywan Riahi, Arnulf Grübler, and Nebojsa Nakicenovic. Scenarios of long-term socio-economic and environmental development under climate stabilization. *Technological Forecasting and Social Change*, 74(7):887–935, 2007. 51

[249] Keywan Riahi, Detlef P Van Vuuren, Elmar Kriegler, Jae Edmonds, Brian C O'neill, Shinichiro Fujimori, Nico Bauer, Katherine Calvin, Rob Dellink, Oliver Fricko, et al. The shared socioeconomic pathways and their energy, land use, and greenhouse gas emissions implications: an overview. *Global Environmental Change*, 42:153–168, 2017. 77, 106

[250] Milton Cezar Ribeiro, Jean Paul Metzger, Alexandre Camargo Martensen, Flávio Jorge Ponzoni, and Márcia Makiko Hirota. The brazilian atlantic forest: How much is left, and how is the remaining forest distributed? implications for conservation. *Biological conservation*, 142(6):1141–1153, 2009. 67

[251] S. E. Robinson, M. G. Everett, and R. M. Christley. Recent network evolution increases the potential for large epidemics in the british cattle population. *J. Roy. Soc. Interface*, 4:669–674, 2007. 21, 28

[252] Ignacio Rodríguez-Iturbe, P D'odorico, A Porporato, and L Ridolfi. On the spatial and temporal links between vegetation, climate, and soil moisture. *Water Resources Research*, 35(12):3709–3722, 1999. 15, 17, 43, 44

[253] Ignacio Rodríguez-Iturbe, Paolo D'Odorico, Amilcare Porporato, and Luca Ridolfi. Tree-grass coexistence in savannas: The role of spatial dynamics and climate fluctuations. *Geophysical Research Letters*, 26(2):247–250, 1999. 15, 17, 43, 44

[254] Sabin Roman, Seth Bullock, and Markus Brede. Coupled societies are more robust against collapse: a hypothetical look at easter island. *Ecological Economics*, 132:264–278, 2017. 18, 71, 72

[255] Elin Röös, Bojana Bajželj, Pete Smith, Mikaela Patel, David Little, and Tara Garnett. Greedy or needy? land use and climate impacts of food in 2050 under different livestock futures. *Global Environmental Change*, 47:1–12, 2017. 70, 180

[256] Max Roser. Fertility rate. *Our World in Data*, 2020. https://ourworldindata.org/fertility-rate. 72, 73

[257] Max Roser and Hannah Ritchie. Food supply. *Our World in Data*, 2020. https://ourworldindata.org/food-supply. 73

[258] S. Rost, D. Gerten, A. Bondeau, W. Lucht, J. Rohwer, and S. Schaphoff. Agricultural green and blue water consumption and its influence on the global water system. *Water Resources Research*, 44(9), 2008. 13, 20

[259] RStudio Team. *RStudio: Integrated Development Environment for R*. RStudio, Inc., Boston, MA, 2015. 25

[260] Mikail Rubinov and O. Sporns. Complex network measures of brain connectivity: uses and interpretations. *Neuroimage*, 52(3):1059–1069, 2010. 28, 30

[261] Mikail Rubinov and Olaf Sporns. Complex network measures of brain connectivity: uses and interpretations. *Neuroimage*, 52(3):1059–1069, 2010. 8, 182

[262] Patricia Guidão Cruz Ruggiero, Marco Antônio Batalha, Vânia Regina Pivello, and Sérgio Tadeu Meirelles. Soil-vegetation relationships in cerrado (brazilian savanna) and semideciduous forest, southeastern brazil. *Plant Ecology*, 160(1):1–16, 2002. 49

[263] M. Sartori and S. Schiavo. Connected we stand: a network perspective on trade and global food security. *Food Policy*, 57:114–127, 2015. 13, 20, 21, 39

[264] Akiko Satake, Thomas K Rudel, and Ayumi Onuma. Scale mismatches and their ecological and economic effects on landscapes: A spatially explicit model. *Global Environmental Change*, 18(4):768–775, 2008. 17, 44

[265] Marten Scheffer, Victor Brovkin, and Peter M Cox. Positive feedback between global warming and atmospheric co2 concentration inferred from past climate change. *Geophysical Research Letters*, 33(10), 2006. 52

[266] E Schertzer, AC Staver, and SA Levin. Implications of the spatial dynamics of fire spread for the bistability of savanna and forest. *Journal of Mathematical Biology*, 70(1-2):329–341, 2015. 17, 44, 48, 49

[267] Christoph Schmitz, Hans van Meijl, Page Kyle, Gerald C Nelson, Shinichiro Fujimori, Angelo Gurgel, Petr Havlik, Edwina Heyhoe, Daniel Mason d'Croz, Alexander Popp, et al. Land-use change trajectories up to 2050: insights from a global agro-economic model comparison. *Agricultural economics*, 45(1):69–84, 2014. 70

[268] F. W. Scholz and M. A. Stephens. K-sample anderson-darling tests. *J. Am. Stat. Assoc.*, 82(399):918–924, 1987. 144

[269] Peter K Schott. Across-product versus within-product specialization in international trade. *The Quarterly Journal of Economics*, 119(2):647–678, 2004. 97

[270] Tim Searchinger, Richard Waite, C Hanson, J Ranganathan, P Dumas, and E Matthews. Creating a sustainable food future: a menu of solutions to feed nearly 10 billion people by 2050. synthesis report. *World Resources Institute*, 2018. 70, 100

[271] Ma Angeles Serrano and Marián Boguná. Topology of the world trade web. *Physical Review E*, 68(1):015101, 2003. 9, 13, 75

[272] R. Sharma. Food export restrictions: review of the 2007-2010 experience and considerations for disciplining restrictive measures. *FAO Commodity and Trade Policy Research Working Papers* http://www.fao.org/fileadmin/templates/est/PUBLICATIONS/Comm_Working_Papers/EST-WP32.pdf, 2011. 21, 31, 147

[273] M. D. Shirley and S. P. Rushton. The impacts of network topology on disease spread. *Ecol. Complex.*, 2(3):287–299, 2005. 30

[274] Shade T Shutters and Rachata Muneepeerakul. Agricultural trade networks and patterns of economic development. *PloS one*, 7(7):e39756, 2012. 27

[275] Lucas CR Silva and Madhur Anand. Mechanisms of araucaria (atlantic) forest expansion into southern brazilian grasslands. *Ecosystems*, 14(8):1354–1371, 2011. 14, 16, 44, 45, 105

[276] U Thara Srinivasan, Susan P Carey, Eric Hallstein, Paul AT Higgins, Amber C Kerr, Laura E Koteen, Adam B Smith, Reg Watson, John Harte, and Richard B Norgaard. The debt of nations and the distribution of ecological impacts from human activities. *Proceedings of the National Academy of Sciences*, 105(5):1768–1773, 2008. 98

[277] Arie Staal, Stefan C Dekker, Marina Hirota, and Egbert H van Nes. Synergistic effects of drought and deforestation on the resilience of the south-eastern amazon rainforest. *Ecological Complexity*, 22:65–75, 2015. 12

[278] Arie Staal, Stefan C Dekker, Chi Xu, and Egbert H van Nes. Bistability, spatial interaction, and the distribution of tropical forests and savannas. *Ecosystems*, 19(6):1080–1091, 2016. 15, 43, 66

[279] A Carla Staver, Sally Archibald, and Simon Levin. Tree cover in sub-saharan africa: rainfall and fire constrain forest and savanna as alternative stable states. *Ecology*, 92(5):1063–1072, 2011. 14, 15, 16, 44, 48, 50, 66

[280] A Carla Staver, Sally Archibald, and Simon A Levin. The global extent and determinants of savanna and forest as alternative biome states. *Science*, 334(6053):230–232, 2011. 15, 43, 49, 50

[281] A Carla Staver, William J Bond, William D Stock, Sue J Van Rensburg, and Matthew S Waldram. Browsing and fire interact to suppress tree density in an african savanna. *Ecological Applications*, 19(7):1909–1919, 2009. 49

[282] A Carla Staver and Simon A Levin. Integrating theoretical climate and fire effects on savanna and forest systems. *The American Naturalist*, 180(2):211–224, 2012. 15, 16, 18, 43, 44, 48, 66

[283] Henning Steinfeld, Pierre Gerber, TD Wassenaar, Vincent Castel, Mauricio Rosales, Mauricio Rosales, and Cees de Haan. *Livestock's long shadow: environmental issues and options*. Food & Agriculture Org., 2006. 180

[284] Nathan L Stephenson, AJ Das, R Condit, SE Russo, PJ Baker, Noelle G Beckman, DA Coomes, ER Lines, WK Morris, N Rüger, et al. Rate of tree carbon accumulation increases continuously with tree size. *Nature*, 507(7490):90, 2014. 67

[285] Thomas Stocker. *Climate change 2013: the physical science basis: Working Group I contribution to the Fifth assessment report of the Intergovernmental Panel on Climate Change*. Cambridge University Press, 2014. 52

[286] Katharine N Suding, Katherine L Gross, and Gregory R Houseman. Alternative states and positive feedbacks in restoration ecology. *Trends in Ecology & Evolution*, 19(1):46–53, 2004. 14, 44

[287] Samir Suweis, Joel A Carr, Amos Maritan, Andrea Rinaldo, and Paolo D'Odorico. Resilience and reactivity of global food security. *Proceedings of the National Academy of Sciences*, 112(22):6902–6907, 2015. 12, 13, 14, 21, 71, 72

[288] Samir Suweis, Megan Konar, Carol Dalin, Naota Hanasaki, Andrea Rinaldo, and Ignacio Rodriguez-Iturbe. Structure and controls of the global virtual water trade network. *Geophysical Research Letters*, 38(10), 2011. 14, 18, 22, 23, 41

[289] S. Tamea, F. Laio, and L. Ridolfi. Global effects of local food-production crises: a virtual water perspective. *Sci. Rep.*, 6:18803; 10.1038/srep18803, 2016. 20, 21, 22

[290] Robert J. Taylor. *Predation*. Population and community biology. Chapman and Hall, New York, 1984. 73

[291] R Core Team and contributors worldwide. *The R Stats Package*, 2018. R package version 3.6.0. 45

[292] Qawi K Telesford, Karen E Joyce, Satoru Hayasaka, Jonathan H Burdette, and Paul J Laurienti. The ubiquity of small-world networks. *Brain connectivity*, 1(5):367–375, 2011. 9, 75, 97, 182

[293] SM Thomas and MW Palmer. The montane grasslands of the western ghats, india: community ecology and conservation. *Community Ecology*, 8(1):67–73, 2007. 15, 16

[294] D. Thompson, P. Muriel, D. Russell, P. Osborne, A. Bromley, M. Rowland, C. Brown, et al. Economic costs of the foot and mouth disease outbreak in the united kingdom in 2001. *Rev. Sci. Tech. Oie.*, 21(3):675–685, 2002. 30, 147

[295] David Tilman, Christian Balzer, Jason Hill, and Belinda L Befort. Global food demand and the sustainable intensification of agriculture. *Proceedings of the national academy of sciences*, 108(50):20260–20264, 2011. 180

[296] C. P. Timmer. Causes of high food prices. *ADB Economics Working Paper Series* https://www.adb.org/sites/default/files/publication/28375/economics-wp128.pdf, 2009. 21, 23, 29, 30, 31, 141, 147

[297] Antony Trewavas. Malthus foiled again and again. *Nature*, 418(6898):668–670, 2002. 10

[298] Miroslav Trnka, Reimund P Rötter, Margarita Ruiz-Ramos, Kurt Christian Kersebaum, Jørgen E Olesen, Zdeněk Žalud, and Mikhail A Semenov. Adverse weather conditions for european wheat production will become more frequent with climate change. *Nat. Clim. Change*, 4(7):637–643, 2014. 23, 39, 40

[299] R. Trostle. Global agricultural supply and demand: factors contributing to the recent increase in food commodity prices. *USDA Economic Research Service* http://www1.eere.energy.gov/bioenergy/pdfs/global_agricultural_supply_and_demand.pdf, 2008. 21, 23, 29, 30, 31, 141, 147

[300] C. Tu, J. Grilli, and S. Suweis. Universality of Resilience Patterns in Generalized Lotka Volterra Dynamics and Beyond. *ArXiv e-prints*, June 2016. 39

[301] Albert W Tucker and Philip D Straffin Jr. The mathematics of tucker: A sampler. *The Two-Year College Mathematics Journal*, 14(3):228–232, 1983. 6

[302] Billie L Turner, Roger E Kasperson, Pamela A Matson, James J McCarthy, Robert W Corell, Lindsey Christensen, Noelle Eckley, Jeanne X Kasperson, Amy Luers, Marybeth L Martello, et al. A framework for vulnerability analysis in sustainability science. *Proceedings of the national academy of sciences*, 100(14):8074–8079, 2003. 12

[303] Graham M Turner. A comparison of the limits to growth with 30 years of reality. *Global environmental change*, 18(3):397–411, 2008. 11, 71

[304] Graham M Turner. Is global collapse imminent? an updated comparison of the limits to growth with historical data. *MSSI Research paper*, 4:21, 2014. 11

[305] James D Turner, Michael J Mazzoleni, Jared A Little, Dane Sequeira, and Brian P Mann. A nonlinear model for the characterization and optimization of athletic training and performance. *Biomedical Human Kinetics*, 9(1):82–93, 2017. 2

[306] BL Turner Ii. Vulnerability and resilience: Coalescing or paralleling approaches for sustainability science? *Global Environmental Change*, 20(4):570–576, 2010. 12

[307] Thomas W Valente, Kathryn Coronges, Cynthia Lakon, and Elizabeth Costenbader. How correlated are network centrality measures? *Connections (Toronto, Ont.)*, 28(1):16, 2008. 86

[308] Ingrid A van de Leemput, Egbert H van Nes, and Marten Scheffer. Resilience of alternative states in spatially extended ecosystems. *PloS One*, 10(2):e0116859, 2015. 17, 44

[309] Guido R Van Der Werf, James T Randerson, Louis Giglio, Nadine Gobron, and AJ Dolman. Climate controls on the variability of fires in the tropics and subtropics. *Global Biogeochemical Cycles*, 22(3), 2008. 54

[310] Egbert H van Nes, Marina Hirota, Milena Holmgren, and Marten Scheffer. Tipping points in tropical tree cover: linking theory to data. *Global change biology*, 20(3):1016–1021, 2014. 16, 18, 44, 48, 50, 53

[311] Egbert H van Nes, Arie Staal, Stijn Hantson, Milena Holmgren, Salvador Pueyo, Rafael E Bernardi, Bernardo M Flores, Chi Xu, and Marten Scheffer. Fire forbids fifty-fifty forest. *PloS One*, 13(1):e0191027, 2018. 15, 17, 43, 44, 49, 50, 54, 66

[312] Detlef P Van Vuuren, Michel GJ Den Elzen, Paul L Lucas, Bas Eickhout, Bart J Strengers, Bas Van Ruijven, Steven Wonink, and Roy Van Houdt. Stabilizing greenhouse gas concentrations at low levels: an assessment of reduction strategies and costs. *Climatic change*, 81(2):119–159, 2007. 51

[313] Detlef P Van Vuuren, Jae Edmonds, Mikiko Kainuma, Keywan Riahi, Allison Thomson, Kathy Hibbard, George C Hurtt, Tom Kram, Volker Krey, Jean-Francois Lamarque, et al. The representative concentration pathways: an overview. *Climatic change*, 109(1-2):5, 2011. 51

[314] Mark T Van Wijk and Ignacio Rodriguez-Iturbe. Tree-grass competition in space and time: Insights from a simple cellular automata model based on ecohydrological dynamics. *Water Resources Research*, 38(9):18–1, 2002. 15, 17, 43, 44, 66

[315] Jeremy VanDerWal, Lorena Falconi, Stephanie Januchowski, Luke Shoo, and Collin Storlie. *SDMTools: Species Distribution Modelling Tools: Tools for processing data associated with species distribution modelling exercises*, 2014. R package version 1.1-221. 47

[316] Brian Walker and David Salt. *Resilience thinking : sustaining ecosystems and people in a changing world*. Island Press, Washington, 2006. 12

[317] X. F. Wang and G. Chen. Complex networks: small-world, scale-free and beyond. *IEEE Circuits Syst. Mag.*, 3(1):6–20, 2003. 28, 30

[318] Zhen Wang, Michael A Andrews, Zhi-Xi Wu, Lin Wang, and Chris T Bauch. Coupled disease–behavior dynamics on complex networks: A review. *Physics of life reviews*, 15:1–29, 2015. 13

[319] Stanley Wasserman, Katherine Faust, et al. *Social network analysis: Methods and applications*, volume 8. Cambridge university press, 1994. 182

[320] Duncan J Watts and Steven H Strogatz. Collective dynamics of 'small-world' networks. *nature*, 393(6684):440, 1998. 5, 7, 9, 28, 30, 75, 97, 181

[321] E. W. Weisstein. Simple directed graph. Retrieved from `http://mathworld.wolfram.com/SimpleDirectedGraph.html`, 2015. 144

[322] T. Wheeler and J. von Braun. Climate change impacts on global food security. *Science*, 341(6145):508–513, 2013. 21

[323] U. Wilensky. Netlogo flocking model, 1998. `http://ccl.northwestern.edu/netlogo/models/Flocking`. 3

[324] U. Wilensky. Netlogo, 1999. `http://ccl.northwestern.edu/netlogo/`. 3, 6

[325] U. Wilensky. Netlogo ising model, 2003. `http://ccl.northwestern.edu/netlogo/models/Ising`. 6

[326] Allen Wilhite. Bilateral trade and 'small-world'networks. *Computational Economics*, 18(1):49–64, 2001. 9, 13, 75, 97

[327] K. Wilkinson, W. P. Grant, L. E. Green, S. Hunter, M. J. Jeger, P. Lowe, G. F. Medley, P. Mills, J. Phillipson, G. M. Poppy, et al. Infectious diseases of animals and plants: an interdisciplinary approach. *Philos. T. Roy. Soc. B*, 366:1933–1942, 2011. 21

[328] RJ Williams, GA Duff, DMJS Bowman, and GD Cook. Variation in the composition and structure of tropical savannas as a function of rainfall and soil texture along a large-scale climatic gradient in the northern territory, australia. *Journal of Biogeography*, 23(6):747–756, 1996. 49

[329] Stefan Wirsenius, Christian Azar, and Göran Berndes. How much land is needed for global food production under scenarios of dietary changes and livestock productivity increases in 2030? *Agricultural systems*, 103(9):621–638, 2010. 70

[330] F. Wu and H. Guclu. Aflatoxin regulations in a network of global maize trade. *PLoS ONE*, 7:e45151; 10.1371/journal.pone.0045151, 2012. 13, 21, 26

[331] F. Wu and H. Guclu. Global maize trade and food security: Implications from a social network model. *Risk Anal.*, 33:2168–2178, 2013. 21

[332] Jianguo Wu. Landscape sustainability science: ecosystem services and human well-being in changing landscapes. *Landscape ecology*, 28(6):999–1023, 2013. 11, 12, 67

[333] Jianguo Wu and Tong Wu. Ecological resilience as a foundation for urban design and sustainability. In *Resilience in ecology and urban design*, pages 211–229. Springer, 2013. 12

[334] Donald J Wuebbles, David W Fahey, and Kathy A Hibbard. Climate science special report: fourth national climate assessment, volume i. 2017. 53

[335] Bert Wuyts, Alan R Champneys, and Joanna I House. Amazonian forest-savanna bistability and human impact. *Nature Communications*, 8:15519, 2017. 17, 44, 49, 50

[336] Li Xue, Gang Liu, Julian Parfitt, Xiaojie Liu, Erica Van Herpen, Åsa Stenmarck, Clementine O'Connor, Karin Östergren, and Shengkui Cheng. Missing food, missing data? a critical review of global food losses and food waste data. *Environmental science & technology*, 51(12):6618–6633, 2017. 73

[337] Florian Zabel, Birgitta Putzenlechner, and Wolfram Mauser. Global agricultural land resources–a high resolution suitability evaluation and its perspectives until 2100 under climate change conditions. *PloS one*, 9(9), 2014. 179

[338] An Zeng, Zhesi Shen, Jianlin Zhou, Jinshan Wu, Ying Fan, Yougui Wang, and H Eugene Stanley. The science of science: From the perspective of complex systems. *Physics Reports*, 714:1–73, 2017. 1, 4, 5, 7

APPENDICES

Appendix A

Supplementary information - Dynamics of the global wheat trade network and resilience to shocks

A.1 Supplementary methods

A.1.1 Defining a continuous trade network

Previously, weighted representations of agri-food trade networks and the associated virtual water trade network have been simplified by considering a "backbone" network. This includes only the dominant links, which are responsible for the majority of the trade volume [89, 174, 122, 238]. We have taken a different approach, considering only continuous trade partnerships to simplify the model. By doing this, we avoid having to determine when and how edges should be deleted from our modelled networks. Additionally, it follows that a trade link that exists over a larger number of years should have a higher probability of being impacted by a shock than one that is only infrequently part of the trade network. Thus, continuous trade partnerships are of interest when considering how shocks impact trade networks. While our network is not a conventional "backbone" network, there is a positive correlation between a country's total degree in the continuous trade network and its total trade volume that is significant at the 5% level (Figure A.1). This would suggest that countries that are important in the continuous trade network would also be influential in a "backbone" network.

We define a continuous trade partnership in the 1986-2013 data set as an import or export that has occurred in at least 3 consecutive years as of the end of 2013; i.e. one has occurred $\forall\ t \in [a, 2013]$ where $a \leq 2011$. A 3-year cut-off is employed to account for the fact that the number of nodes and edges in the network drastically increases if trade partnerships that existed in 2012 and 2013, or only in 2013 are included (Figure A.2). This suggests that many trade partnerships do not persist for more than 2 years. In order to account for the fact that shocks to the real-world network may have interrupted the continuity of otherwise well-established trade relationships, all trade partnerships for which trades have occurred in 90% or more of the years since they were initiated are included. The 90% threshold ensures that an otherwise continuous long-term trade relationship, spanning decades, will not be excluded from the network due to a lack of trade in 1 or 2 years. Since the majority of shocks to the wheat network, and other staple crop networks such as rice and maize, only persist for a single year, this translates to roughly 1 or 2 shocks [205, 299, 76, 296, 83, 132, 100, 10]. The continuity condition has the added benefit of ensuring that countries that have ceased to exist since 1986 are excluded from the network, a logical assumption if any predictions of the future of the network are to be made.

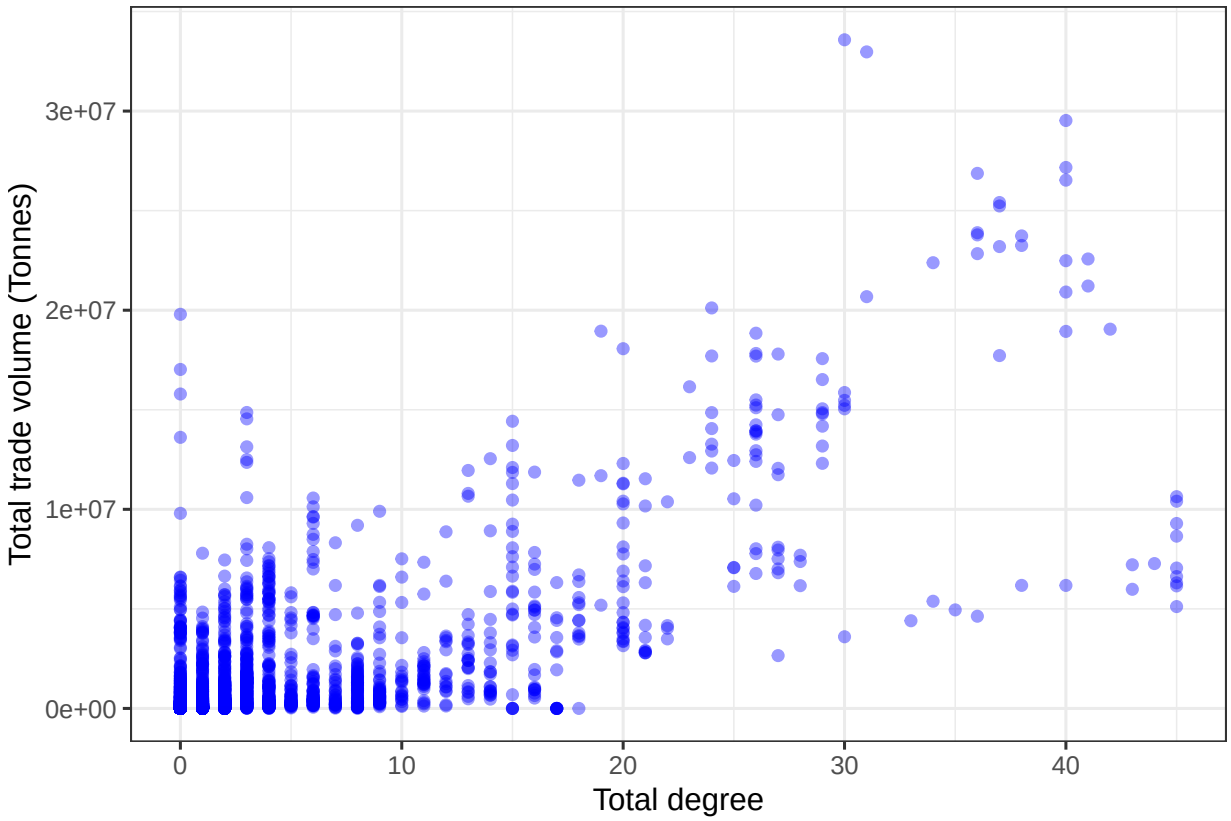

Figure A.1: **Relationship between total degree in the continuous trade network and total trade volume from 1986-2011.** Each point represents a single country in a single year, with a total degree of 0 corresponding to a country not included in the continuous trade network in that year. The darker the point, the higher the number of countries with that combination of total degree and trade volume. The correlation between total degree and trade volume is significant at the 5% level (p-value $< 2.2 \times 10^{-16}$).

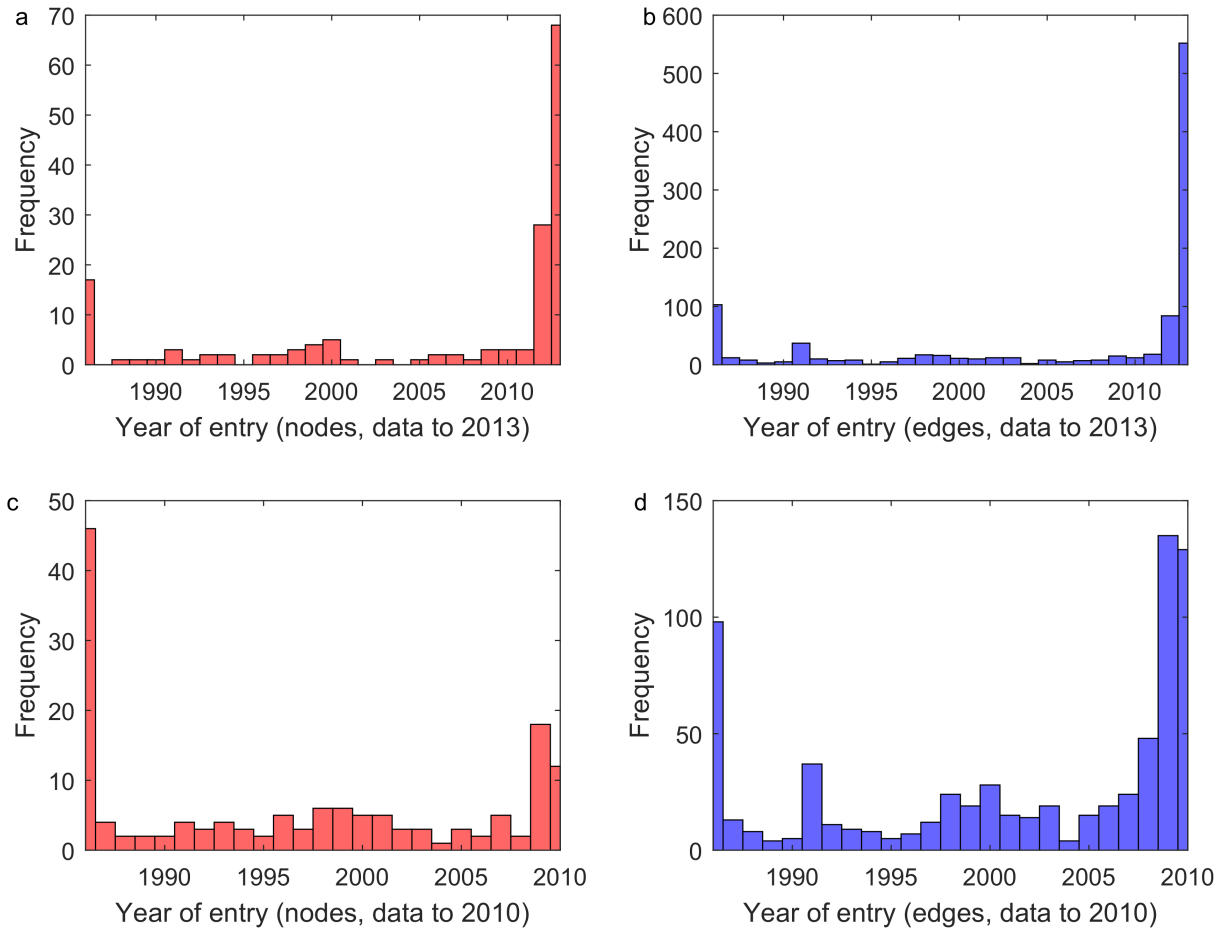

Figure A.2: **Year of entry for nodes and edges to the global wheat trade network.** (a) Year in which some country i not previously engaged in any continuous trade partnerships first initiated a continuous trade partnership with another country that has occurred in all subsequent years up to (and including) 2013. (b) year in which a continuous trade partnership between countries i and j was initiated that has existed for all subsequent years up to (and including) 2013. (c) year in which some country i not previously engaged in any continuous trade partnerships first initiated a continuous trade partnership with another country that has occurred in all subsequent years up to (and including) 2000. (d) year in which a continuous trade partnership between countries i and j was initiated that has existed for all subsequent years up to (and including) 2000. Plots (a) and (b) use data for 1986-2013, (c) and (d) use data for 1986-2000. For all cases, the 90% threshold on continuity is applied, and an export partnership is considered as separate to an import partnership.

A.1.2 Estimating rate of network growth

In order to estimate the passage of time during network formation, a logistic growth model was fit to the cumulative number of edges in the wheat trade network by year, $m(t)$, for 1986-2013 [107]. This $m(t)$ cannot exceed the maximum possible number of edges in a directed graph with $n(t)$ nodes where $\max(m) = n(n-1)$ [321]. We assume that the network can be fully saturated, or have total reciprocity, as the wheat trade network includes reciprocal trades (Figure A.3c). Using the 244 countries and dependent territories in the world as of 2015, $n_{max} = 244$, the largest possible wheat trade network would contain $m_{max} = 59292$ edges [213]. This value was held constant throughout the fitting process, with the slope and midpoint of the sigmoid estimated using linear regression. A 2-sample Anderson-Darling test (version 1) comparing the fit to data for 1986-2010 gives $p = 0.66728$ [268]. As $p > 0.05$, we concluded that both samples came from the same distribution at the 5% significance level.

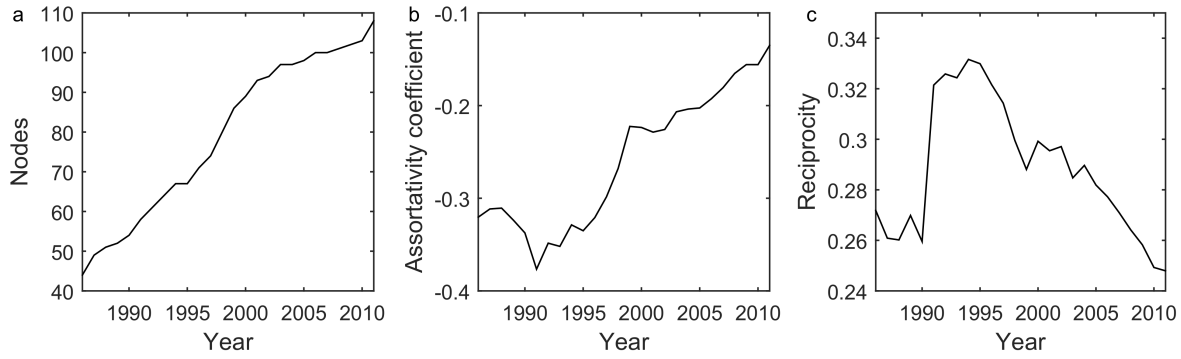

Figure A.3: **Temporal metric evolution for the continuous wheat trade network.** (a) Number of nodes. (b) assortativity. (c) reciprocity. Data shown for 1986-2013.

Using the fit (Figure A.4) we estimated the number of edges added to the network each year, running all simulations for $t \in [1875, 2060]$. The logistic growth model will allow us to introduce shocks with realistic durations. Even if no new countries enter the trade network post-2013, meaning $n_{max} = 108$, we would have $m_{max} = 11556$, a threshold not exceeded by our logistic model for $t \in [1875, 2060]$, though the parameters chosen for the logistic model with $m_{max} = 59292$ would provide a poor fit for the new upper bound on the possible number of edges. However, the number of nodes in the network has increased over time (Figure A.2a, Figure A.3a), and thus such a scenario is unlikely. We acknowledge that without empirical data on $m(t)$ for $t < 1986$ or $t > 2013$, it is difficult to justify the use of one functional form over another; it is possible that a linear or exponential function better describes $m(t)$ than the logistic form we assume.

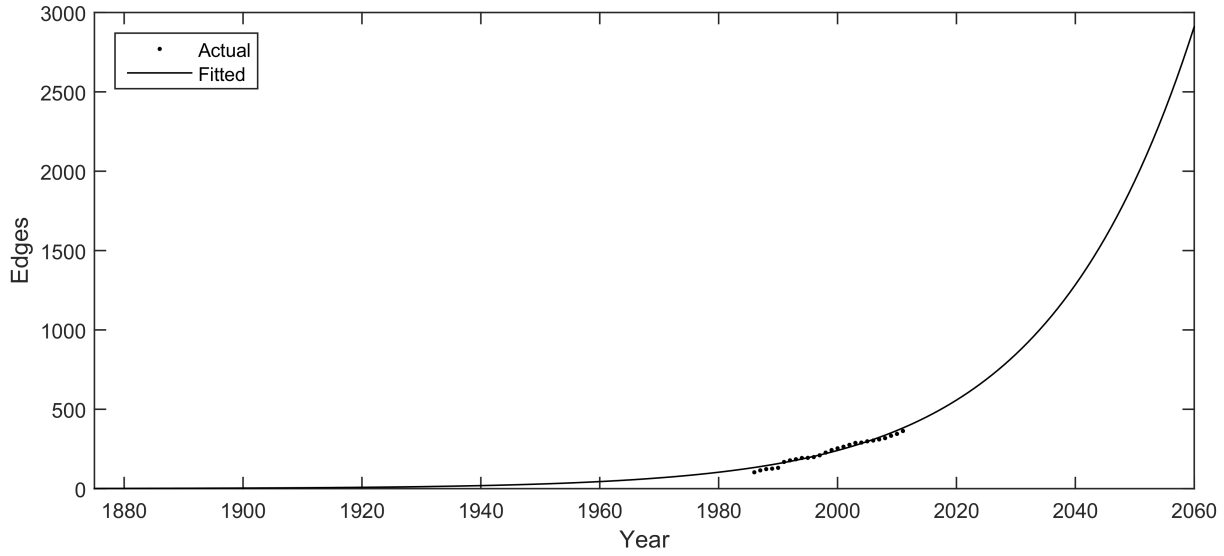

Figure A.4: **Growth of the number of continuous trade partnerships in the wheat trade network over time.** The equation of the logistic growth model for number of edges is $m(t) = 59292/(1 + e^{-(t-2130)/23.62})$, the fit gives p=0.66728.

A.1.3 Model parametrization

We ran approximately 5000 simulations for combinations of α and β from Equation 2.1 as well as C and λ from Equation 2.3, across ranges for all parameters. Ranges for α and β were set to $[1, 200]$, based on the parameters used in previous similar models [117, 116]. For C, λ and ϵ we experimentally determined ranges that led to reasonable model outcomes in terms of the network parameters. These ranges are $C \in [25, 1500]$, $\lambda \in [0.01, 0.1]$ and $\epsilon \in [9.0 \times 10^{-5}, 1.2 \times 10^{-5}]$. Once suitable ranges had been determined, we began testing parameter sets using large increments for all parameter ranges. This allowed us to focus on a smaller portion of the parameter space; $\alpha,\ \beta \in [1, 5]$, $C \in [25, 1025]$, $\lambda \in [0.01, 0.05]$ and $\epsilon \in [9.5 \times 10^{-5}, 1.15 \times 10^{-5}]$, where model outputs for assortativity, reciprocity, and number of nodes were reasonably close to those for the real world network. Our 100 best networks had parameter sets drawn from these reduced ranges (Figure A.5).

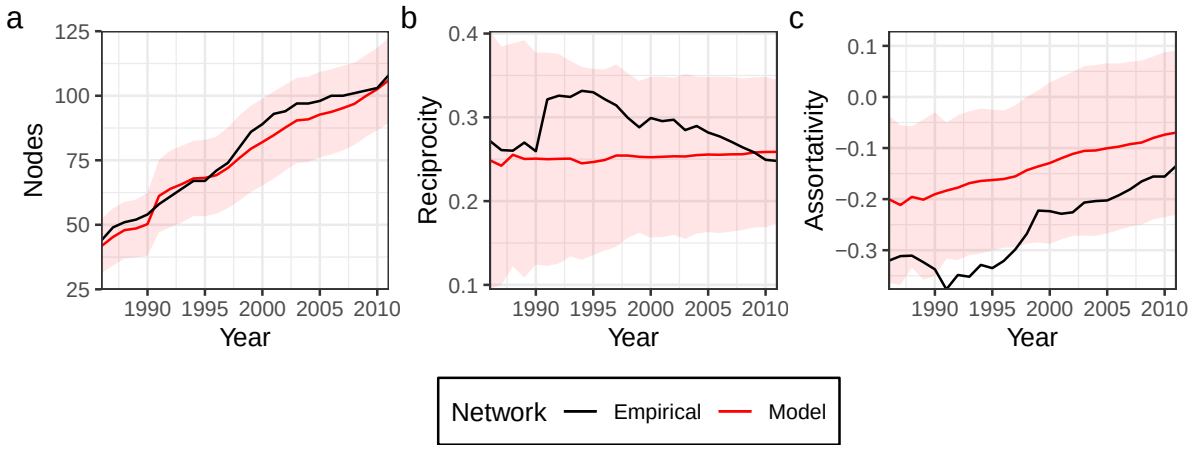

Figure A.5: **Network metrics for model parametrization 1986-2011.** Solid red line represents the mean metric value for networks generated using the top 100 parameter sets ranked by least MSE normalized over assortativity, number of nodes, and reciprocity. The envelope represents a range of ±2 standard deviations from the mean.

A.1.4 Implementing shocks

For attacks, countries are targeted based on their connectivity. Connectivity can be determined using various centrality measures such as degree, out-degree, closeness, and betweenness centrality [4, 244, 183, 169, 164, 157]. We define connectivity in terms of total degree centrality. This means that an attack will cause the sequential removal of the outgoing edges belonging to the countries with the highest total number of trade links. We limit ourselves to considering sudden shocks where production level adjustments occur on too long a timescale to counter their effects [119]. For the duration of a shock, affected countries will not export; existing export links are removed, and new export links cannot be formed. After the shock, the affected countries, which no longer have any exports, can begin to establish new export links. Following the removal of export links for affected countries, new links are formed to replace those removed. The formation of new links represents 2 occurrences whereby countries who previously imported from the affected countries seek to replace their lost trade volume; they may form new trade partnerships themselves or rely more on existing partnerships. This increased dependence on existing trade partners, in turn, means those countries either rely more heavily on *their* partners or form new trade links. While we do not explicitly model how the weights of trade flows are redistributed due to a shock, this rewiring of the network to account for changes in the availability of exports is conceptually similar.

A.1.5 Determining realistic shock durations and sizes

Each shock will be introduced for 1-5 years and impact 1-15 countries, as, depending on the type of shock, the duration and severity will vary. For example, the late Victorian Great Drought of 1876-1878 had a protracted effect on global trade networks of rice products [238]. Another case, the 2001 outbreak of foot and mouth disease in the United Kingdom caused shocks to the global beef, sheep, and pig meat trade networks lasting approximately a year until the lifting of export bans in 2002 [294]. Our ranges were drawn from a survey of the literature on recent export restrictions. These export restrictions include bans, quotas, and taxes resulting from food shortages that have influenced global trade. During the 2007/08 global food crisis, 15 countries (including 6 of the top 17 wheat exporters) restricted wheat exports, in some cases implementing complete export bans [205, 299, 76, 296, 83, 238]. Additionally, rice export was restricted in 14 countries (including 4 of the top 9 rice exporters), grain export in 15, maize in 3, palm oil in 2, and oilseed & vegetable oils in 1 [205, 299, 76, 296, 132, 238]. Six of the 17 largest wheat exporters (responsible for 90% of total trade) introduced trade restrictions, as did 4 of the 9 largest rice exporters [238, 272]. India maintained bans and restrictions on rice and wheat exports from February 2007 to September 2011 [125]. In 2010/11 Russia, Ukraine, and Kazakhstan all implemented export restrictions on grain [100, 10]. While not all of these restrictions have resulted in the complete cessation of exports, they provide us with a rough estimate of the appropriate size and length of shocks. Additionally, we use the 07/08 and 10/11 shocks as a template for our multiple shock scenario; for all cases of multiple shocks a gap of 2 years will be observed between shocks.

A.2 Network analysis for agri-food commodities

A.2.1 Materials and methods

Trade data for 549 commodities from 1986-2010 was obtained from the United Nations Food and Agriculture Organization's FAOSTAT database [107]. These commodities included crops, animal products, and crop-derived products. A $N \times N$ trade matrix, where N is the number of countries in the network, was used to represent the trade network for each commodity. Trades were extracted from the FAOSTAT database of imports, within the 25 year period. All cases where a value of 0 was reported for a trade were excluded, as these are generally caused by rounding small trade values to 0, or due to missing data. We believe that these excluded trades would not significantly alter the overall commodity-specific trade networks, in regards to the metrics we measured. The $(i, j)^{th}$ element of

the matrix represents the export of the commodity under consideration from country j to country i. The value of this $(ij)^{th}$ element is the volume of the export from country j to country i. When comparisons were carried out, commodity-specific networks were given equal weighting, regardless of their size, in order to remove any bias towards the larger networks. These matrices were used to calculate diameter, average path length (AvPL), assortativity, density, average clustering coefficient (transitivity), average degree (AvDeg), the unweighted normalized average betweenness centrality coefficient (BCC), and reciprocity. Finally, the number of nodes and edges and the total value of the trade conducted with each network were recorded. These values were averaged over all commodity networks.

To determine relationships between metrics, the Pearson product-moment correlation coefficient, r, was calculated for all possible pairs of metrics. The associated p-values used were adjusted using the Holm-Bonferroni method to reduce the frequency of "false positives" resulting from multiple comparisons. Using a similar method as Jamakovic *et al.* the number of metrics required to describe the network was reduced [166]. Any correlation with a p-value > 0.05 was discarded as not significant at the 5% level and those where $|r| \leq 0.6$ were discarded as weak. Once groups of highly correlated metrics were identified, 1 metric from each group was selected for further analysis, to avoid redundancy. All metrics not significantly correlated with others were kept. For the purposes of describing our results, Jamakovic *et al.*'s definitions of correlation strength were used: $0 \leq |r| \leq 0.3$ (no correlation); $0.3 \leq |r| \leq 0.6$ (mild correlation); $0.6 \leq |r| \leq 0.9$ (significant correlation); $0.9 \leq |r| \leq 1.0$ (strong correlation) [166].

A.2.2 Results

When network metrics were calculated to give correlations (Figure A.6) the number of commodity networks within the sample was reduced to 524. This was necessary as some networks contained an extremely low number of nodes and edges, meaning certain metrics could not be properly calculated. Two groups of metrics had significant to strong intra-group correlation: a size group containing the average path length, network diameter, and betweenness centrality coefficient, and a connectivity group of average node degree, density, average clustering coefficient, reciprocity and the number of nodes and edges (Figure A.6). The highly correlated metric groups for the agri-food trade network are not the same as those found by Jamakovic *et al.* in their study of a variety of real-world networks, though there is some overlap [166].

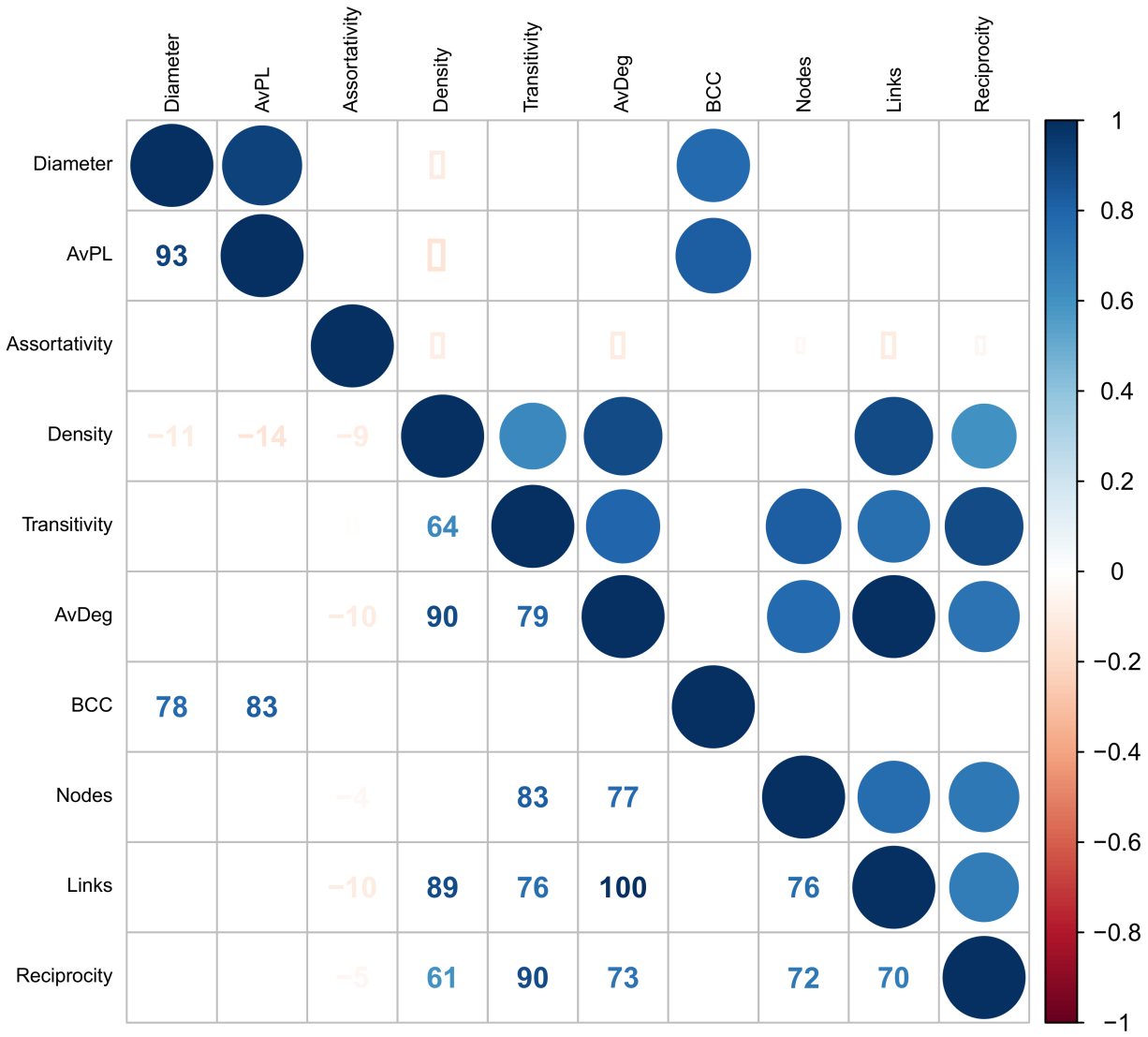

Figure A.6: **Correlation heat map for network metrics using 524 commodity networks for 1986-2010.** All correlations shown are significant at the 5% level, non-Holm's-adjusted, and are given as % values.

A.3 Supplementary figures

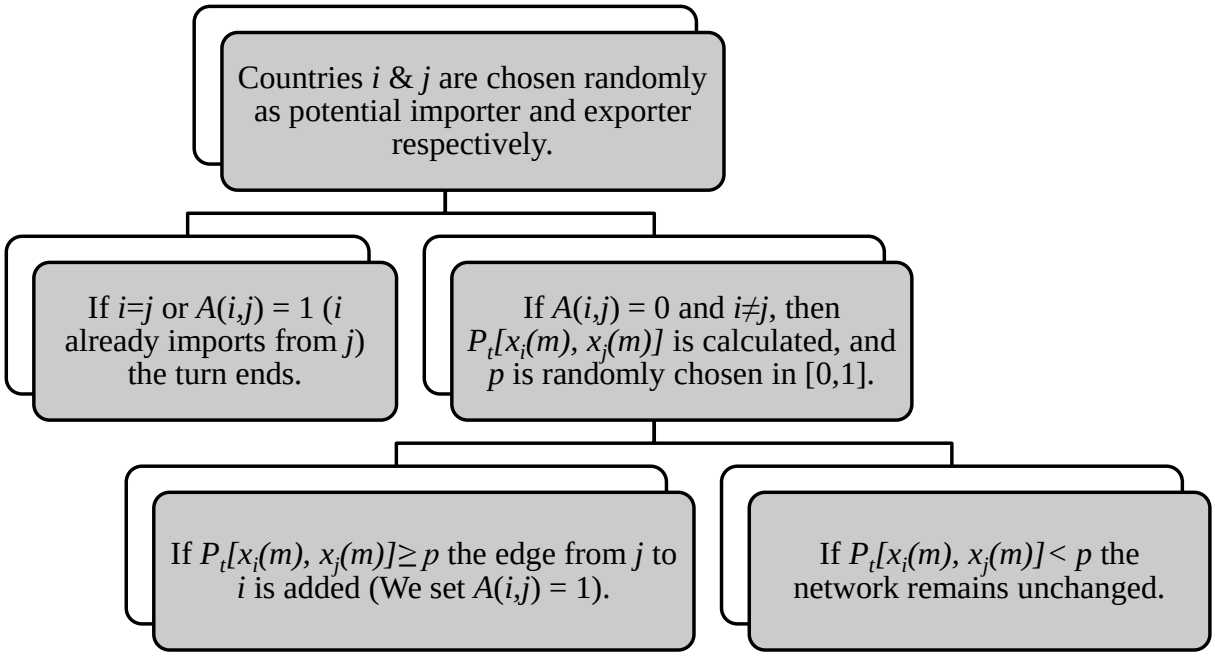

Figure A.7: **Decision-making process at each turn of dynamic network model.** If the final $P_t[x_i(m), x_j(m)] \geq p$ condition is not met, the turn ends with no new edges formed.

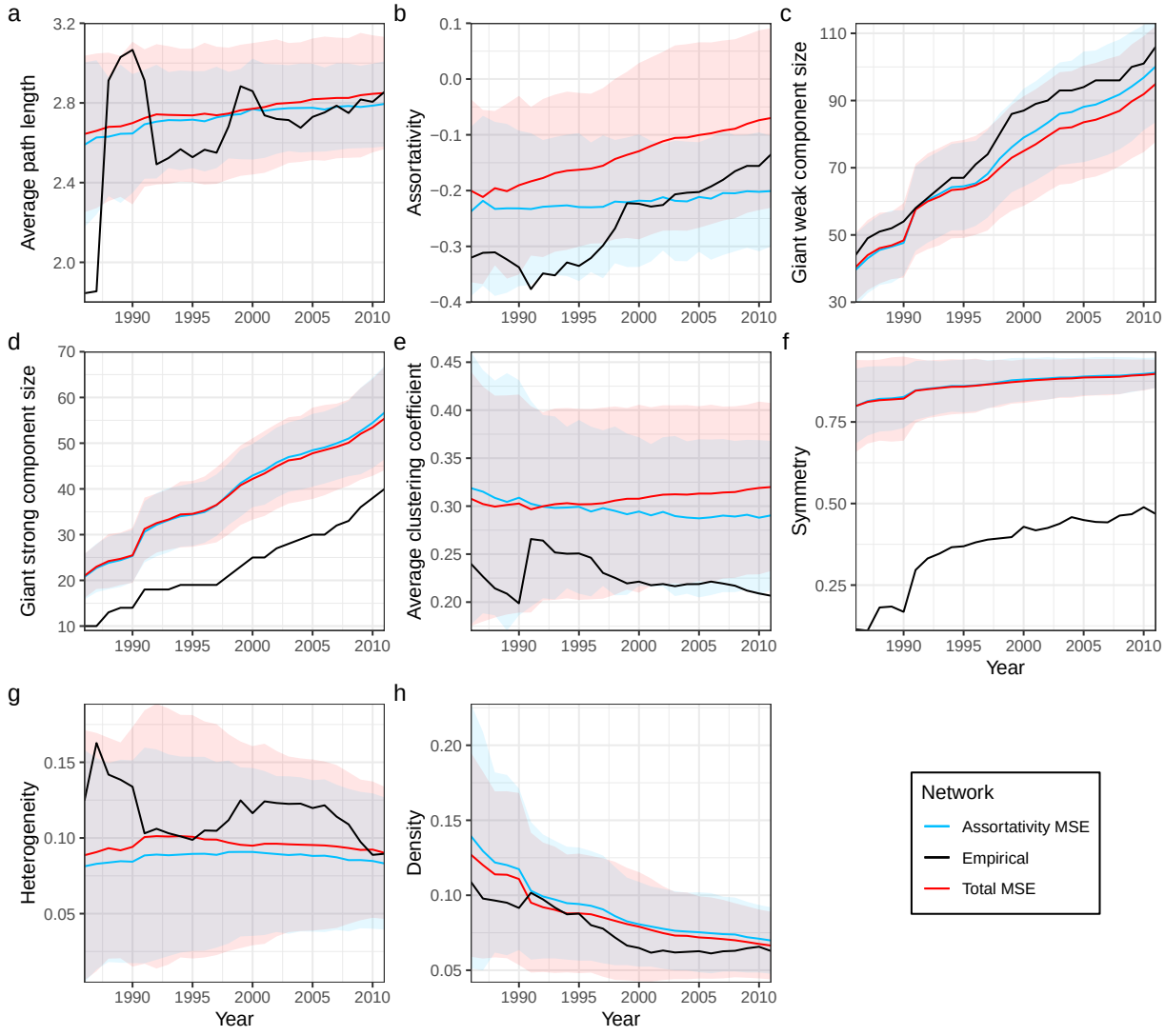

Figure A.8: **Selected network metrics 1986-2011.** Lines represents the mean metric value for networks generated using the top 100 parameter sets ranked by least MSE for assortativity (dotted) and normalized across assortativity, number of nodes, and reciprocity (solid). The envelopes represent a range of ±2 standard deviations from the mean.

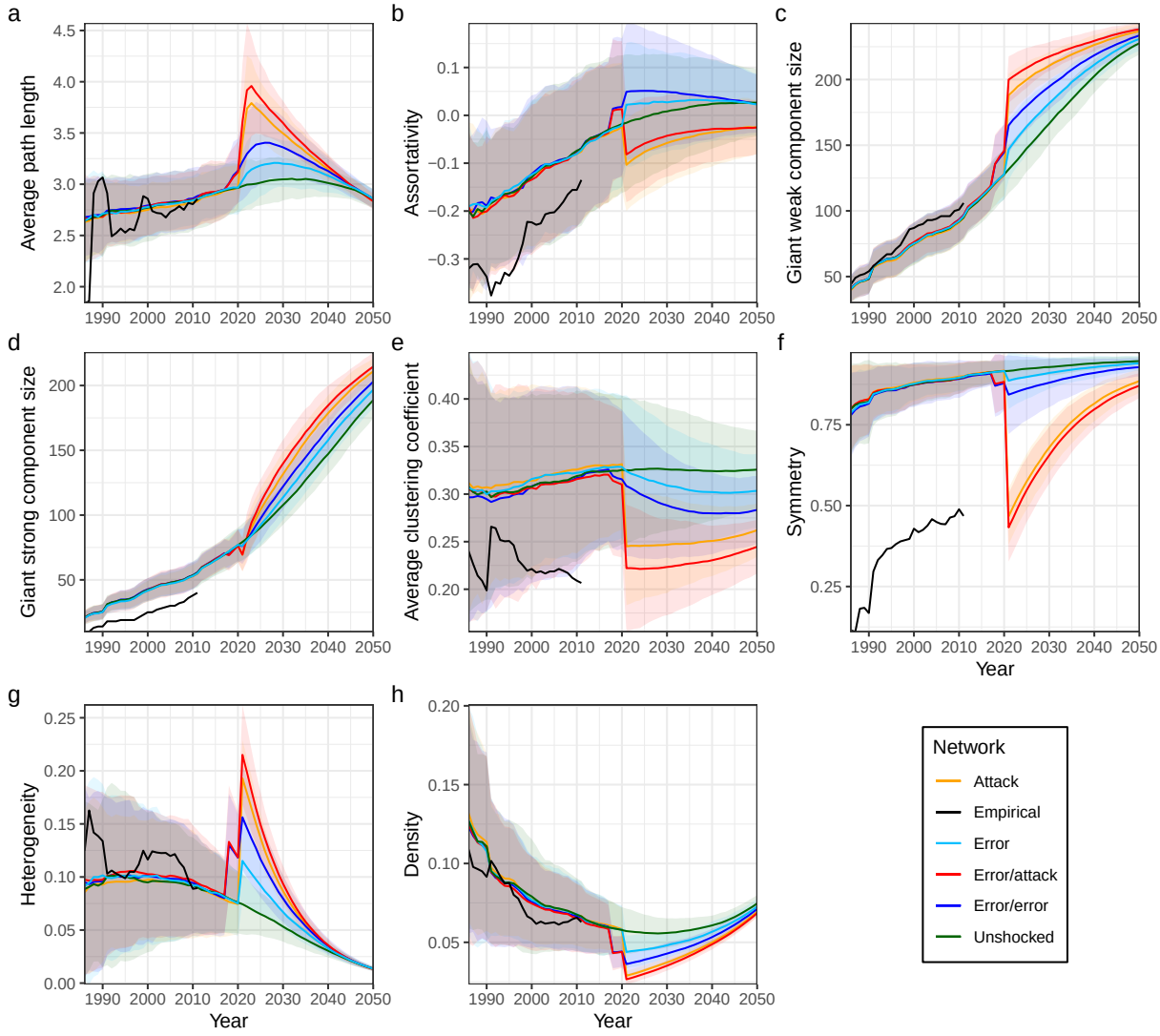

Figure A.9: **Impact of previous errors on changes in network metrics due to a subsequent shock.** Initial error to double shocked networks (shown in blue and red) occurred in 2017-18, all networks shocked in 2020-21. All shocks were low severity/short duration. Solid lines represent the mean metric value for networks generated using the top 100 parameter sets ranked by least MSE normalized over assortativity, number of nodes, and reciprocity. The envelopes represent a range of ±2 standard deviations from the mean for each shock scenario.

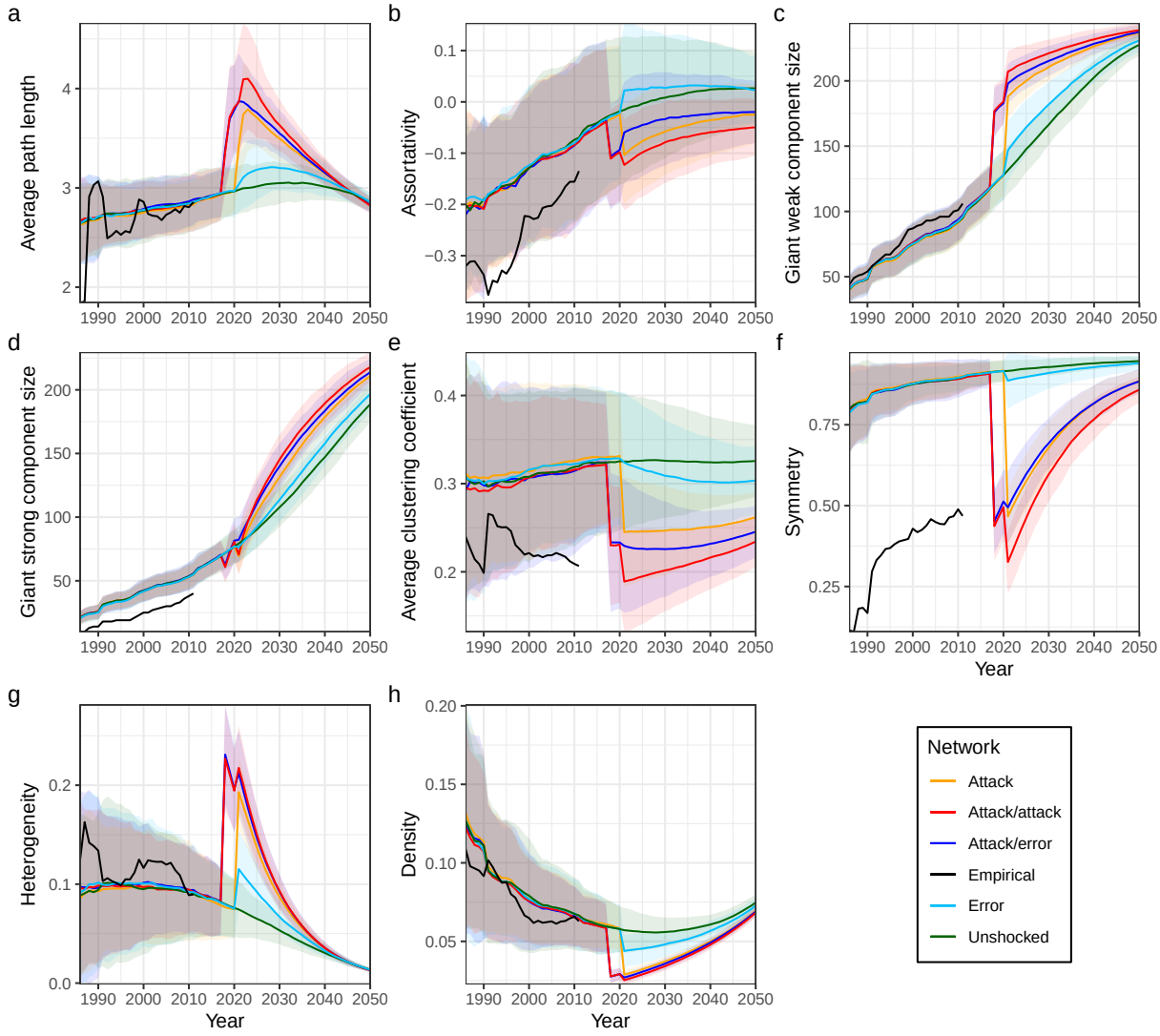

Figure A.10: **Impact of previous attacks on changes in network metrics due to a subsequent shock.** Initial attack on double shocked networks (shown in blue and red) occurred in 2017-18, all networks shocked in 2020-21. All shocks were low severity/short duration. Solid lines represent the mean metric value for networks generated using the top 100 parameter sets ranked by least MSE normalized over assortativity, number of nodes, and reciprocity. The envelopes represent a range of ±2 standard deviations from the mean for each shock scenario.

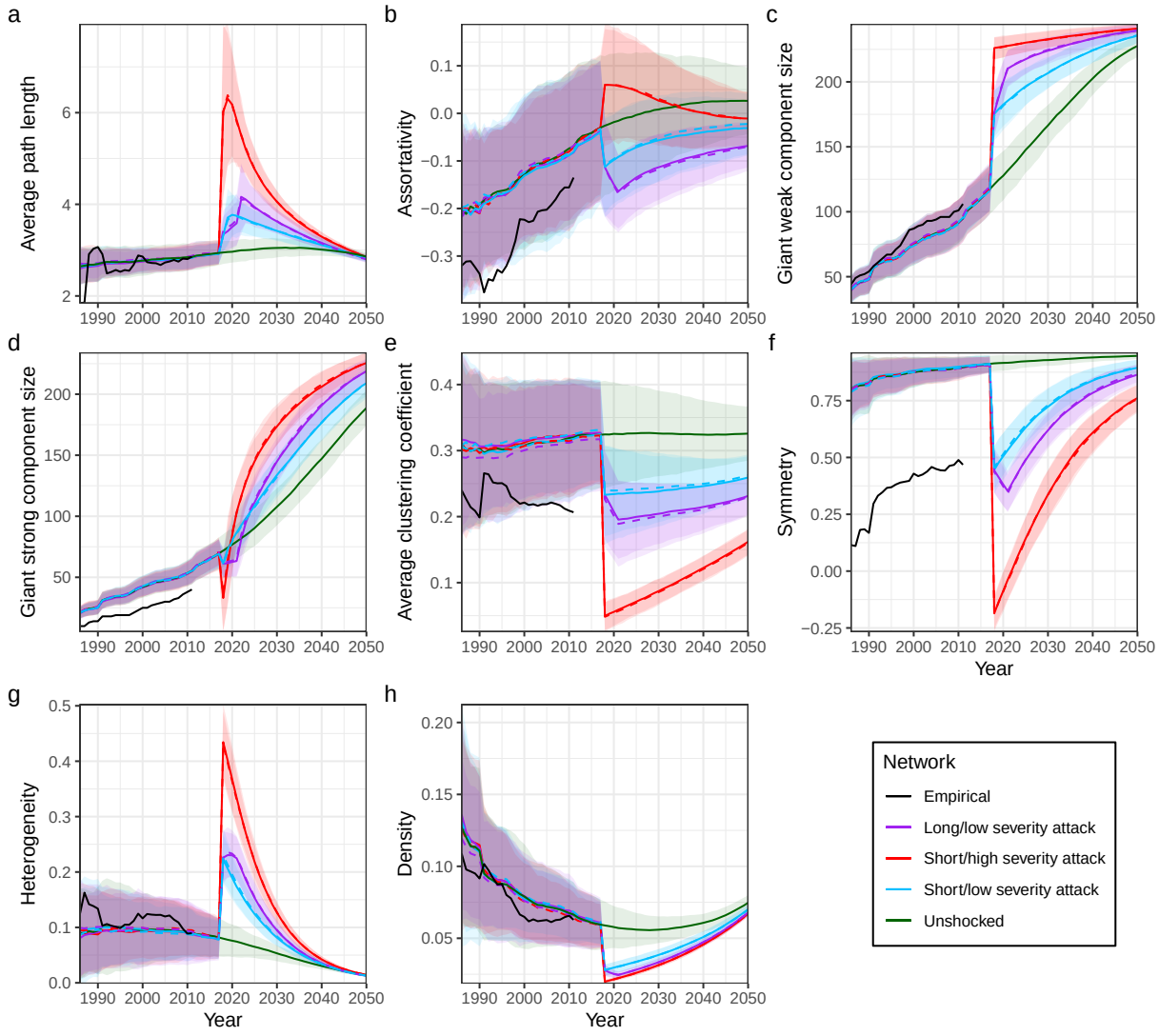

Figure A.11: **Comparison of sequential and simultaneous attacks.** Shocks occurred in 2017-18. Solid lines represent the mean metric value for networks generated using the top 100 parameter sets ranked by least MSE normalized over assortativity, number of nodes, and reciprocity. The envelopes represent a range of ±2 standard deviations from the mean for each shock scenario. Targets are selected by largest total degree.

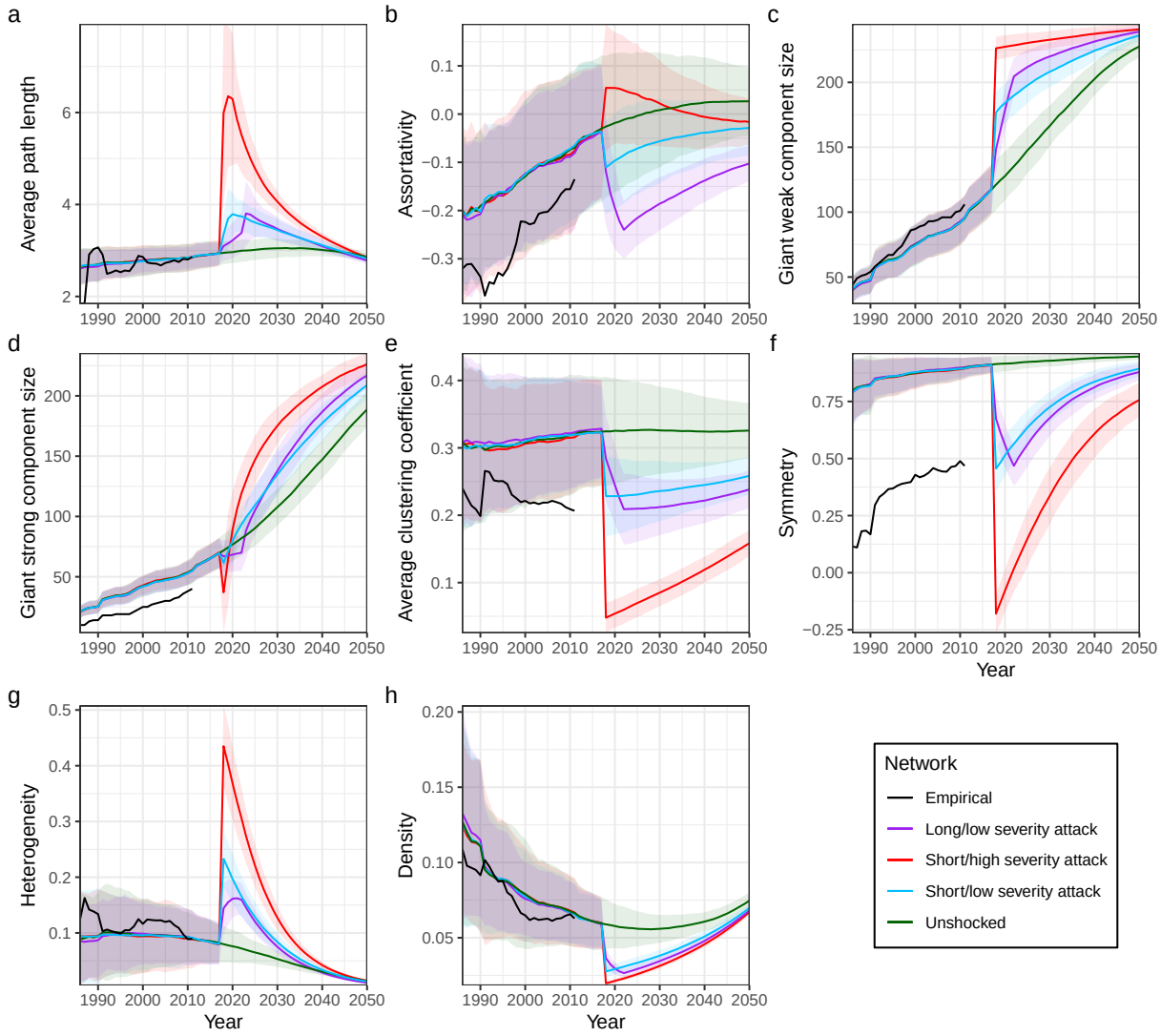

Figure A.12: **Impact of out-degree attacks on network metrics.** Shocks occurred in 2017-18. Solid lines represent the mean metric value for networks generated using the top 100 parameter sets ranked by least MSE normalized over assortativity, number of nodes, and reciprocity. The envelopes represent a range of ±2 standard deviations from the mean for each shock scenario. Targets are selected by largest out-degree.

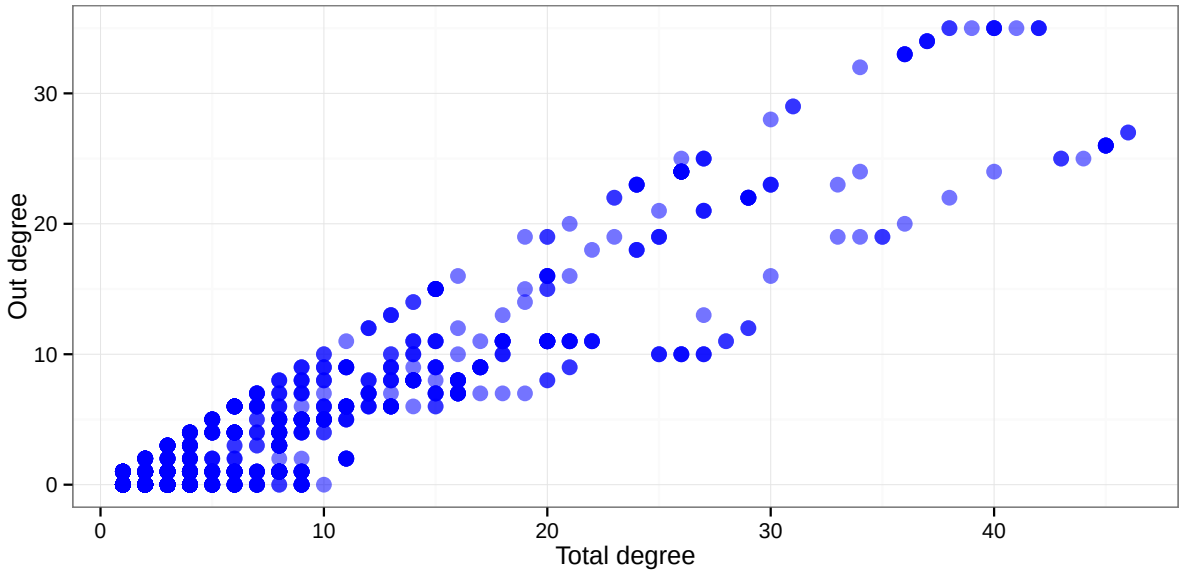

Figure A.13: **Relationship between total degree and out-degree in the continuous wheat trade network from 1986-2011.** Each point represents a single country in a single year, with a total degree of 0 corresponding to a country not included in the continuous trade network in that year. The darker the point, the higher the number of countries with that combination of total and out-degree. The correlation between total and out-degree is significant at the 5% level (p-value $< 2.2 \times 10^{-16}$).

Appendix B

Supplementary information - Spatial structure in protected forest-grassland mosaics: exploring futures under climate change

B.1 Supplementary figures

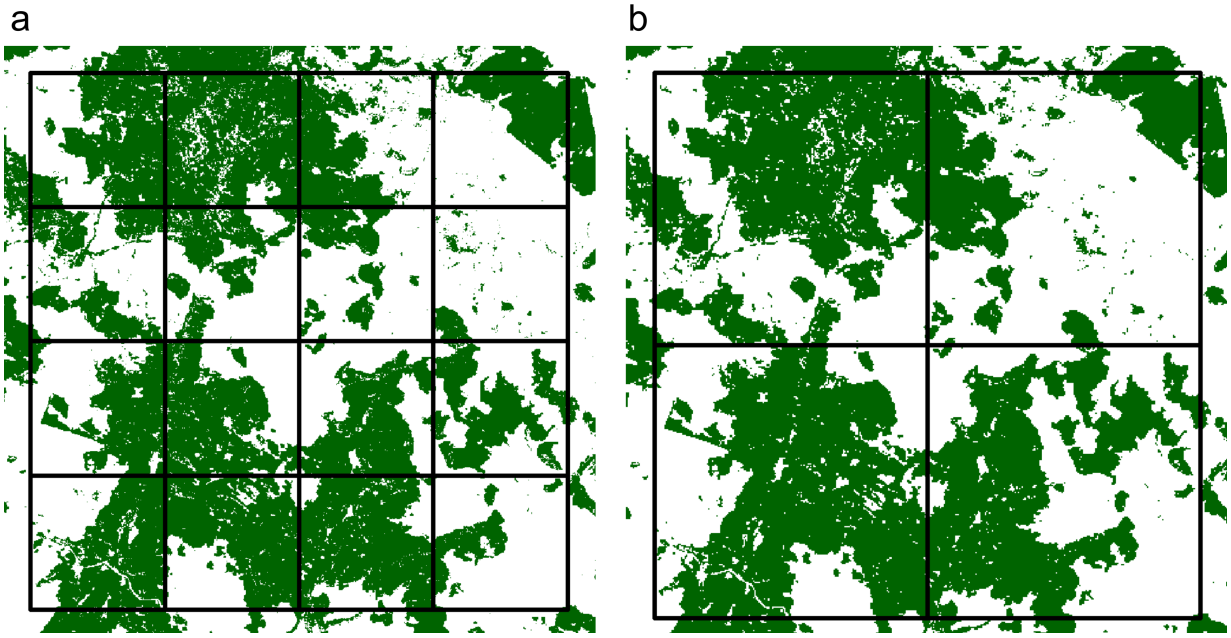

Figure B.1: **Forest-grassland mosaics in Aparados da Serra national park display distinct clustering.** 200×200 cell landscapes resulting from classifying the NDVI image of the AdS mosaics at (a) 10m resolution (b) 20m resolution into forest/non-forest clusters using a k-means clustering algorithm.

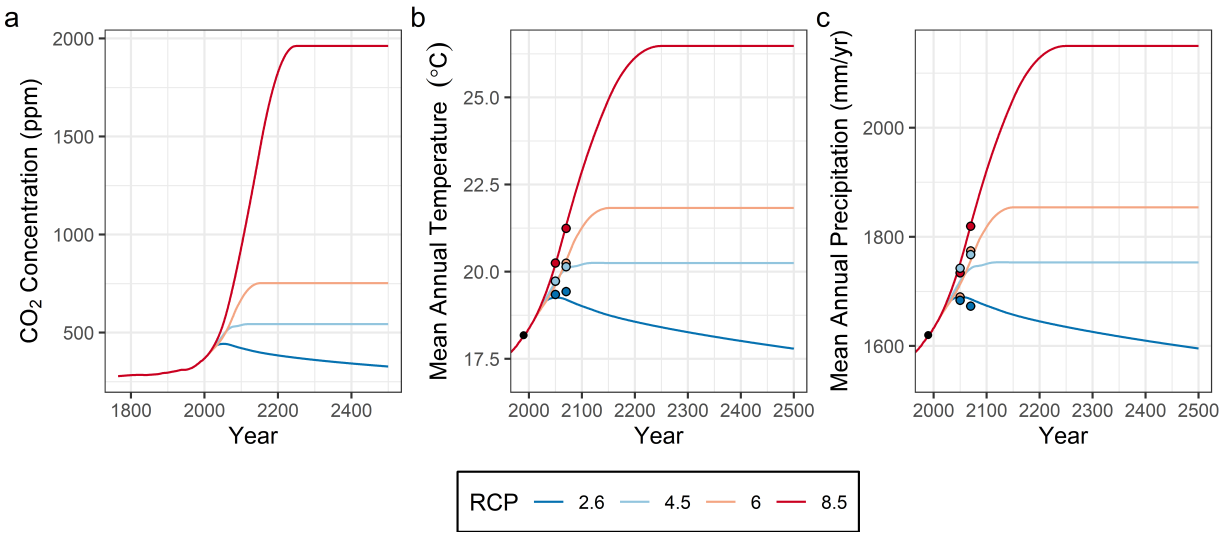

Figure B.2: **Rising global CO_2 concentrations will result in increased mean annual temperature and precipitation for Southern Brazil's forest-grassland mosaics.** (a) Global trends in atmospheric CO_2 concentration. Lines in (b) and (c) indicate MAT and MAP trajectories for Southern Brazil's forest-grassland mosaics generated using Equation 3.5 and Equation 3.6, with coloured circles corresponding to GCM-based MAT and MAP estimates at 2050 and 2070, and black circles corresponding to MAT and MAP in 1990.

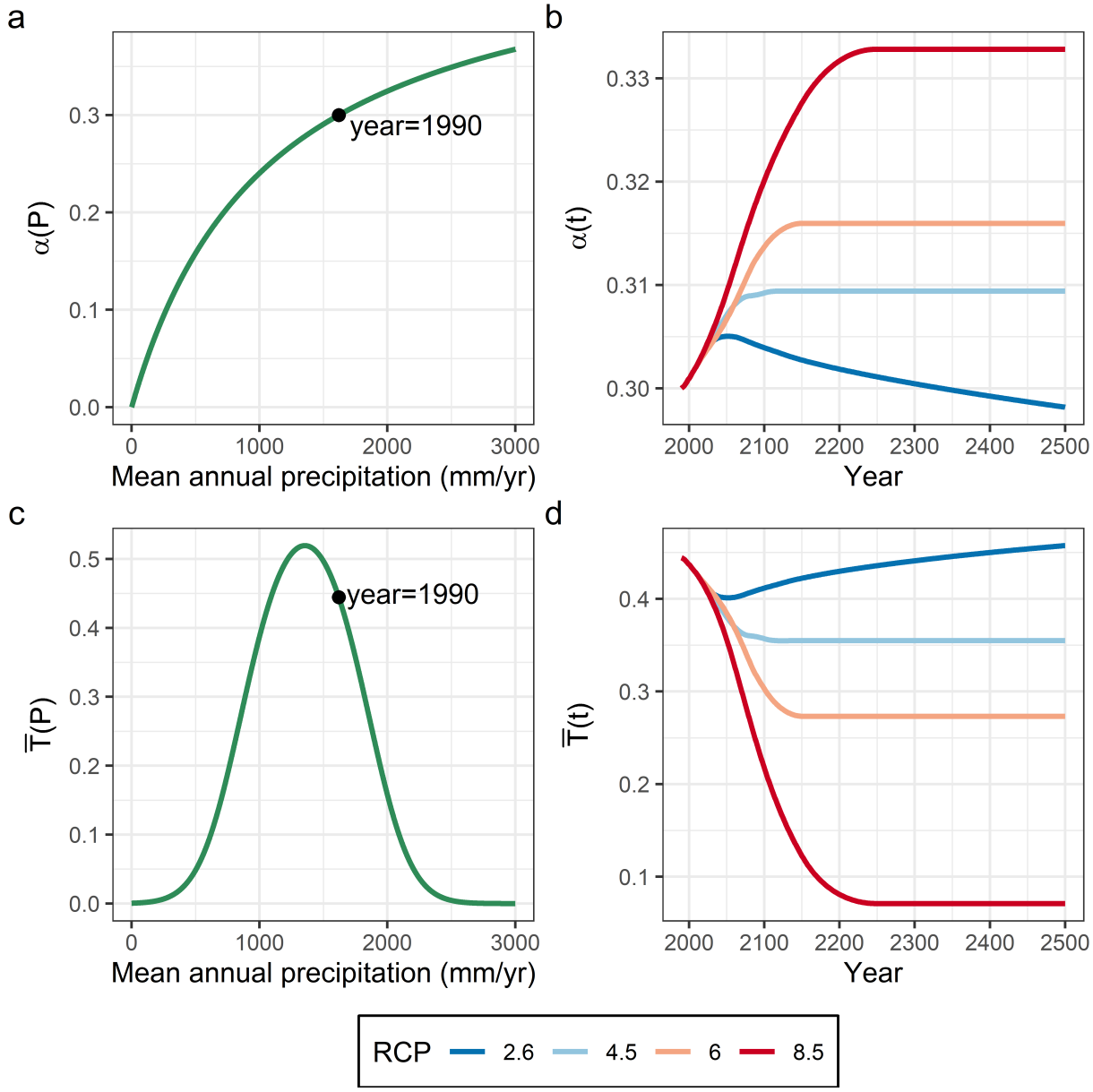

Figure B.3: **Forest recruitment, and the fire-mediated threshold to recruitment, are impacted by changes in mean annual precipitation.** Recruitment as (a) a function of precipitation and (b) time under different RCPs. Threshold as a function of (c) precipitation and (d) time under different RCPs.

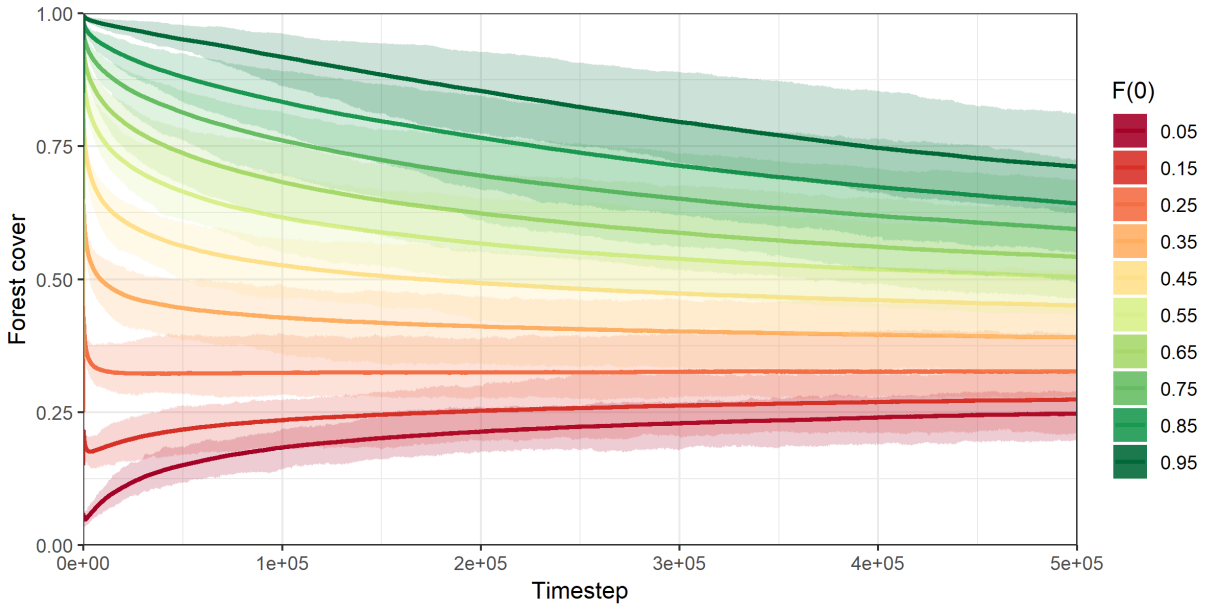

Figure B.4: **Long-term trends in forest cover depend strongly on initial forest cover.** Lines show the mean forest cover level across all simulations with a given $F(0)$, with envelopes indicating the maximum and minimum forest cover levels for simulations with that $F(0)$. Simulations use base parameter set, and 250 simulations are run for each $F(0)$, discarding any that do not stabilize.

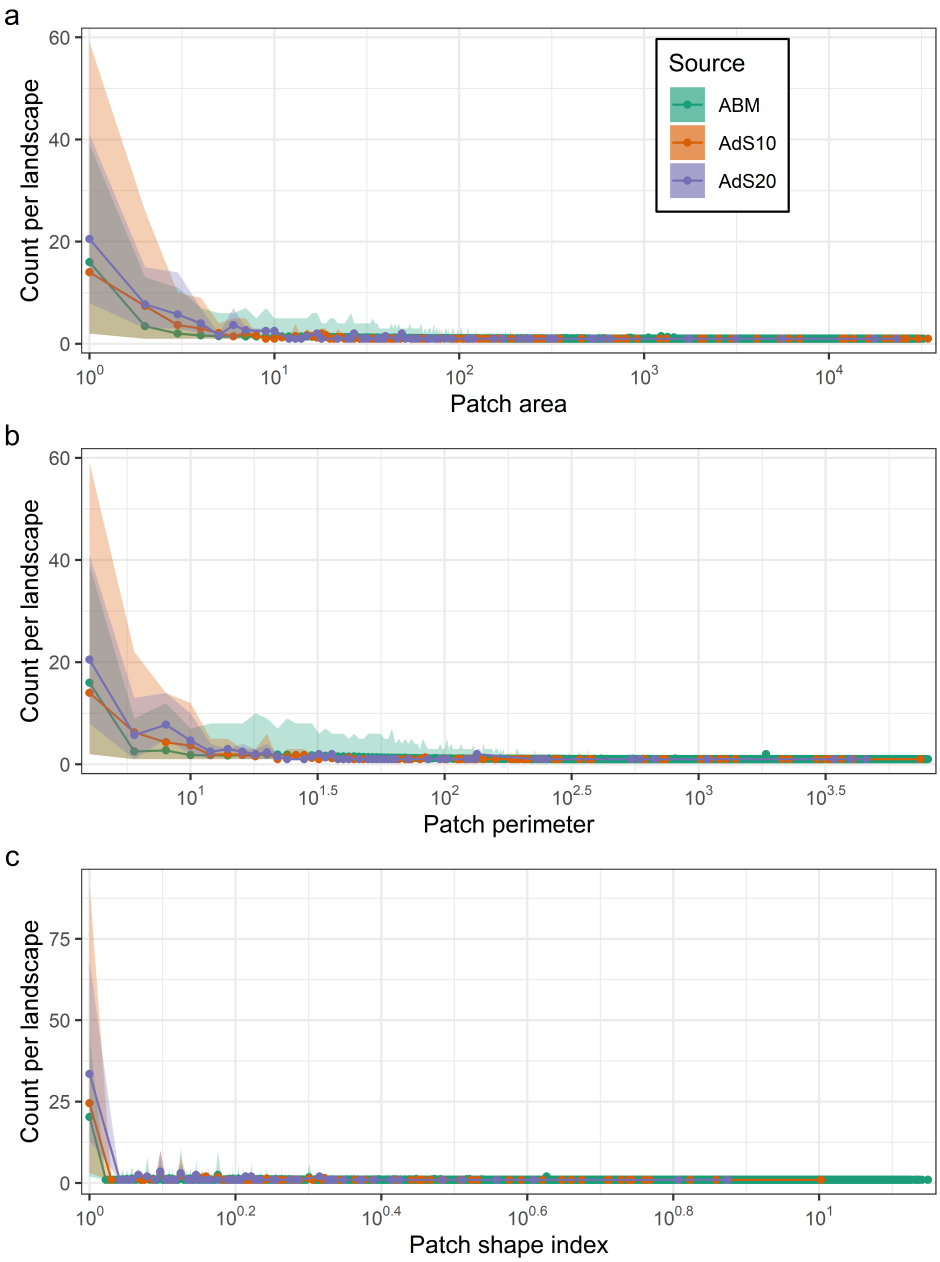

Figure B.5: **Simulated and real-world mosaics display similar patch-level metric distributions.** Patch (a) area, (b) perimeter, and (c) shape index distributions for 10m and 20m resolution satellite images of mosaic landscapes in AdS national park compared to simulated landscapes. Lines trace mean count across all landscapes from a source, coloured envelopes enclose all observations. 250 simulations are run for each $F(0)$, discarding any that do not stabilize.

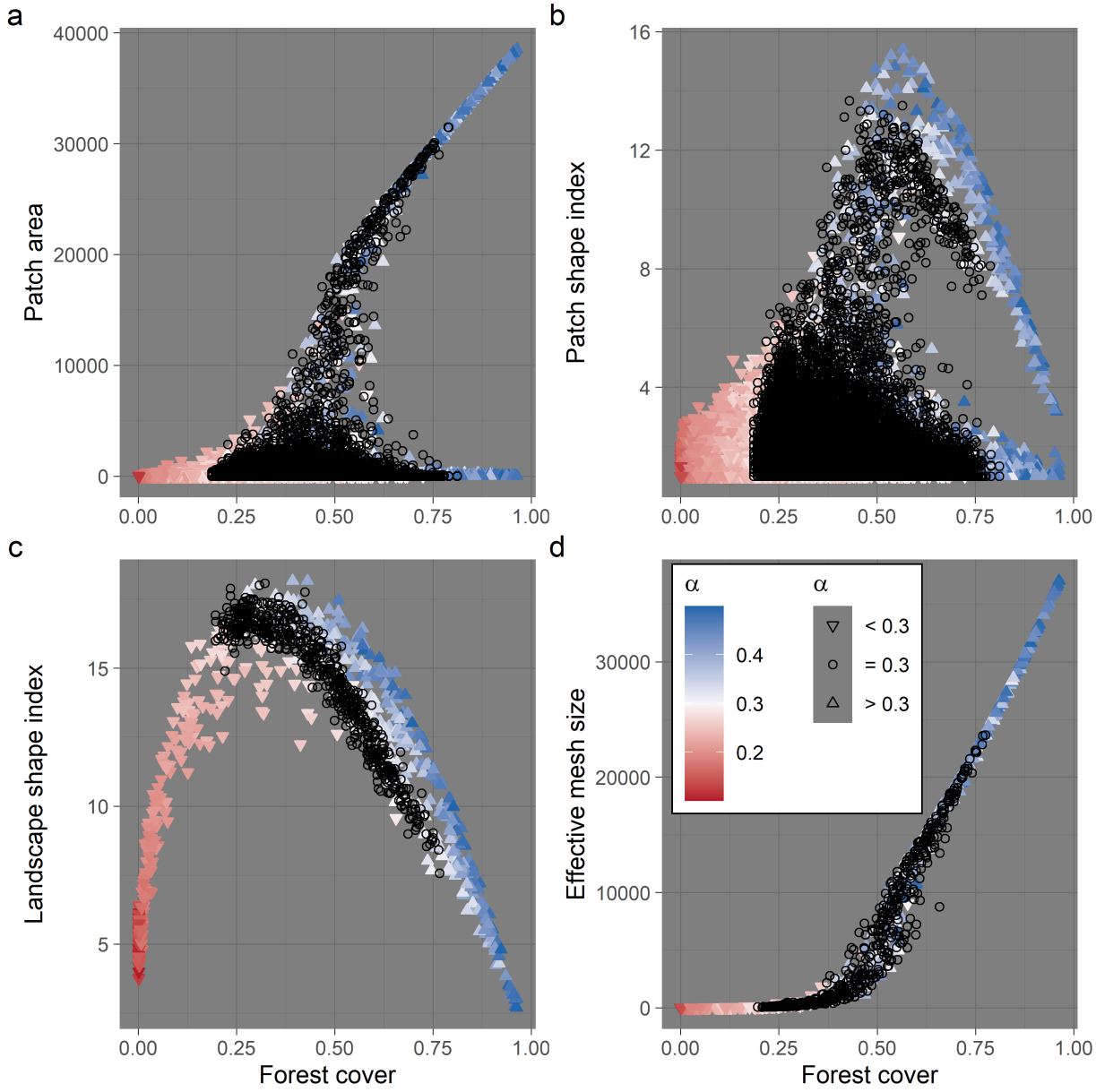

Figure B.6: **Forest recruitment impacts spatial structure at the patch and landscape level.** Impact of forest recruitment on (a) patch area, (b) patch shape index, (c) landscape shape index and (d) effective mesh size. Colour corresponds to α-value for each α-vary run (black for base), shape indicates the value in relation to base α. 250 simulations are run for each $F(0)$, discarding any that do not stabilize, with 25% of points shown to avoid overplotting.

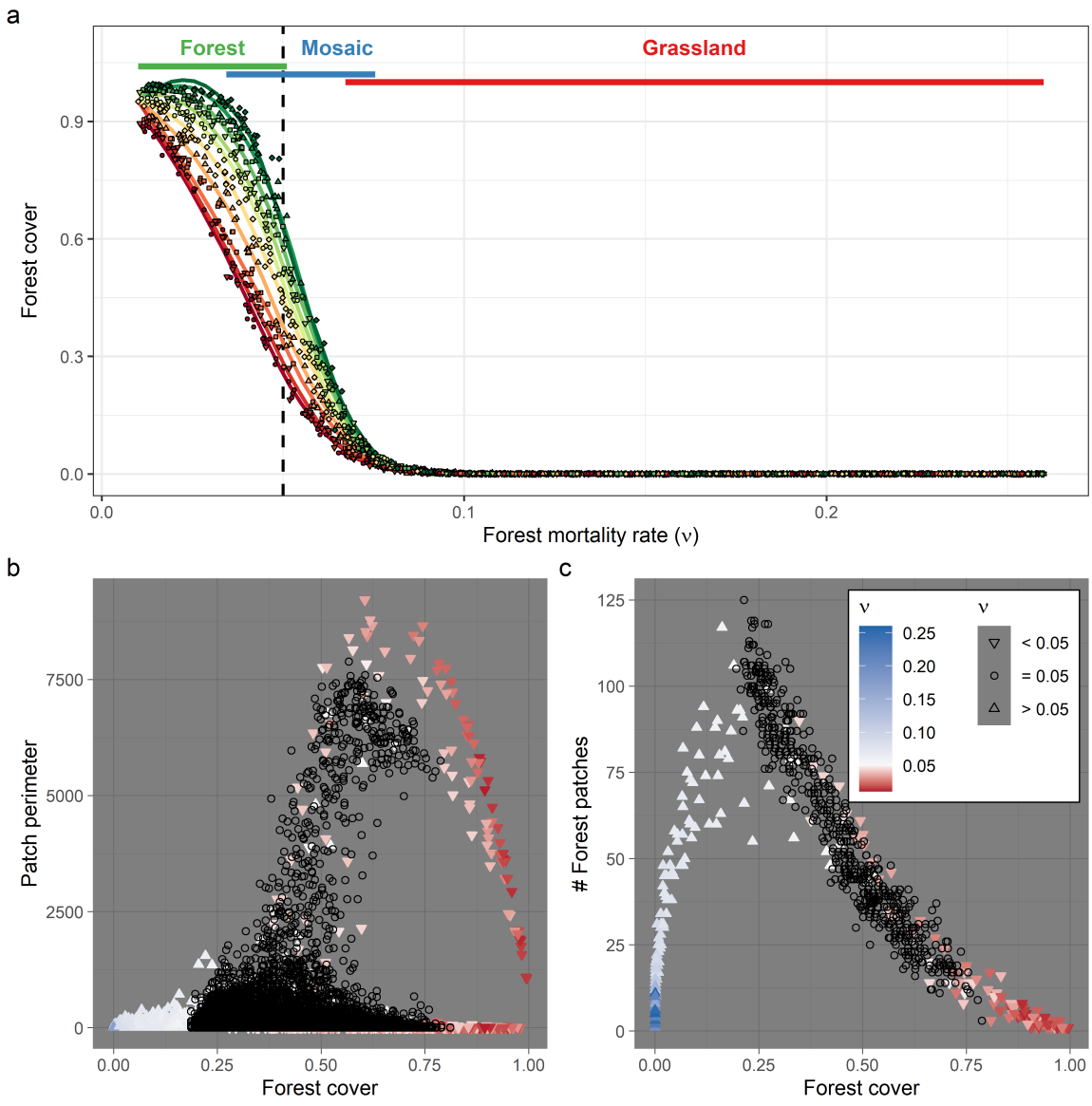

Figure B.7: **Forest mortality impacts landscape forest cover and spatial structure.** (a) Effect of mortality on forest cover. Points indicate individual simulation runs, lines show a LOESS curve for each $F(0)$. Vertical dashed line indicates the base mortality rate, horizontal bars indicate ranges of ν for which different landscape outcomes are possible. (b) and (c) indicate effect of mortality on perimeter and number of forest patches respectively. Here colour corresponds to ν-value for each ν-vary run (black for base), shape indicates the value in relation to base ν. 250 simulations are run for each $F(0)$, discarding any that do not stabilize, with 25% of points shown in (b) and (c) to avoid over plotting.

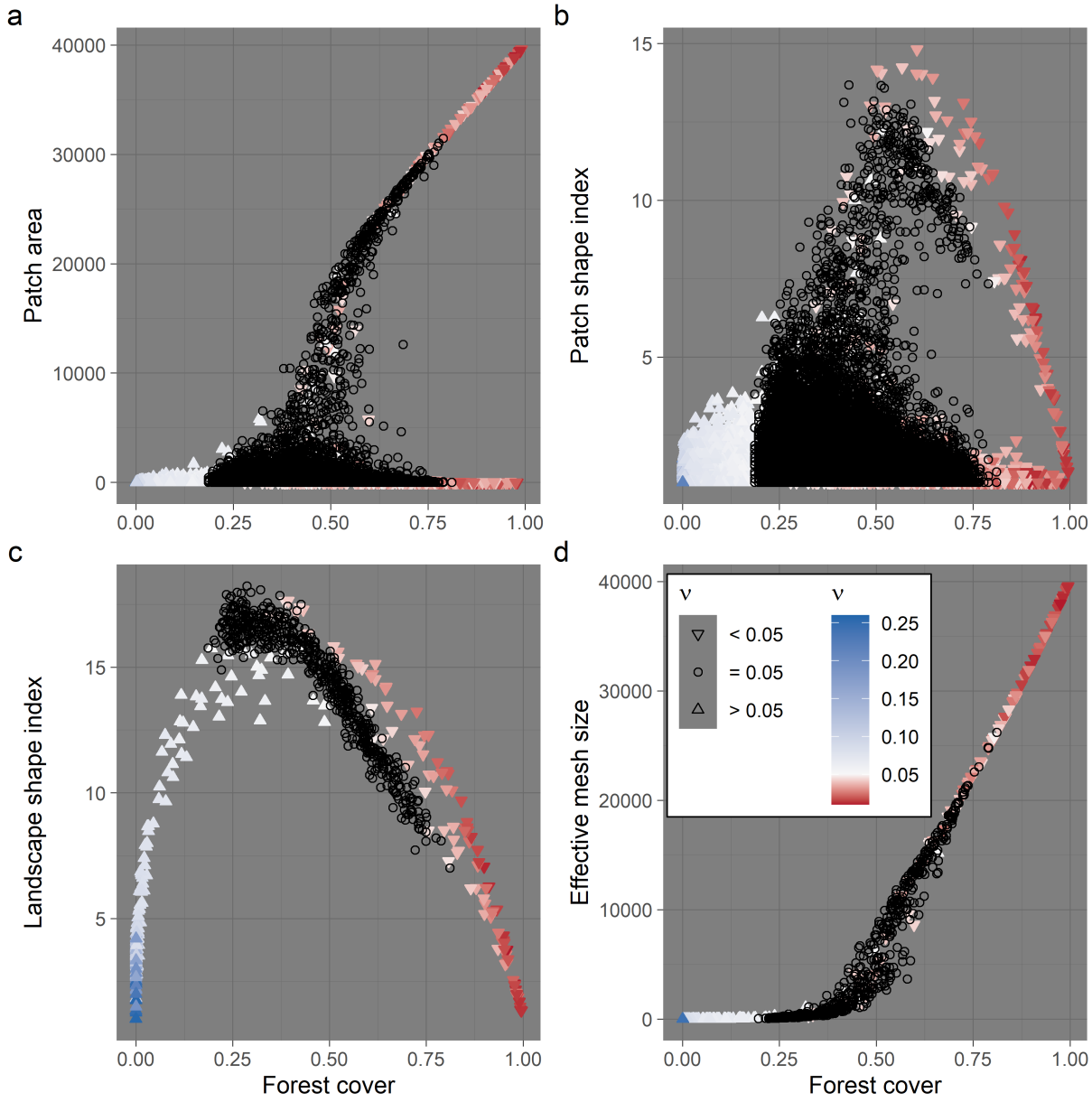

Figure B.8: **Forest mortality impacts spatial structure at the patch and landscape level.** Impact of forest mortality on (a) patch area, (b) patch shape index, (c) landscape shape index and (d) effective mesh size. Colour corresponds to ν-value for each ν-vary run (black for base), shape indicates the value in relation to base ν. 250 simulations are run for each $F(0)$, discarding any that do not stabilize, with 25% of points shown to avoid overplotting.

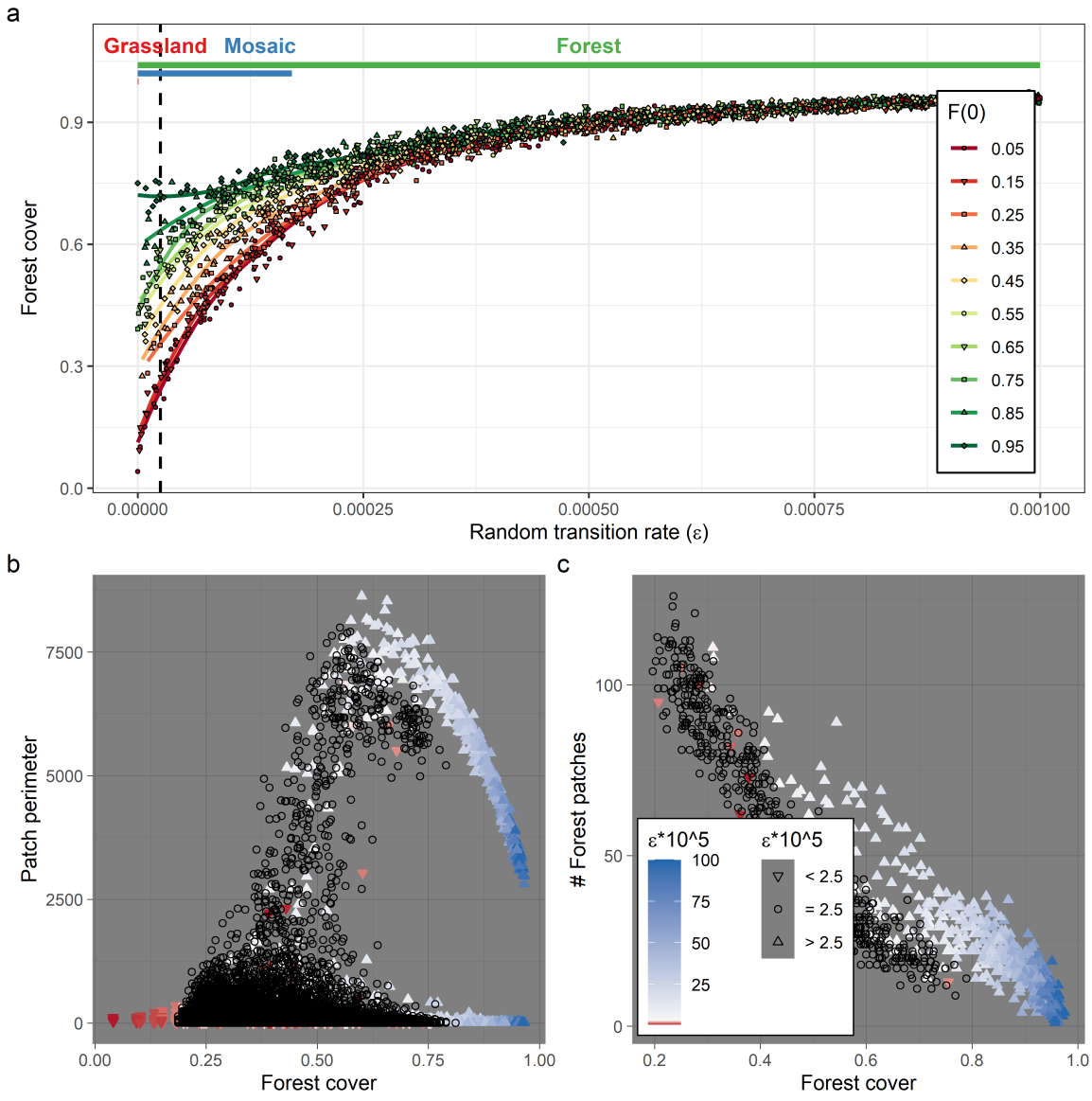

Figure B.9: **Random land-state transitions impact landscape forest cover and spatial structure.** (a) Effect of random land-state transitions on forest cover. Points indicate individual simulation runs, lines show a LOESS curve for each $F(0)$. Vertical dashed line indicates base mortality rate, horizontal bars indicate ranges of ε for which different landscape outcomes are possible. (b) and (c) display effect of random land-state transitions on perimeter and number of forest patches respectively. Here colour corresponds to ε-value for each ε-vary run (black for base), shape indicates value in relation to base ε. 250 simulations are run for each $F(0)$, discarding any that do not stabilize, with 25% of points shown in (b) and (c) to avoid overplotting.

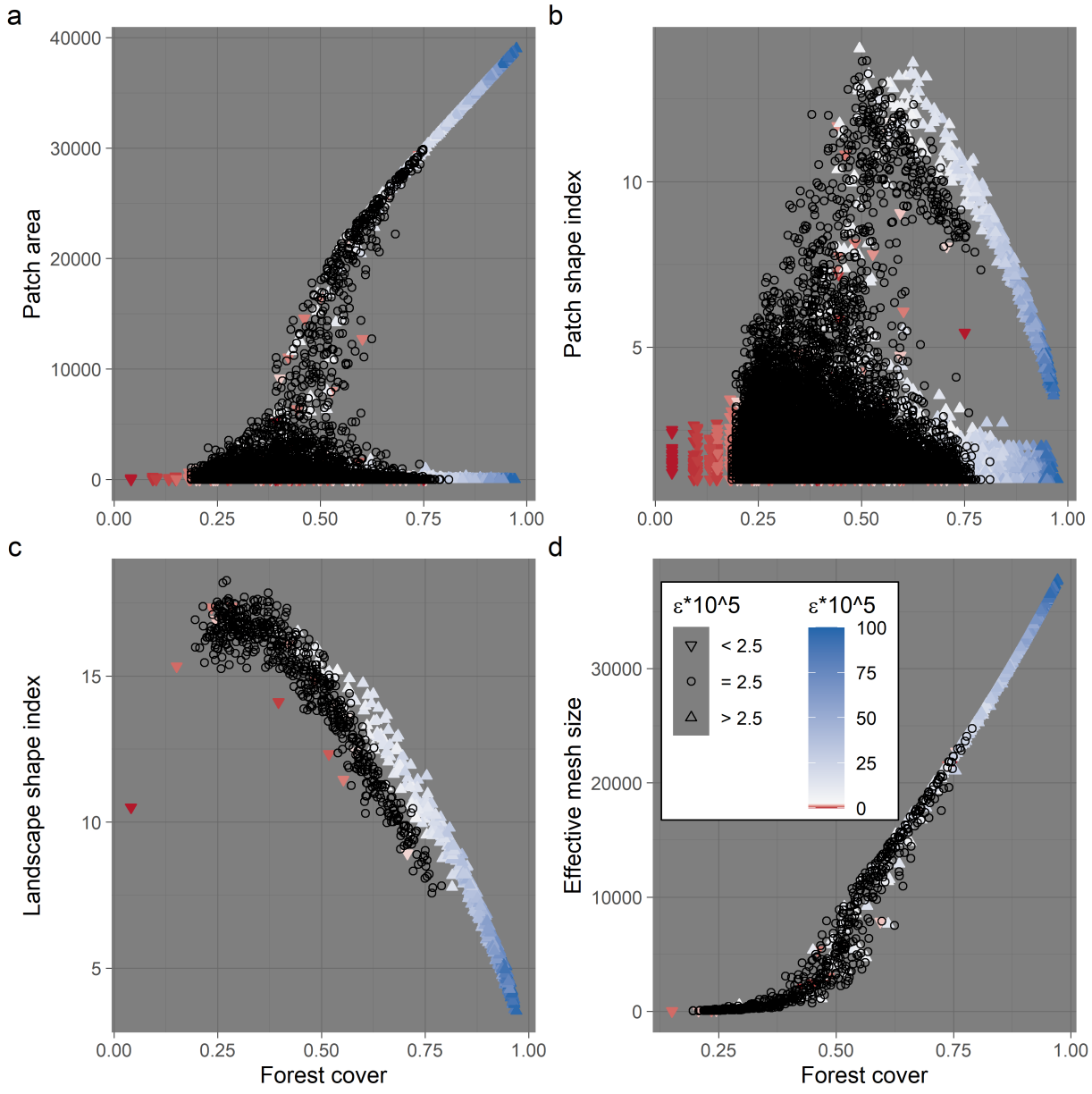

Figure B.10: **Random land-state transitions impact spatial structure at the patch and landscape level.** Impact of random land-state transitions on (a) patch area, (b) patch shape index, (c) landscape shape index and (d) effective mesh size. Colour corresponds to ε-value for each ε-vary run (black for base), shape indicates value in relation to base ε. 250 simulations are run for each $F(0)$, discarding any that do not stabilize, with 25% of points shown to avoid overplotting.

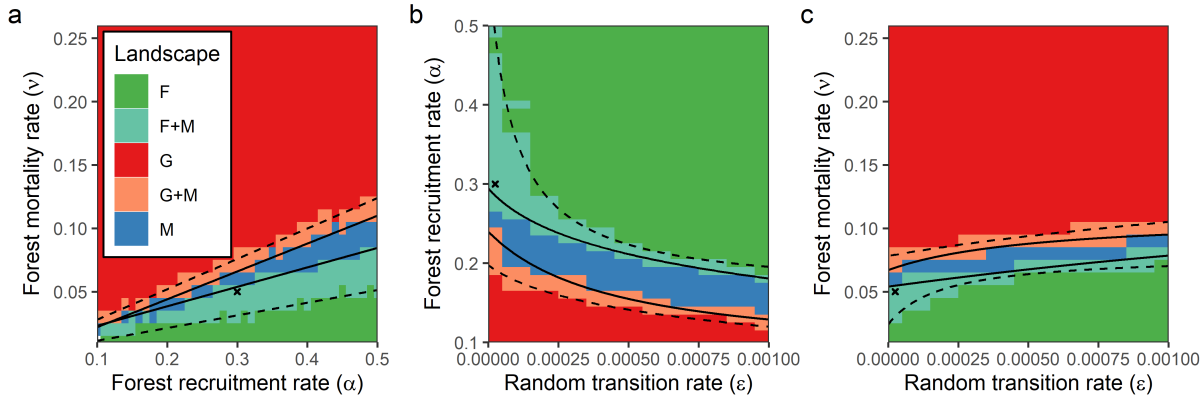

Figure B.11: **Land-state transition rates determine possible landscape states.** Landscape state due to combined effect of (a) forest recruitment and mortality, (b) forest recruitment and random land-state transitions, and (c) forest mortality and random land-state transitions. Location of base rates are indicated with $\times$. For each parameter plane 10000 simulations are run (1000 for each $F(0)$), discarding any that do not stabilize. Dashed lines enclose the region where mosaics occur, with solid lines enclose the region where only mosaics are possible.

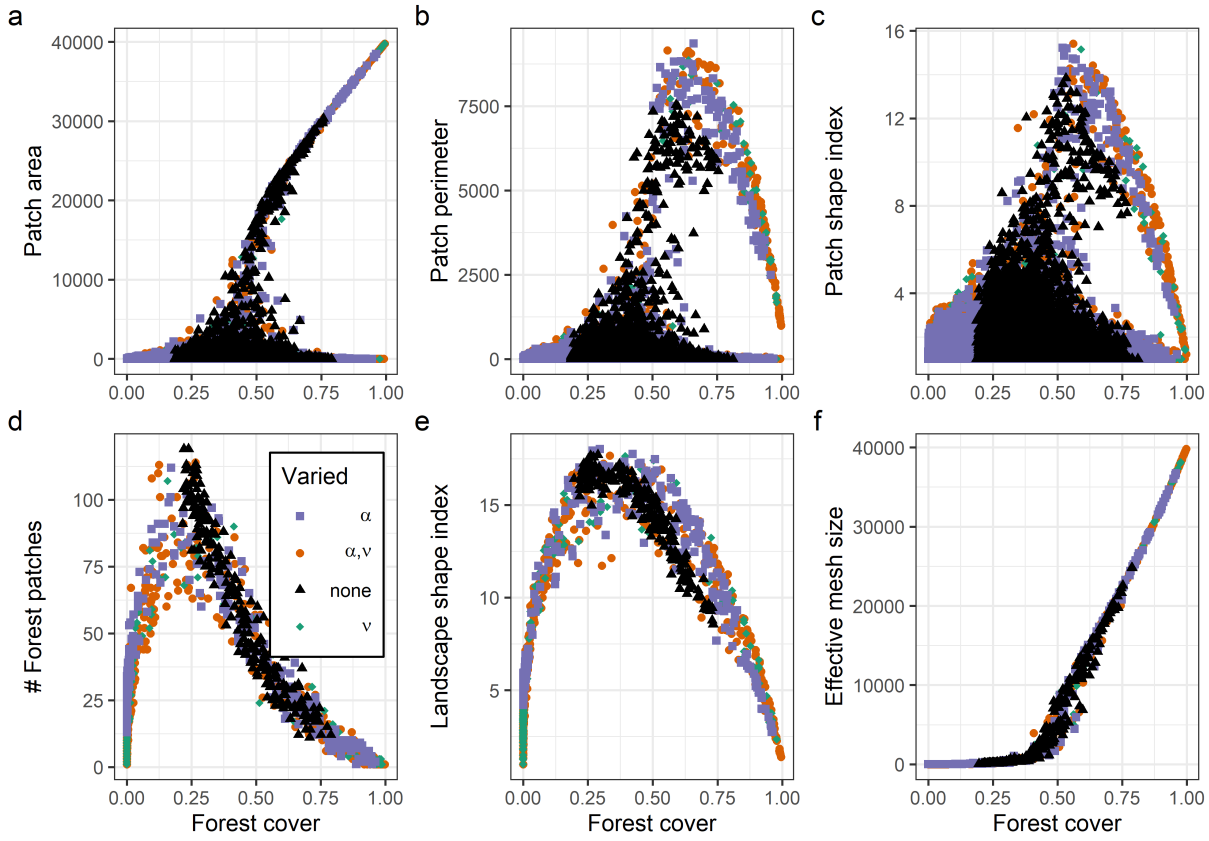

Figure B.12: **Varying both tree recruitment and mortality does not substantially alter spatial structure, as compared to varying only one of these rates.** Effects of varying tree recruitment, mortality, both, and neither on (a) patch area (b) patch perimeter (c) patch shape index (d) number of forest patches (e) landscape shape index and (f) effective mesh size. For Base, α-vary, and ν-vary 250 simulations are run for each $F(0)$, with 1000 each in the α, ν-vary case. In all cases we discard any simulations that do not stabilize, and only 10% of points are shown to avoid overplotting.

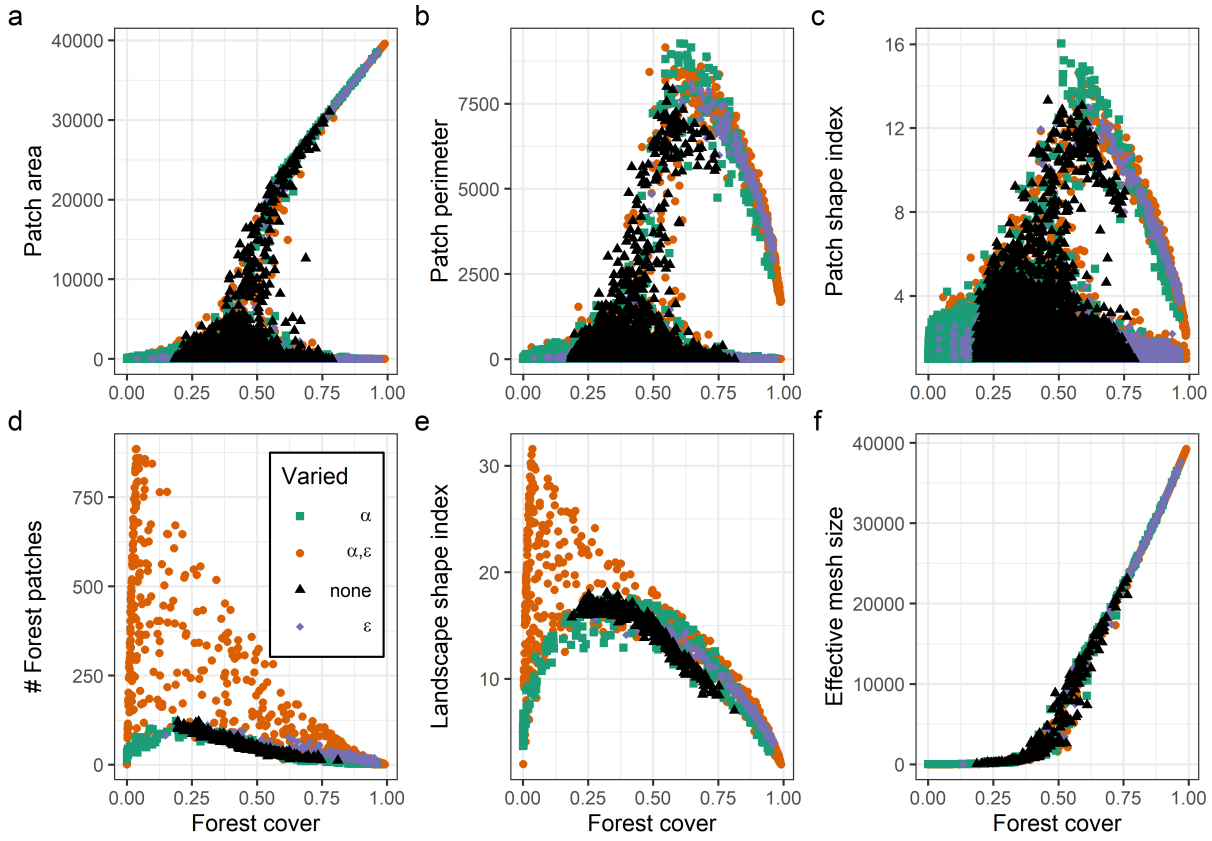

Figure B.13: **Varying both tree recruitment and the rate of random land-state transitions results in changes to landscape structure not observed when only one rate is varied.** Effects of varying tree recruitment, random land-state transitions, both, and neither on (a) patch area (b) patch perimeter (c) patch shape index (d) number of forest patches (e) landscape shape index and (f) effective mesh size. For Base, α-vary, and ε-vary 250 simulations are run for each $F(0)$, with 1000 each in the α, ε-vary case. In all cases we discard any simulations that do not stabilize, and only 10% of points are shown to avoid overplotting.

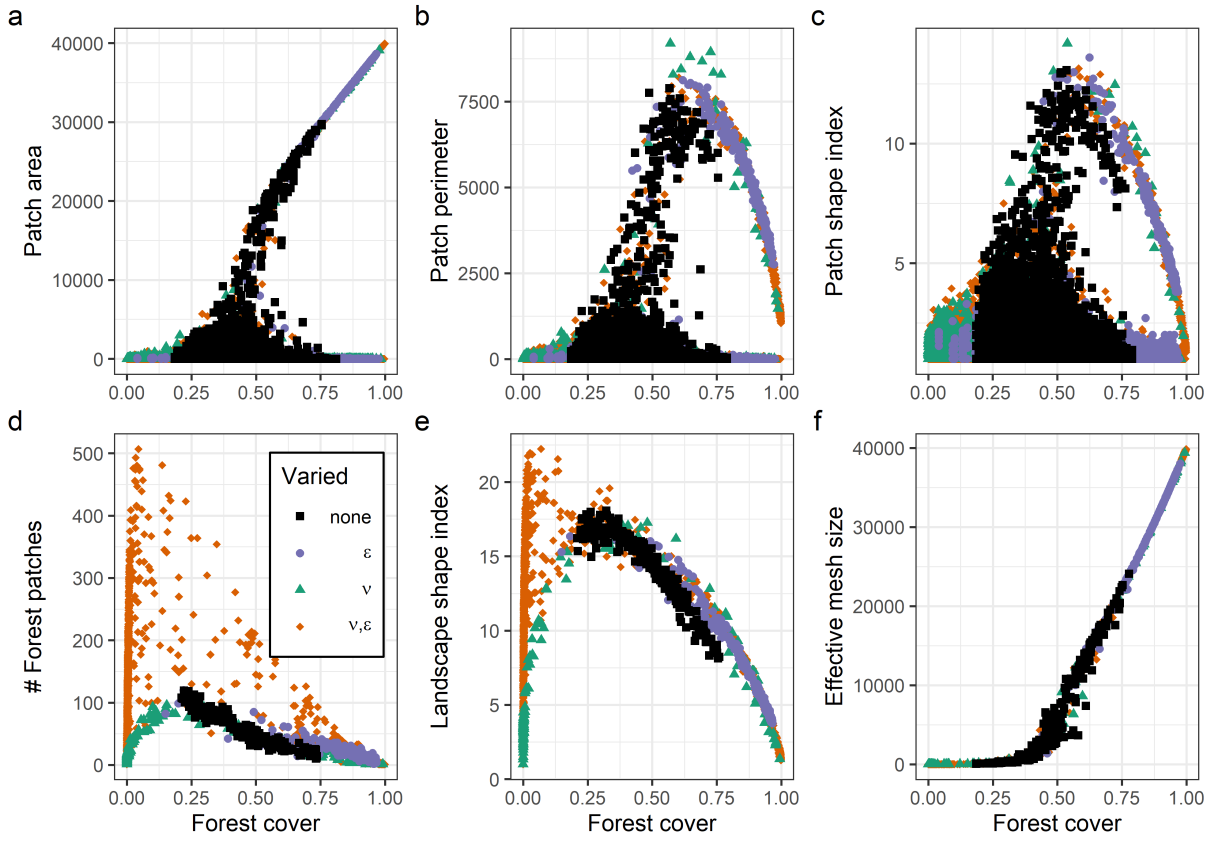

Figure B.14: **Varying both tree mortality and the rate of random land-state transitions results in changes to landscape structure not observed when only one rate is varied.** Effects of varying tree mortality, random land-state transitions, both, and neither on (a) patch area (b) patch perimeter (c) patch shape index (d) number of forest patches (e) landscape shape index and (f) effective mesh size. For Base, ν-vary, and ε-vary 250 simulations are run for each $F(0)$, with 1000 each in the ν, ε-vary case. In all cases we discard any simulations that do not stabilize, and only 10% of points are shown to avoid overplotting.

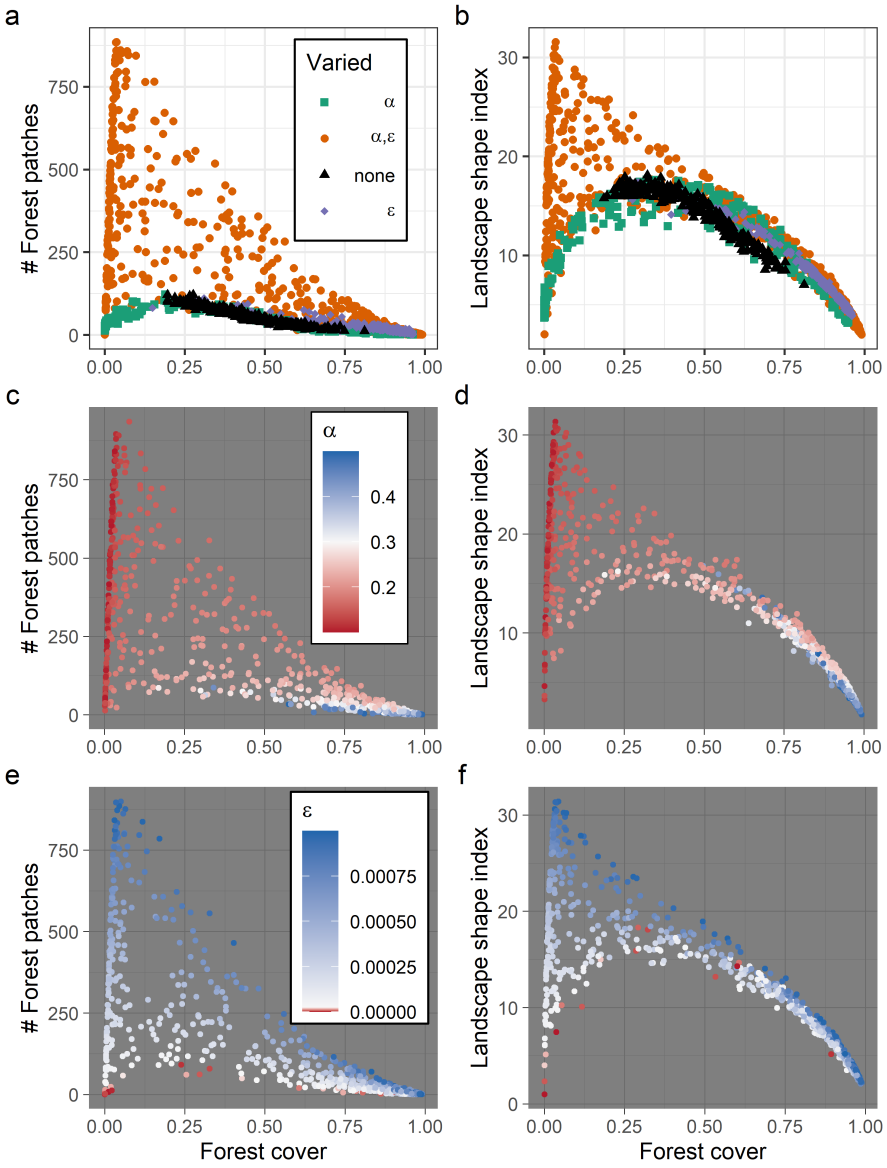

Figure B.15: **Low tree recruitment accompanied by a high rate of random land-state transitions leads to complex landscapes with large numbers of forest patches.** Impacts of forest recruitment and random land-state transitions rate on the number of forest patches and LSI when exploring the $\alpha - \varepsilon$ parameter plane. (a) and (b) show combined effect, with (c) and (d) highlighting the impact of recruitment and (e) and (f) the impact of random transition rates. For Base, α-vary, and ε-vary 250 simulations are run for each $F(0)$, with 1000 each in the α, ε-vary case. We discard simulations that do not stabilize, 10% of points are shown to avoid over plotting

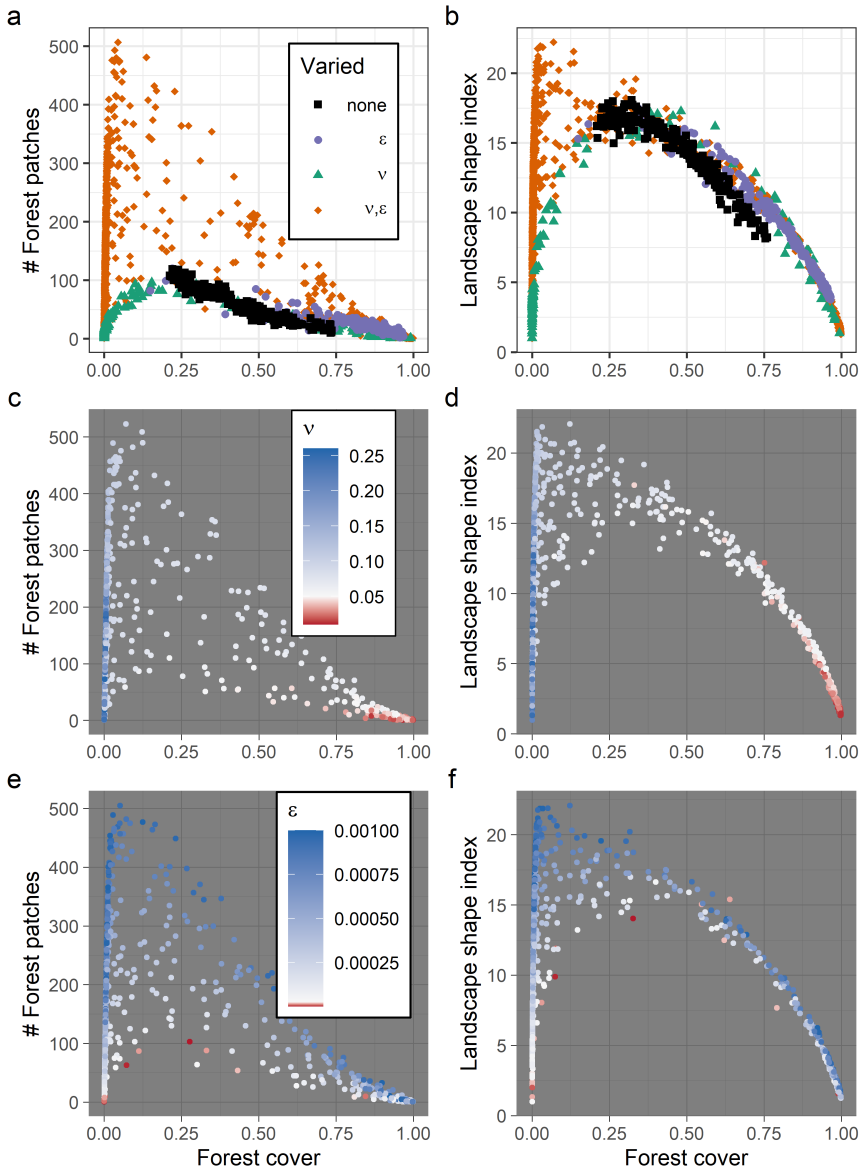

Figure B.16: **Combining high rates of tree mortality and random land-state transitions leads to complex landscapes with large numbers of forest patches.** Impacts of forest mortality and random land-state transitions rate on the number of forest patches and LSI when exploring the $\nu - \varepsilon$ parameter plane. (a) and (b) show combined effect, , with (c) and (d) highlighting the impact of mortality and (e) and (f) the impact of random transition rates. For Base, ν-vary, and ε-vary 250 simulations are run for each $F(0)$, with 1000 each in the ν, ε-vary case. We discard simulations that do not stabilize, 10% of points are shown to avoid over plotting

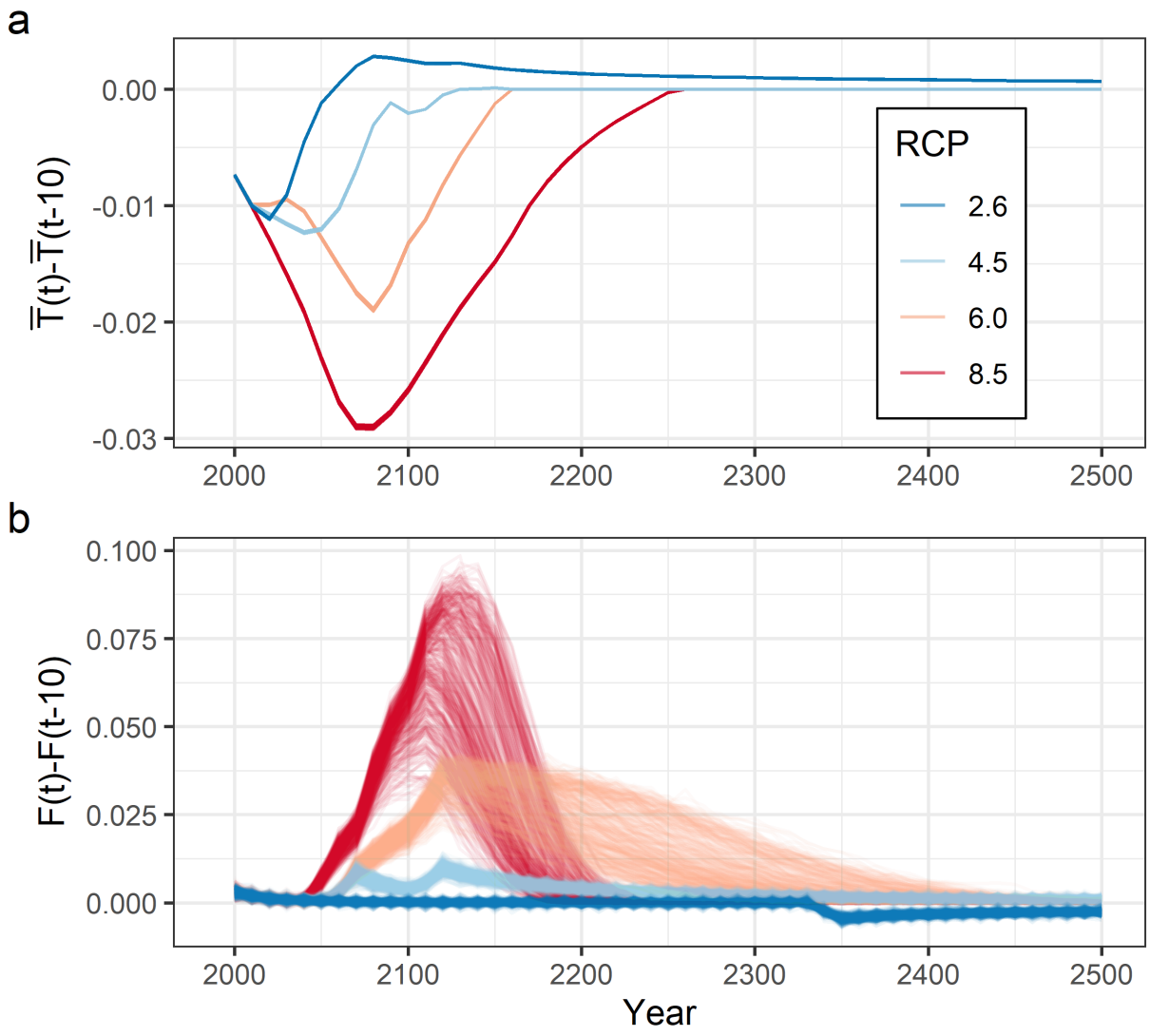

Figure B.17: **Decadal changes in recruitment threshold precede corresponding changes in forest cover.** a) decadal change in mean threshold value, b) change in forest cover for each simulation. 500 simulations are run for each scenario.

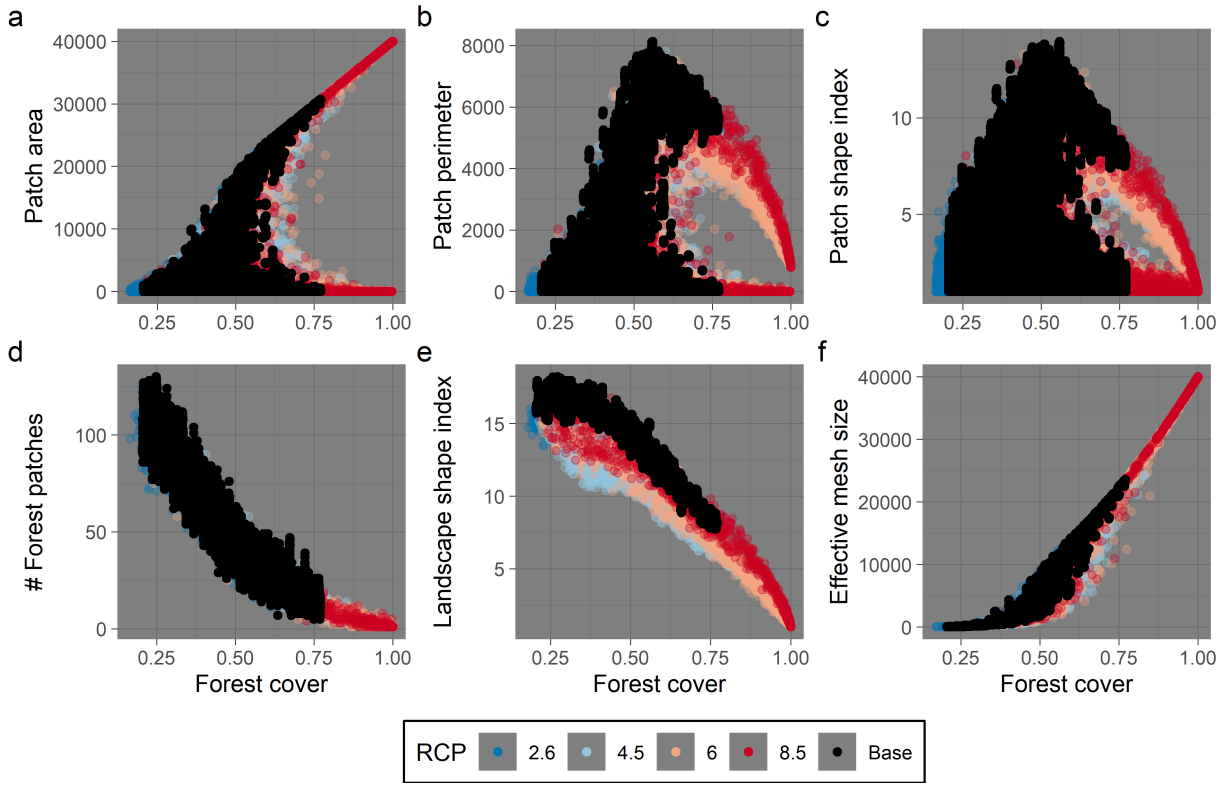

Figure B.18: **Climate impacts on the tree recruitment threshold result in alterations to landscape spatial structure.** Effect of climate-impacted forest recruitment threshold on (a) patch area (b) patch perimeter (c) patch shape index (d) number of forest patches (e) landscape shape index and (f) effective mesh size. For each scenario 500 simulations are run.

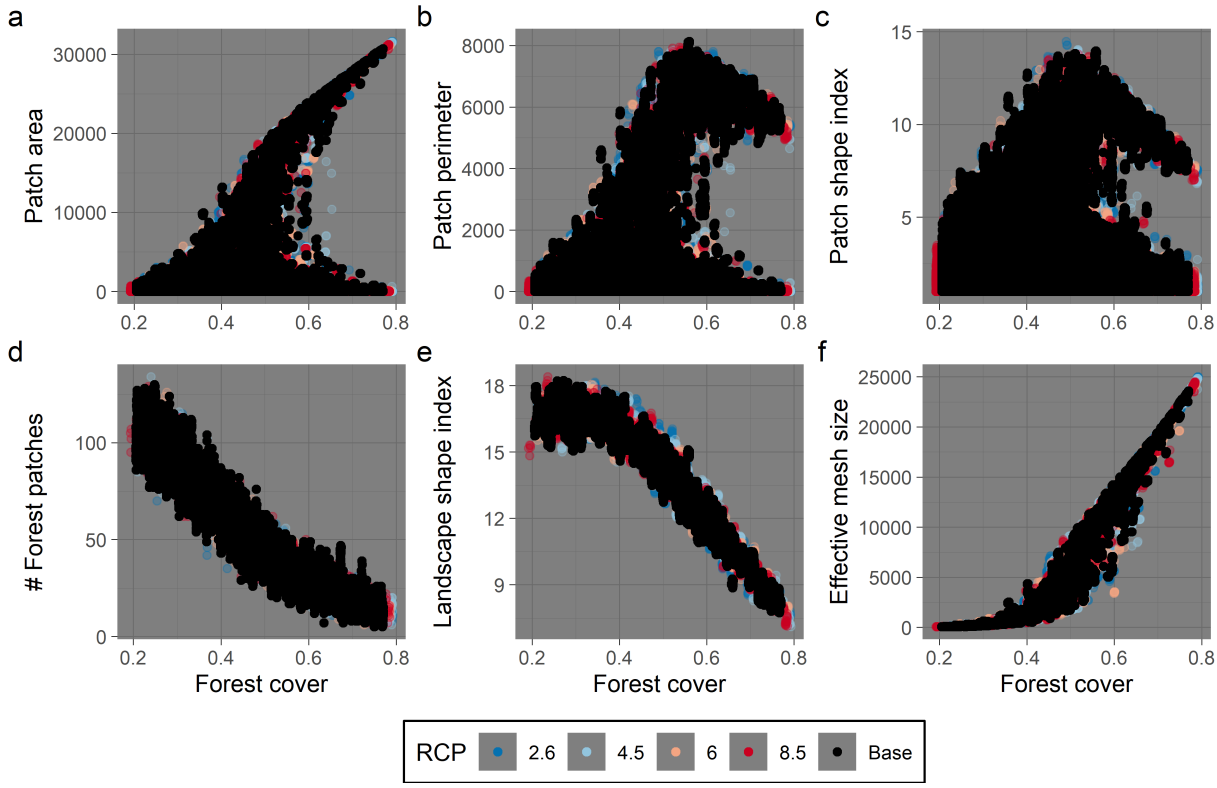

Figure B.19: **Climate impacts on the tree recruitment rate do not result in substantial alterations to landscape spatial structure.** Effect of climate-impacted forest recruitment on (a) patch area (b) patch perimeter (c) patch shape index (d) number of forest patches (e) landscape shape index and (f) effective mesh size. For each scenario 500 simulations are run.

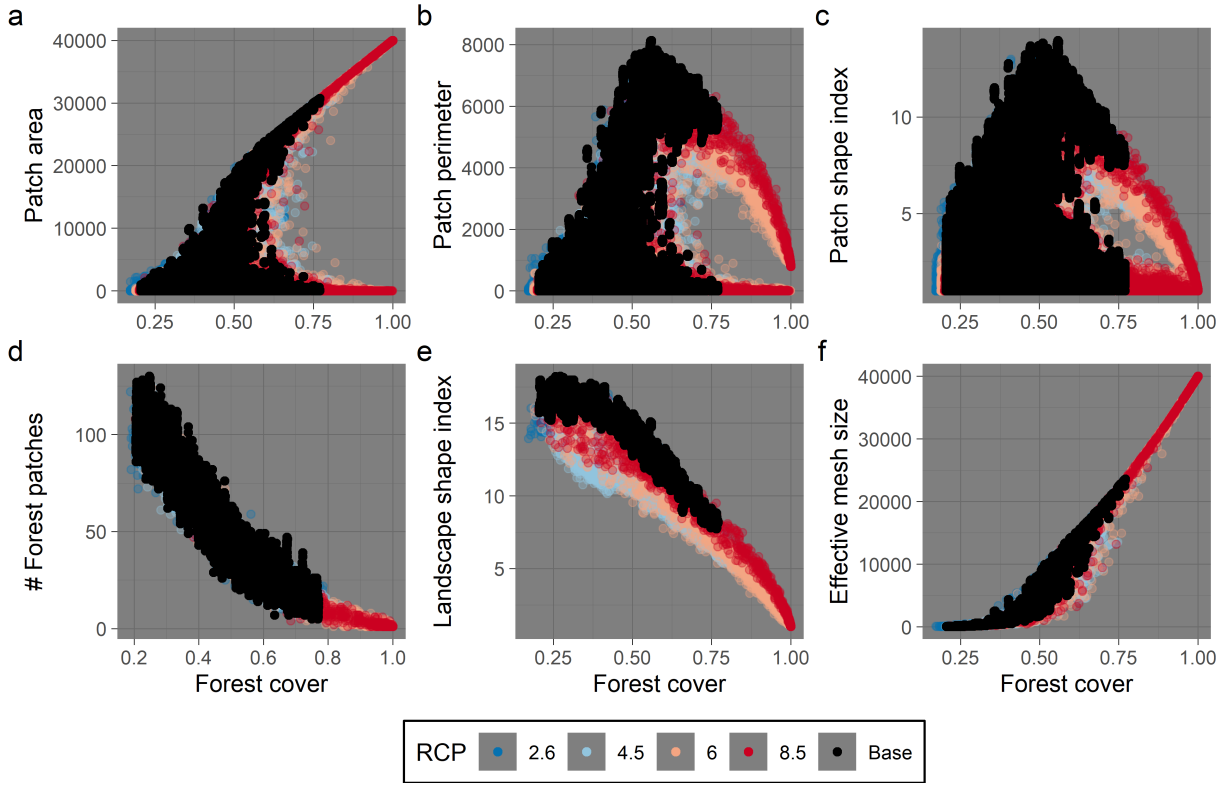

Figure B.20: **Climate impacts on both the tree recruitment rate and threshold to recruitment result in alterations to landscape spatial structure similar to those resulting from impacts on recruitment threshold only.** Effect of climate-impacted forest recruitment and recruitment threshold on (a) patch area (b) patch perimeter (c) patch shape index (d) number of forest patches (e) landscape shape index and (f) effective mesh size. For each scenario 500 simulations are run.

Appendix C

Supplementary information - Human metapopulation interactions on a trade network: implications for food security & equality

C.1 Supplementary methods

C.1.1 Global model parametrization

The model is parameterized at the global level using empirical data from the United Nations Food and Agriculture Organization (FAO). We collect data on global population ("Total population", 1961-2018, and projected "Total population", 2019-2100), food supply ("Food; the total amount of agricultural products available as food", 1961-2013), agricultural land ("Agricultural land; land used for cultivation of crops and animal husbandry. The total of areas under Cropland and Permanent meadows and pastures.", 1961-2017), total land area ("Land area; country area excluding area under inland waters and coastal waters", 1961-2017), uninhabitable land area (sum of "Terrestrial barren land" and "Permanent snow and glaciers" land cover areas from CCI-LI, 1992-2015), and food production ("Production quantity", excluding aquatic products, 1961-2013) [108]. We use a conservative estimate of the total land available for agriculture, taken as the total habitable land area (total area - uninhabitable area) in 2015, the most recent year for which all necessary data is available. While this undoubtedly leads to an overestimation of the amount of available land, the amount of land suitable for agriculture will vary widely depending on the production being considered (crops vs. livestock, type of crop, type of irrigation, etc.) [337, 102] so an accurate total across all production types is difficult to obtain.

To reduce the complexity of fitting our system of differential equations to our time series data, we independently fit the parameters from our net growth rate function (Equation 4.2) as listed above the line in Table 4.1, to data on global net population growth rate and per capita food supply from 1962-2013. We assume $\delta = 0.0113$, the mean of the global crude death rate from 1950-2020, to focus our fitting on those parameters that do not have a direct biological interpretation [222, 108]. Through this assumption, we attribute all variation in the net population growth rate to per capita food supply driven changes to the fertility rate. We use a Levenberg-Marquardt type nonlinear least squares fitting algorithm implemented in R to obtain values for α_0, ρ, and σ (Table 4.1) [88, 241]. The resulting fit (Figure C.1) has a peak in net growth rate of 0.0343/yr when the annual food per capita is approximately 0.3673 tonnes. We note that the fitted value of ρ is located at the upper bound of possible values ($\rho = 6.25$) however we feel that allowing for a lower value would create an unrealistic lower bound on the per capita food values for which net growth is positive, as our fit here is already fairly conservative (based on a comparison to the country-level data, as shown in Figure C.1).

We also obtain values for r_y and K_y to yield data prior to fitting parameters for the food supply and agricultural land (Equation 4.3, Equation 4.4), as the yield DE (Equation 4.1)

does not depend on the dynamics in the remainder of the system. For yield, we consider 2 scenarios; a "conservative" maximum yield scenario using the estimated maximum annual yield from [228] (K_Y^C=3.5), and a "high" yield scenario where we assume $K_Y^H = 2K_Y^C = 7$. We consider these contrasting scenarios as, given the roughly linear increase in yield from 1961-2013 and the potential for technological advances, the upper bound on yield may be higher than estimated by [228]. Alternatively, this "high" yield scenario can be thought of as a future where there is a global shift towards more plant-based diets, as livestock production requires a substantial amount of land and plant calories [295, 283, 255].

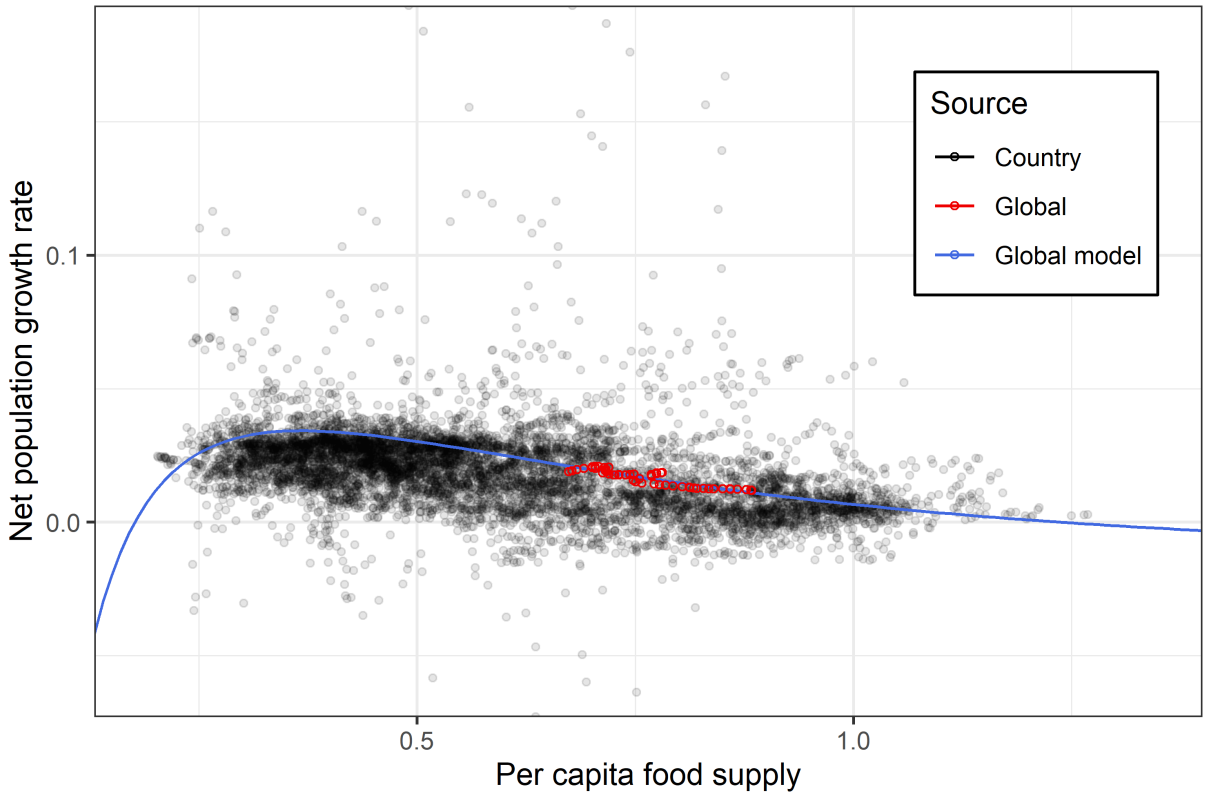

Figure C.1: **Functional form developed for net population growth rate provides reasonable fit to empirical data.** Fitting is performed using global data on net population growth rate vs. per capita food for 1962-2013. Country-level data points shown for comparison.

Once values for the parameters in the net growth rate function (Equation 4.2), and yield (Equation 4.1) have been determined, fitted values for the remaining parameters are obtained. Fitted values for parameters (excluding those related to the net growth rate

function) are obtained using the Matlab function lsqcurvefit applied to the global model. This function is a nonlinear-least squares curve fitting method utilizing the trust-region-reflective algorithm. We note that the value of μ is fixed, as trade is not considered in the global model, meaning it cannot be included in our fitting exercise. We instead chooose $\mu = 0.16$, the country-level average value for exports as a fraction of production in 2013, calculated using FAO data [108].

C.1.2 Network science concepts for analyses

We provide a brief overview of network science concepts required for analysis of our model. Our trade network is made up of nodes (on which the patches of our metapopulation model are situated) connected by edges (representing trade links between patches). Nodes are "neighbours" if they are connected by an edge. Throughout the remainder of the paper, when we refer to patch-level characteristics we are indicating properties of the dynamic behaviour in patch i, resulting from the parameterization of Equation 4.6-Equation 4.9. When we describe node-level characteristics, we refer to the metrics describing the position of node i (that patch i is situated on) within the trade network. The metrics we will employ to characterise nodes and networks are listed in Table C.1. We include several centrality metrics to explore which measures of node "importance" (centrality, by various definitions) in a network have clear relationships to patch-level outcomes [217].

Throughout our analysis we generate networks using the Watts-Strogatz algorithm. This algorithm takes a ring lattice – a regular network, where the number of nodes and edges is fixed – and randomly rewires edges with some probability p. As the rewiring probability, p, increases the networks generated become less regular and more random. If $p = 0$ we retain the lattice, if $p = 1$ we have a completely random network, and for rewiring probabilities in $(0, 1)$, we may obtain small-world networks. This algorithm accepts as input a number of nodes, the "neighbourhood" in which to connect each node (equivalent to the average degree centrality of the network/2 for our undirected network), and the rewiring probability, p [320]. All networks are generated using an implementation of the Watts-Strogatz algorithm from the igraph package (Version 1.2.4.2) for R (Version 3.6.3) [68, 241]. Network analysis is performed using both igraph the Network Toolbox package (Version 1.4.0) [68, 58].

Table C.1: **Metrics for describing network topology.** A subset of common metrics from the field of network science useful to our analyses.

Metric	Description	Source
Degree centrality	Number of edges connected to a node.	[18, 261]
Betweenness centrality	Extent to which a node is located on paths between other nodes.	[217, 261, 111]
Closeness centrality	Average distance from a node to all other nodes within a network.	[217, 261]
Eigenvector centrality	Measures influence in a network by accounting both for number and "quality" of edges, being connected to nodes with high eigenvector centrality scores contributes more to a nodes' eigenvector centrality than being connected to nodes with low scores.	[217, 37]
Local clustering coefficient	Average probability that a node's neighbours are themselves connected to eachother.	[217, 261]
Density (d)	Ratio of the number of edges in a network to the maximum possible number of edges.	[319]
Average path length	Average length of the shortest paths (along edges) between pairs of nodes in a network.	[18]
Small-world measure (ω)	Quantifies the extent to which a network displays small-world properties by measuring its average path length against that of a comparable random network, and its average clustering coefficient against that of a comparable lattice. This metric has a range of $[-1, 1]$ where values near 0 are indicative of a small-world network, more negative values point to a more regular (lattice-like) network, and more positive values point to a more random network.	[292]

C.2 Supplementary results: global model

Our work with the global model focuses on determining parameter values which allow the model to obtain a good fit to the empirical data we retrieved from the FAO (fitting method and data described in Subsection C.1.1). Fitting was carried out using data from the years 1961-2013 (additionally 2014-2100 for human population), with $t = 1961$ as our initial condition. In the "low-yield" scenario (Figure C.2), our parameter fitting exercise

indicates that the projected increasing global population trajectory will be accompanied by an increase in agricultural land area (and thus an increase in food supply). Fitted values for γ^A and β^A in this scenario are effectively meaningless, as any combination of (γ^A, β^A) that results in $b^A = 1 \; \forall \; t \; \in [2013, 2100]$ will have the same outcome for variable trajectories. In the "high-yield" scenario (Figure C.3), the higher value for maximum yield (K_Y) means that a larger food supply can be obtained, even with decreases in agricultural area past 2040. Additionally, this leads the population to experience a demographic transition to lower birth rates, causing a decrease in global population towards the end of the century. Here, a unique fit for β^A, γ^A is obtained.

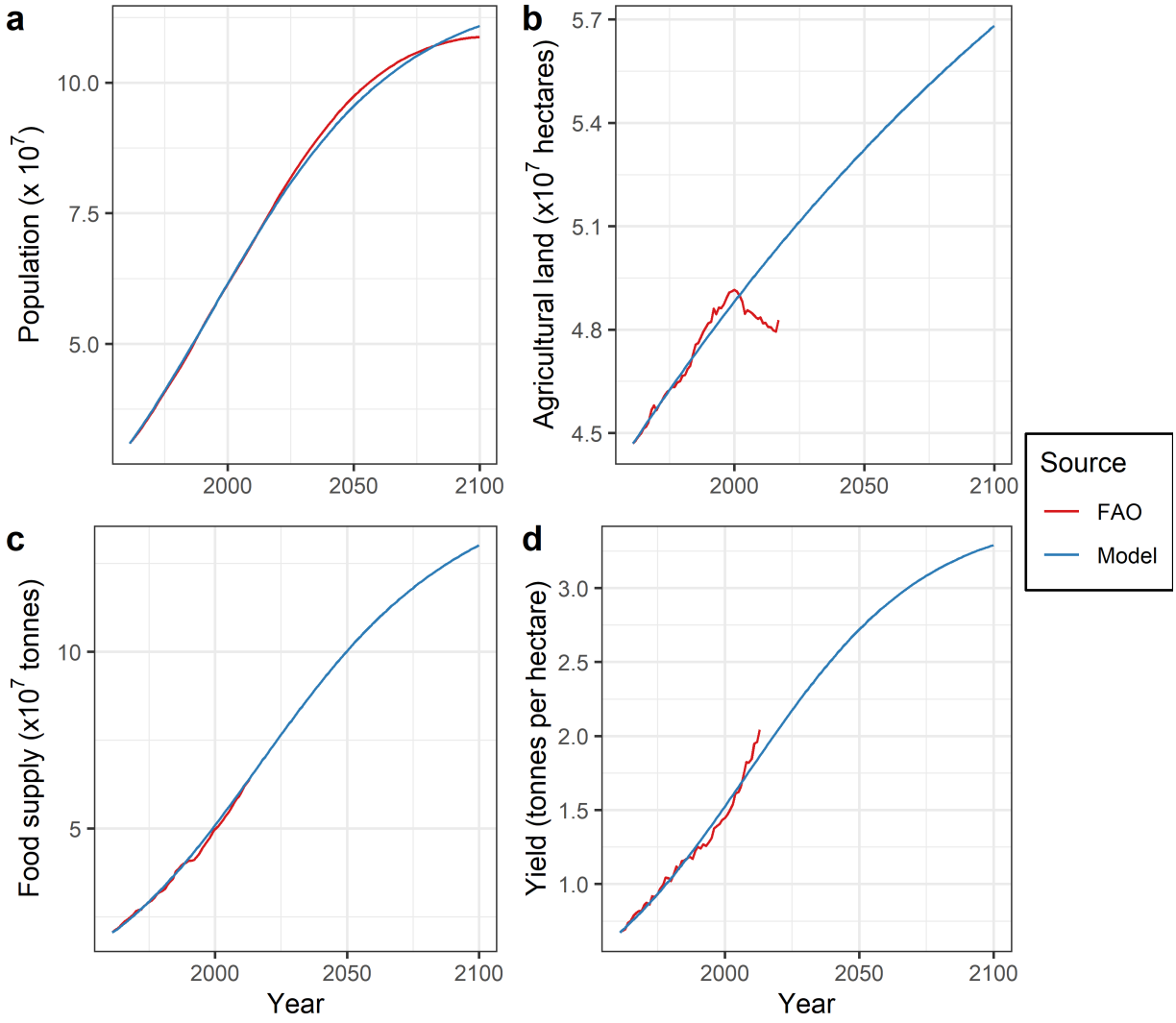

Figure C.2: **Global model using low yield scenario provides reasonable fit to real-world trajectories.** Trajectories for a) population b) agricultural land c) food supply and d) agricultural yield from global model (low yield scenario) and empirical data.

Though we obtain values for β^A and γ^A in these global fits, we do not fix these values for our metapopulation model. This is motivated both by the lack of a unique fit in the "low-yield" scenario, and a desire to explore how β^A and γ^A interact with β^I and γ^I. This exploration allows us to observe how the response curves for fulfilling food demand through expansion of agriculture (b_i^A), and imports (b_i^I), impact model outcomes.

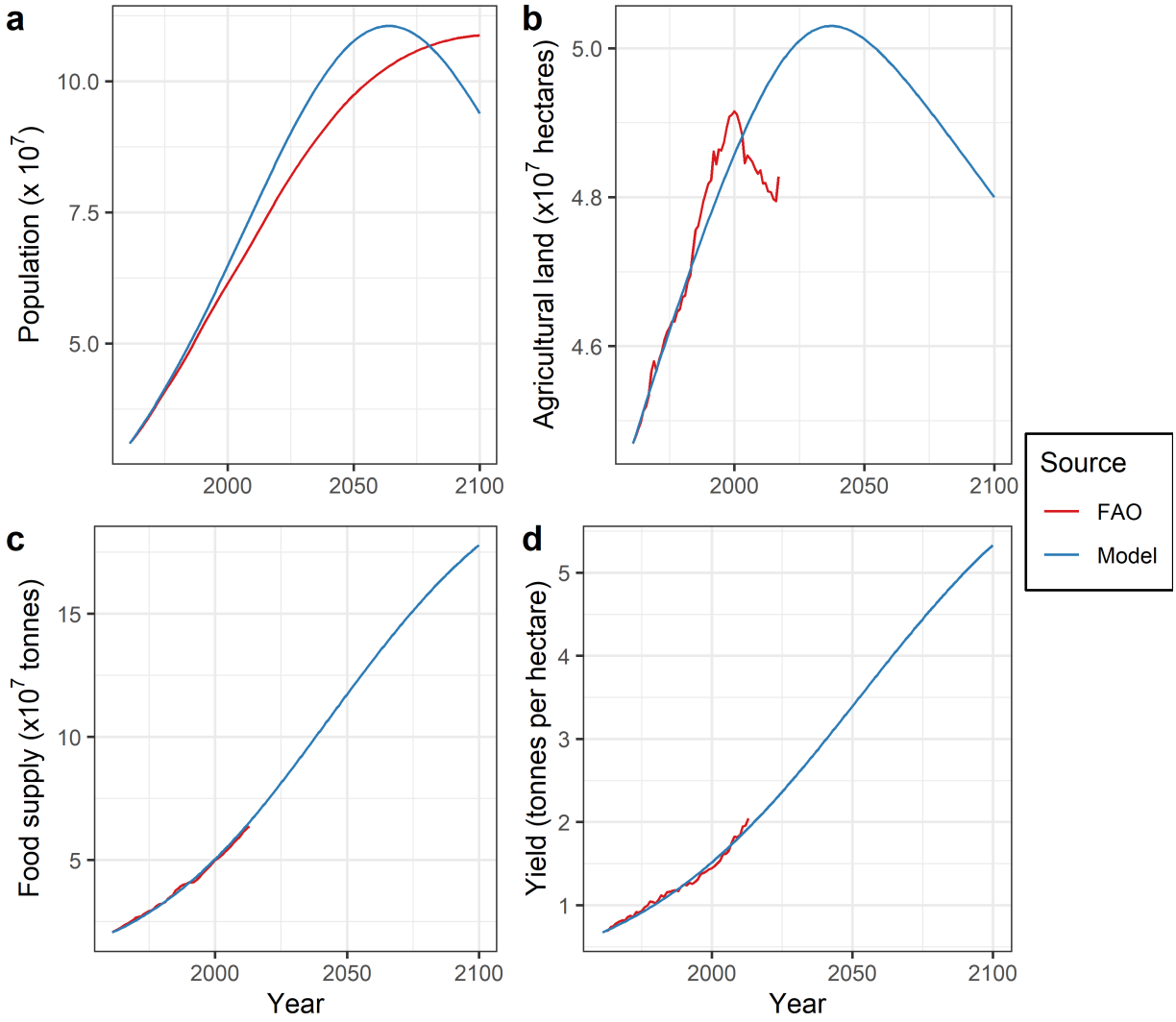

Figure C.3: **High yield variation of global model alters trajectories to 2100.** Trajectories for a) population b) agricultural land c) food supply and d) agricultural yield from global model (high yield scenario) and empirical data.

C.3 Supplementary figures

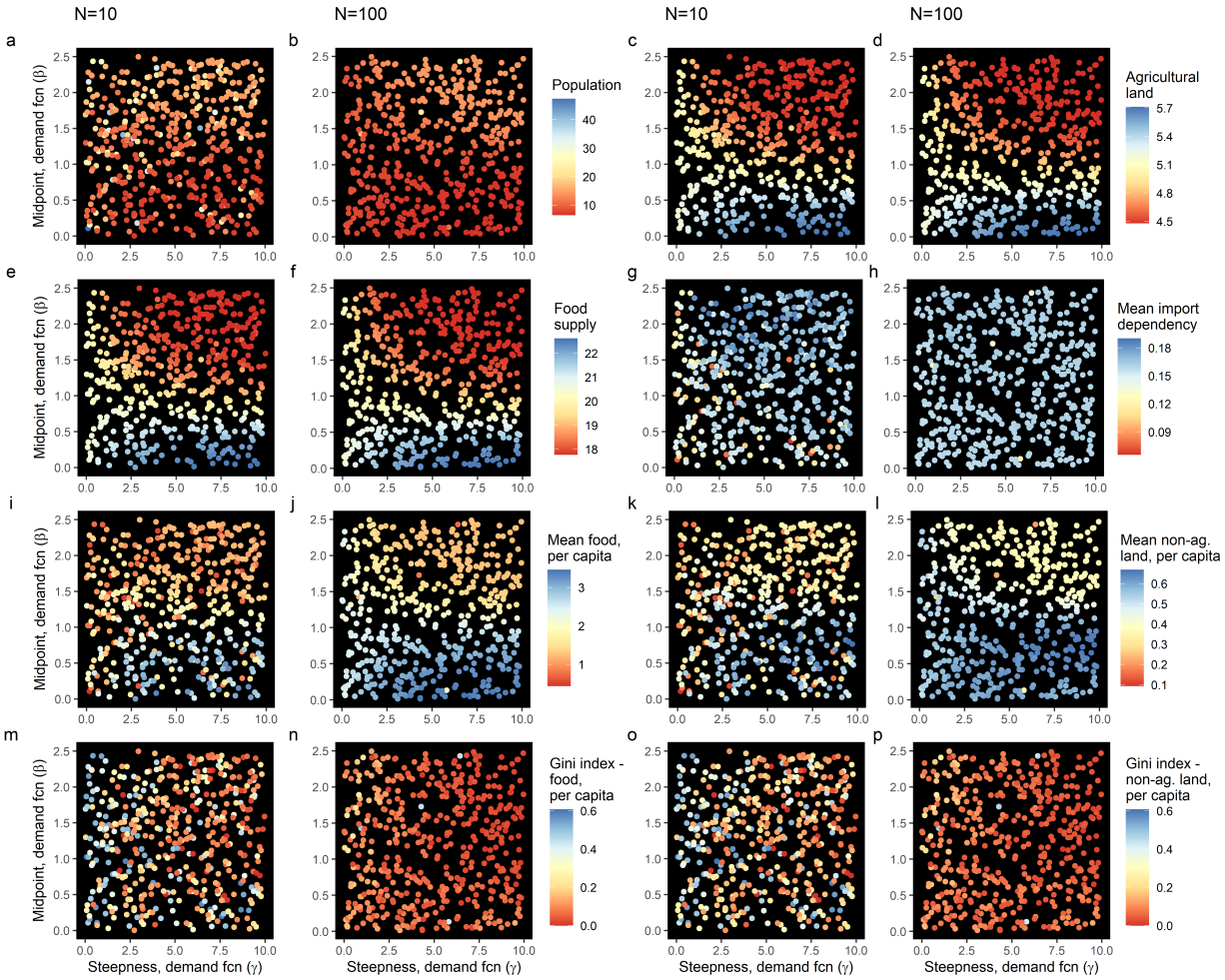

Figure C.4: **Steepness and midpoint of demand response sigmoid influence global system outcomes in a "high" yield scenario.** (γ, β) parameter planes for global values of (a)-(b) population ($\times 10^7$) (c)-(d) agricultural land ($\times 10^7$ hectares) (e)-(f) food supply ($\times 10^7$ tonnes) (g)-(h) mean level of import dependency, mean per capita (i)-(j) food (tonnes/person) and (k)-(l) non-agricultural land (hectares/person and Gini index, per capita (m)-(l) food and (o)-(p) non-agricultural land. 500 simulations run for each of $N = 10$, $N = 100$, randomly selecting a network and parameter values.